

Diss.- No. ETH 25949

**Ecohydrological sensitivity to climatic variables:
dissecting the water tower of Europe**

A thesis submitted to attain the degree of
DOCTOR OF SCIENCES of ETH ZURICH
(Dr. sc. ETH Zurich)

presented by

THEODOROS MASTROTHEODOROS

Diploma in Civil Engineering, National Technical University of Athens

born on 14.06.1990

citizen of Greece

accepted on the recommendation of

Prof. Dr. Peter Molnar, examiner

Prof. Dr. Paolo Burlando, co-examiner

Prof. Dr. Christina (Naomi) Tague, co-examiner

Prof. Dr. Valeriy Ivanov, co-examiner

Dr. Simone Fatichi, co-examiner

2019

*Dedicated to my parents and grandparents
and especially to my grandmother Eleni,
who left us the very first day of my PhD studies*

Abstract

The water balance in mountain regions describes the relations between precipitation, snow accumulation and melt, evapotranspiration and soil moisture and determines the availability of water for runoff in downstream areas. Climate change is affecting the water budget of mountains at a fast pace and it has thus become a priority for hydrologists to quantify the vulnerability of each hydrological component to climate change, in order to assess the availability of water in the near future. However, our incomplete understanding of mountain hydrology implies that our knowledge about the future water supply of billions of people worldwide is limited. In this thesis, I use the ecohydrological model Tethys-Chloris (T&C) to (1) explore the responses of forests to the increasing atmospheric CO₂, (2) quantify the major drivers of ecohydrological processes and their vulnerability to climate change across the European Alpine environments, and (3) partition the water budget into blue (hydrological) and green (biological) water fluxes and quantify the sensitivity of each component to temperature and precipitation change at the pan-Alpine scale.

The first part of the thesis focuses on vegetation parameterization in ecohydrological models. It is a common practice to apply static vegetation parameters, although recently several studies have questioned this approach, showing that vegetation may adjust to climate change at shorter timescales than previously thought. This implies that traditional model approaches using temporally constant parameters might be biased. Recent evidence suggests that one such example of vegetation plasticity may be related to the increasing atmospheric CO₂ concentrations. Through numerical simulations with T&C, I show that plasticity in key vegetation parameters can explain the changes in water and carbon vegetation fluxes in 20 forest sites in the northern Hemisphere; changes that otherwise cannot be explained.

In the second part of the thesis, I explore the key drivers of Alpine ecohydrology. Applying T&C on three case studies, I quantified the drivers of ecohydrological fluxes and explored the vulnerability of different Alpine ecosystems to climate change. By correlating the spatial distribution of ecohydrological responses with that of meteorological and topographic attributes, I computed spatially explicit sensitivities of net primary productivity, transpiration, and snow cover to air temperature, radiation, and water availability to evaluate their absolute and relative importance. The results demonstrate the sharp differences between different parts of the Alps, thus highlighting the need for a high-resolution assessment of the Alpine water budget.

The third part of the thesis addresses the ecohydrological sensitivity to climatic variables across the Alps. I collected a dataset from meteorological and environmental agencies and universities from six countries and combined it with new distributed products of meteorological forcing, soil properties, vegetation and snow cover to perform and validate large-scale, high-resolution ecohydrological simulations of the entire Alpine region for a period of three years (2001-2003). The focus in these simulations is on the partitioning of the pan-Alpine water budget into runoff and evapotranspiration. These simulations allowed us to quantify the sensitivity of each component of the pan-Alpine water budget to climate change and show that even during major heatwaves, Alpine vegetation keeps high transpiration rates, thus amplifying the decrease in streamflow. These unique simulations permitted

for the first time a very detailed understanding of water sinks and sources at the scale of the Alps, and a correlation analysis revealed the potential “hot spots” of changes in the water cycle in space and time under climate change. This study also shows that recent advances in ecohydrological modeling, combined with large scale datasets and new computational capabilities, can bridge the gap between coarse-scale Earth system models and detailed catchment analyses, providing more reliable, high-resolution climate change impact assessments in the world’s mountain regions.

Zusammenfassung

Der Wasserhaushalt in Gebirgsregionen beschreibt die Zusammenhänge von Niederschlag, Schneefall und -schmelze, Evapotranspiration und Bodenfeuchte und bestimmt die Wasserverfügbarkeit in Gebieten im Unterlauf. Diese, für den Wasserhaushalt entscheidenden, Prozesse werden stark vom Klimawandel beeinflusst. Daher ist es für Hydrologen zur Priorität geworden, die Anfälligkeit von jeder hydrologischen Komponente in Bezug auf den Klimawandel zu quantifizieren, um die Verfügbarkeit von Wasser in naher Zukunft beurteilen zu können. Unser Verständnis der hydrologischen Prozesse im Gebirge ist jedoch begrenzt, gleichermassen sind dadurch auch unsere Möglichkeiten die zukünftige Wasserversorgung von Milliarden Menschen zu planen eingeschränkt.

In dieser Arbeit verwende ich das öko-hydrologische Modell Tethys Chloris (T&C), um (1) die Reaktionen der Wälder auf das zunehmende atmosphärische CO₂ zu untersuchen, (2) die wichtigsten Faktoren für ökohydrologische Prozesse und ihre Anfälligkeit in Bezug auf den Klimawandel in verschiedenen Regionen der europäischen Alpen zu quantifizieren und (3) den Wasserhaushalt in blaue (hydrologische) und grüne (biologische) Wasserflüsse aufzuteilen und die Empfindlichkeit jeder Komponente gegenüber Temperatur- und Niederschlagsänderungen in den gesamten Alpen zu quantifizieren.

Der erste Teil der Arbeit beschäftigt sich mit der Parametrisierung von Vegetation in ökohydrologischen Modellen. Es ist allgemein üblich, statische Vegetationsparameter zu verwenden, obwohl kürzlich mehrere Studien diesen Ansatz in Frage gestellt haben. Diese Studien haben gezeigt, dass sich die Vegetation - in kürzeren Zeitabständen als bisher angenommen - an den Klimawandel anpassen kann. Dies bedeutet, dass mit traditionellen Modellansätzen, die zeitlich konstante Parameter verwenden, möglicherweise voreingenommene Schlüsse gezogen werden. Jüngste Ergebnisse legen nahe, dass diese rasche Veränderung der Vegetation mit steigenden atmosphärischen CO₂-Konzentrationen in Zusammenhang stehen könnte. Durch numerische Simulationen mit T&C zeige ich, dass wie die Veränderung von wesentlichen Vegetationsparametern die Veränderungen der Wasser- und Kohlenstoffvegetationsflüsse an 20 Waldstandorten in der nördlichen Hemisphäre erklären kann. Dabei handelt es sich um Veränderungen, die bisher nicht zu erklären waren.

Im zweiten Teil der Arbeit untersuche ich die wichtigsten Einflussfaktoren auf die alpine Ökohydrologie. Anhand von T&C quantifizierte ich in drei Fallstudien die massgebenden Einflüsse ökologischer Flüsse und untersuche die Anfälligkeit verschiedener alpiner Ökosysteme auf den Klimawandel. Durch Korrelation von räumlicher Verteilung ökohydrologischer Reaktionen sowie meteorologischen und topographischen Gebietseigenschaften berechnete ich - räumlich aufgelöst - die Sensitivität der primären Nettoproduktivität, Transpiration, die Schneedecke im Bezug zur Lufttemperatur, Strahlung und Wasserverfügbarkeit, um deren absolute und relative Bedeutung zu bewerten. Die Ergebnisse zeigen die starken Unterschiede zwischen verschiedenen Teilen der Alpen und unterstreichen die Notwendigkeit einer hochaufgelösten Bewertung des alpinen Wasserhaushalts.

Der dritte Teil der Arbeit befasst sich mit der ökohydrologischen Sensitivität auf klimatischen Variablen in den Alpen. Ich sammelte einen Datensatz von Meteorologie- und Umweltbehörden und Universitäten aus sechs Ländern und kombinierte ihn mit neuen flächendeckenden Produkten meteorologischer Variablen, Bodeneigenschaften, Vegetation und Schneebedeckung. Die Daten wurden verwendet um ökohydrologische Simulationen für gesamten Alpenraum mit hoher räumlicher Auflösung für einen Zeitraum von drei Jahren (2001-2003) durchzuführen und zu validieren. Der Fokus dieser Simulationen liegt auf der Aufteilung des alpinen Wasserhaushalts in Abfluss und Evapotranspiration. Diese Simulationen ermöglichten es, die Sensitivität jeder Komponente des alpinen Wasserbudgets für den Klimawandel zu quantifizieren, und zeigen, dass die alpine Vegetation auch bei großen Hitzewellen hohe Transpirationsraten beibehält, was eine verstärkte Abnahme des Abflusses während Trockenperioden bewirkt. Mit Hilfe dieser einzigartigen Simulationen, konnten zum ersten Mal – räumlich hochaufgelöst - Wassersenken und Quellen für den gesamten Alpenraum aufgezeigt werden. Eine Korrelationsanalyse ergab die potenziellen „Hot Spots“ der Veränderungen des Wasserkreislaufs in Raum und Zeit unter Einbeziehung des Klimawandels. Diese Studie zeigt auch, dass die jüngsten Fortschritte in der ökohydrologischen Modellierung in Verbindung mit umfangreichen Datensätzen und neuen Berechnungsfähigkeiten die Lücke zwischen groben Erdsystemmodellen und detaillierten Einzugsgebietsanalysen schließen können und zuverlässigere, hochauflösendere Abschätzungen der Klimafolgen für Bergregionen der Welt ermöglichen können.

Acknowledgements

I take this opportunity to thank all the people who have helped me. It is dedicated teachers already from the kindergarten, in the Greek countryside, and then through the primary and secondary school to the National Technical University of Athens. I really wish to thank all those people for their inspiration and patience, especially Andreas Efstratiadis and Demetris Koutsoyiannis, who prepared the way for this PhD, which I had never wished or thought about before. It is also all the good friends, with whom I shared so much during my studies in NTUA.

I want to thank Paolo Burlando and Peter Molnar, not just for trusting me, but also because they have always been morally intact, in an environment where ethics become looser. I want to thank Simone Fatichi, for all the time we spent together. I know it took him a lot of patience until we could speak the same language and I appreciate that. I want to thank also Christoforos Pappas for his support, and especially Panagiotis Hadjidoukas for his indescribable serenity with the most frustrating part of my research; without him, I doubt I would have made it to the end.

I want to thank all my colleagues in the hydrology group, for all the nice experiences we had together. Especially, Daniela Anghileri for her valuable help. Very special thanks to Anna Costa, for her invaluable understanding.

I owe a warm thank you to Marianne Schmid, my good friend who welcomed me in this wonderful country, to all my dear friends from the Greek Orthodox Church, and especially to father Emmanouel Simandirakis. All these people taught me so much and made me feel at home; I will keep them in my heart and thank them one by one.

Surprisingly, some people outside Academia persuaded me that I should go on with research, when I thought that this is not for me. They taught me I should accept some bitter advice and they saved me from a big mistake. I want to thank them.

I want to thank my brothers and sisters along with their families. I am so blessed to have them; each one has a unique spot in my heart; spots that multiply as they have more kids! Of course, we owe this blessing to our parents. I cannot imagine how much they have sacrificed to raise us. I am sorry they had to suffer with me whenever I was suffering, but this was more than a relief for me at that time. What shall I return to them for all their patience and love?

Table of contents

1. INTRODUCTION	1
1.1 MOTIVATION	1
1.2 RESEARCH QUESTIONS	3
1.2.1 How are ecohydrological models able to capture the response of forests to increasing CO ₂ ? ..	4
1.2.2 What is the role of temperature, radiation and soil water for Alpine ecohydrology? ..	5
1.2.3 What is the sensitivity of the pan-Alpine water budget to changes in temperature and precipitation?	7
2. LINKING PLANT FUNCTIONAL TRAIT PLASTICITY AND THE LARGE INCREASE IN FOREST WATER USE EFFICIENCY	9
2.1 INTRODUCTION.....	10
2.2 MATERIALS AND METHODS.....	12
2.2.1 Data Set.....	12
2.2.2 Inherent Water Use Efficiency	13
2.2.3 Trend Estimation and Uncertainty.....	13
2.2.4 Numerical Experiments.....	14
2.3 RESULTS	16
2.4 DISCUSSION	19
2.4.1 Observed Trends in IWUE	19
2.4.2 Plasticity in Plant Functional Traits.....	20
2.4.3 Challenges for the future	24
3. ECOHYDROLOGICAL DYNAMICS IN THE ALPS: INSIGHTS FROM A MODELLING ANALYSIS OF THE SPATIAL VARIABILITY	27
3.1 INTRODUCTION.....	28
3.2 METHODS	30
3.2.1 The T&C model	30
3.2.2 Model simulations.....	30
3.2.3 Sensitivity analysis.....	34
3.2.4 Variance across spatial scales.....	36
3.3 RESULTS	37
3.3.1 Ecohydrological sensitivity to temperature, radiation, and topographic index.....	37
3.3.1.1 The Kleine Emme catchment	37
3.3.1.2 Synthetic domain.....	40
3.3.1.3 The role of catchment orientation.....	43
3.3.2 Variability across spatial scales.....	44
3.3.2.1 The Kleine Emme catchment	44
3.3.2.2 Synthetic domain.....	45
3.4 DISCUSSION	47
3.4.1 Ecosystem sensitivities.....	47
3.4.1.1 Ecosystem sensitivity to air temperature	48
3.4.1.2 Ecosystem sensitivity to shortwave radiation	48
3.4.1.3 Ecosystem sensitivity to water availability	49
3.4.1.4 Which is the dominant driver of Alpine ecohydrological processes?.....	49
3.4.2 How important is catchment orientation?	50
3.4.3 Cross-scale spatial variability in Alpine ecohydrology	51
3.4.4 Limits of interpretation.....	52
3.4.4.1 Lateral water flows and soil moisture.....	52
3.4.4.2 Synthetic mountain set-up.....	53
3.4.4.3 The use of the “space-for-time” approach.....	53
3.4.4.4 Simulating vegetation fitness and mortality.....	54

3.5	CONCLUSIONS	55
4.	MORE GREEN AND LESS BLUE WATER IN THE ALPS DURING WARMER SUMMERS	57
4.1	INTRODUCTION	58
4.2	DISSECTING THE WATER TOWER OF EUROPE	59
4.3	BLUE VS GREEN WATER DURING EXCEPTIONALLY DRY SUMMERS	60
4.4	DISCUSSION	64
4.4.1	Limitations	64
4.4.2	Conclusions	64
5.	CONCLUSIONS	67
5.1	MAJOR CONCLUSIONS	67
5.1.1	Plasticity in plant traits	67
5.1.2	Drivers of Alpine ecohydrology	67
5.1.3	Pan-Alpine water budget	68
5.2	OUTLOOKS	69
5.2.1	Adapting model parameterization	69
5.2.2	Ecohydrological models as tools for developing new theories	69
5.2.3	Towards hyper-resolution ecohydrology	70
5.2.4	Linking Earth system models to ecohydrology	70
APPENDIX A: LINKING PLANT FUNCTIONAL TRAIT PLASTICITY AND THE LARGE INCREASE IN FOREST WATER USE EFFICIENCY		71
A.1	Water use efficiency definition	71
A.2	Fluxnet data	72
A.3	The T&C model	72
A.4	Data-related uncertainties	75
APPENDIX B: ECOHYDROLOGICAL DYNAMICS IN THE ALPS: INSIGHTS FROM A MODELLING ANALYSIS OF THE SPATIAL VARIABILITY		87
B.1	The T&C model	87
B.2	Details about the independent variables	88
APPENDIX C: MORE GREEN AND LESS BLUE WATER IN THE ALPS DURING WARMER SUMMERS		111
C.1	The Tethys-Chloris model (T&C)	111
C.2	Domain setup	112
C.3	Meteorological input	113
C.4	Space-for-time substitution	115
C.5	Model validation	115
REFERENCES		143
CURRICULUM VITAE		177

List of Figures

Figure 2.1 Observed (green) and simulated (purple and red) annual time series of (a) inherent water use efficiency (IWUE, computed as in Eq. 2.1, using the annual means of GEP, ET and VPD), (b) gross ecosystem production (GEP) and (c) evapotranspiration (ET) at the US-UMB site (details in Table A.1). Purple represents the base simulations and red shows the numerical experiment which best approximates each variable's slope for this site, i.e. $[+V_{\max}-a_1]$ for IWUE, $[-a_1+K_{\text{nit}}]$ for GEP and $[-a_1]$ for ET. Linear least squares fitting is shown with dashed lines. The shaded green areas show the 95% uncertainty bounds for the observed slopes in the three variables.16

Figure 2.2 Linear slopes of (a) inherent water use efficiency (IWUE), (b) gross ecosystem production (GEP), and (c) evapotranspiration (ET) for the 20 investigated sites. The box length provides the interquartile range (I_{QR}), the bottom of the box the 25th percentile (first quartile, q_1), the top of the box the 75th percentile (third quartile, q_3), and the horizontal line within the box the median value. The lower whisker corresponds to $q_1 - 1.5I_{\text{QR}}$, or to the minimum estimate, and the upper whisker corresponds to $q_3 + 1.5I_{\text{QR}}$, or to the maximum estimate. The green represents the observations, the black stands for base simulations, the blue for the experiments in which only one parameter was perturbed, and the magenta for the experiments in which two parameters were perturbed. The red dashed line represents the expected rate of IWUE increase.18

Figure 2.3 Relative frequency distributions of median slopes in (a) observed inherent water use efficiency (IWUE), (b) gross ecosystem production (GEP), and (c) evapotranspiration (ET). For each site, a slope was selected randomly from the uniform distribution that is bounded by the 95% confidence interval of the estimated linear slope. The histograms show the results of 10,000 Monte Carlo runs. The dotted lines show the median reported by Keenan et al. (2013), and the dashed green line shows the expected IWUE increase ($0.5\% \text{ yr}^{-1}$). In each subplot we show the median slopes of base T&C simulations (circles), the median slopes of base simulations with detrended temperature and relative humidity (dots), and the numerical experiment which best approximates each variable's slope (crosses), i.e., $[+V_{\max} + \text{LtR}]$ for IWUE, $[-a_1-K_{\text{nit}}]$ for GEP, and $[a_1]$ for ET.19

Figure 3.1 Location and topographic map of the Kleine Emme catchment in central Switzerland. ...31

Figure 3.2 Four-year mean annual (a) temperature, (b) shortwave radiation, (c) precipitation that are used as input meteorological variables to the model and 4-year mean annual simulated (d) transpiration, (e) leaf area index (LAI), (f) net primary production (NPP), (g) soil evaporation, (h) fraction of time with soil saturation, and (i) fraction of time with snow cover for the Kleine Emme catchment.32

Figure 3.3 Three-dimensional (3D) representation of the symmetric synthetic domain. The vertical axis has been stretched to improve clarity.33

Figure 3.4 Four-year mean annual (a) temperature, (b) shortwave radiation, (c) precipitation that are used as input meteorological variables to the model and 4-year mean annual simulated (d) transpiration, (e) leaf area index (LAI), (f) net primary production (NPP), (g) soil evaporation, (h)

fraction of time with soil saturation, and (i) fraction of time with snow cover for the dry grassland experiment in the synthetic domain.....35

Figure 3.5 Sensitivity of transpiration (T), evapotranspiration (ET), net primary production (NPP), and leaf area index (LAI) to air temperature, shortwave radiation, and topographic index in the Kleine Emme catchment. Green represents areas where an increase in the explanatory variable leads to an increase in the dependent variable (positive sensitivity), and magenta is for the areas where an increase in the explanatory variable leads to a decrease in the dependent variable (negative sensitivity). Areas shown in dark colour are those where the dependent variable is insensitive to the respective explanatory variable.....38

Figure 3.6 Normalized sensitivity of net primary production (NPP) to air temperature, shortwave radiation, and topographic index in the Kleine Emme catchment. The red colour represents areas where temperature is the main control for NPP, green represents the radiation-limited areas, and blue is for areas where the topographic index is the dominant control. Inset scatter plots show the comparison between the original model output (“original”) and the values that are calculated with the regression formula that was used for the sensitivity analysis (“regressed”) for (a) evergreen forest, (b) mixed forest, and (c) grassland (the R² values of each regression are also shown). All variables are normalized.39

Figure 3.7 Sensitivity of net primary production (NPP) to air temperature, shortwave radiation, and topographic index in the four experiments on the synthetic domain. Green represents areas where an increase in the explanatory variable leads to an increase in NPP (positive sensitivity), and magenta is for areas where an increase in the explanatory variable leads to a decrease in NPP (negative sensitivity). Areas shown in dark colour are those where NPP is insensitive to the respective explanatory variable.....41

Figure 3.8 Normalized sensitivity of net primary production (NPP) to air temperature, shortwave radiation, and topographic index in the four experiments on the synthetic domain. The red colour represents areas where temperature is the main control for NPP, green represents the radiation-limited areas, and blue is for areas where the topographic index is the dominant control. Inset scatter plots show the comparison between the original model output (“original”) and the values that are calculated with the regression formula that was used for the sensitivity analysis (“regressed,” R² values are also shown). All variables are normalized.43

Figure 3.9 Departure of the mean of each catchment from the mean of the whole domain (expressed in % of the latter) for (a) shortwave radiation; (b) transpiration; (c) leaf area index (LAI); (d) net primary production (NPP); (e) runoff; and (f) fraction of time with snow cover (snoFra). S, E, N, and W on the y-axis denote the orientation of the catchment (south, east, north, and west, respectively). The blue lines represent the wet climate, and the red lines represent the dry climate. Continuous lines are used for the grassland and dashed for the evergreen forest (w_g, w_e, d_g, and d_e stand for wet grassland, wet evergreen forest, dry grassland, and dry evergreen forest, respectively). Subplot (e)

shows only the runoff of the wet experiments, because the runoff of the dry experiments is almost zero.44

Figure 3.10 Meteorological, topographic, and ecosystem spatial variability in the Kleine Emme catchment. Normalized Standard deviation as a function of spatial scale for air temperature, shortwave radiation, and topographic index in green, magenta, and black, respectively. Blue lines represent the spatial variability of several ecohydrological variables: the continuous line is for transpiration, the dotted line for net primary production (NPP), the dashed line for leaf area index (LAI), and the line with the star markers corresponds to the time fraction with snow cover (snoFra). Temperature and topographic index create an envelope that contains all the ecohydrological variables (shaded). All variables are normalized so that the standard deviation equals one for the original resolution of the simulations (100-m grid). For an explanation of the aggregation, see Fig. B.9 (Appendix B).....45

Figure 3.11 Range of spatial variability in the four experiments in the synthetic domain. Boxplots of (a) temperature, (b) shortwave radiation (ShRad), (c) precipitation, (d) transpiration, (e) leaf area index (LAI), (f) net primary production (NPP), (g) soil evaporation (sEvap), (h) fraction of time with soil saturation (satFra), and (i) fraction of time with snow cover (snoFra). For the meteorological forcing (a–c), we distinguish between the wet and dry experiments and for the ecohydrological variables we distinguish also between grassland and evergreen (using the symbols w_g, w_e, d_g, and d_e for wet grassland, wet evergreen forest, dry grassland, and dry evergreen forest, respectively). Each boxplot represents the 4-year average annual values for each simulated cell of the domain. The box length provides the interquartile range (I_{QR}), the bottom of the box the 25th percentile (first quartile, q_1), the top of the box the 75th percentile (third quartile, q_3), and the horizontal line within the box the median value. The lower whisker corresponds to $q_1 - 1.5I_{QR}$, or to the minimum estimate, and the upper whisker corresponds to $q_3 + 1.5I_{QR}$, or to the maximum estimate. The number on the x-axis is the range of variability (RV), as defined in Appendix A.4. Outliers outside the whiskers are not shown.....46

Figure 3.12 Meteorological, topographic, and ecosystem spatial variability in the four experiments on the synthetic domain. Normalized standard deviation as a function of spatial scale for (a) air temperature, shortwave radiation, and topographic index in green, magenta, and black, respectively; (b) transpiration; (c) leaf area index (LAI); (d) net primary production (NPP); and (e) fraction of time with snow cover (snoFra). In subplots (b–e), red lines represent the dry ecosystems and blue the wet ones; dashed lines are used for evergreen forest, and continuous lines are used for grassland (w_g, w_e, d_g, and d_e stand for wet grassland, wet evergreen forest, dry grassland, and dry evergreen forest, respectively). The three variables of subplot (a) create an envelope that contains most ecohydrological variables in all experiments (shaded). All variables are normalized so that the standard deviation equals one for the original resolution of the simulations (100-m grid). X-axis in subplot (a) also shows the area that is aggregated for each spatial scale (in km²).....47

Figure 4.1 Simulation results reflect the high spatial heterogeneity in latent heat (evapotranspiration in energy units). (a) The spatial extent of the European Alps. (b) Three-year average latent heat flux ($W m^{-2}$) for the entire 257,000 km² domain simulated with Tethys-Chloris. (c) and (d) focus on the

Bernese highlands, Switzerland, to reveal the small-scale spatial heterogeneity and the high-resolution simulation (250 m x 250 m pixels).....60

Figure 4.2 Relationship between elevation and blue and green water fluxes. (a) Percent contribution of each elevation class (grouped in 100 m elevational bins) to precipitation (P), evapotranspiration (ET) and P-ET, including the fractional area of each class (the fluxes are averaged over the entire simulation period, i.e. 2001-2003). The highlighted magenta bars show the most runoff-productive zone (1300-3000 m a.s.l.). (b) P-ET in mm yr⁻¹. The dashed line and the shaded area represent the median P-ET (averaged over the entire simulation period) over the entire domain and the interquartile range, respectively. Coloured lines show P-ET elevational distribution for selected catchments to illustrate the spatial variability. A locator map is included. (c) ET anomalies (solid lines-left y-axis) and ET contribution to the runoff deficits compared with the precipitation deficit during the 2003 growing season (scatter-right y-axis). The anomalies were computed based on the 2001-2003 mean and the fluxes were averaged in space based on the 100 m elevational bins. Each point of the scatter represents one of the 334 catchments (out of the 381 in total) for which both precipitation and runoff were lower in 2003 compared with the long-term average and the 2001-2003 mean, respectively. .62

Figure 4.3 Analysis of anomalies in blue and green water fluxes during the 2003 drought. (a) Histogram of observed 2003 runoff anomalies in percentage for 381 locations (2003 compared with the long-term mean of each station), coloured according to the magnitude of the anomaly (>-75%: cyan, -50 to -75%: red, -25 to -50%: yellow and >-25%: black). (b) Spatial distribution of the simulated ET anomaly in mm during the 2003 growing season (May-September, here 2003 ET is compared with the 2001-2003 mean). The dots represent the locations of the 381 locations with hydrological measurements and are coloured as described in (a). The three insets in the lower right part show the boxplots of simulated ET anomaly for three different vegetation types (evergreen, deciduous, and grassland) in three elevational classes (<1000 m a.s.l., 1000-2000 m a.s.l. and >2000 m a.s.l.).63

Appendices

Figure A.1 Location of the 20 flux tower sites used in the study.....75

Figure A.2 Correlation and corresponding coefficients (r) between linear regression and Sen slope of the inherent water use efficiency (IWUE) computed in the 20 sites. We show the corresponding values obtained from both observations and Tethys-Chloris base simulations.76

Figure A.3 Inherent water use efficiency (IWUE) response to perturbation of five parameters for the US-UMB site. Linear fit is also shown for each parameter.76

Figure A.4 Observed inherent water use efficiency (IWUE), gross ecosystem production (GEP) and evapotranspiration (ET) linear slopes in evergreen needleleaf forests (ENF) and deciduous broadleaf forests (DBF).77

Figure A.5 Discrepancies between CarboEurope (dashed lines) and Fluxnet 2015 (continuous lines) in the reported observations of latent heat flux (LE), in RU-Fyo (magenta) and DE-Tha (green). ...	77
Figure A.6 Linear slopes in simulated C_i/C_a , where C_i is the intercellular CO_2 concentration estimated as the simple average of the annual C_i of sunlit and shaded leaves at the ecosystem scale and C_a is the annual atmospheric CO_2 concentration. Black represents the base simulations; blue the simulations for which only one parameter was perturbed, and magenta the simulations in which two parameters were perturbed.	78
Figure A.7 Linear slopes in simulated C_i (intercellular CO_2 concentration estimated as the simple average of the annual intercellular CO_2 concentration of sunlit and shaded leaves at the ecosystem scale) for the 20 sites examined. Black represents the base simulations; blue the simulations for which only one parameter was perturbed, and magenta the simulations in which two parameters were perturbed.	79
Figure A.8 Inherent water use efficiency (IWUE), gross ecosystem production (GEP) and evapotranspiration (ET) linear slopes in evergreen needleleaf forests (ENF) and deciduous broadleaf forests (DBF) for the base simulations.	80
Figure A.9 Inherent water use efficiency (IWUE), gross ecosystem production (GEP) and evapotranspiration (ET) linear slopes in evergreen needleleaf forests (ENF) and deciduous broadleaf forests (DBF) for the numerical experiment in which we perturbed a_1 parameter (which connects stomatal aperture and net assimilation) by $-1\% \text{ yr}^{-1}$	80
Figure B.1 The Kleine Emme catchment; elevation (a), land cover (b) and soil texture (c).	89
Figure B.2 Simulated and observed hourly discharge in Littau (a) and Werthenstein (b). For details about the two hydrological stations, refer to Table B.1.	90
Figure B.3 Simulated and observed discharge seasonality for the simulated period (1/10/2000-30/9/2005) in Littau (a) and Werthenstein (b). For details about the two hydrological stations, refer to Table B.1.	90
Figure B.4 Simulated and observed hourly (a and c) and daily (b and d) discharge in Littau (upper plots) and Werthenstein (lower plots) in logarithmic scale.	91
Figure B.5 Observed and simulated flow duration curves for Littau (a) and Werthenstein (b).	92
Figure B.6 Summary of the meteorological input and simulated ecohydrological variables for the dry evergreen forest experiment in the synthetic domain. The subplots show the four-year average of annual (a) temperature, (b) shortwave radiation, (c) precipitation, (d) transpiration, (e) leaf area index (LAI), (f) net primary production (NPP), (g) soil evaporation, (h) fraction of time with soil saturation, and (i) fraction of time with snow cover.	93

Figure B.7 Summary of the meteorological input and simulated ecohydrological variables for the wet grassland experiment in the synthetic domain. The subplots show the four-year average of annual (a) temperature, (b) shortwave radiation, (c) precipitation, (d) transpiration, (e) leaf area index (LAI), (f) net primary production (NPP), (g) soil evaporation, (h) fraction of time with soil saturation, and (i) fraction of time with snow cover.....94

Figure B.8 Summary of the meteorological input and simulated ecohydrological variables for the wet evergreen forest experiment in the synthetic domain. The subplots show the four-year average of annual (a) temperature, (b) shortwave radiation, (c) precipitation, (d) transpiration, (e) leaf area index (LAI), (f) net primary production (NPP), (g) soil evaporation, (h) fraction of time with soil saturation, and (i) fraction of time with snow cover.95

Figure B.9 Analysis of variance across spatial scales. The green colour shows the aggregation area, which is stepwise increased.....95

Figure B.10 Normalized sensitivity of leaf area index (LAI) to air temperature, shortwave radiation and topographic index in Kleine Emme. The red colour represents areas where temperature is the main control for LAI. Green represents the radiation-limited areas and blue is for areas where the topographic index is the dominant control. Inset scatter plots show the comparison between the original model output (“original”) and the values that are calculated with the regression formula that was used for the sensitivity analysis (“regressed”) for (a) evergreen forest, (b) mixed forest, and (c) grassland (the R^2 value of each regression is also shown). All variables are normalized.....96

Figure B.11 Normalized sensitivity of transpiration (T) to air temperature, shortwave radiation and topographic index in Kleine Emme. The red colour represents areas where temperature is the main control for T. Green represents the radiation-limited areas and blue is for areas where the topographic index is the dominant control. Inset scatter plots show the comparison between the original model output (“original”) and the values that are calculated with the regression formula that was used for the sensitivity analysis (“regressed”) for (a) evergreen forest, (b) mixed forest, and (c) grassland (the R^2 value of each regression is also shown). All variables are normalized.97

Figure B.12 Normalized sensitivity of evapotranspiration (ET) to air temperature, shortwave radiation and topographic index in Kleine Emme. The red colour represents areas where temperature is the main control for ET. Green represents the radiation-limited areas and blue is for areas where the topographic index is the dominant control. Inset scatter plots show the comparison between the original model output (“original”) and the values that are calculated with the regression formula that was used for the sensitivity analysis (“regressed”) for (a) evergreen forest, (b) mixed forest, and (c) grassland (the R^2 value of each regression is also shown). All variables are normalized.....98

Figure B.13 Normalized sensitivity of the fraction of time with snow cover (snoFra) to air temperature, shortwave radiation and topographic index in Kleine Emme. The red colour represents areas where temperature is the main control for snoFra. Green represents the radiation-limited areas and blue is for areas where the topographic index is the dominant control. Inset scatter plots show the comparison between the original model output (“original”) and the values that are calculated with the

regression formula that was used for the sensitivity analysis (“regressed”) for (a) evergreen forest, (b) mixed forest, and (c) grassland (the R^2 value of each regression is also shown). All variables are normalized.99

Figure B.14 Sensitivity of evapotranspiration (ET) to air temperature, shortwave radiation and topographic index in the four experiments on the synthetic domain. Green represents areas where an increase in the explanatory variable leads to an increase in ET and magenta is for areas where an increase in the explanatory variable leads to a decrease in ET. Areas shown in dark colour are those where ET is insensitive to respective explanatory variable.100

Figure B.15 Sensitivity of leaf area index (LAI) to air temperature, shortwave radiation and topographic index in the four experiments on the synthetic domain. Green represents areas where an increase in the explanatory variable leads to an increase in LAI and magenta is for areas where an increase in the explanatory variable leads to a decrease in LAI. Areas shown in dark colour are those where LAI is insensitive to respective explanatory variable.101

Figure B.16 Sensitivity of transpiration (T) to air temperature, shortwave radiation and topographic index in the four experiments on the synthetic domain. Green represents areas where an increase in the explanatory variable leads to an increase in T and magenta is for areas where an increase in the explanatory variable leads to a decrease in T. Areas shown in dark colour are those where T is insensitive to respective explanatory variable.102

Figure B.17 Normalized transpiration (T) to air temperature, shortwave radiation and topographic index in the four experiments on the synthetic domain. The red colour represents areas where temperature is the main control for T. Green represents the radiation-limited areas and blue is for areas where the topographic index is the dominant control. Inset scatter plots show the comparison between the original model output (“original”) and the values that are calculated with the regression formula that was used for the sensitivity analysis (“regressed”, R^2 values are also shown). All variables are normalized.103

Figure B.18 Normalized sensitivity of evapotranspiration (ET) to air temperature, shortwave radiation and topographic index in the four experiments on the synthetic domain. The red colour represents areas where temperature is the main control for ET. Green represents the radiation-limited areas and blue is for areas where the topographic index is the dominant control. Inset scatter plots show the comparison between the original model output (“original”) and the values that are calculated with the regression formula that was used for the sensitivity analysis (“regressed”, R^2 values are also shown). All variables are normalized.104

Figure B.19 Normalized sensitivity of leaf area index (LAI) to air temperature, shortwave radiation and topographic index in the four experiments on the synthetic domain. The red colour represents areas where temperature is the main control for LAI. Green represents the radiation-limited areas and blue is for areas where the topographic index is the dominant control. Inset scatter plots show the comparison between the original model output (“original”) and the values that are calculated with the

regression formula that was used for the sensitivity analysis (“regressed”, R^2 values are also shown). All variables are normalized.....105

Figure B.20 Normalized sensitivity of the fraction of time with snow cover (snoFra) to air temperature, shortwave radiation and topographic index in the four experiments on the synthetic domain. The red colour represents areas where temperature is the main control for snoFra. Green represents the radiation-limited areas and blue is for areas where the topographic index is the dominant control. Inset scatter plots show the comparison between the original model output (“original”) and the values that are calculated with the regression formula that was used for the sensitivity analysis (“regressed”, R^2 values are also shown). All variables are normalized.....106

Figure C.1 Decomposition of the pan-Alpine domain into eight independent subdomains. The aim was to subdivide the computational load without affecting lateral connectivity and topographic influences, thus we followed the ridgelines and assumed no exchange between the different subdomains.117

Figure C.2 Difference in fraction of time with snow cover [-] between MODIS observations for the period November 2000 to October 2003 and T&C simulations. The inset shows the respective histogram, including all the simulated pixels.118

Figure C.3 Model validation against measured daily runoff (a-c) and snow depth (d-f). The latter was conducted accounting for the period with observed snow cover only. The maps (a, d) include the locations of each station, coloured according to model performance, as explained in subplots c and f for runoff and snow depth, respectively. Subplots B and E show the histogram of the percent bias and bias in cm, respectively for all the stations. For runoff, we used the Spearman R and the percent bias (c) and for snow we used the bias in snow duration and average snow depth (d). Both runoff (b) and snow depth (e) biases are close to zero for the majority of the stations.119

Figure C.4 Comparison between simulated (Q_{sim}) and observed (Q_{obs}) mean runoff for the entire simulation period in 381 locations (in $mm\ hr^{-1}$). The colour of the markers shows the degree of glaciation of each catchment. Closed circles are used for the natural catchments and open circles are used for the heavily regulated ones, the R^2 is reported separately for those two groups. The inset shows the comparison of catchment-averaged P-ET against measured runoff (Q_{obs}), using the same symbols. In both plots, the one-one line is also plotted.120

Figure C.5 ET elevational distribution. ET is averaged over 100 m elevation bins for the entire pan-Alpine domain (dashed line) and for selected catchments (solid lines, their locations are shown in the inset map). The shaded area represents the interquartile range of ET distribution across the entire pan-Alpine domain.....121

Figure C.6 Relationship between water fluxes (km^3) and elevation (a) annually and (b) for the growing season (May-September). Negative values on the y-axis denote supply of water from soil storage.122

Figure C.7 Time series of mean annual (black) and growing season (blue bold) precipitation (a) and temperature (b) for the period 1992-2008 and 1992-2017, respectively. The growing season of 2002 and 2003, were the wettest and driest in the record, respectively; 2003 growing season was also the warmest. Hydrological years for computing the annual means, are defined as the period between November 1st of the previous year to October 31st, to be consistent with model simulations.....123

Figure C.8 Blue and green water daily fluxes averaged over the entire domain for the three simulated years (November 2000 excluded). Liquid precipitation (i.e. excluding snow), runoff (Q), snowmelt, icemelt and ET are shown in mm. All variables have been smoothed using a 30-days moving average. The three growing seasons (May-September) are highlighted (shaded areas).124

Figure C.9 Relative contribution of ET in comparison to P to the runoff deficit in 2003. Anomalies in ET and P are computed in comparison to the 2001-2003 mean in 334 catchments for which both precipitation and runoff were lower in 2003 compared with the 2001-2003 mean. The map shows the location of each runoff station coloured according to $ET_{anomaly}$ and the ratio $ET_{anomaly}/P_{anomaly}$, as displayed in the inset. Yellow colour denotes the catchments for which ET increased in 2003, but the precipitation deficit was larger than the ET excess. Black colour shows the catchments in which ET excess in 2003 was larger than precipitation deficit. Magenta is used for the catchments where ET decreased in 2003 less than precipitation, and cyan for the catchments in which ET decreased more than precipitation. The green and the red dot on the y-axis show the median $ET_{anomaly}/P_{anomaly}$ across all catchments and in the catchments with mean elevation between 1300-3000 m a.s.l., respectively.125

Figure C.10 Relative contribution of ET in comparison to precipitation to the runoff deficit in 2003. The maps show the ratio of the anomaly in ET over the anomaly in P (anomalies computed as the difference between 2003 and the mean over the entire simulation period, i.e. 2001-2003) over the entire Alps (a) and focusing in central Switzerland (b) to show the spatially complex patterns of changes in ET. Black represents the areas in which precipitation in 2003 was higher than the 2001-2003 mean.....126

List of Tables

Table 2.1 Parameters of T&C model that were modified in the numerical experiments.....15

Table 3.1 Summary of the meteorological stations used in the study (source: Swiss meteorological service).....31

Appendices

Table A.1 Summary of the 20 flux tower sites and of the periods used in the analysis. All sites represent temperate or boreal forest ecosystems. DBF = Deciduous broadleaf forest; ENF = Evergreen needleleaf forest; MF = Mixed Forest.81

Table A.2 Linear slopes of inherent water use efficiency (IWUE), gross ecosystem production (GEP) and evapotranspiration (ET) for the 20 sites in [% yr⁻¹]; observed and base simulation slopes are shown as well as the slopes computed from simulations with de-trended temperature and relative humidity. We also show the output of the numerical experiments in which we perturbed the a_1 parameter (which connects stomatal aperture and net assimilation) by -1% yr⁻¹ ($[-a_1]$ simulations). For observations, the 5-95% uncertainty range is shown in parenthesis (the range is computed based on the normality assumption that residuals follow the Gaussian distribution).82

Table A.3 Correlation coefficients between modelled and observed latent heat (LE) and gross primary production (GPP) at the hourly and daily scale for the entire period modelled for each site (in parenthesis the coefficients for the filtered data, i.e. summer, non-rainy days and daytime only). The amount of data missing is also given (gaps in % of the total data). ‘-’ is used when no estimate of the gaps is available.83

Table A.4 Annual trends in temperature and relative humidity.84

Table A.5 Parameters of the Tethys-Chloris (T&C) model included in the initial screening.....84

Table A.6 Median linear slopes (in [% yr⁻¹]) of inherent water use efficiency (IWUE), gross ecosystem production (GEP) and evapotranspiration (ET) for observations and all T&C simulations and Euclidean distance between simulations and observations for all the experiments. Values for Sen slopes are given in parenthesis. Bold denotes the simulations in which the Euclidean distance is lower than that of the base simulations.85

Table A.7 Median linear slopes (in [% yr⁻¹]) of inherent water use efficiency (IWUE), gross ecosystem production (GEP) and evapotranspiration (ET) for observations and all T&C simulations and Euclidean distance between simulations and observations for all the experiments weighing by the length of time series. Values for Sen slopes are given in parentheses. Bold denotes the simulations in which the Euclidean distance is lower than that of the base simulations.86

Table B.1. River discharge measurement stations in the Kleine Emme catchment.....107

Table B.2 Initial screening for the third explanatory variable to express water limitations. The table shows the explanatory power (R^2) of the regressions for transpiration (T), evapotranspiration (ET), net primary production (NPP), leaf area index (LAI), snow water equivalent (SWE) and the fraction of time with snow cover (snoFra) using air temperature, shortwave radiation and topographic index (upstream area).....	107
Table B.3 Correlation between the three explanatory variables in the wet and dry synthetic domains and in the Kleine Emme catchment.....	107
Table B.4 Regression-derived relationships for transpiration (T), evapotranspiration (ET), net primary production (NPP) and leaf area index (LAI) in the Kleine Emme catchment (on normalized variables). y is the dependent variable and x_1 , x_2 and x_3 are the explanatory variables (air temperature, shortwave radiation and topographic index, respectively). The R^2 values are given in parenthesis after each equation.	108
Table B.5 Normalized sensitivity of T, ET, NPP and LAI to air temperature, shortwave radiation and topographic index for transpiration (T), net primary production (NPP) and leaf area index (LAI) along the altitudinal gradient in the Kleine Emme catchment. The values in the table represent the respective partial derivative (equation 3.2).	108
Table B.6 Normalized sensitivity of T, ET, NPP and LAI to air temperature, shortwave radiation and topographic index for transpiration (T), net primary production (NPP) and leaf area index (LAI) along the altitudinal gradient in the dry grassland numerical experiment. The values in the table represent the respective partial derivative (equation 3.2).....	109
Table C.1 Classification in the original Corine land cover product and correspondence with the classification used in this study. The contribution of each class to the total domain is shown. Original classes covering less than 0.005% of the pan-Alpine domain are omitted.....	127
Table C.2 List of meteorological stations that were used for disaggregating daily precipitation provided by the Alpine precipitation to hourly values. The stations are presented in alphabetical order for each country, along with the ETRS coordinates and the online source, when available. The asterisk denotes stations that were also used for the computation of radiation input.	127
Table C.3 List of the discharge measurement stations that were used for validation.	129
Table C.4 List of stations with daily snow depth measurements used for validation.	133
Table C.5 List of online data sources.	142

Introduction

1.1 MOTIVATION

ἀλλὰ Θαλῆς μὲν ὁ τῆς τοιαύτης ἀρχηγὸς φιλοσοφίας ὕδωρ φησὶν τὴν ἀρχὴν εἶναι

Thales, the founder of this school of philosophy, says the permanent entity is water

Aristotle, *Metaphysics*, 983b, 20-21

The profound necessity of water for every form of life and the natural hazards that are associated with it render the understanding of the water cycle crucial for the humanity. Climate being in an ever-changing state, it is unavoidable that the water cycle is also under perpetual movement. Historically, sudden changes in the water cycle have often been devastating enough to trigger the demise of civilisations (e.g., Evans et al., 2018; Stager, Ryves, Chase, & Pausata, 2011). Although humanity has become more resilient to climatic variability in recent times, we now realize that predicting water resources dynamics in the era of climate change is more than ever important (Fan et al., 2019; Montanari et al., 2013).

To better understand the water cycle and its interactions with environmental changes, hydrologists combine observations and models. Measurements of water (e.g., precipitation, streamflow, evaporation) and energy fluxes (e.g., latent and sensible heat) are necessary, but they do not suffice to provide a deep understanding of the underlying mechanisms, because the physical laws that shape the water cycle act at multiple spatiotemporal scales that are practically impossible to monitor in a comprehensive way. This renders numerical models necessary tools to explore the water cycle. The cornerstone of hydrological models is the conservation of mass, which implies that precipitation (in liquid or solid phase over the land surface) is partitioned to changes in water storage and water losses through evapotranspiration, surface and subsurface runoff and deep drainage.

Each of the components of the water budget inserts a layer of uncertainty in hydrological modelling, but what is particularly interesting and challenging is evapotranspiration, because it links the water and the energy budgets, triggering a domino of effects and feedbacks between the land surface and the atmosphere. This link emerges because of the latent heat of vaporization, i.e. the heat flux from the Earth's surface to the atmosphere that is associated with evaporation or transpiration at the surface and the subsequent condensation of water vapour in the atmosphere.

The biggest component of land evapotranspiration is plant transpiration (Good, Noone, & Bowen, 2015). Thousands of tiny pores on every leaf, the so-called stomata, open and close to serve the needs of the plants in carbon (Berry, Beerling, & Franks, 2010; Hetherington & Woodward, 2003). Through

the stomata, an astonishing amount of water leaves the surface of the earth, equivalent to roughly 40% of precipitation falling on the land surface (Fatichi, Pappas, & Ivanov, 2016). Modelling transpiration is an important challenge, because parameterizing the energy and water needs of plants is complicated. Model attempts include simplified equations based on meteorological variables and land-surface attributes (e.g., Penman, 1948; Priestley & Taylor, 1972), biochemical models (e.g., Ball, Wood, & Berry, 1987; Buckley, Mott, & Farquhar, 2003; Farquhar, von Caemmerer, & Berry, 1980) and optimization theories (e.g., Manzoni, Vico, Palmroth, Porporato, & Katul, 2013; A. Wolf, Anderegg, & Pacala, 2016).

The links between vegetation and hydrology were recognized long ago (e.g., Bonell, 2002 and references therein), but the term “ecohydrology” first appeared only in the 90s (Wassen & Grootjans, 1996). In the last twenty years, ecohydrology has become an independent research field with numerous applications and model developments (Fatichi, Pappas, et al., 2016 and references therein). These are physically-based models, which simulate processes related to vegetation, such as stomata functioning, root controls, plant hydraulics, phenology, stand dynamics. Such models have shed light on the interactions between vegetation and hydrology, and help us also to evaluate the importance of plants for climate itself, through complicated land surface-atmosphere feedbacks (e.g., Arneth et al., 2010). Modelling studies have also investigated the sensitivity of ecosystems to climate change, by quantifying, for example, the different effects on transpiration and net primary productivity (e.g., Tague et al., 2009). In general, many studies have focused on semi-arid ecosystems (e.g., Ivanov, Bras, & Vivoni, 2008a; Tague, McDowell, & Allen, 2013; Vivoni, Rodríguez, & Watts, 2010), but there is also increasing evidence that other less water-limited ecosystems, such as the European Alps, are sensitive to climate change (e.g., Bertoldi et al., 2010; Della Chiesa et al., 2014; Zierl, Bugmann, & Tague, 2007).

Ecohydrological models have proven to be particularly useful for understanding the water cycle where both its importance and complexity peak: in mountainous areas. Mountains are referred to as the water towers for humanity (Viviroli, Messerli, Meybeck, & Weingartner, 2007; Viviroli & Weingartner, 2004), because they supply roughly half of the world’s rivers (Beniston, 2003) and more than four billion people worldwide with fresh water (Vörösmarty, Lévêque, & Revenga, 2005). The profound difficulties inherent in mountain hydrology were detected long ago; Klemeš (1987) stated that modelling of mountain hydrology is the ultimate challenge, because the observations of the state of nature in mountains are very difficult and the involved processes are far beyond our theoretical understanding (e.g., spatially variable soil texture, soil depth and vegetation). More than 30 years later, monitoring networks remain sparse, even in the best-monitored mountains, which creates uncertainty in the meteorological forcing (Elsner et al., 2014) and several processes are still not well understood. For instance, some snow-related processes, such as sublimation, remain poorly constrained (e.g., Strasser, Bernhardt, Weber, Liston, & Mauser, 2008), while lateral redistribution of water and topographic shading (both known to be of paramount importance for the water cycle) are still ignored by most Earth system models (Fan et al., 2019).

Mountains are particularly vulnerable to climate change (Goulden & Bales, 2014; Immerzeel, van Beek, & Bierkens, 2010), because as temperature rises, glaciers melt, snow cover is reduced and

precipitation regimes shift (e.g., Barnett, Adam, & Lettenmaier, 2005; Beniston, Farinotti, Stoffel, Andreassen, Coppola, Eckert, et al., 2018). In addition, the increase in atmospheric CO₂ concentrations impacts the water cycle, by increasing the water use efficiency of vegetation, although the exact biochemical mechanisms remain unclear (Ma, Baldocchi, Mambelli, & Dawson, 2011) and the magnitude of this effect is spatially variable (Keenan et al., 2013). The hydrological impact of these climatic changes has already been profound and is projected to intensify (Samaniego et al., 2018). It is thus crucial to better understand mountain hydrology in order to assess the effects of climate change worldwide (Viviroli et al., 2011). Indeed, mountains are the target of an increasing number of studies (e.g., Rössler, Dieckkrüger, & Löffler, 2012; Tague, Heyn, & Christensen, 2009) that have to face several challenges, that arise from the aforementioned complexities. For instance, interpolating meteorological station data (Frei, 2014) or downscaling from the synoptic to the regional scale (Addor, Rohrer, Furrer, & Seibert, 2016) create biases that propagate through water balance simulations affecting the results. Thus, improving the meteorological forcing of models is an active research field (e.g., Ko, Mascaro, & Vivoni, 2018). Obtaining reliable data for soil and vegetation cover in complex terrain is challenging, although high-resolution datasets have been recently released (e.g., Hengl et al., 2014); this is particularly important, as the effects of changes in vegetation may be comparable to those of climate change (Duethmann & Blöschl, 2018; Köplin, Schädler, Viviroli, & Weingartner, 2013).

Indeed, vegetation is the cornerstone of the coupling between the land surface and the atmosphere and between water and carbon cycles and represents a large source of uncertainty for understanding the water cycle vulnerability to climate change (Teuling et al., 2010). The biogeophysical functioning of vegetation is changing, which provides indirect feedbacks, through changes in stomatal conductance, leaf area index, and species composition. For instance, decreased stomatal conductance due to the increased atmospheric CO₂ reduces evapotranspiration and reinforces warming (Bonan, 2008). Recent research has found that physiological effects (e.g., changes in leaf area index) due to increased atmospheric CO₂ can have a more important impact on the water cycle compared with the direct effects of changes in precipitation and radiative forcing (Lemordant, Gentine, Swann, Cook, & Scheff, 2018). Vegetation sensitivity to climate change is also linked to changes in the disturbance regimes, which can have major implications for the water cycle. For instance, fire frequency is increasing in many forested mountains worldwide (Dupire, Curt, & Bigot, 2017; Tague, Seaby, & Hope, 2009), but only recent modelling attempts take disturbances into account (e.g., Hanan et al., 2018). Given these complexities, detailed analyses with high spatial resolution are warranted for a more reliable estimation of the ecosystem responses to climate change and the effects on the water cycle (Fan et al., 2019).

1.2 RESEARCH QUESTIONS

This thesis summarizes the research done under the project ALPHSENS (A pan-Alpine high-resolution carbon and water budget and its sensitivity to climate changes). The research aim of this project is to obtain a comprehensive understanding of the water and carbon cycle over the entire Alpine region and quantify their sensitivity to climate change combining newly available datasets and state-of-the-art ecohydrological modelling. Given the large uncertainties in simulating forests'

responses to environmental changes (and since this area is largely forested) the focus of the research was initially on forests in general, with the aim to improve model parameterization. Subsequently, my research focused on the Alps; at first, I investigated the role of vegetation and climate in shaping the sensitivity of several ecohydrological processes to environmental forcing in different Alpine locations with contrasting vegetation and climate. Finally, I set up high-resolution, massively parallel, pan-Alpine ecohydrological simulations to quantify the different water budget components and their sensitivity to climate change, with a focus on droughts.

1.2.1 How are ecohydrological models able to capture the response of forests to increasing CO₂?

Here, as already mentioned, the focus is on ecohydrological modelling. Ecohydrological models remain far from complete. Mechanistic knowledge and parameterization to describe several biochemical and ecological processes related to the water and carbon cycles are still debated (e.g., phenological thresholds), while for other processes we either have limited data (e.g., biophysical responses to drought) or models that do not reflect the current knowledge (e.g., plant hydraulics, Venturas, Sperry, & Hacke, 2017). Upscaling stomata responses from the leaf to the plant and further to the stand or larger scales is also complicated (Jarvis & McNaughton, 1986) and remains a field of active research despite several achievements (e.g., Ding, Kang, Du, Hao, & Zhang, 2014). Additionally, environmental variables affect several plant physiological processes in various ways, which are often difficult to understand and simulate; for example, higher temperatures may increase respiration rates (Ryan, 1991) and photosynthesis, by relaxing the energy limitations (Boisvenue & Running, 2006). Changes in soil water and in atmospheric vapour pressure deficit are also an increasingly important control on the functioning of terrestrial ecosystems (Novick et al., 2016).

In Chapter 2, I examine the effects of increasing atmospheric CO₂ ([CO₂]) on ecosystem functioning. Increasing [CO₂] creates a very important source of uncertainties about simulating water and carbon cycles, which lies actually on the link between these two cycles. Recent studies have found that the water use efficiency (WUE, which expresses the ratio of the amount of carbon assimilated by a plant over the amount of water it transpires, Beer et al., 2009) is changing. In order to assimilate carbon, plants inevitably lose water (Berry et al., 2010). Plants regulate stomatal aperture and photosynthesis so that the ratio between intercellular and atmospheric [CO₂] remains roughly constant in time (Ainsworth & Long, 2005; Drake, Gonzalez-Meler, & Long, 1997; Leonardi et al., 2012; Morison, 1985; Peñuelas, Canadell, & Ogaya, 2011; Saurer, Siegwolf, & Schweingruber, 2004). Thus, the intrinsic water use efficiency (the ratio between carbon assimilation and stomatal conductance, Beer et al., 2009) should increase at ~0.5% yr⁻¹ in the last decades on the assumption of a linear scaling with [CO₂]. By analogy, ecosystem inherent water use efficiency should also scale with [CO₂] if the canopy is well coupled with the atmosphere (Beer et al., 2009; De Kauwe et al., 2013; Medlyn & De Kauwe, 2013). However, data from many forests show that the increase in WUE exceeded the theoretical expectations in the last two decades and many studies attempted to explain this phenomenon (e.g., Keenan et al., 2013) with conflicting findings. Some researchers examined meteorological forcing such as changes in wind and vapour pressure deficit (Novick et al., 2016;

Schymanski & Or, 2015) or even interactions between climate covariates (Leonardi et al., 2012) as possible triggers of the increase in WUE.

Other studies tried to link the observed WUE increase with a possible co-occurrence of synergistic effects of several factors beyond climatic variables (e.g., J.-G. Huang, Bergeron, Denneler, Berninger, & Tardif, 2007). Changes in climatic variables seem to be capable of triggering plasticity in key physiological traits (Aubin et al., 2016; S. J. Franks, Sim, & Weis, 2007; Galmés et al., 2014; Nicotra et al., 2010; Valladares, Gianoli, & Gómez, 2007), but until recently, plasticity had not been examined as a possible reason behind the increase in WUE (Knauer et al., 2017). The study presented in Chapter 2 is based on the hypothesis that subtle trends in key physiological parameters could explain the unexpected increase in WUE in forest sites in Europe and North America. These temporal variations in model parameters do not necessarily express plasticity at the leaf or plant scale, but they may imply subtle changes in species composition, which has occurred in some of the examined sites (e.g., Hardiman et al., 2013; Urbanski et al., 2007). In this study, I used the mechanistic ecohydrological model Tethys-Chloris (T&C; extensively validated in various ecosystems worldwide, see Appendix C.1) to test this hypothesis through numerical experiments, aiming at providing novel ways of parameterizing ecohydrological models.

1.2.2 What is the role of temperature, radiation and soil water for Alpine ecohydrology?

The Alps extend across seven countries in central Europe and are a particularly interesting case study for mountain ecohydrology, not only because they constitute the water tower of Europe (Viviroli et al., 2007), but also because they are the best-monitored mountainous area in terms of hydrometeorological variables (Beniston, 2006). Understanding the pan-Alpine water cycle and its vulnerability to climate change is necessary in order to answer questions regarding the fresh water and energy supply for millions of people (European Environment Agency (EEA), 2009), tourism (Elsasser & Bürki, 2002; Rixen et al., 2011), forestry (Lexer et al., 2001), agriculture (Perroud & Bader, 2013) and river navigation (Middelkoop et al., 2001).

Climate change impacts on the Alpine ecohydrology are already apparent: temperature increases faster than the global average (e.g., Brunetti et al., 2009), humidity decreases especially in spring (e.g., Fatichi, Molnar, Mastrotheodoros, & Burlando, 2015) and evapotranspiration generally increases (e.g., Duethmann & Blöschl, 2018). Snow cover duration is reduced and glaciers have retreated (Beniston et al., 2018), while droughts have intensified (Timofeeva et al., 2017). These changes have triggered a domino of effects that are spatially highly heterogeneous. For example, in the drier parts of the Alps, droughts are associated with higher tree mortality and more frequent wildfires (Dupire et al., 2017; Rebetez & Dobbertin, 2004), whereas in north pre-Alpine hills extreme droughts have enhanced vegetation activity (Seneviratne et al., 2012). The contrasting responses of the Alpine ecosystems to climate change reflect the very high spatial variability of this area. The complex terrain and the position of the Alps in the confluence of different atmospheric influences create steep climatic gradients (Beniston, 2006), which implies that despite the dense network of meteorological stations, our knowledge about the micro- and mesoscale spatial variability in the

Alpine climate and hydrology is incomplete. Soil and land cover are also highly heterogeneous, and although new products have become available (e.g., Hengl et al., 2014) the uncertainties remain large.

Detailed ecohydrological studies have examined the Alpine ecohydrology in the recent years. However, most of these studies have typically focused on small-scale case studies with special local features (often well-monitored hillslopes or experimental catchments, e.g., Bertoldi et al., 2010; Della Chiesa et al., 2014; Rössler et al., 2012; Zierl et al., 2007). Given the high spatial heterogeneity of the ecosystem responses, conclusions from these studies are not generalizable to larger areas. Thus, quantifying the sensitivity of ecohydrological fluxes to environmental forcing (e.g., temperature, precipitation, and incoming shortwave radiation) and the role of different land cover (e.g., grasslands and forests respond in different ways, as pointed by the aforementioned studies), soil types and climate remain open scientific questions.

Although overall the European Alps receive considerable precipitation throughout the entire year, in the dry inner-Alpine valleys long dry periods and low annual precipitation (~500 mm) imply that the ecosystems might be sporadically (in space and/or time) water-limited. Identifying these ecosystems is particularly interesting: for instance, water limitations cause species compositions to shift (e.g. Rigling et al., 2013), which might have important implications for ecosystem services and the water cycle in general. Moreover, the way ecosystems will respond to climate change depends on the extent to which initial vegetation is water-limited or temperature-limited (Tague, Heyn, et al., 2009). Variations in topography pose another impediment in our understanding of the water resources vulnerability to climate change. Previous research has shown that in areas where snowmelt is an important fraction of the water cycle, hillslope aspect can affect ecosystem functioning (Tague & Peng, 2013; Williams, McNamara, & Chandler, 2009). Since a large part of the Alps is covered by snow during a considerable fraction of the year, understanding the effect of slope orientation on ecohydrological processes is important.

Chapter 3 addresses these open questions with the ecohydrological model T&C. This model is suitable for investigating the water cycle in complex terrain, because it simulates key processes, such as lateral soil water move and feedbacks between soil water and ET, which are often omitted by Earth System models. The first case study is a wet pre-Alpine catchment, which is typical of a large fraction of the European Alps. Multiple simulations were also performed with T&C on a synthetic domain with two different uniform vegetation covers (i.e., grassland and evergreen forest) and for two contrasting Alpine climatic regimes (i.e., wet pre-Alpine and dry inner-Alpine), to disentangle the roles of climate and vegetation. The design of the virtual topography of this synthetic domain also permitted the investigation of the role of catchment orientation (through the alteration of the amount of the incoming shortwave radiation) on ecohydrological processes. Through this analysis, I specifically addressed the following questions: (a) How will forests and grasslands respond to changes in meteorological variables in climatically contrasting Alpine areas? (b) Which areas are water-limited and thus prone to droughts and which areas are energy-limited? (c) What is the role of catchment orientation in controlling ecohydrological processes? (d) How does the spatial variability of ecohydrological variables change across spatial scales?

1.2.3 What is the sensitivity of the pan-Alpine water budget to changes in temperature and precipitation?

Studying the pan-Alpine water budget is particularly important for the European water resources, because the Alps, considering their small size, contribute a disproportionately large amount of water, especially during summer, to four major European rivers (Weingartner & Viviroli, 2007), in the basins of which reside roughly 170 million people (European Environment Agency (EEA), 2009). The droughts of 2003, 2010, 2015 and 2018 showed that the European water budget is sensitive to climate change, and water resource management needs to adapt (European Environment Agency (EEA), 2009; Teuling, 2018). These droughts indeed affected more than 17% of the European population (European Commission, 2007) with an annual economic impact exceeding USD 6.8 billion between 2001 and 2006 and there is consensus that such climatic extreme events will become more frequent (Barnett et al., 2005; Beniston, 2012; Gobiet et al., 2014; Samaniego et al., 2018). The way vegetation responded during these droughts was investigated by previous studies, which showed that some forests and grasslands benefited by the increased radiation and the higher temperatures during these heatwaves (Leuzinger, Zotz, Asshoff, & Korner, 2005; Seneviratne et al., 2012; Jolly et al., 2005); this led to a quicker depletion of soil moisture (“drought paradox”, Teuling et al., 2013). This feedback might have implications for the water cycle, but the responses of ecosystems to heatwaves at the pan-Alpine scale remain unclear.

Given the unsuitability of small-scale studies for predicting changes in the water cycle over the entire Alpine domain (as explained in the previous section), larger-scale approaches are a useful tool to explore the European water budget under climate change (e.g., Orth & Destouni, 2018; Zhu et al., 2016). However, datasets typically used in such studies are too coarse to encapsulate the effects of microclimate and spatial heterogeneity in land surface characteristics. Moreover, land-surface models often represent the links between soil moisture and transpiration in a simplistic way (Seneviratne, Lüthi, Litschi, & Schär, 2006; Sheffield, Wood, & Roderick, 2012; Teuling, 2018). They also rarely resolve the land-surface energy and water fluxes at sufficient resolutions to account for local topographic and microclimatic effects and they often ignore lateral water transfer (Bierkens et al., 2015; Fan et al., 2019; Rouholahnejad Freund & Kirchner, 2017; Viviroli et al., 2011; Wood et al., 2011). Such simplifications may impact model predictions at both water- and energy-limited conditions (Fan et al., 2019) but hyper-resolution approaches can provide more realistic alternatives (Bierkens et al., 2015; Potter, Arthur Woods, & Pincebourde, 2013; Wood et al., 2011). Thus, recently, many studies aim at high-resolution modelling of mountainous areas (e.g., Rössler et al., 2012; Vicente-Serrano et al., 2015), but usually their domains are too small to infer about climate change impacts at scales relevant for water resource management (Fan et al., 2019).

In this part of my research, I bridge this gap between detailed small-scale analyses and coarse/simplified large-scale simulations, by applying the mechanistic ecohydrological model T&C at the pan-Alpine scale and at a very high spatiotemporal resolution to shed light on the water towers of Europe and provide insights into the pan-Alpine water budget (Chapter 4). The very high spatial resolution of this study also provides the necessary background to capture the small-scale topographic, vegetation and microclimatic heterogeneities in much more detail than any other previous study of

this area at that scale, which is important for a realistic representation of the water cycle (Fan et al., 2019). However, due to computational limitations long-term dynamics associated with changes in WUE or forest demography (e.g., Chapter 2) could not be fully addressed. To drive and test T&C at the pan-Alpine scale, I selected meteorological, discharge and snow depth measurements from 1212 stations and combined them with distributed products of meteorological variables, soil texture and land cover (Dee et al., 2011; European Environment Agency, 2006; Hall & Riggs, 2016; Isotta et al., 2014; Panagos, Van Liedekerke, Jones, & Montanarella, 2012). I performed massively parallel simulations (6.1×10^5 CPU hours) at an unprecedented high resolution (250 m grid) for the entire Alpine region ($257,000 \text{ km}^2 - 4.12$ million pixels) for three years, including a very wet and a very dry year (2001 and 2003, respectively). Analysing the data and the model output, I partitioned the pan-Alpine water budget into blue and green water fluxes (runoff and evapotranspiration, respectively), I quantified the sensitivity of each component to precipitation and air temperature therefore assessing the elasticity of the Alpine water budget in space and time. This allows evaluating the impact of climate change on the Alpine hydrology. The final part of this analysis was the quantification of the relative contribution of increased ET on runoff deficits compared with precipitation during the 2003 heatwave.

Linking plant functional trait plasticity and the large increase in forest water use efficiency

Abstract

Elevated atmospheric CO₂ concentrations are expected to enhance photosynthesis and reduce stomatal conductance, thus increasing plant water use efficiency. A recent study based on eddy covariance flux observations from Northern Hemisphere forests showed a large increase in inherent water use efficiency (IWUE). Here we used an updated version of the same data set and robust uncertainty quantification to revisit these contemporary IWUE trends. We tested the hypothesis that the observed IWUE increase could be attributed to interannual trends in plant functional traits, potentially triggered by environmental change. We found that IWUE increased by $\sim 1.3\% \text{ yr}^{-1}$, which is less than previously reported but still larger than theoretical expectations. Numerical simulations with the Tethys-Chloris ecosystem model using temporally static plant functional traits cannot explain this increase. Simulations with plant functional trait plasticity, i.e., temporal changes in model parameters such as specific leaf area and maximum Rubisco capacity, match the observed trends in IWUE. Our results show that trends in plant functional traits, equal to $1.0\% \text{ yr}^{-1}$, can explain the observed IWUE trends. Thus, at decadal or longer time scales, trait plasticity could potentially influence forest water, carbon, and energy fluxes with profound implications for both the monitoring of temporal changes in plant functional traits and their representation in Earth system models.¹

Mastrotheodoros, T., Pappas, C., Molnar, P., Burlando, P., Keenan, T. F., Gentine, P., Gough C. M., Fatichi, S. (2017). Linking plant functional trait plasticity and the large increase in forest water use efficiency. *Journal of Geophysical Research: Biogeosciences*, 122(9), 2393–2408. <https://doi.org/10.1002/2017JG003890>

2.1 INTRODUCTION

During the last two decades, the atmospheric CO₂ concentration ([CO₂]) has been increasing at a rate of 2 ppm yr⁻¹, corresponding to ~0.5% yr⁻¹ (Francey et al., 2013). The effects of increasing [CO₂] on plant physiology at the leaf scale are well documented: at elevated [CO₂], stomatal conductance tends to be lower than in ambient [CO₂] in most plant species, and photosynthesis rates increase for C₃ plants in the absence of other limiting factors (Ainsworth & Rogers, 2007; Long, Ainsworth, Rogers, & Ort, 2004; Wullschleger, Tschaplinski, & Norby, 2002). Plants tend to regulate stomatal aperture and photosynthesis so that the ratio between intercellular and atmospheric [CO₂] (C_i:C_a) remains relatively constant (Ainsworth & Long, 2005; Drake et al., 1997; Katul, Manzonni, Palmroth, & Oren, 2010; Leonardi et al., 2012; Morison & Gifford, 1984; Peñuelas et al., 2011; Saurer et al., 2004). This implies that intrinsic water use efficiency (iWUE, the ratio between carbon assimilation and stomatal conductance; see Appendix A.1, Beer et al., 2009) should scale linearly with [CO₂], thus increasing at ~0.5% yr⁻¹ in the last 20 years (Appendix A.1). By analogy, ecosystem inherent water use efficiency (IWUE, the ecosystem-scale version of iWUE; see Appendix A.1) should also scale with atmospheric [CO₂] if ecosystem C_i:C_a is constant (Medlyn & De Kauwe, 2013) and the canopy is well coupled with the atmosphere (Beer et al., 2009; De Kauwe et al., 2013). The rate of increase in IWUE with constant C_i:C_a is called hereafter the “expected” rate of increase.

Elevated [CO₂] affects plant functioning through various physiological mechanisms that go beyond the leaf scale (Ainsworth & Long, 2005; Cao, Bala, Caldeira, Nemani, & Ban-Weiss, 2010; Gedney et al., 2006; Leakey et al., 2009; Wullschleger, Gunderson, Hanson, Wilson, & Norby, 2002). Upscaling leaf-level responses to increased [CO₂] at the ecosystem-level remains challenging (Faticchi et al., 2016; Field, Jackson, & Mooney, 1995; Knauer et al., 2017; Koutavas, 2013; Leuzinger et al., 2011; Nelson et al., 2004; Way, Oren, & Kroner, 2015), and accounting for interactions between environmental covariates and vegetation dynamics is even more complex (J.-G. Huang et al., 2007; Leonardi et al., 2012). Remote sensing observations provide spatial patterns of water use efficiency (WUE) trends; global trends vary on the order of -0.3 to +0.2% yr⁻¹ over the last 15 years (M. Huang et al., 2015; Tang et al., 2014; Xue et al., 2015). Estimates based on the isotope content of tree rings suggest that iWUE increased by 0.1% yr⁻¹ between 1850 and 2000 (Leonardi et al., 2012) 0.1–0.3% yr⁻¹ over the last century (Frank et al., 2015; Peñuelas et al., 2011; Saurer et al., 2004; van der Sleen et al., 2015), and more rapidly (up to 0.7% yr⁻¹) during the last 40 years (Maseyk, Hemming, Angert, Leavitt, & Yakir, 2011; Silva & Anand, 2013). A recent study combined tree ring, eddy covariance, and atmospheric observations and reported an overall increase of 0.4% yr⁻¹ between 1900 and 2010 (Dekker, Groenendijk, Booth, Huntingford, & Cox, 2016). Model analyses also report iWUE increases on the order of 0.2–0.3% yr⁻¹ for the 21st century (M. Huang et al., 2015; Ito & Inatomi, 2012).

Trends in IWUE can also be estimated using eddy covariance observations of carbon, water, and energy fluxes between the land surface and the atmosphere (Keenan et al., 2013; S. Zhou, Yu, Huang, & Wang, 2015). However, these data sets are restricted to relatively short periods and are subjected to measurement and methodological uncertainties. Gross ecosystem production (GEP) is not a direct observation (Reichstein et al., 2005), and it might be overestimated due to the eddy covariance flux

partitioning algorithms (Wehr et al., 2016; Wohlfahrt & Gu, 2015). Transpiration is also not directly measured but is inferred from latent heat estimates which are uncertain because of the lack of energy budget closure (Leuning, van Gorsel, Massman, & Isaac, 2012) and relatively frequent data gaps. Latent heat includes not only transpiration but also other evaporation fluxes, and partitioning between canopy interception, soil evaporation, and transpiration is also uncertain (Fatichi & Pappas, 2017; Miralles et al., 2015; Van Dijk et al., 2015). Despite these limitations, eddy covariance observations have provided important insights into IWUE trends. Using eddy covariance observations, Keenan et al. (2013) detected an unexpectedly large increase ($2.3\% \text{ yr}^{-1}$) in contemporary IWUE across forest sites in the Northern Hemisphere. This increase is more than five times larger than expected from assumptions of constant $C_i:C_a$, from Free-Air Carbon dioxide Enrichment experiments (FACE) and from laboratory experiments (Medlyn & De Kauwe, 2013). The authors found that this increase is consistent with a strong CO_2 fertilization effect, suggesting that stomata partially close to maintain a near-constant C_i . An open question remains, however, as to what mechanisms explain this larger-than-expected IWUE increase.

Environmental changes, such as the increasing atmospheric $[\text{CO}_2]$, are potential drivers of plasticity in plant functional traits that link plant physiology and the carbon cycle (Aubin et al., 2016; S. J. Franks et al., 2007; Galmés et al., 2014; Nicotra et al., 2010; Valladares et al., 2007). A recent study by Knauer et al. (2017) tested with numerical simulations whether an increase in the stomatal conductance sensitivity to $[\text{CO}_2]$ would be a plausible explanation for the observed IWUE increase. To reproduce the IWUE trends showed by Keenan et al. (2013), the authors imposed a $-2.1\% \text{ yr}^{-1}$ trend on the model parameter linking stomatal conductance and net assimilation and found that the simulated trends in evapotranspiration and gross ecosystem productivity are incompatible with both local- and global-scale observed trends in evapotranspiration, discharge, and atmospheric $[\text{CO}_2]$ seasonal amplitude. Thus, they concluded that variables beyond $[\text{CO}_2]$ might have triggered the observed changes in IWUE and that IWUE trends of such magnitude are not a large-scale phenomenon. Other studies have investigated the interactions between WUE and meteorological forcing, such as wind (Schymanski & Or, 2015) or solar radiation (McAusland et al., 2016). Studies across Europe and the U.S. found that ecosystem IWUE is also sensitive to the vapour pressure deficit (VPD) (Frank et al., 2015; Novick et al., 2015), while low soil moisture availability may offset the positive effect of increasing $[\text{CO}_2]$ in the IWUE (De Kauwe et al., 2013).

Instead of linking changes in meteorological variables to trends in WUE, some researchers attributed the observed WUE increase to complex interactions between different climate covariates (Leonardi et al., 2012) or to a possible occurrence of synergistic effects of several factors beyond changes in climate variables (J.-G. Huang et al., 2007). Possible explanations of the observed increase in WUE also include long-term metabolic shifts (Ehlers et al., 2015) or changes in stomatal density, mesophyll conductance or biochemical and molecular processes, all of which could be driven by plasticity in plant functional traits (de Boer et al., 2016; Flexas et al., 2016; P. J. Franks, W. Doheny-Adams, Britton-Harper, & Gray, 2015; Lawson & McElwain, 2016; Moore, Cheng, Sims, & Seemann, 1999; Sun et al., 2014).

Here we revised the trend estimates of IWUE for the same sites used by Keenan et al. (2013), using an updated data set and extending the period of analysis to the most recent years whenever possible. Subsequently, we tested by means of model simulations the hypothesis that plant trait plasticity driven by environmental changes could explain the observed increase in IWUE at the ecosystem scale. This hypothesis is based on recent evidence that plants can acclimate at shorter timescales than previously thought (e.g., Lammertsma et al., 2011; Ma et al., 2011). In this study, the plasticity hypothesis is tested by implementing trends in model parameters that directly affect the simulation of ecosystem processes related to IWUE (e.g., the sensitivity of stomatal conductance to $[\text{CO}_2]$, maximum photosynthetic capacity, maximum leaf-to-root ratio). These trends, affect how key physiological processes are modelled through the simulation period to mimic the observed patterns.

2.2 MATERIALS AND METHODS

2.2.1 Data Set

We analysed eddy covariance data from 20 forest sites in the Northern Hemisphere (Figure A.1 and Table A.1, Aubinet, Heinesch, & Longdoz, 2002; Berbigier, Bonnefond, & Mellmann, 2001; Carrara et al., 2003; Cook et al., 2004; Curtis et al., 2005; Davidson, Savage, Trumbore, & Borken, 2006; Dolman, Moors, & Elbers, 2002; Dunn, Barford, Wofsy, Goulden, & Daube, 2007; Goldstein et al., 2000; Gough et al., 2013; Granier et al., 2000; Grünwald & Bernhofer, 2007; Hadley & Schedlbauer, 2002; Hollinger et al., 2004; Jenkins et al., 2007; Pilegaard, Ibrom, Courtney, Hummelshøj, & Jensen, 2011; Schmid, Grimmond, Cropley, Offerle, & Su, 2000; Suni et al., 2003; Thum et al., 2007; Urbanski et al., 2007). Eddy covariance observations from the freely available gap-filled “Fluxnet 2015” database (<http://fluxnet.fluxdata.org/data/fluxnet2015-dataset/>; release July 2016, Tier 1, more details in Appendix A.2) were used when available and Ameriflux or CarboEurope databases were used for the remaining sites (Table A.1). We excluded all negative values in evapotranspiration, gross ecosystem productivity, and vapour pressure deficit (ET, GEP, and VPD, respectively) before computing IWUE. Gaps in meteorological variables used as model input (e.g., air temperature, relative humidity, wind speed, VPD, and shortwave radiation) were filled linearly or with the mean for that specific hour and day of the year. Data from the European Centre for Medium-Range

Weather Forecasts ERA-Interim data set (<http://apps.ecmwf.int/datasets/data/interim-full-daily/levtype=sfc/>) or information from local rain gauges were used to replace missing values in precipitation time series or for sites where long-term “Fluxnet” precipitation considerably deviates from climatological precipitation. Following the approach of Keenan et al. (2013), we computed the IWUE only for summer months (June–August) and daytime (shortwave radiation $> 100\text{Wm}^{-2}$). Rainy days (defined as days with daily precipitation larger than 1 mm) and 1 day after every rainy day were excluded from the analysis to minimize the influence of ground evaporation and evaporation from canopy interception. Although our analysis focuses on summer months, we used only continuous years without any long gaps (roughly longer than a month), because model simulations are conducted continuously and not only during the summer months. The resulting data set includes 20 sites with a median duration of 13 years.

2.2.2 Inherent Water Use Efficiency

WUE characterizes the ecosystem balance between assimilated carbon and transpired water and is commonly used to describe ecosystem functioning. Linking the water and carbon cycles, WUE provides insights into water resource availability and land surface-atmosphere feedback (Lemordant, Gentine, Stéfanon, Drobinski, & Fatichi, 2016; Medlyn et al., 2017). WUE can be expressed in various ways based on how the water and carbon fluxes are defined and according to the spatial (leaf, plant, or ecosystem) and temporal scales (instantaneous or averaged over a period). Either evapotranspiration or transpiration and net or gross ecosystem production can be used for computing WUE (M. Huang et al., 2015; Ito & Inatomi, 2012). Additional variations of these basic WUE definitions include the intrinsic water use efficiency (iWUE) (Battipaglia et al., 2013; Beer et al., 2009; Frank et al., 2015), the underlying water use efficiency (S. Zhou et al., 2015), and the inherent water use efficiency (IWUE) (Beer et al., 2009; Keenan et al., 2013; Vickers, Thomas, Pettijohn, Martin, & Law, 2012). Here we used the ecosystem-scale IWUE, because it scales roughly proportionally to C_a under the assumption of a constant $C_i:C_a$ (see A.1):

$$IWUE = \frac{GEP}{ET} VPD \quad (2.1)$$

where IWUE is in $\text{mgC g}^{-1} \text{H}_2\text{O hPa}$, ET is in $\text{gH}_2\text{O m}^{-2} \text{h}^{-1}$, GEP is in $\text{mgC m}^{-2} \text{h}^{-1}$, and VPD is in hPa (for a detailed description of how water and carbon fluxes are simulated in T&C, refer to Fatichi, Ivanov, & Caporali, 2012a).

For the calculation of IWUE, we used the average over the summer period of the daytime hourly ET, GEP, and VPD values. Thus, we obtain a single mean IWUE value per year and site, which is much less sensitive to very small or large ET and GEP values at the hourly scale.

2.2.3 Trend Estimation and Uncertainty

Linear regression and the nonparametric Theil-Sen (Sen, 1968) estimator were applied to quantify the slopes of observed and simulated IWUE, GEP, and ET. The dependent variables are annual IWUE, GEP, or ET, and the independent variable is the corresponding year of the time series. GEP and ET were included because IWUE is a derived quantity (computed from GEP and ET as shown in Eq. 2.1). The two methods (linear regression and the non-parametric Theil-Sen estimator) gave slopes that are highly correlated (Figure A.2). Thus, in the following, we only report results for the linear regression slopes, unless otherwise specified. Based on the normality assumption that residuals follow the Gaussian distribution, we applied t-statistics to the estimator of the slope coefficient to obtain the 95% confidence intervals of the linear slope. Uncertainties in the IWUE slope at individual sites are large (Table A.2); yet we expected that a combination of 20 sites would result in a robust estimation of the median and mean slope of the ensemble.

To quantify the uncertainties of the slope computed for the ensemble and verify its statistical robustness, we assumed that for each location the slope could be described by a uniform distribution bounded by the 95% confidence interval of the linear regression slope estimate. While a normal

distribution would be a closer approximation of the slope uncertainty at each site, we adopted the most conservative assumption of a uniform distribution in order to indirectly account for other uncertainties such as the lack of surface energy budget closure in the eddy covariance measurements (Foken, 2008; Leuning et al., 2012; Wohlfahrt & Gu, 2015). For each site, a random value was selected from the corresponding uniform distribution for each of the three variables (i.e., slope of IWUE, GEP, and ET) using a Monte Carlo sampling. In total, 10,000 values were sampled for each location and the corresponding mean and median slopes of the ensemble were computed at each time. With this procedure, we were able to quantify the overall uncertainty of the ensemble mean and median slope. In the following, we mostly refer to median rather than mean values, since the median is a better indicator for small data sets, in being less sensitive to outliers (Kenney & Keeping, 1962). Time series duration varies across sites and further complicates the analysis. Ideally, a common period should be used for all sites, but given data availability, this would lead to a very small data set. Considering that longer records are more reliable in the slope estimation and given the relatively large variability in time series length between the sites (from six to 19 years), we repeated our analysis weighting the slopes by the time series length.

2.2.4 Numerical Experiments

We used the state-of-the-art mechanistic ecosystem model Tethys-Chloris (T&C), which simulates the main components of the hydrological and carbon cycle (Fatichi, Ivanov, & Caporali, 2012b). It resolves the mass and energy budgets at the land surface and describes physiological processes including photosynthesis, phenology, carbon allocation, and tissue turnover. A detailed model description is provided in Appendix A.3, with emphasis on the components of interest in this study (Bonan et al., 2011; Farquhar et al., 1980; Krinner et al., 2005; Rutter, Kershaw, Robins, & Morton, 1971; Rutter, Morton, & Robins, 1975). The model has been extensively validated at various sites worldwide (Fatichi & Ivanov, 2014; Fatichi et al., 2012a; Fatichi, Pappas, et al., 2016; Pappas, Fatichi, & Burlando, 2016; Paschalis, Fatichi, Katul, & Ivanov, 2015).

For each of the examined sites, T&C simulations were conducted with static, site-specific parameterizations, which were tested to satisfactorily reproduce the energy and carbon fluxes and vegetation phenology through a manual calibration procedure (“base simulations”; Table A.3). Considering that VPD is rising along with $[\text{CO}_2]$ (Brzostek et al., 2014; Rigden & Salvucci, 2017) and that this may have profound impact on ecosystem functioning (Novick et al., 2016), we computed the linear trend of temperature and relative humidity based on annual mean values (Table A.4). We removed these trends from the hourly time series and repeated the simulations with the same parameterizations in order to assess the effect of trends in VPD on ecosystem response.

Subsequently, we ran the model using time-variable plant functional traits; i.e., we assumed that the parameters are not static and reflect temporal changes in plant functional traits and forest structure. For each time step, ET was calculated as the sum of transpiration and evaporation from the ground and intercepted water. GEP was calculated as gross assimilation, i.e., the sum of net assimilation and leaf maintenance respiration. Subsequently, we followed exactly the same approach we used for the

observed data. For each year, we computed an annual mean value over summer, daytime non-rainy days for GEP, ET, and VPD and we calculated the annual mean IWUE before computing the slopes.

After an initial screening of nine T&C vegetation parameters (Table A.5), the following five most sensitive parameters for estimating IWUE were chosen (Table A.6): empirical parameter linking stomatal aperture and net assimilation in the Leuning model of stomatal conductance (a_1 Leuning, 1995), top-of-the-canopy maximum Rubisco capacity at 25°C (V_{\max}), canopy nitrogen decay coefficient (K_{nit}), specific leaf area (S_{LA}), and maximum leaf-to-root biomass ratio (LtR). The latter affects model performance only when its value is reached, acting as an upper threshold. The selected parameters represent biochemical (a_1 and V_{\max}) and structural (S_{LA} and LtR) properties of the vegetation or a combination of the two (K_{nit}). Appendix A.3 provides a list of the equations in which these parameters are involved.

Table 2.1 Parameters of T&C model that were modified in the numerical experiments.

Symbol	Description	Units	Typical Range
a_1	Empirical parameter connecting stomatal aperture and net assimilation	[-]	3-11
K_{nit}	Canopy nitrogen decay coefficient	[-]	0.1-0.5
V_{\max}	Top-of-the-canopy maximum Rubisco capacity at 25°C	[$\mu\text{mol CO}_2 \text{ m}^{-2} \text{ s}^{-1}$]	20-120
S_{LA}	Specific leaf area	[$\text{m}^2 \text{ g}^{-1} \text{C}$]	0.006-0.050
LtR	Maximum leaf to root biomass ratio	[-]	0.2-1.5

After evaluating single-parameter perturbations, we also conducted the analysis by concurrently perturbing two parameters in each run (10 combinations) in order to account for parameter interactions (Pappas, Fatichi, Leuzinger, Wolf, & Burlando, 2013; Saltelli & Annoni, 2010). For each parameter, the value adopted in the base simulation (which corresponds to site-specific model calibration over the entire period) was assigned to the centre of the time series and a linear trend was imposed according to a given slope expressed as percent change per year ($\% \text{ yr}^{-1}$). The sign of the slope was chosen for each parameter so that IWUE was enhanced (see Figure A.3). It is worth emphasizing that the selected parameters are representative of the ecosystem scale. Thus, trends in vegetation parameters might be partly driven by changes in forest demography (e.g., species composition, forest structure, or both, as has happened, for example, in the US-Ha1 and US-UMB, Hardiman et al., 2013; Urbanski et al., 2007) rather than an actual trend in the plant-level functional trait itself.

For two sites (US-UMB and NL-Loo, the latter not shown) we tested several rates of parameter change in the range of 0.5–3% yr^{-1} and examined the relationship between trends in IWUE and the hypothesized trends in plant functional traits by keeping the model setup and all other parameters identical to the base simulations. We found that this relationship is almost linear for all parameters, which is expected for relatively low parameter perturbations (Figure A.3). We chose a 1% yr^{-1} rate of change in the parameters for all the numerical experiments applied over periods of up to 20 years. This value is small enough to ensure that all parameters remain well within the ranges reported in

literature (see Table 2.1) but large enough to modify considerably the ecosystem response, given the expected influence of plant trait variability in ecosystem carbon and water dynamics (Pappas et al., 2016; Wang et al., 2012). Clearly, our analysis does not suggest that this rate of change might last indefinitely. Rather our experiment is based on the simplifying hypothesis of linear trends to investigate the implications for the ecosystems at the decadal timescale. At longer timescales, such acclimation pace would potentially lead to unrealistic parameter values.

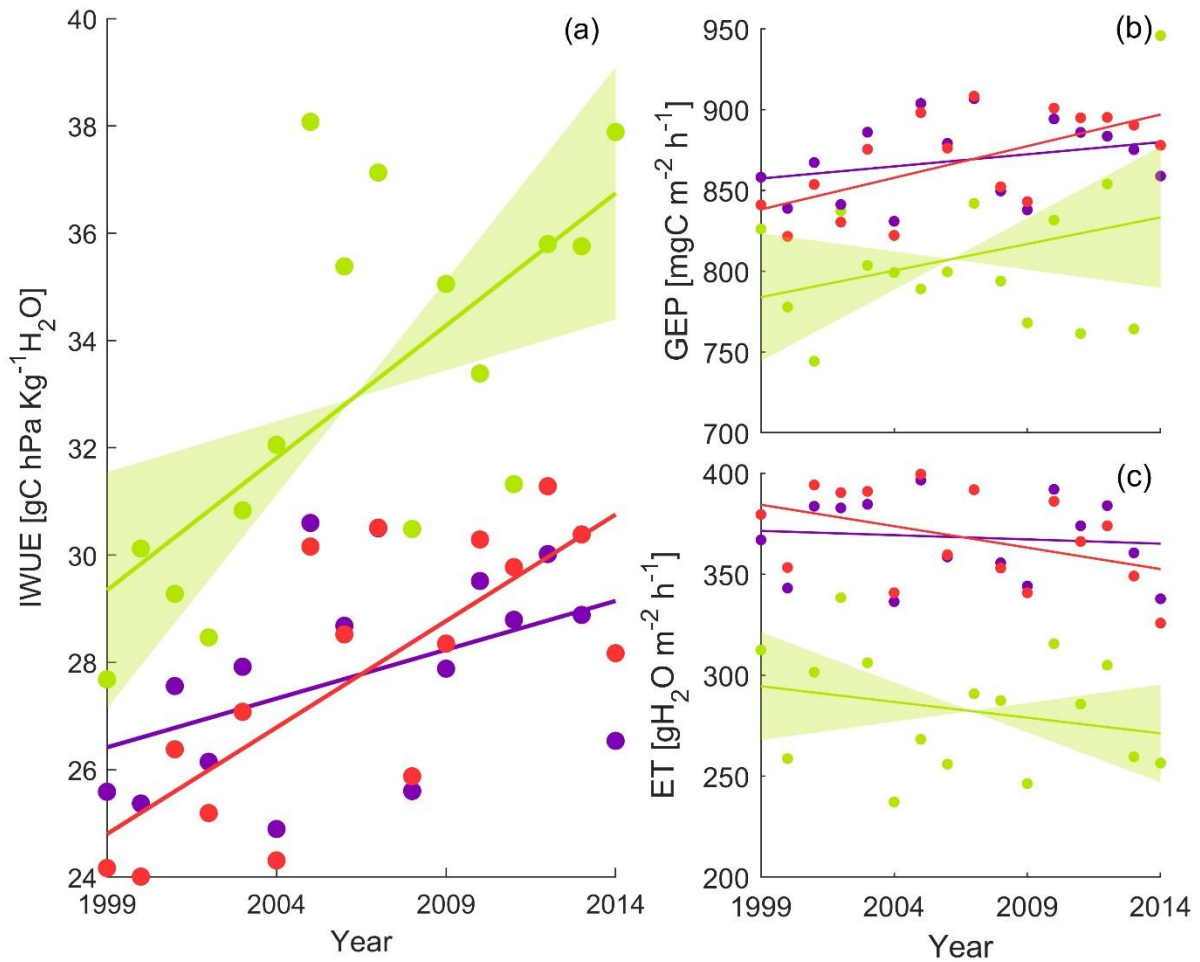


Figure 2.1 Observed (green) and simulated (purple and red) annual time series of (a) inherent water use efficiency (IWUE, computed as in Eq. 2.1, using the annual means of GEP, ET and VPD), (b) gross ecosystem production (GEP) and (c) evapotranspiration (ET) at the US-UMB site (details in Table A.1). Purple represents the base simulations and red shows the numerical experiment which best approximates each variable's slope for this site, i.e. $[+V_{\max}-a_1]$ for IWUE, $[-a_1+K_{\text{nit}}]$ for GEP and $[-a_1]$ for ET. Linear least squares fitting is shown with dashed lines. The shaded green areas show the 95% uncertainty bounds for the observed slopes in the three variables.

2.3 RESULTS

Figure 2.1 shows example time series of IWUE, GEP, and ET from observations and numerical experiments for the US-UMB site. The deviation of the simulated annual means from the observations can be mostly attributed to an underestimation of latent heat in the flux tower measurements at this

site (Schmid et al., 2000; Su, Schmid, Grimmond, Vogel, & Oliphant, 2004). The energy budget is indeed not closed in the flux tower data. Observations suggest that IWUE of the 20 sites increased on average by $1.3\% \text{ yr}^{-1}$ (equivalent to $1\% \text{ ppm}^{-1}$), due to the combination of increasing GEP ($0.6\% \text{ yr}^{-1}$) and decreasing ET ($0.3\% \text{ yr}^{-1}$) (Figure 2.2 and Table A.2 and A.6). Median slopes weighted by the time series length were of smaller magnitude, but they preserved the general pattern; in this case IWUE increased by $1.0\% \text{ yr}^{-1}$ (Table A.7). Despite the large uncertainties of the single-site slopes, the ensemble median slope of IWUE exceeded the expectations ($0.5\% \text{ yr}^{-1}$) with a probability of 95% (Figure 2.3).

Using static vegetation parameters (base simulations), the modelled IWUE increased by $0.9\% \text{ yr}^{-1}$, GEP increased by $0.2\% \text{ yr}^{-1}$, and ET also increased by $0.2\% \text{ yr}^{-1}$ (Figure 2.2 and Table A.6). Weighted median slopes differ only slightly among sites, with a simulated trend in IWUE of $0.7\% \text{ yr}^{-1}$ (Table A.7). Simulations with detrended temperature and relative humidity show a $0.4\% \text{ yr}^{-1}$ increase in IWUE (which corresponds closely to the theoretical expectations), while median GEP and ET trends only slightly differ from the base simulations (Figure 2.3 and Table A.2).

The observed IWUE trend is best reproduced by simulations with increased V_{max} or decreased a_1 alone or together with other parameters (Figure 2.2 and Table A.6 and Table A.7). In order to assess the performance of each numerical experiment regarding both IWUE and its components (GEP and ET), we computed the Euclidean distance between simulated and observed median slopes of IWUE, GEP, and ET. When all three parameters are considered together, a change in a_1 describes best the observed trends. Decreasing a_1 (alone or together with decreasing K_{mit} or increasing S_{LA} or LtR) by $1\% \text{ yr}^{-1}$ led to an increase in IWUE similar to the observed trend, mainly improving the simulated trend of ET (Figure 2.2 and Tables A.6 and A.7). Overall, differences in reproducing the observed trends among these combinations are rather small, suggesting that they can be considered practically equivalent.

The comparison of observed IWUE slopes between sites reveals different patterns across different vegetation types. Evergreen forests (10 sites) show almost no increase in IWUE ($0.1\% \text{ yr}^{-1}$), while in broadleaf deciduous forests (eight sites) IWUE increased by $3.0\% \text{ yr}^{-1}$ (Figure A.4).

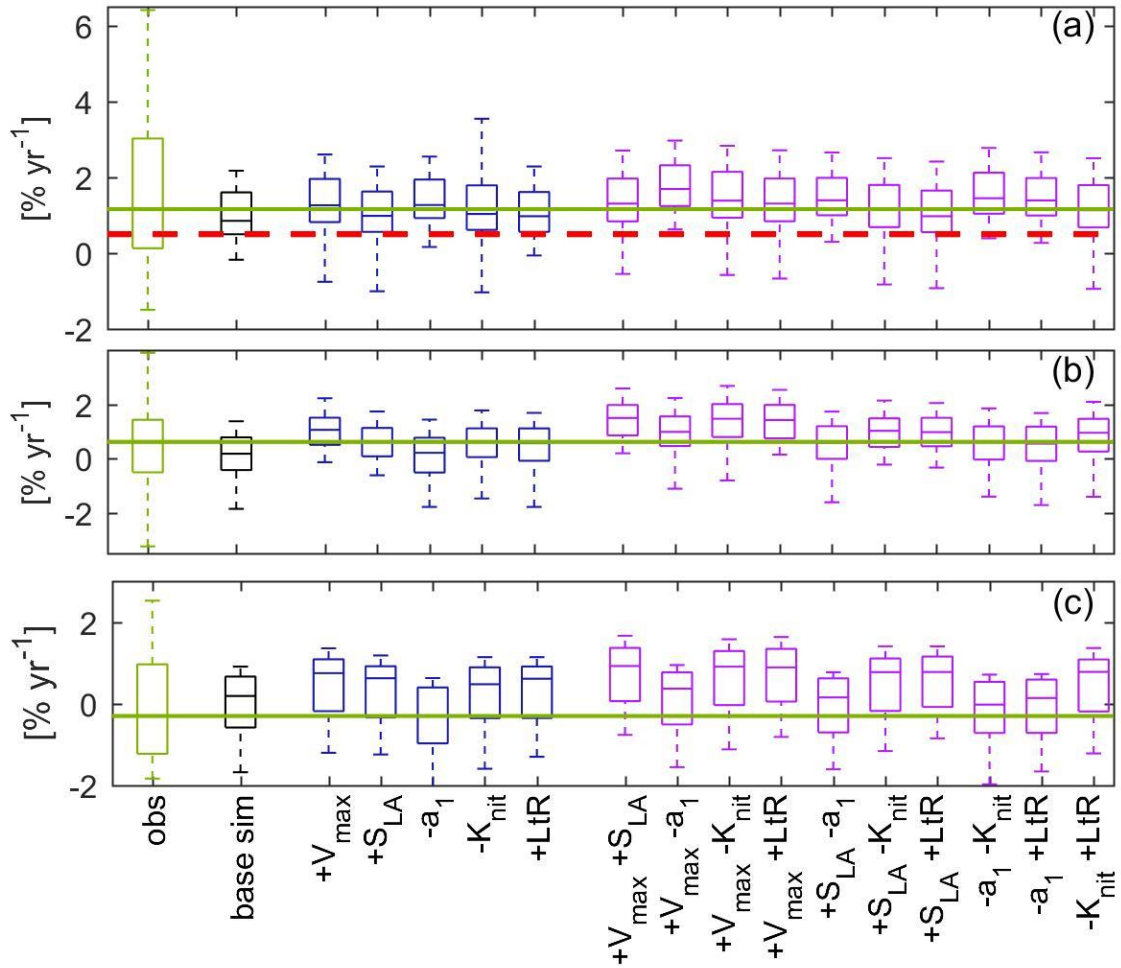


Figure 2.2 Linear slopes of (a) inherent water use efficiency (IWUE), (b) gross ecosystem production (GEP), and (c) evapotranspiration (ET) for the 20 investigated sites. The box length provides the interquartile range (I_{QR}), the bottom of the box the 25th percentile (first quartile, q_1), the top of the box the 75th percentile (third quartile, q_3), and the horizontal line within the box the median value. The lower whisker corresponds to $q_1 - 1.5I_{QR}$, or to the minimum estimate, and the upper whisker corresponds to $q_3 + 1.5I_{QR}$, or to the maximum estimate. The green represents the observations, the black stands for base simulations, the blue for the experiments in which only one parameter was perturbed, and the magenta for the experiments in which two parameters were perturbed. The red dashed line represents the expected rate of IWUE increase.

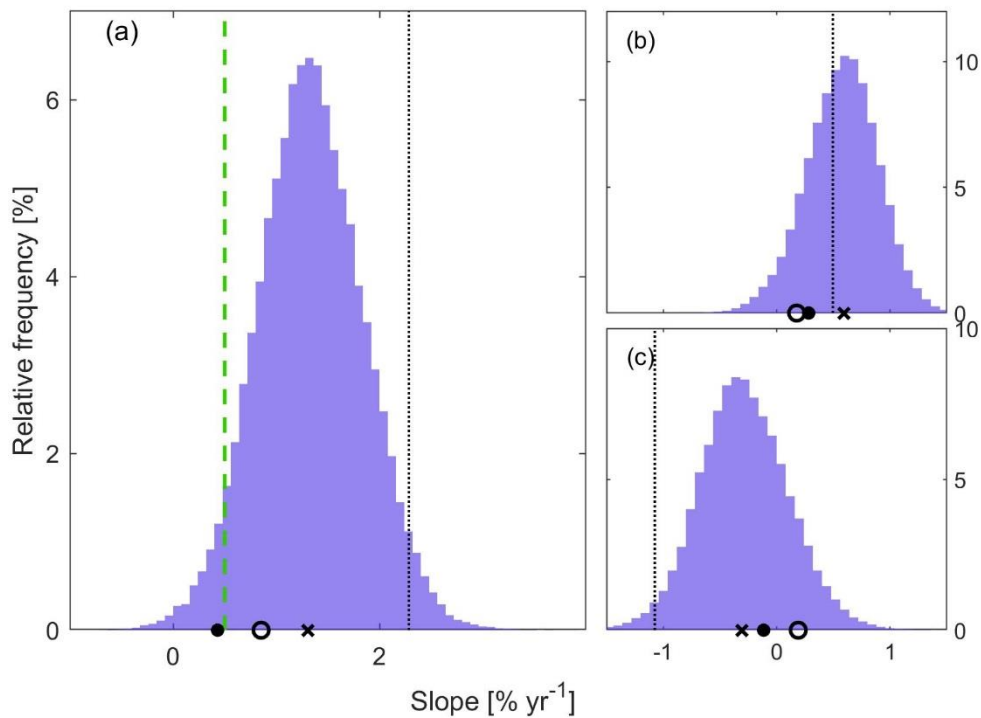


Figure 2.3 Relative frequency distributions of median slopes in (a) observed inherent water use efficiency (IWUE), (b) gross ecosystem production (GEP), and (c) evapotranspiration (ET). For each site, a slope was selected randomly from the uniform distribution that is bounded by the 95% confidence interval of the estimated linear slope. The histograms show the results of 10,000 Monte Carlo runs. The dotted lines show the median reported by Keenan et al. (2013), and the dashed green line shows the expected IWUE increase ($0.5\% \text{ yr}^{-1}$). In each subplot we show the median slopes of base T&C simulations (circles), the median slopes of base simulations with detrended temperature and relative humidity (dots), and the numerical experiment which best approximates each variable's slope (crosses), i.e., $[+V_{\max} + \text{LtR}]$ for IWUE, $[-a_1 - K_{\text{nit}}]$ for GEP, and $[a_1]$ for ET.

2.4 DISCUSSION

2.4.1 Observed Trends in IWUE

We found a median increase in IWUE of $1.3\% \text{ yr}^{-1}$ across 20 Northern Hemisphere forest sites in the last two decades. This increase more than doubles the expected increase under the assumption of a constant $C_i:C_a$ but is considerably lower than what Keenan et al. (2013) reported for the same sites ($2.3\% \text{ yr}^{-1}$).

The difference in IWUE trends found in our study compared to Keenan et al. (2013) is mostly due to recent differences in ET trends arising from the inclusion of site years not available at the time of the previous analysis. Recent droughts (e.g., in 2010 and 2012 in Europe and the U.S., respectively) may have contributed to the strong decreasing ET trend found by Keenan et al. (2013) through soil moisture limitations. Indeed, the positive trend in ET seems to be interrupted in recent years (Jung et al., 2011), but it remains unclear if this was an effect of climate variability or rather a sign of a

geographical reorganization of ET. Thus, ET trends are uncertain and the inclusion of additional data as well as shifting the analysis to more recent years may change the results (Appendix A.4).

The trends in IWUE were lower when we computed the median increase weighted by the time series length of each site. This is mainly because of reduced ET slopes, while GEP was less dependent on the time series length (Tables A.6 and A.7). The sensitivity of the slope of ET (and therefore IWUE) on the time series length further verifies that the inclusion of 30% more data in our study potentially improves the robustness of the slope estimation. It further depicts the uncertainties in latent heat observations, as indicated by the lack of energy balance closure (Foken, 2008; Leuning et al., 2012). It could also be the manifestation of feedback between the surface energy budget and the atmospheric boundary layer, where reduction in latent heat increases atmospheric evaporative demand (higher temperature and VPD) or maintains higher soil moisture, therefore preventing a persistent negative trend in latent heat (Lemordant et al., 2016). The preprocessing of eddy covariance data in the different Fluxnet products is also not identical (Figure A.5); while GEP slopes are similar in the two studies, ET slopes diverge considerably (Figure 2.3), which can partly explain the discrepancies with previous results.

The confidence in the magnitude of the trend in IWUE for any single site is particularly low (Table A.2), testifying that strong conclusions cannot be drawn from a single site or only few sites. However, combining 20 sites increases the robustness of the analysis. We verified the statistical robustness of the median change in IWUE using a Monte Carlo analysis with a very conservative assumption on the uncertainty in the single site slopes.

This analysis showed that the probability that IWUE increases more than the expected ($0.5\% \text{ yr}^{-1}$) is larger than 95% (Figure 2.3). In other words, despite the large site-to-site variability in IWUE slopes, it is very unlikely that the overall trend in IWUE can be explained by theoretical expectations of a constant $C_i:C_a$ at the ecosystem scale. In the deciduous forests the IWUE increase was larger (Figure A.4), in agreement with some previous studies (Keenan et al., 2013; Y. Liu et al., 2015; Saurer et al., 2014). This may be due to the fact that the stomata of conifers are less responsive to environmental stimuli, such as $[\text{CO}_2]$ (Brodrigg & McAdam, 2013; Medlyn et al., 2001; Tor-ngern et al., 2015). A comparison between the Duke and the ORNL sites in the U.S. shows the same pattern; IWUE increases more in the deciduous forest mostly because of the negative ET trend (De Kauwe et al., 2013). However, a tree ring analysis at three FACE sites showed similar IWUE increase in evergreen and deciduous but for different physiological reasons (Battipaglia et al., 2013), while a recent study showed that IWUE of conifers responds to increasing $[\text{CO}_2]$ more than that of broadleaves (Frank et al., 2015).

2.4.2 Plasticity in Plant Functional Traits

Model results show that plasticity in ecosystem-scale physiological and structural traits could explain the observed increase in IWUE. A $1\% \text{ yr}^{-1}$ change in one or two key vegetation parameters combined with changes in relative humidity and temperature is sufficient to explain a 2.6 times larger change in IWUE when compared to theoretical expectations and other modelling results (Medlyn & De Kauwe,

2013). We emphasize that model parameters are representative of the ecosystem scale. This means that a trend in S_{LA} , a_1 , or V_{max} may not necessarily imply a trend in this parameter for a given species but might be the effect of a change in stand demography, as for example previously documented for the US-Ha1 site (Urbanski et al., 2007) and other ecosystems (Hardiman et al., 2013; Knapp, Briggs, & Smith, 2012). While this is unlikely to occur concurrently in all sites, it may partially drive the median trend in IWUE. This has also direct consequences for the interpretation of $C_i:C_a$ and iWUE inferred from tree ring studies, which may not necessarily reflect the trend in IWUE if ecosystem traits are changing because of a shift in forest demographic distribution or composition. Indeed, several of the ecosystems studied here might still be in a growing state and have not yet reached an equilibrium (Table A.1). It is also possible that changes in ecosystem functioning arise as a result of very subtle changes in species composition (Knapp et al., 2012).

Many models estimate generally lower WUE increase than the theoretically expected ($0.5\% \text{ yr}^{-1}$) (Dekker et al., 2016; Ito & Inatomi, 2012; Keenan et al., 2013). However, the T&C model, even using static parameters, predicts an increase of $0.9\% \text{ yr}^{-1}$ in IWUE, which is larger than the expected, while simulating a constant $C_i:C_a$ (Figure A.6). This result is independent of changes in the growing season length, because we restricted our analysis to summer months, but it is related to trends in climate variables, because simulations without trends in temperature and relative humidity show a median increase of $0.4\% \text{ yr}^{-1}$ roughly following the expectations. Indeed, T&C accounts not only for temperature, but also for the actual and saturated vapour pressure, thus changes in these variables can affect the model output. Hydrometeorological variability shapes ecosystem functioning (Pappas, Mahecha, Frank, Babst, & Koutsoyiannis, 2017) and changes in local meteorological drivers (such as VPD; Figure 2.3 and Table A.2) and the occurrence of favourable weather conditions are indeed capable of modifying long-term ecosystem response as shown by both observations and models (Faticchi & Ivanov, 2014; Forkel et al., 2016; Paschalis et al., 2015; Zscheischler et al., 2016).

We found that the perturbations of V_{max} and a_1 (by $+1\% \text{ yr}^{-1}$ and $-1\% \text{ yr}^{-1}$, respectively) best simulate the observed IWUE trend. The physiological acclimation of decreasing a_1 (the parameter which connects stomatal aperture and net assimilation rate) could concurrently explain the observed IWUE, GEP, and ET trends, although with lower GEP trends, compared to observations. When pairing a_1 with other parameters, the most effective in terms of performance was the combination with increasing maximum leaf-to-root ratio (LtR) or specific leaf area (S_{LA}) and with decreasing canopy nitrogen decay coefficient (K_{nit}).

The parameter a_1 is the most influential for the IWUE trend, which is not surprising because a_1 represents the sensitivity of stomatal conductance (g_s) to assimilation rate and environmental drivers ($[CO_2]$ and VPD) in the Leuning model of stomatal conductance which is implemented in T&C (Faticchi & Leuzinger, 2013; Leuning, 1995; Leuning, Kelliher, de Pury, & Schulze, 1995). Indeed, a_1 directly affects diffusivity in our experiments; imposing a negative slope in a_1 leads to a slight reduction in $C_i:C_a$, while in all other experiments $C_i:C_a$ was roughly constant (Figure A.6). While this result is partially expected, it reinforces the concept that the representation and parameterization of the “closure equation” in the photosynthesis-stomatal model is a cornerstone of model behaviour in a

changing climate (Damour, Simonneau, Cochard, & Urban, 2010; Medlyn et al., 2015; Paschalis, Katul, Fatichi, Palmroth, & Way, 2016).

Given the importance of the a_1 parameter, assessing the magnitude of its plasticity is pivotal. A recent study, in which the authors followed a similar modelling approach to reproduce the larger IWUE trends originally reported by Keenan et al. (2013), showed that a 2.1% yr⁻¹ trend in g_1 (similar to a_1 in our study) would imply (i) unrealistic site-level GEP negative trends, (ii) a decrease in C_i , and most importantly (iii) inconsistencies with large-scale trends in evapotranspiration, discharge, and seasonal amplitude of [CO₂] (Knauer et al., 2017). However, in all our simulations, both C_i and GEP increase on average (Figure A.7 and Tables A.6 and A.7), in accordance with theoretical expectations and observations (Ainsworth & Long, 2005), and the most negative ET slopes (0.3% yr⁻¹) are considerably smaller in magnitude compared to findings of Knauer et al. (2017) (i.e., 1% yr⁻¹). Thus, our simulations support the hypothesis that a 1% yr⁻¹ trend in one or more key physiological parameters could be a plausible explanation for the observed trend in IWUE in Northern Hemisphere forests not only at site level but potentially also at larger scales.

The fact that a_1 is variable among vegetation types and across temperature and moisture gradients was already explicit in the work of Leuning (1995). Recent work corroborated that the g_1 parameter of an optimal stomatal conductance model (Katul et al., 2010; Medlyn et al., 2011), a parameter closely related to a_1 , spans a quite large range of values (Lin et al., 2015). Other studies have also shown that this parameter is not constant (Bunce, 2004; Valentini, Gamon, & Field, 1995). For instance, g_1 can be parameterized as a function of soil moisture content (Medlyn et al., 2011); this parameterization can improve the results of models based on stomatal optimality theory (Manzoni et al., 2011). Other support comes from studies showing some plasticity in maximum stomatal conductance and leaf epidermal area with changes in [CO₂], mostly occurring through a decrease in stomatal density, which can be directly translated in a decrease in a_1 (de Boer, Eppinga, Wassen, & Dekker, 2012; de Boer et al., 2011, 2016; Lammertsma et al., 2011). While such plasticity is well acknowledged for geological time scales (P. J. Franks et al., 2013), it has been also demonstrated for decadal trends (Lammertsma et al., 2011), even though the latter finding is rather uncertain (Miglietta, Peressotti, Viola, Korner, & Amthor, 2011; Reid et al., 2003). Two studies from the Duke FACE site further support this hypothesis: a study in a loblolly pine plantation (Domec et al., 2009) showed that increased [CO₂] decreased the sensitivity of stomatal conductance to VPD, while a similar result was also found for *Liquidambar styraciflua* (Ward et al., 2013). Overall, while at the ecosystem and decadal scale we cannot bring specific evidence beyond model simulations, we suggest that it is reasonable to hypothesize that a_1 is adapting to environmental changes, such as increasing [CO₂].

Previous research has also shown that V_{max} is not constant but acclimates to [CO₂], temperature, or soil moisture availability (Jens Kattge & Knorr, 2007; Sage, 1994; S. X. Zhou, Medlyn, & Prentice, 2016). Across 12 FACE experiments, V_{max} generally decreased in time (Ainsworth & Long, 2005), as happened, for instance, in the Oak Ridge FACE experiment, where photosynthesis was downregulated (V_{max} was reduced) because of nutrient limitations (Warren, Jensen, Medlyn, Norby, & Tissue, 2015). However, other FACE experiments also showed that trees growing in elevated [CO₂] have only a marginal decrease in V_{max} (Ainsworth & Rogers, 2007). A modelling study showed that

the observed changes in the fluxes at Harvard forest can be explained by increases in V_{\max} (Keenan, Davidson, Moffat, Munger, & Richardson, 2012). Our results suggest that the increase in V_{\max} increases the ratio between net assimilation and stomatal conductance since V_{\max} has a direct effect on carbon assimilation but only an indirect influence on stomatal conductance. Thus, the net outcome is an enhanced IWUE.

Decreasing K_{nit} (canopy nitrogen decay coefficient) implies that leaf nitrogen content declines less steeply throughout the canopy profile (i.e., more evenly distributed). In other words, for a given top-of-the-canopy V_{\max} , the total canopy nitrogen content is increasing. This can be a result of increasing nitrogen deposition or simply of an increased height or structural rearrangement of the examined forest canopies (Guerrieri et al., 2011; Leonardi et al., 2012). However, any conclusion about changes in K_{nit} remains quite speculative.

Elevated $[\text{CO}_2]$ influences allocation (Palmroth et al., 2006; Poorter & Nagel, 2000), but it is unclear in which direction, since confounding factors complicate the observed dynamics. Some studies reported both increasing and decreasing leaf-to-root ratio (H. H. Rogers, Stephen, Runion, & Mitchell, 1996), and others detected limited $[\text{CO}_2]$ effect on root-to-shoot ratio (Morison & Gifford, 1984). Some researchers found that under increasing $[\text{CO}_2]$ usually more carbon is allocated to roots, although it is difficult to quantify the change relative to foliage biomass since many factors affect root production (Matamala & Schlesinger, 2000 and references therein).

Previous studies have shown that S_{LA} decreases rather than increases under elevated $[\text{CO}_2]$ (Ainsworth & Long, 2005; De Kauwe et al., 2014; Eamus & Jarvis, 1989; Ishizaki, Hikosaka, & Hirose, 2003; Maillard, Guehl, Muller, & Gross, 2001; Medlyn et al., 2015; Morison & Gifford, 1984; Peñuelas & Matamala, 1990; Yin, 2002). However, our hypothesis of increasing S_{LA} is plausible since other environmental changes could be the potential drivers. Overall, the patterns of change in the physiological parameters we perturbed can be considered realistic. Rapid physiological and structural acclimation to environmental change has occurred in several temperate forests recently (Gough et al., 2013; Granier, Bréda, Longdoz, Gross, & Ngao, 2008; Niinemets, 2007; Stuart-Haëntjens, Curtis, Fahey, Vogel, & Gough, 2015). Our results demonstrate that such acclimation -in combination with changes in VPD and temperature- could explain the observed trend in IWUE.

The fact that even trends of $1\% \text{ yr}^{-1}$ can be so important demands for more observations not only of the current values of the different plant physiological properties but also of their potential change with time or due to environmental change. Trends in plant functional traits at the ecosystem scale within this magnitude are currently difficult to detect because measurements are usually available as snapshots on individual plants. For many vegetation parameters (such as V_{\max} , S_{LA} , and a_1) even considerable changes at the ecosystem scale would be difficult to detect experimentally due to the large heterogeneity within different canopy levels (Niinemets, Keenan, & Hallik, 2015) or at the interspecies (J. Kattge et al., 2011) and intraspecies levels (Albert, Grassein, Schurr, Vieilledent, & Violle, 2011; Siefert et al., 2015). Intraspecific trait variability is currently not sufficiently documented for any plant trait (Aubin et al., 2016) hampering the assessment of possible trends at the ecosystem level.

Regardless of the choice of the exact vegetation parameter or parameter combinations, we deem as critical the fact that trends in plant functional traits, which are assumed constant in time in most vegetation models, can potentially modify the ecosystem capacity to metabolize water and carbon under changing environmental conditions. The parameterization of vegetation models should be thus revised, considering that plant trait variability in both space and time can lead to more realistic predictions of the ecosystem response to changing environmental conditions (Fyllas et al., 2014; Pappas et al., 2016; Pavlick, Drewry, Bohn, Reu, & Kleidon, 2013; Sakschewski et al., 2015; Scheiter, Langan, & Higgins, 2013). We advocate that pioneering observation campaigns including forest demography monitoring and many replicates of plant physiological measurements over decadal periods could quantify the velocity of plant trait plasticity and acclimation to environmental change.

2.4.3 Challenges for the future

To improve our understanding of ecosystem responses to changes in climatic variables, we need to reduce the uncertainties in measurements of hydrometeorological variables. For instance, the lack of energy balance closure in several sites implies important biases in the derived fluxes (e.g., Foken, 2008; Leuning et al., 2012; Schmid et al., 2000; Su et al., 2004).

Our numerical experiment shows that trends in vegetation parameters, reflecting plant trait plasticity, and/or changes in forest demography and composition, could explain the higher-than-expected IWUE increase. Tracing plant trait plasticity is challenging. Beyond CO₂ fertilization (Battipaglia et al., 2013; J.-G. Huang et al., 2007; Keenan et al., 2013), droughts can alter forest structure and plant functional traits (Camarero, Gazol, Tardif, & Conciatori, 2015; Hereş, Voltas, López, & Martínez-Vilalta, 2014; Koutavas, 2013; S. X. Zhou et al., 2016). Plant acclimation to rising air temperature (Reichstein et al., 2007; Smith & Dukes, 2013) and to changes in VPD (Novick et al., 2016) can also affect ecosystem functioning; thus, forecasting future changes in IWUE would require more accurate projections of changes in climatic variables, such as near surface humidity. The drivers of plant trait plasticity remain unclear, but it seems unlikely that the changes are merely driven by the increase in [CO₂].

Variability among species and plant functional types introduces another source of uncertainty (Pappas et al., 2016), which cannot be sufficiently captured by current approaches. We found that evergreen and deciduous tree species exhibited markedly different rates of change in IWUE, while currently T&C can only partially reproduce this difference (Figures A.4, A.8 and A.9). To model such diverging responses, we need a better description of plant physiological behaviour over time. This might be achieved through more mechanistic models of stomatal functioning (Damour et al., 2010) together with trait-based approaches (Fyllas et al., 2009; Pappas et al., 2016; Pavlick et al., 2013; Sakschewski et al., 2015) and potentially stochastic parameterizations that account for biotic and abiotic spatiotemporal heterogeneities (Fatichi, Leuzinger, et al., 2016; Pappas et al., 2016; Pappas, Fatichi, Rimkus, Burlando, & Huber, 2015; Prentice, Liang, Medlyn, & Wang, 2015). Temperature- or [CO₂]-driven acclimation of photosynthesis and respiration (Buckley, 2008; Lombardozzi, Bonan, Smith, Dukes, & Fisher, 2015; Reich et al., 2016; Smith, Malyshev, Shevliakova, Kattge, & Dukes, 2016) is another source of uncertainty, which might also be tackled in future analyses since it is not modelled

here, but it is expected to reduce rather than increase IWUE. The lack of an explicit representation of mesophyll conductance by most ecosystem models (including T&C) poses another impediment in the simulation of WUE trends (Flexas et al., 2016; Sun et al., 2014) because a response of mesophyll conductance to increased [CO₂] and other environmental variables modifies WUE. Finally, interactions between the nutrient cycles and changes in WUE remain challenging (M. Huang et al., 2016; Ito & Inatomi, 2012; Jennings, Guerrieri, Vadeboncoeur, & Asbjornsen, 2016; X. Liu et al., 2014; Peñuelas et al., 2011; Radoglou, Aphalo, & Jarvis, 1992; Saurer et al., 2014). Yet many ecosystem models, including the current version of T&C, do not explicitly simulate nutrient dynamics. Using models that explicitly describe nutrient cycles and their interaction with plant growth and performance could likely further improve our understanding of changes in WUE.

Short-term plants' acclimation can be crucial for the survival of forests under climate change (Aubin et al., 2016), but our current knowledge about plasticity and climate change interactions is limited (Valladares et al., 2007). Evidence of plasticity is still limited to a few species (S. J. Franks et al., 2007; Galmés et al., 2014), but there is increasing interest in the significance of including trait plasticity in ecological studies (Albert et al., 2011; Nicotra et al., 2010). Our results suggest that even small changes in plant physiological traits could possibly affect forest functioning at the decadal time scale. Clearly, any attempt to better model the ecosystems' responses to environmental changes requires detailed long-term monitoring of plant functional traits.

Author contribution

S.F., T.M., C.P. and P.M. designed the study. T.M. performed the simulations and the analyses and plotted the figures. T.M. wrote the manuscript with contributions from all authors.

Acknowledgements

This work used eddy covariance data acquired and shared by the FLUXNET community (<http://fluxnet.fluxdata.org/>, last access 30.08.2016), including these networks: AmeriFlux, AfriFlux, AsiaFlux, CarboAfrica, CarboEuropeIP, CarboItaly, CarboMont, ChinaFlux, Fluxnet-Canada, GreenGrass, ICOS, KoFlux, LBA, NECC, OzFlux-TERN, TCOS-Siberia, and USCCC. The FLUXNET eddy covariance data processing and harmonization were carried out by the ICOS Ecosystem Thematic Center, AmeriFlux Management Project and Fluxdata project of FLUXNET, with the support of CDIAC, and the OzFlux, ChinaFlux, and AsiaFlux offices. Funding for AmeriFlux data resources (<http://ameriflux.lbl.gov/>, last access 16 March 2017) was provided by the U.S. Department of Energy's Office of Science. The data sources are listed in Table A.1. T.M. and S.F. thank the support of the Stavros Niarchos Foundation and the ETH Zurich Foundation (grant ETH-29 14-2). C.P. acknowledges the support of the Stavros Niarchos Foundation and the ETH Zurich Foundation (grant P2EZP2_162293) through a Swiss National Science Foundation (SNSF) Early Postdoc. Mobility fellowship. T.F.K. acknowledges supported from the Laboratory Directed Research and Development Program of Lawrence Berkeley National Laboratory under U.S. Department of Energy contract DEAC02-05CH11231. P.G. acknowledges support from the National Science Foundation CAREER grant (1552304) and Department of Energy Early Career grants.

Ecohydrological dynamics in the Alps: Insights from a modelling analysis of the spatial variability

Abstract

Mountain ecosystems are experiencing rapid warming resulting in ecological changes worldwide. Projecting the response of these ecosystems to climate change is thus crucial, but also uncertain due to complex interactions between topography, climate, and vegetation. Here, we performed numerical simulations in a real and a synthetic spatial domain covering a range of contrasting climatic conditions and vegetation characteristics representative of the European Alps. Simulations were run with the mechanistic ecohydrological model Tethys–Chloris to quantify the drivers of ecosystem functioning and to explore the vulnerability of Alpine ecosystems to climate change. We correlated the spatial distribution of ecohydrological responses with that of meteorological and topographic attributes and computed spatially explicit sensitivities of net primary productivity, transpiration, and snow cover to air temperature, radiation, and water availability. We also quantified how the variance in several ecohydrological processes, such as transpiration, quickly diminishes with increasing spatial aggregation, which highlights the importance of fine spatial resolution for resolving patterns in complex topographies. We conducted controlled numerical experiments in the synthetic domain to disentangle the effect of catchment orientation on ecohydrological variables, such as streamflow. Our results support previous studies reporting an altitude threshold below which Alpine ecosystems are water-limited in the drier inner-Alpine valleys and confirm that the wetter areas are temperature-limited. High-resolution simulations of mountainous areas can improve our understanding of ecosystem functioning across spatial scales. They can also locate the areas that are the most vulnerable to climate change and guide future measurement campaigns.

3.1 INTRODUCTION

Climate change poses challenges for mountain ecosystems, and the quantification of their responses is crucial for their management. The European Alps—situated in the transition between the Mediterranean Sea and the Atlantic Ocean—comprise a unique mosaic of microclimates and vegetation types, which renders this area particularly interesting, but also complicates modelling attempts (Beniston, 2006). In the European Alps, air temperature is rising faster than the global average (Brunetti et al., 2009), reducing snow cover duration (Beniston et al., 2018) and increasing drought occurrence (Timofeeva et al., 2017), tree mortality (Rebetez & Dobbertin, 2004), and wildfires (Dupire et al., 2017). Observations show that vegetation species composition is changing in certain areas (Rigling et al., 2013); these changes might accelerate in the future (Booth et al., 2012; Schumacher & Bugmann, 2006). At higher elevations, grassland species are either profiting from the reduced snow cover or diminishing due to higher temperatures (Carlson et al., 2017; Gottfried et al., 2012; Pauli, Gottfried, Reiter, Klettner, & Grabherr, 2007). Models project negative impacts on forests (including more frequent wildfires) especially in the dry and warm regions (Elkin et al., 2013). Tree-ring studies in certain Alpine areas also suggest that water stress is becoming more frequent (Büntgen et al., 2006; Timofeeva et al., 2017).

Process-based numerical models are widely used for simulating ecohydrological dynamics in different ecosystems. In mountainous areas such efforts are challenging because the complex terrain creates variability and gradients in vegetation patterns and in several meteorological variables, such as air temperature, precipitation, shortwave radiation and wind speed, thus confounding the relationship between climate and ecosystem functioning (Ivanov, Bras, & Vivoni, 2008a). Studies with spatially explicit numerical models have investigated mountain ecohydrology, principally in water-limited areas (e.g., Gutiérrez-Jurado & Vivoni, 2013; Ivanov, Bras, & Vivoni, 2008b; Klos et al., 2018; C. Tague, Heyn, & Christensen, 2009; Vivoni, Rodríguez, & Watts, 2010; Williams, McNamara, & Chandler, 2009; Zapata-Rios, Brooks, Troch, McIntosh, & Guo, 2016), but the quantification of the spatial variability of the related ecohydrological processes remains limited. Research in the semi-arid western US cascades has shown that the responses of ecosystems to climate change and management practices varies spatially (Tague, Heyn, et al., 2009), and the uncertainties related to the aspect peak in areas where precipitation might shift from snow-dominated to rain-dominated (Tague & Peng, 2013; Williams et al., 2009).

To date, very few distributed ecohydrological studies have focused on the European Alpine ecosystems (Zierl et al., 2007) and they typically investigated few sites with special local features (e.g., Bertoldi et al., 2010; Della Chiesa et al., 2014; Rössler, Diekkrüger, & Löffler, 2012). Conclusions from these studies are not generalizable to larger areas. For example, Della Chiesa et al., 2014 found an altitudinal threshold below which grass is water-limited in a dry inner Alpine hillslope and call for more research to quantify this threshold. Since this threshold seems to characterize also evergreen forests in another inner Alpine catchment (Rössler et al., 2012), it becomes clear that a more comprehensive analysis of the spatial variability of ecohydrological drivers and responses in the Alpine region is warranted.

Contrary to the western US (e.g., Hinckley et al., 2014; Zapata-Rios et al., 2016), no modelling study has explored the role of aspect on ecohydrology in the European Alps, although previous research has shown that slope orientation influences the sensitivity of plants to climate in this region (Leonelli, Pelfini, Battipaglia, & Cherubini, 2009). These knowledge gaps in vegetation-climate-topography interactions in the Alpine region hinder our ability to assess the impacts of climate and land use changes on mountain ecosystems (Viviroli et al., 2011; Voepel et al., 2011). Additionally, recent research has shown that the cross-scale temporal variability of ecosystem processes is enveloped by the variability of hydrometeorological variables (Pappas et al., 2017). Distributed ecohydrological models offer the opportunity to explore the cross-scale variability of these processes not only in time but also in space. Indeed, modelling insights on the spatial scale dependence of ecohydrological processes may help understanding the controls of spatial distribution of vegetation (Thompson, Harman, Troch, Brooks, & Sivapalan, 2011), which is crucial for predicting the response of the ecosystems to climate change (Voepel et al., 2011). In summary, studying the spatial variability of ecohydrological variables might enhance our understanding of the climatic drivers of the various processes and thus help assessing climate change effects in mountainous ecosystems.

In this study, we used the distributed ecohydrological model Tethys-Chloris (T&C) to simulate the ecohydrology of an Alpine catchment (Kleine Emme, central Switzerland) and a synthetic domain to address the following questions: (1) How will different vegetation types (forest and grassland) respond to changes in meteorological variables in Alpine areas with distinct climates? (2) Which areas are water-limited and thus prone to droughts and which areas are energy-limited? (3) Is there a role of catchment orientation in controlling ecohydrological processes? (4) How does the spatial variability of ecohydrological variables change across spatial scales?

A way to evaluate the response of ecosystems to climate change is through multiple simulations based on climate projections, which are very uncertain, especially in mountainous areas, where the downscaling is necessary and constitutes an additional source of uncertainty (e.g., Rössler et al., 2012). Instead, here we applied the “space-for-time” approach, in which ecological variables are correlated to naturally occurring topographic gradients (e.g., Dunne, Saleska, Fischer, & Harte, 2004; Goulden & Bales, 2014; Sundqvist, Sanders, & Wardle, 2013). This approach hypothesizes that vegetation will respond to climate change following the same principles that determine its spatial distribution under current climate. While this is not generally true across large climatic gradients (e.g., Fatichi & Ivanov, 2014; Goward & Prince, 1995; Huxman et al., 2004), it is a reasonable assumption at the spatial scales of few tens of square kilometres of this study. We correlated the spatial patterns of several simulated ecohydrological variables (including net primary production, leaf area index, transpiration, evapotranspiration and snow cover duration, hereafter referred as “ecohydrological variables”) to the spatial patterns of temperature, radiation and water availability. Through a correlation analysis, we quantified how each of the dependent variables will respond to a unit change in each of the three drivers in a spatially explicit way for different vegetation types and climatic conditions. To generalize these sensitivities for a broader climatic spectrum, we repeated the same sensitivity analysis on a synthetic domain with simple topography and uniform vegetation cover for two contrasting climates of the Alpine region (the wet Bernese highlands and the dry inner valley of

the upper Rhone basin). Using the same experimental setup, we quantified the role of catchment orientation on ecohydrological processes, such as streamflow.

3.2 METHODS

3.2.1 The T&C model

We used the mechanistic ecohydrological model Tethys-Chloris (T&C, Fatichi, Ivanov, & Caporali, 2012; Fatichi & Leuzinger, 2013; Fatichi & Pappas, 2017; Manoli, Ivanov, & Fatichi, 2018; Pappas, Fatichi, & Burlando, 2016). T&C simulates the principal processes of the hydrological cycle, such as precipitation interception, transpiration, ground evaporation, infiltration, and surface/subsurface water fluxes, including the lateral transfer of water. It further simulates plant-related processes, such as photosynthesis, phenology, carbon allocation and tissue turnover. It resolves the mass and energy budgets over complex topography, explicitly considering the spatial variability of meteorological fields, soil properties, vegetation and the topography effect on the distribution of incoming radiation. More details about the model are presented in the supplementary information (see Appendix B.1).

3.2.2 Model simulations

The first case study of this analysis investigates the wet pre-Alpine environment, which is representative of a large fraction of the European Alps. We selected the Kleine Emme catchment in central Switzerland (Figure 3.1) as a typical wet Alpine case study. The Kleine Emme catchment (478 km²) is mostly covered by grassland, evergreen forest, and mixed (evergreen-deciduous) forest and the dominant soil type is silt/sandy loam (Figure B.1). The mean catchment elevation is 1050 m a.s.l. (range: 431-2329 m a.s.l.). The long-term catchment-average mean for precipitation and air temperature are 1650 mm yr⁻¹ and 7.7 °C, respectively (Pappas et al., 2015). Vegetation cover was derived by the Corine 2006 product (<https://www.eea.europa.eu/data-and-maps/data/clc-2006-raster-4>, downloaded in December 2016) and soil texture data were derived from the Swiss soil map (GEOSTAT, 2000). We used a uniform soil depth of 0.6 m in the whole catchment in the absence of more precise information.

Data from three meteorological stations in (or near) the catchment were used to derive the meteorological input for the model (Table 3.1). Based on the elevational lapse rates, which were estimated for every hour of the simulation period assuming linear regressions according to the elevation of the stations, T&C computed the maps of air temperature (Figure 3.2a), air pressure, wind speed and dew point temperature (to subsequently use vapour pressure). Shortwave radiation was computed based on local and remote topographic effects (Figure 3.2b). For precipitation, we used a distributed product with 2 km resolution and daily time step (Wüest et al., 2010, Figure 3.2c). Daily to hourly disaggregation of precipitation was based on the rainfall timing observed at the three stations (as described in Fatichi, Rimkus, Burlando, Bordoy, & Molnar (2015)). The model was run on 100 m spatial resolution and hourly temporal resolution for a period of five years (2000-2005). The first year of the simulation period was discarded to eliminate issues related to model spin-up, thus only four years were finally analysed.

We used vegetation parameterizations derived from previous applications of T&C for sites of the Swiss FluxNet network (S. Wolf et al., 2013), which reproduce realistically carbon, water and energy responses (Faticchi & Pappas, 2017; Faticchi, Zeeman, Fuhrer, & Burlando, 2014). Only discharge data from two sites are available for validating the hydrological response in the Kleine Emme catchment (Table B.1). The good model performance at the hourly and daily time scales (Figures B.2, B.3 and B.4) and the comparison between the observed and modelled flow duration curves (Figure B.5) confirm the suitability of the employed vegetation parameterizations and soil properties for the scope of this study.

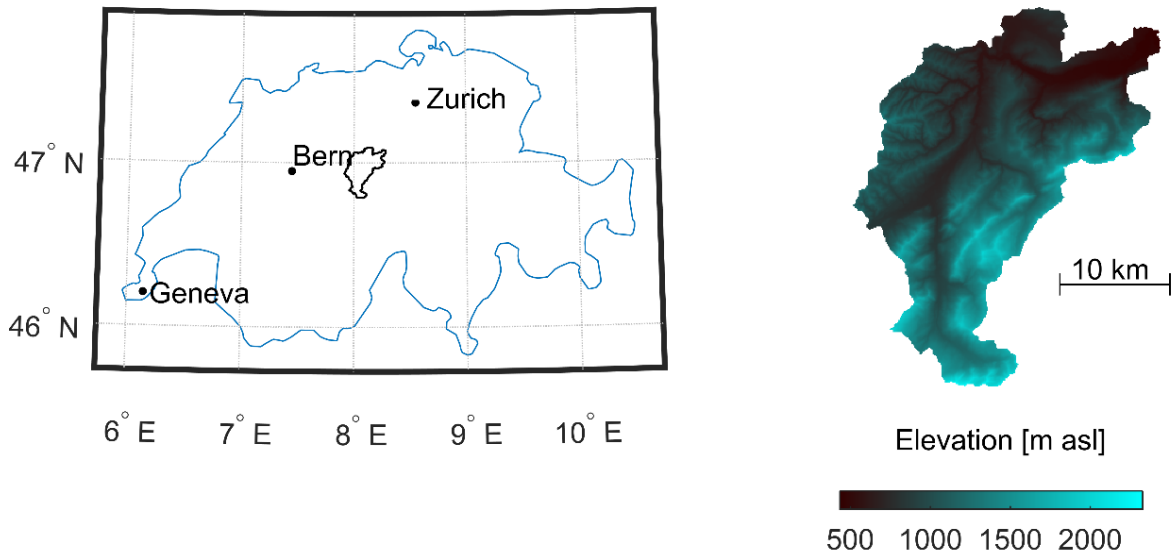


Figure 3.1 Location and topographic map of the Kleine Emme catchment in central Switzerland.

Table 3.1 Summary of the meteorological stations used in the study (source: Swiss meteorological service).

Experiments	Kleine Emme			Wet synthetic domain		Dry synthetic domain	
Station name	Luzern	Napf	Pilatus	Interlaken	Adelboden	Visp	Zermatt
Elevation [m a.s.l.]	454	1403	2106	577	1320	639	1638
Latitude	N 47.03	N 47.00	N 46.98	N 46.67	N 46.50	N 46.30	N 46.03
Longitude	E 8.30	E 7.93	E 8.25	E 7.87	E 7.56	E 7.85	E 7.75
Time period used	1.10.2000-30.9.2005			1.10.1990-30.9.1995		1.1.1982-31.12.1986	

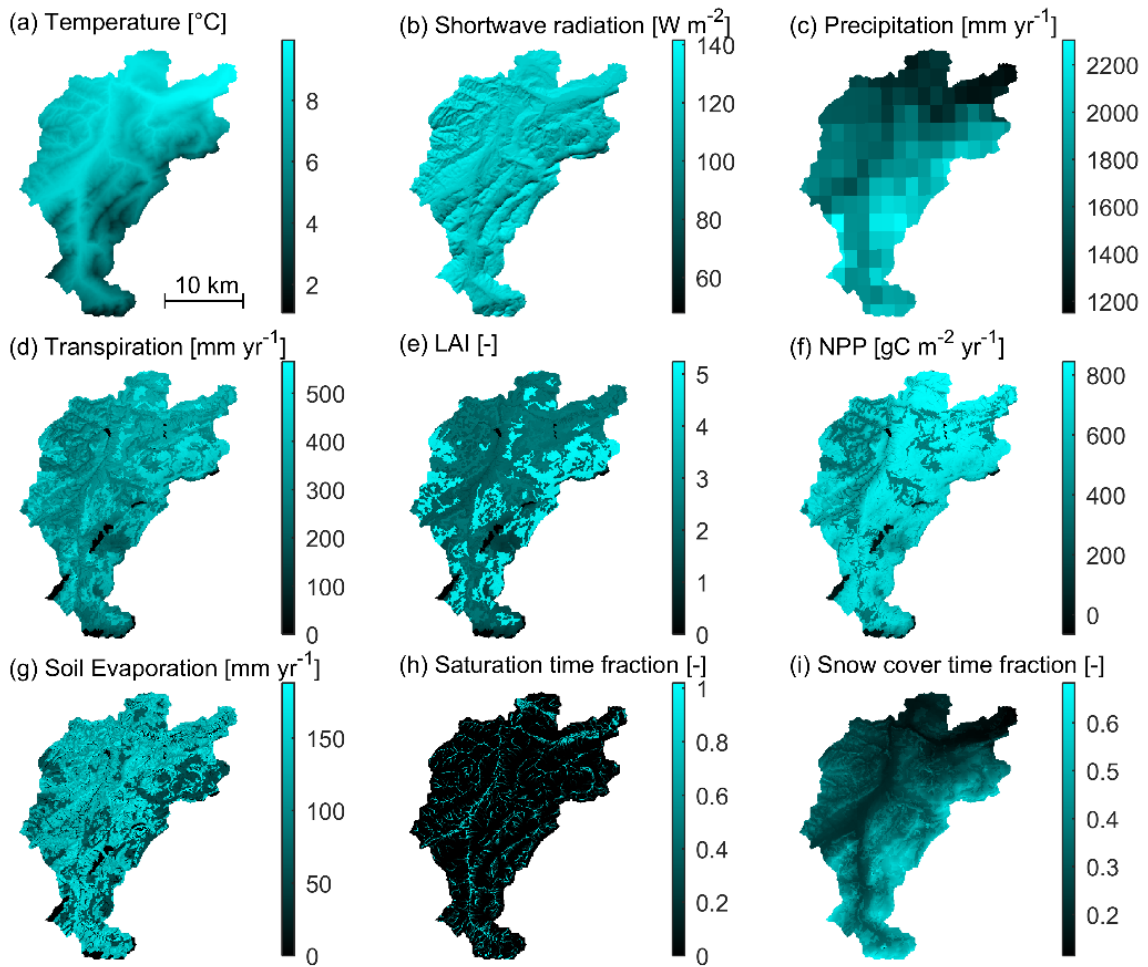


Figure 3.2 Four-year mean annual (a) temperature, (b) shortwave radiation, (c) precipitation that are used as input meteorological variables to the model and 4-year mean annual simulated (d) transpiration, (e) leaf area index (LAI), (f) net primary production (NPP), (g) soil evaporation, (h) fraction of time with soil saturation, and (i) fraction of time with snow cover for the Kleine Emme catchment.

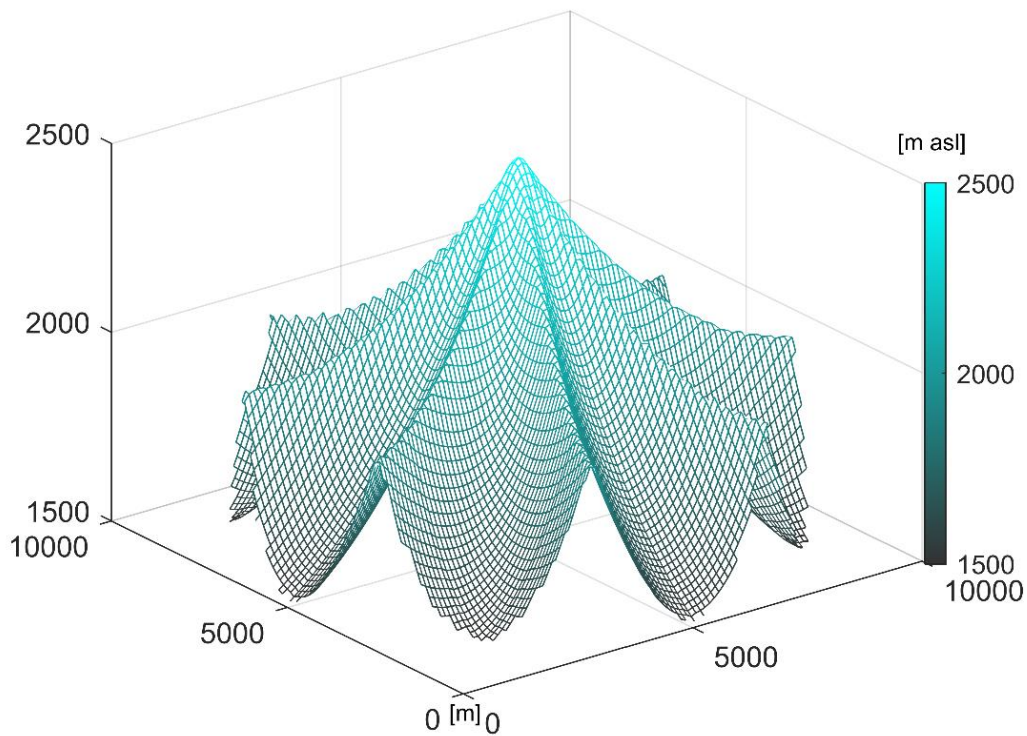


Figure 3.3 Three-dimensional (3D) representation of the symmetric synthetic domain. The vertical axis has been stretched to improve clarity.

We also performed multiple simulations with T&C on a synthetic domain with different vegetation covers and for contrasting climatic regimes, to disentangle the roles of climate and vegetation. The synthetic domain comprises one peak in the middle with eight catchments draining along the cardinal and intercardinal directions (Figure 3.3). The total area of the domain is 78 km², the area of each catchment is 8.7 km² (cardinal) and 9.1 km² (intercardinal) and the elevation range is 1500-2500 m (typical elevation of Alpine headwater catchments). The soil was assumed uniform in the whole domain (clay loam with 30% clay and 20% sand, Hengl et al., 2014). Air temperature, wind speed and precipitation change with elevation and thus are similar in all catchments (all catchments have a similar elevation profile). The eight catchments differ only in terms of incoming radiation, which makes this experimental setup suitable for isolating the effects of radiation on ecohydrological processes.

We performed four simulations on this domain to explore different climates and vegetation characteristics. We considered two areas with very contrasting climatic regimes in the Alps, although they are close to each other, the Bernese Highlands (wet climate) and the inner-Alpine upper Rhone valley (dry climate) with mean annual precipitation ca. 1450 and 620 mm, respectively. For each of the two climates (hereafter “wet” and “dry”), data from a low- and a high-elevation station were used (Table 3.1) to compute the elevational lapse rates for every hour for all meteorological variables (e.g., precipitation).

We investigated the differences between two common Alpine vegetation covers, i.e. evergreen forest and managed grassland. Each vegetation cover was assigned in the entire domain and model parameterization followed previous T&C studies, assigning different plant functional type parameterizations to evergreen forests and grasslands (Fatichi et al., 2014, 2015; Fatichi & Pappas, 2017). We conducted four simulations to combine the different climates and vegetation types (i.e. wet evergreen forest, wet grassland, dry evergreen forest and dry grassland). We excluded the first simulated year in each case to eliminate problems related with the spin-up, and we thus used the four-year average for the subsequent analyses. The spatial resolution of the simulations is 100 m and we used hourly time step. Figure 3.4 shows an overview of meteorological input and simulated ecohydrological variables for the dry grassland (for the other three experiments, see Figures B.6, B.7 and B.8).

3.2.3 Sensitivity analysis

To quantify the sensitivity of ecohydrological processes, ideally, we would perform several virtual experiments perturbing one explanatory variable at a time to compute the corresponding change in the ecohydrological variables. However, this is infeasible, because the simulations with T&C are computationally very demanding due to the fine spatiotemporal resolution. Instead, we applied the so-called gradient method, which is common in ecological research (e.g., Dunne, Saleska, Fischer, & Harte, 2004); we related the spatial distribution of several simulated ecohydrological variables (such as transpiration and NPP) to the spatial distribution of topographic or meteorological variables. Three main environmental controls express the energy and water limitations: air temperature, solar radiation and water availability (e.g., Churkina & Running, 1998; Nemani et al., 2003; Seddon, Macias-Fauria, Long, Benz, & Willis, 2016). Since soil moisture is a model output (and thus it is influenced by many factors), we preferred to use a topographic proxy to express water availability. We compared two indexes: the upstream area and the topographic wetness index (hereafter “topographic index”) and retained the latter because it has a better explanatory power to describe moisture availability (more details in Appendix B.2, Tables B.2 and B.3).

We performed one regression for each ecohydrological variable (separately for each vegetation type in the Kleine Emme catchment) using the three explanatory variables (i.e. air temperature, shortwave radiation and topographic index) and taking into account interaction effects between them (Table B.4). We first visually inspected the scatter plot of each dependent variable against each explanatory variable to decide if their relationship is linear or quadratic. A generalized equation in its full version is the following:

$$y = a_1x_1 + a_2x_2 + a_3x_3 + a_4x_1x_2 + a_5x_1x_3 + a_6x_2x_3 + a_7x_1^2 + a_8x_2^2 + a_9x_3^2 \quad (3.1)$$

where y is the dependent variable (e.g., leaf area index, LAI) and x_1 , x_2 , and x_3 are the three explanatory variables (i.e., air temperature, radiation, and topographic index).

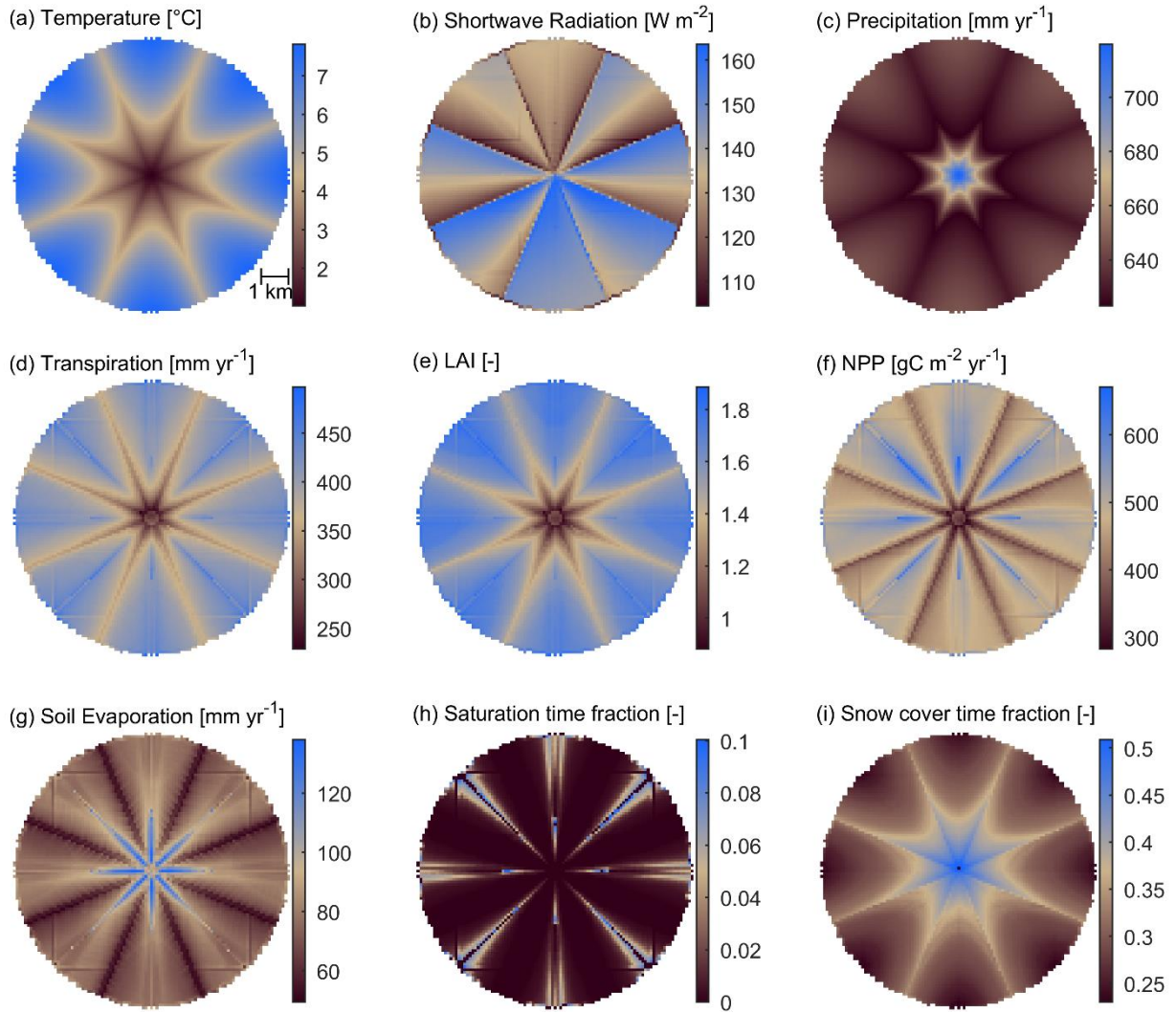


Figure 3.4 Four-year mean annual (a) temperature, (b) shortwave radiation, (c) precipitation that are used as input meteorological variables to the model and 4-year mean annual simulated (d) transpiration, (e) leaf area index (LAI), (f) net primary production (NPP), (g) soil evaporation, (h) fraction of time with soil saturation, and (i) fraction of time with snow cover for the dry grassland experiment in the synthetic domain.

Statistical metrics from these regressions were used to detect outliers: every pixel for which the leverage or the Cook distance was outside of the 99.9 percentile of the corresponding distribution was excluded as an outlier, and the regressions were recomputed. Based on the final regressions, we computed the sensitivity of the dependent variables to each explanatory variable as the respective partial derivative. For example, the sensitivity of the dependent variable y to the explanatory variable x_1 in Equation (3.1) is

$$\frac{\partial y}{\partial x_1} = a_1 + a_4 x_2 + a_5 x_3 + 2a_7 x_1 \quad (3.2)$$

Equation 3.2 shows that the sensitivity of every dependent variable to one explanatory variable is a function of all the three explanatory variables, since the sensitivity is affected by where the dependent variable is located in the three-dimensional domain (where the three dimensions correspond to air

temperature, shortwave radiation and topographic index). Note that in the following, when we refer to the sensitivity of a dependent variable y to an independent variable x , we mean how much y will change for a unit change in x , i.e., we use the mathematical partial derivative of a multivariate field to compute the sensitivity. This differs from how sensitivity is strictly defined in statistical terms (e.g., Pappas, Fatichi, Leuzinger, Wolf, & Burlando, 2013; Saltelli et al., 2008) and allows sensitivity values to be positive and negative according to the sign of the derivative.

This analysis provided three maps for each ecohydrological variable showing their distributed sensitivity to the three explanatory variables (one value for each grid cell and each explanatory variable based on the long-term mean values for each variable). However, the comparison of the relative importance of each explanatory variable with this analysis alone is infeasible, because the sensitivity to each explanatory variable has different units; that is, the sensitivity of annual transpiration to temperature, radiation, and topographic index is expressed in $\text{mm yr}^{-1}/^{\circ}\text{C}$, $\text{mm yr}^{-1}/(\text{W m}^{-2})$, and $\text{mm yr}^{-1}/(-)$, respectively.

To estimate the relative importance of each explanatory variable, we standardized all the variables using the Z-scores, so that the mean equals zero and the standard deviation equals one. We repeated the sensitivity analysis as described above and computed the partial derivatives of each dependent variable to the three explanatory variables. In this analysis, we used the absolute values of the partial derivatives, because the sign does not affect the relative importance of each explanatory variable (besides, including the sign would be redundant, because this information emerges from the previously described non-normalized analysis). For each pixel of the domain, we computed the total sensitivity by summing the three partial derivatives and we divided each derivative by the total sensitivity. These normalized sensitivities were visualized using Red-Green-Blue (RGB) representation with one colour for each explanatory variable. The exact relationships for the normalized variables in the Kleine Emme catchment are given in Table B.4 for four ecohydrological variables.

3.2.4 Variance across spatial scales

To compare the spatial variability of the analysed meteorological and ecohydrological variables, we defined a range of variability (RV) of each variable, as an indicator of the scatter of the values around the mean. RV equals the double of its interquartile range (I_{QR}), which— assuming a normal distribution—corresponds to $2.698 * \sigma$ (σ is the standard deviation), expressed as percentage of the

$$RV = \frac{2 * I_{QR}}{mean} * 100 \quad (3)$$

We investigated how the variance of several ecohydrological variables decreases with increased spatial aggregation, in both the synthetic domain and the Kleine Emme catchment. We used the 4-year average of simulated net primary production (NPP), transpiration, and other ecohydrological and meteorological variables. First, we standardized all the variables using the Z-scores, so that the standard deviation of the original 100-m resolution equals one, in order to combine different variables

in a single figure. Then, we aggregated the model output by assigning to each pixel the mean value of an area, which is increased stepwise (see Figure B.9 for an illustrative explanation). After computing the spatial variability of the original model output, the second step was to aggregate the surrounding cells of each pixel (e.g., three times larger resolution implies that nine pixels are aggregated). At each step, we extended the aggregation area to include the surrounding pixels of the pixels considered in the previous step; thus, the size of the aggregation area increases by 200 m in each direction at every step (Figure B.9).

3.3 RESULTS

3.3.1 Ecohydrological sensitivity to temperature, radiation, and topographic index

3.3.1.1 *The Kleine Emme catchment*

Low temperatures limit all ecosystem variables in most parts of the domain, which translates into a positive sensitivity to air temperature (Figure 3.5a–d). This sensitivity peaks in the higher (and colder) parts of the domain, where a one-degree increase in temperature can lead to up to more than 60 mm increase in annual ET, 70 gC m⁻² increase in annual NPP, and 0.2 increase in LAI. When moving to lower elevations, the sensitivity of ET and NPP to air temperature declines, whereas for the ET of the evergreen forest, the sensitivity to air temperature becomes even negative locally (Figure 3.5b).

The sensitivity to shortwave radiation differs between variables. The radiation sensitivity of transpiration and ET is generally positive (Figure 3.5e–f), whereas NPP and LAI are radiation-saturated in the south-facing slopes and radiation-limited in the north-facing slopes (Figure 3.5g–h). A radiation increase of 1 W m⁻² could increase annual transpiration by up to 3 mm and decrease annual NPP by up to 4 gC m⁻².

Almost all ecosystem variables are negatively correlated to the topographic index (Figure 3.5i–l), which means that there are no major water limitations in this catchment. Only in the ridges of the lower parts of the catchment, NPP and LAI are slightly positively correlated to topographic index.

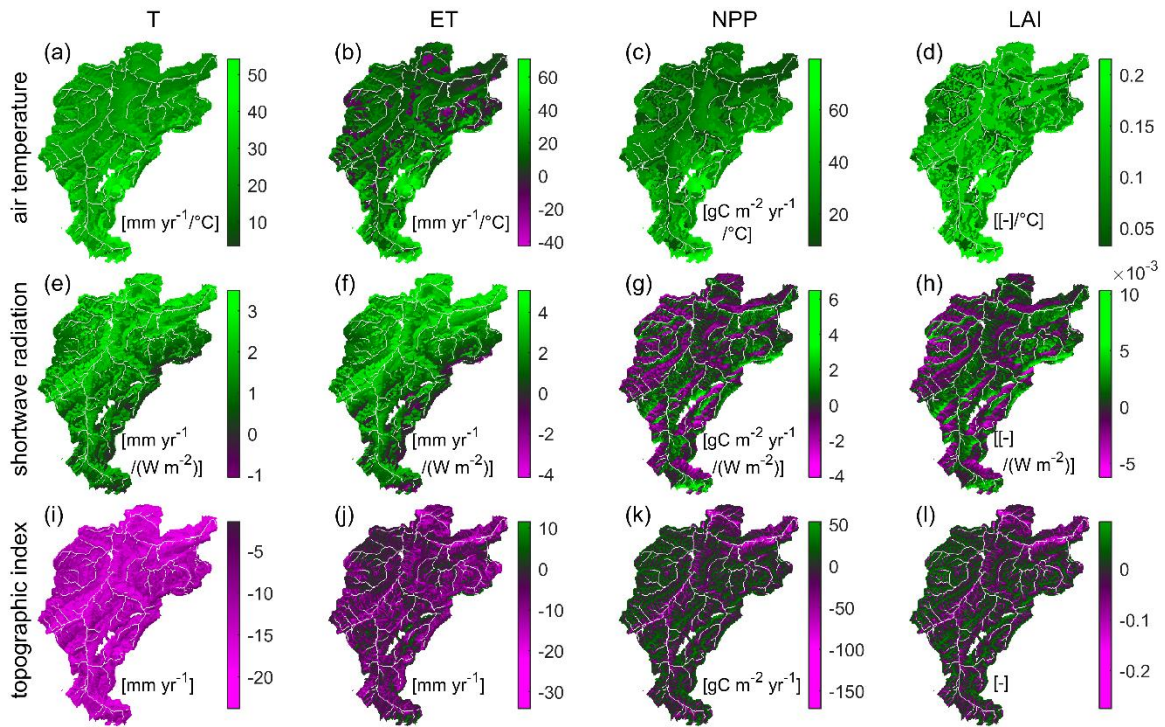


Figure 3.5 Sensitivity of transpiration (T), evapotranspiration (ET), net primary production (NPP), and leaf area index (LAI) to air temperature, shortwave radiation, and topographic index in the Kleine Emme catchment. Green represents areas where an increase in the explanatory variable leads to an increase in the dependent variable (positive sensitivity), and magenta is for the areas where an increase in the explanatory variable leads to a decrease in the dependent variable (negative sensitivity). Areas shown in dark colour are those where the dependent variable is insensitive to the respective explanatory variable.

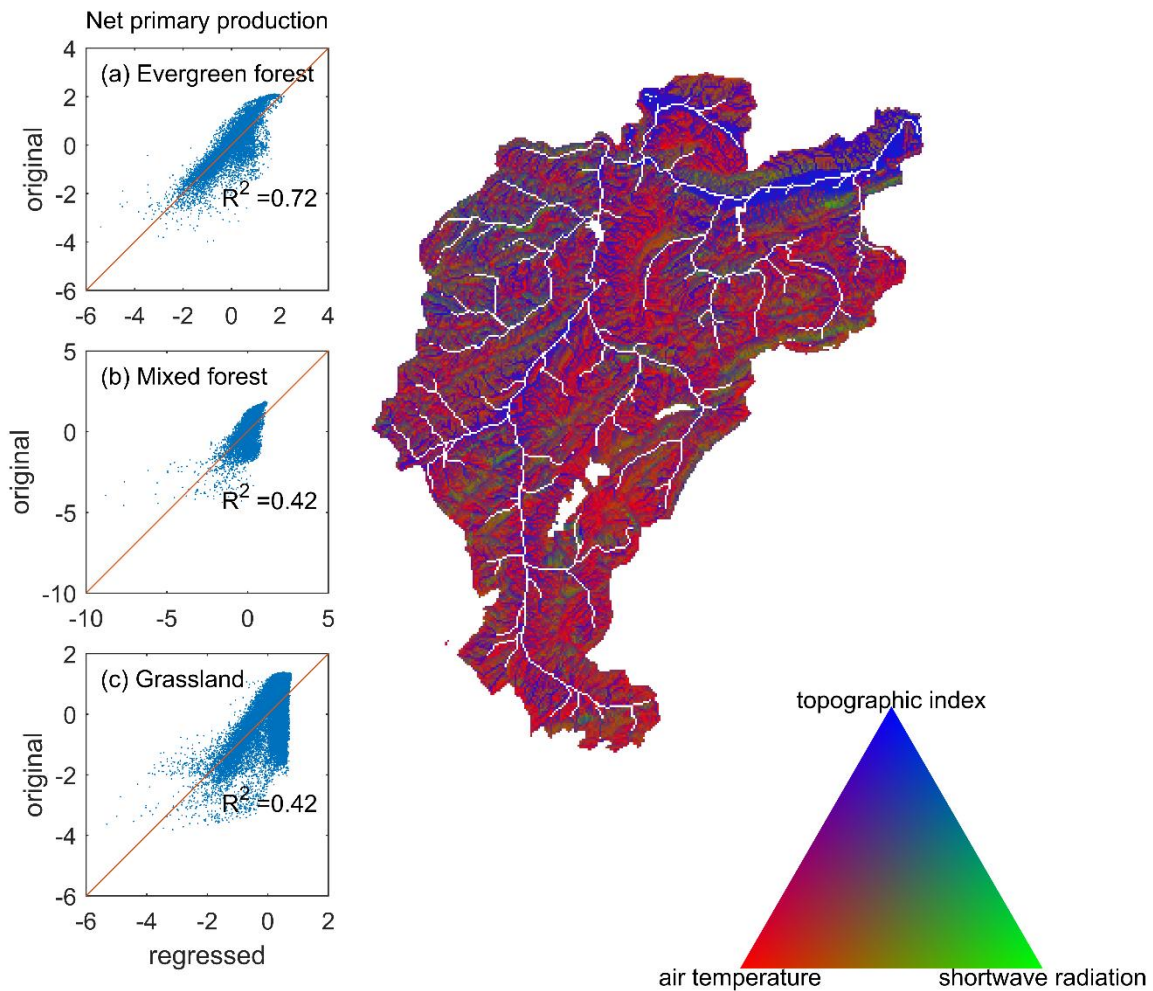


Figure 3.6 Normalized sensitivity of net primary production (NPP) to air temperature, shortwave radiation, and topographic index in the Kleine Emme catchment. The red colour represents areas where temperature is the main control for NPP, green represents the radiation-limited areas, and blue is for areas where the topographic index is the dominant control. Inset scatter plots show the comparison between the original model output (“original”) and the values that are calculated with the regression formula that was used for the sensitivity analysis (“regressed”) for (a) evergreen forest, (b) mixed forest, and (c) grassland (the R^2 values of each regression are also shown). All variables are normalized.

The analysis of the normalized variables shows that air temperature is the dominant control for NPP in most parts of the catchment (Figure 3.6 and Table B.5). The subplots in Figure 3.6 show the scatter of the originally modelled NPP against the regressed NPP (both normalized) for the different ecosystems. The three explanatory variables describe relatively well the spatial distribution of NPP for the evergreen forest ($R^2 > 0.7$) but do less efficiently so for the mixed forest and the grassland ($R^2 \sim 0.4$). It is important to notice that the maps of normalized sensitivity should be viewed through the lens of the magnitude of the absolute sensitivities: For example, one variable might appear to be the

dominant control for an ecohydrological variable in a specific area only because the sensitivity to the other two drivers is closer to zero.

Air temperature is the primary control for most ecosystem variables in large parts of the domain. Not only for NPP, but also for LAI, air temperature is at least three times more important than radiation or topographic index in all elevation bands above 800 m (Table B.5 and Figure B.10). In the lower parts, all three explanatory variables are roughly equally important for transpiration whereas for ET, radiation is the dominant control (Table B.5 and Figures B.11 and B.12). Snow processes are mainly driven by air temperature (Figure B.13). The scatter subplots in the aforementioned figures show that the three explanatory variables provide a good regression for all variables in all three ecosystems ($R^2 > 0.6$); they only perform poorly for evergreen forest ET ($R^2 = 0.2$).

3.3.1.2 *Synthetic domain*

Results from the experiments on the synthetic domain show very distinct patterns of NPP sensitivity (Figure 3.7). A comparison between different vegetation types shows that grassland NPP is much more sensitive to all three explanatory variables compared with evergreen forests (e.g., for sensitivity to air temperature, compare subplots 7a and 7b). Depending on the ecosystem and the location, an increase in air temperature by one degree would lead up to more than 150 gC m⁻², or equivalently, more than 45% (40 gC m⁻², or 10%) increase in annual NPP of the wet grassland (wet evergreen forest).

The climatic signal on NPP sensitivity is even more striking for the dry ecosystems: although the wet ecosystems are limited by low temperatures in the whole elevation range (Figure 3.7a,b), the dry ecosystems show a transition from areas limited by low temperatures to areas negatively influenced by relatively high temperatures when moving below 1,700 m a.s.l. (Figure 3.7c,d and Table B.6). NPP sensitivity to radiation is very small in the wet ecosystems (Figure 3.7e–f) but larger and negative everywhere in the dry ecosystems (Figure 3.7g–h and Table B.6). Water limitations (e.g., the combination of negative sensitivity to temperature and positive sensitivity to topographic index in the low parts of the dry domain) are stronger in the grassland and less pronounced in the evergreen forest in absolute values (Figure 3.7c–d, k–l). Together with the sensitivity to topographic index of the wet experiments (Figure 3.7i–j), these results show that although the wet Alpine ecosystems are primarily energy-limited, the lower parts of dry Alpine valleys are water-limited.

In general, air temperature is low and limiting for all ecosystem variables (T, ET, and LAI), at least at the highest elevations, in all simulations. The only exception is the ET in the wet evergreen forest, which shows a negative sensitivity to air temperature (Figure B.14a). Similarly with NPP, in the dry experiments, ET and LAI are negatively correlated to temperature in the low areas of the evergreen forest (Figures B.14c–d and B.15c–d).

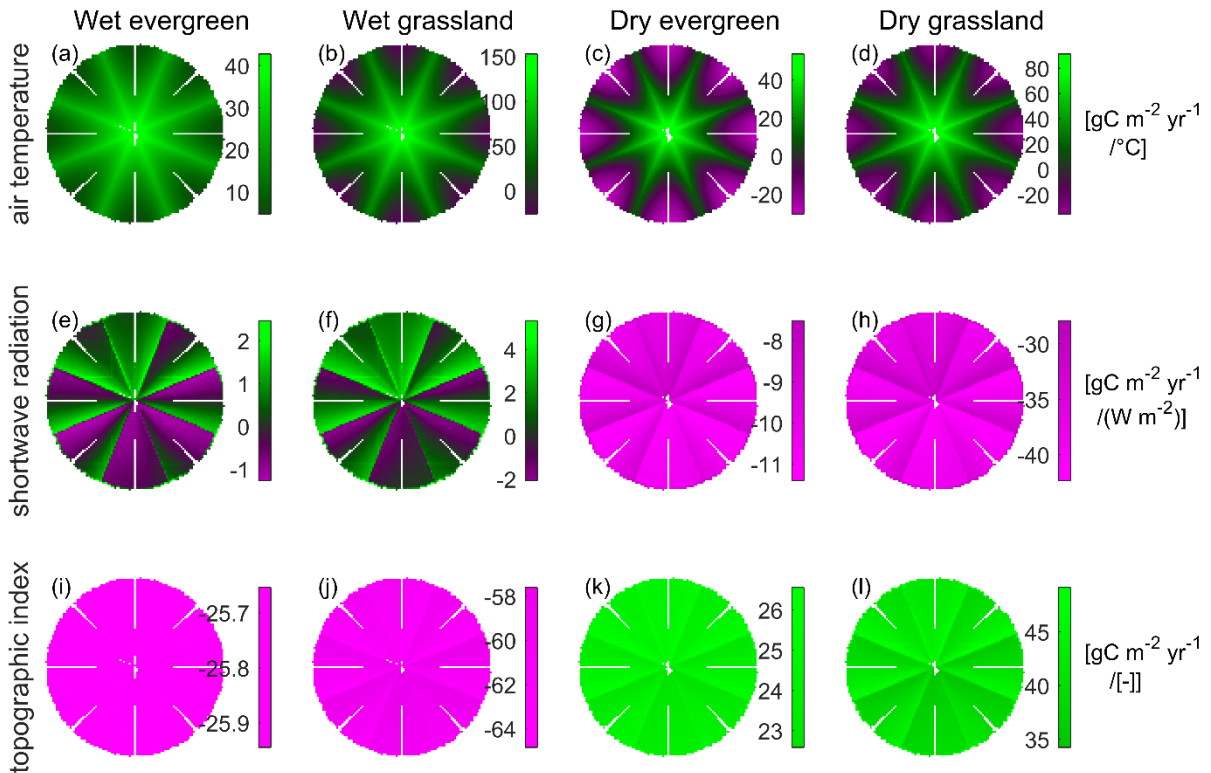


Figure 3.7 Sensitivity of net primary production (NPP) to air temperature, shortwave radiation, and topographic index in the four experiments on the synthetic domain. Green represents areas where an increase in the explanatory variable leads to an increase in NPP (positive sensitivity), and magenta is for areas where an increase in the explanatory variable leads to a decrease in NPP (negative sensitivity). Areas shown in dark colour are those where NPP is insensitive to the respective explanatory variable.

In the dry climate, all ecosystem variables are negatively related to radiation (Figure 3.7g–h, B.14g–h, B.15g–h, and B.16g–h). A 1-W m^{-2} increase in shortwave radiation could reduce dry grassland annual NPP by up to 40 gC m^{-2} (12%), LAI by up to 0.04, and annual ET by up to 22 mm (4%). In the wet climate, the sensitivity to shortwave radiation is much smaller. In both climates, grasslands are more sensitive to radiation than evergreen forests (in terms of transpiration, ET, and NPP).

Ecosystem sensitivity to topographic index is uniform in space; the sensitivity of all ecosystem variables to topographic index is negative in the wet and positive in the dry experiments. Increasing the topographic index by one unit could increase ET by up to 30 mm yr^{-1} in the dry climate and decrease it by up to 25 mm yr^{-1} in wet climate (Figure B.14).

Air temperature is the dominant control for NPP in large parts of the domain in all four numerical experiments (Figure 3.8; for the dry grassland, see also Table B.6). In areas where the sensitivity to air temperature is small (either in the low elevations in the wet experiments, e.g., Figure 3.8a–b, or in the transition zones between positive and negative sensitivity to temperature in the dry experiments,

e.g., Figure 3.8c–d), topographic index emerges as the dominant driver, but its effect is generally smaller compared with air temperature (Table B.6).

Compared with the other ecosystem variables, NPP is the most sensitive to high temperature in the low elevations of the dry experiments (Table B.6). All variables are limited by low temperature at higher elevations (Figures B.17, B.18 and B.19), with the exception of the wet evergreen forest transpiration and ET. Radiation limitations are important for transpiration and ET in the north-facing slopes of the wet evergreen forest and grassland (Figures B.17a–b and B.18a–b). In the dry climate, the transition from low-temperature limitations at high elevations to detrimental high temperatures at low elevations is evident in all variables mostly in the evergreen forest (Figures B.17c–d, B.18c–d, and B.19c–d). The duration of snow cover is driven by air temperature in all four experiments (Figure B.20). The insets in the figures of relative sensitivity show (as for Kleine Emme) the scatter plots of the original against the regressed normalized dependent variables. For all ecohydrological variables, the best fit is achieved in the dry grassland ($R^2 > 0.9$) and the poorest in the wet evergreen forest ($R^2 \sim 0.7$).

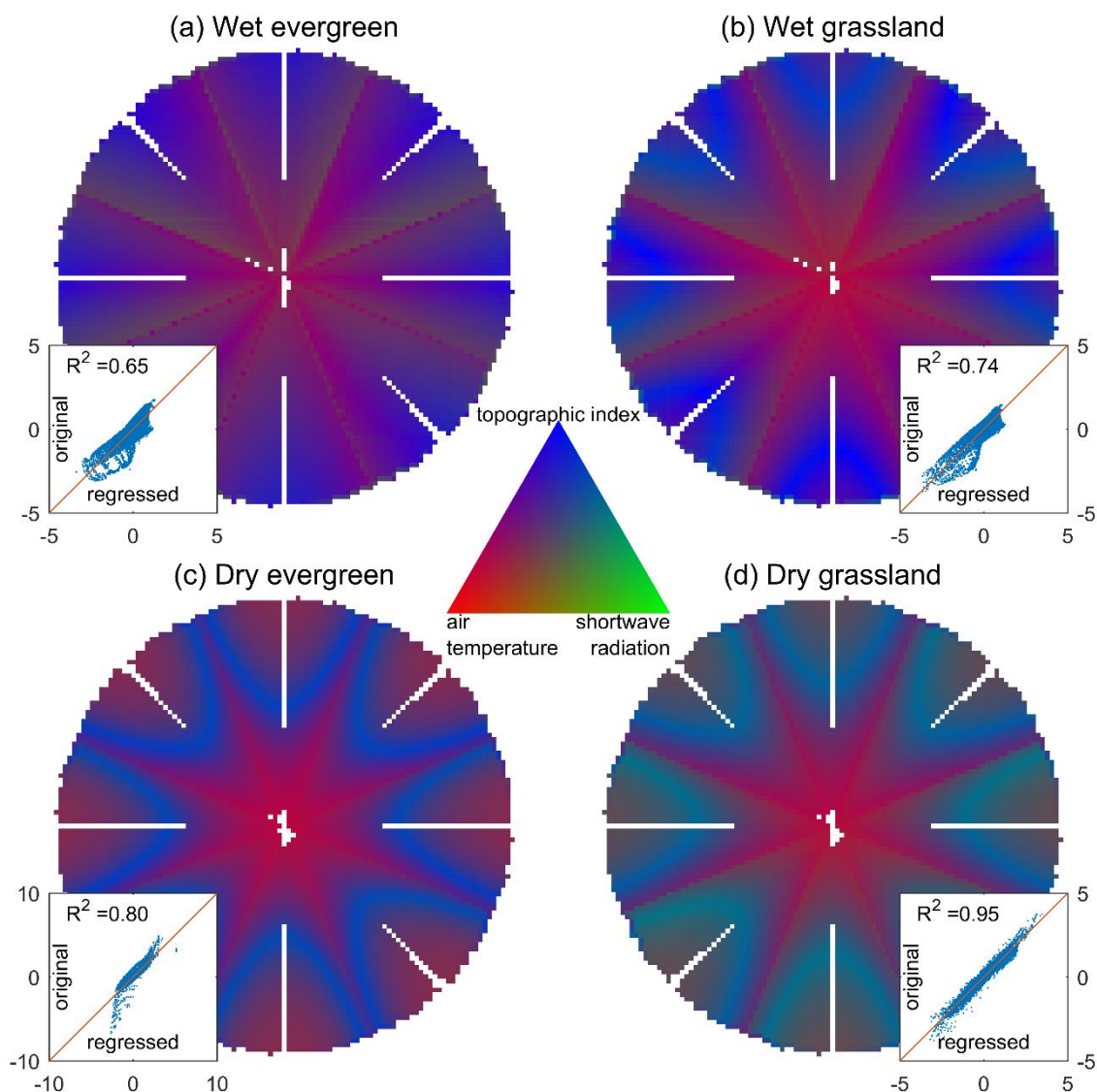


Figure 3.8 Normalized sensitivity of net primary production (NPP) to air temperature, shortwave radiation, and topographic index in the four experiments on the synthetic domain. The red colour represents areas where temperature is the main control for NPP, green represents the radiation-limited areas, and blue is for areas where the topographic index is the dominant control. Inset scatter plots show the comparison between the original model output (“original”) and the values that are calculated with the regression formula that was used for the sensitivity analysis (“regressed,” R^2 values are also shown). All variables are normalized.

3.3.1.3 The role of catchment orientation

When aggregating the model output to the catchment level of the synthetic domain (eight catchments along the cardinal and intercardinal directions), the differences in mean annual radiation between the north- and south-facing catchments are roughly 16% (Figure 3.9a) and only up to 12% for most ecosystem variables in all four synthetic experiments (Figure 3.9b–f). Transpiration of the wet evergreen forest peaks in the south-facing catchment, whereas NPP of the dry grassland peaks in the north-facing catchments (Figure 3.9b, d).

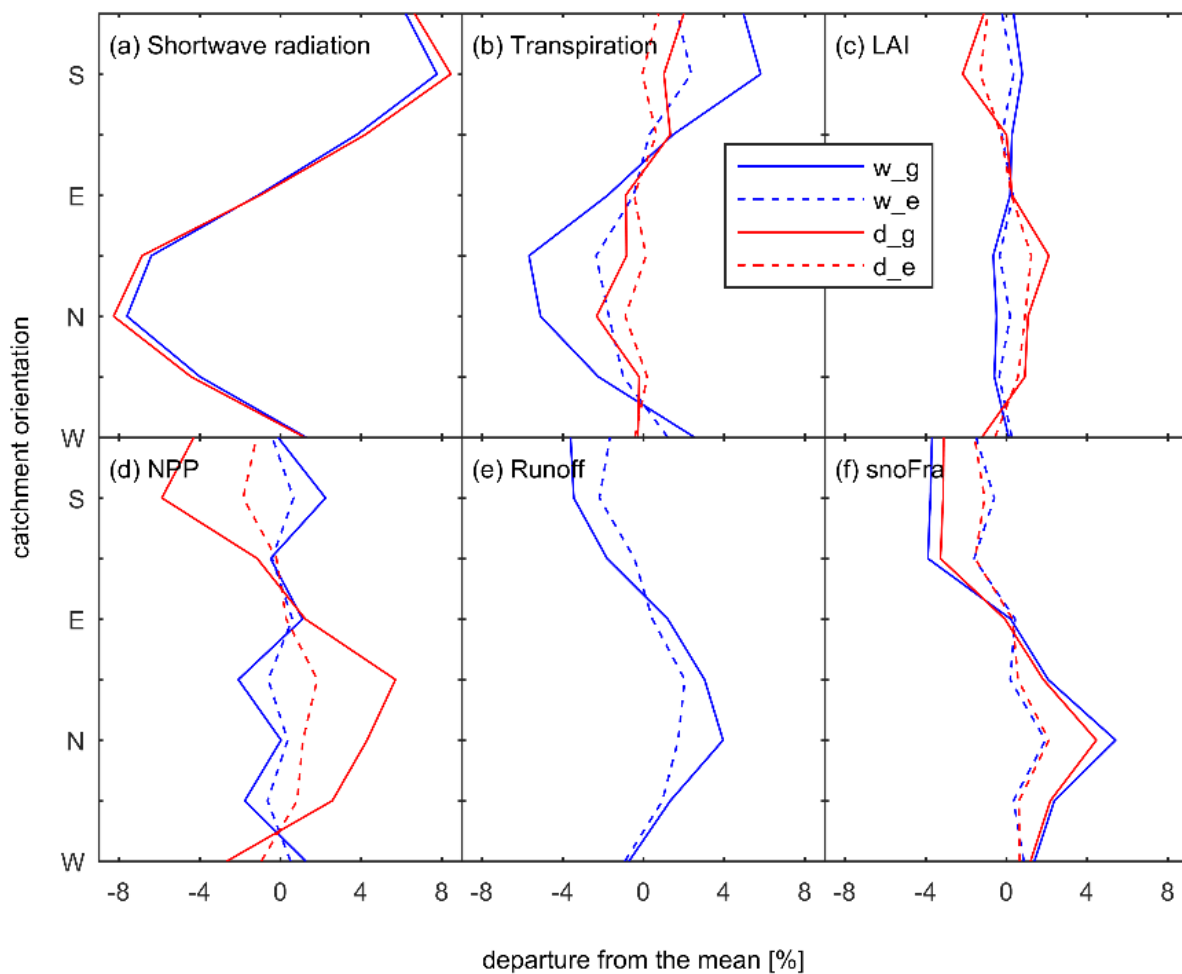


Figure 3.9 Departure of the mean of each catchment from the mean of the whole domain (expressed in % of the latter) for (a) shortwave radiation; (b) transpiration; (c) leaf area index (LAI); (d) net primary production (NPP); (e) runoff; and (f) fraction of time with snow cover (snoFra). S, E, N, and W on the y-axis denote the orientation of the catchment (south, east, north, and west, respectively). The blue lines represent the wet climate, and the red lines represent the dry climate. Continuous lines are used for the grassland and dashed for the evergreen forest (w_g, w_e, d_g, and d_e stand for wet grassland, wet evergreen forest, dry grassland, and dry evergreen forest, respectively). Subplot (e) shows only the runoff of the wet experiments, because the runoff of the dry experiments is almost zero.

The radiation signature in hydrological variables is consistent with expectations that north exposed catchments produce higher runoff because of the longer snow cover duration and lower evapotranspiration, but the differences are relatively small in magnitude, typically between $\pm 4\%$ of the total domain average (Figure 3.9e, f).

3.3.2 Variability across spatial scales

3.3.2.1 *The Kleine Emme catchment*

Figure 3.2 shows the spatial distribution of several simulated vegetation and hydrological variables (Figure 3.2d–i). Spatial aggregation decreases the variability of topographic index faster than the variability of air temperature, which coincides with the spatial variability of elevation (as expected, since air temperature was computed based on elevational gradients, Figure 3.10). This is because the topographic index is more sensitive to the smoothing of the complex terrain (lower correlation length scale) that is induced by aggregation compared with elevation. The spatial variability of these two topography-related variables envelops the spatial variability of transpiration, NPP, LAI, and snow cover duration (snoFra) across the whole spectrum of spatial scales, that is, from 100-m to 20-km spatial resolution (Figure 3.10). The decrease of spatial variability with aggregation is rapid; aggregating the results to 40 cells (~4-km resolution, instead of the original 100-m resolution) leads to at least 50% lower standard deviation in several ecosystem variables, which is a signal of the high spatial variability in the catchment and the low correlation length scale (Figure 3.10). The spatial variability of the time fraction with snow cover follows the spatial variability of air temperature, which implies that the two variables are closely related, as expected, because temperature is the most important driver of snow cover duration. However, the main driver of the spatial variability in the other ecohydrological variables (such as transpiration and NPP) cannot be estimated with this analysis, because the spatial variability of topographic index and shortwave radiation follow similar trajectories (Figure 3.10).

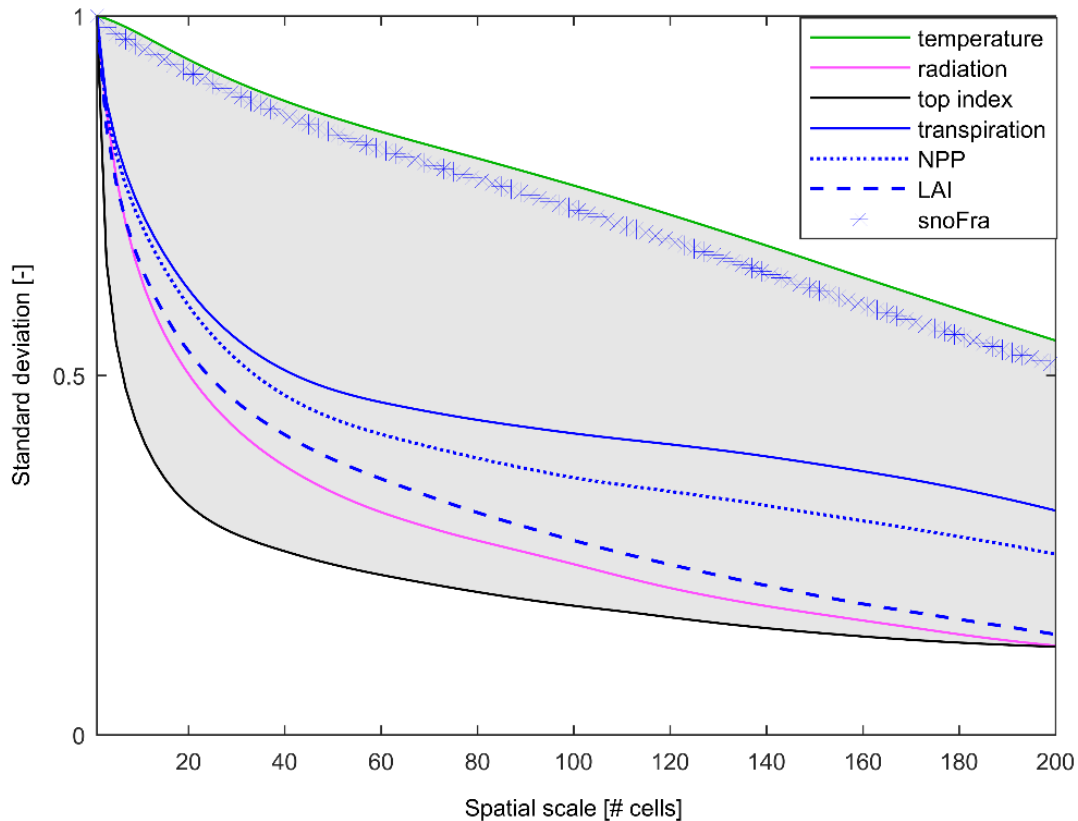


Figure 3.10 Meteorological, topographic, and ecosystem spatial variability in the Kleine Emme catchment. Normalized Standard deviation as a function of spatial scale for air temperature, shortwave radiation, and topographic index in green, magenta, and black, respectively. Blue lines represent the spatial variability of several ecohydrological variables: the continuous line is for transpiration, the dotted line for net primary production (NPP), the dashed line for leaf area index (LAI), and the line with the star markers corresponds to the time fraction with snow cover (snoFra). Temperature and topographic index create an envelope that contains all the ecohydrological variables (shaded). All variables are normalized so that the standard deviation equals one for the original resolution of the simulations (100-m grid). For an explanation of the aggregation, see Fig. B.9 (Appendix B).

3.3.2.2 Synthetic domain

The four experiments on the synthetic domain reveal considerable differences among vegetation types and climates (Figure 3.11). The most variable meteorological input in both examined climates is air temperature, the RV of which exceeds 50%. The RV of shortwave radiation is approximately 26%, and precipitation is almost uniform throughout the synthetic domain in the dry climatic conditions (Figure 3.11a–c). Results from the T&C simulations show that the RV for transpiration, LAI, and NPP is lower in dry conditions (RV < 30%) compared with wet conditions (up to 40%) and lower in evergreen forests (<20%) compared with grasslands (up to 40%, Figure 3.11d–f). Hydrological variables follow the same pattern: The wet grassland shows the largest spatial variability, and the dry evergreen forest is the least variable (Figure 3.11g–i). The analysis of variance when aggregating to larger spatial scales shows that the ecosystem variables of the wet ecosystems decline with aggregation scale similarly to Kleine Emme (Figure 3.12b–c), but the variability of NPP in the dry

cases drops much faster (Figure 3.12d), and even falls out of the topographic index-temperature envelope. The decline of spatial variability of snow cover duration follows that of air temperature as in the case of the Kleine Emme catchment (Figure 3.12e).

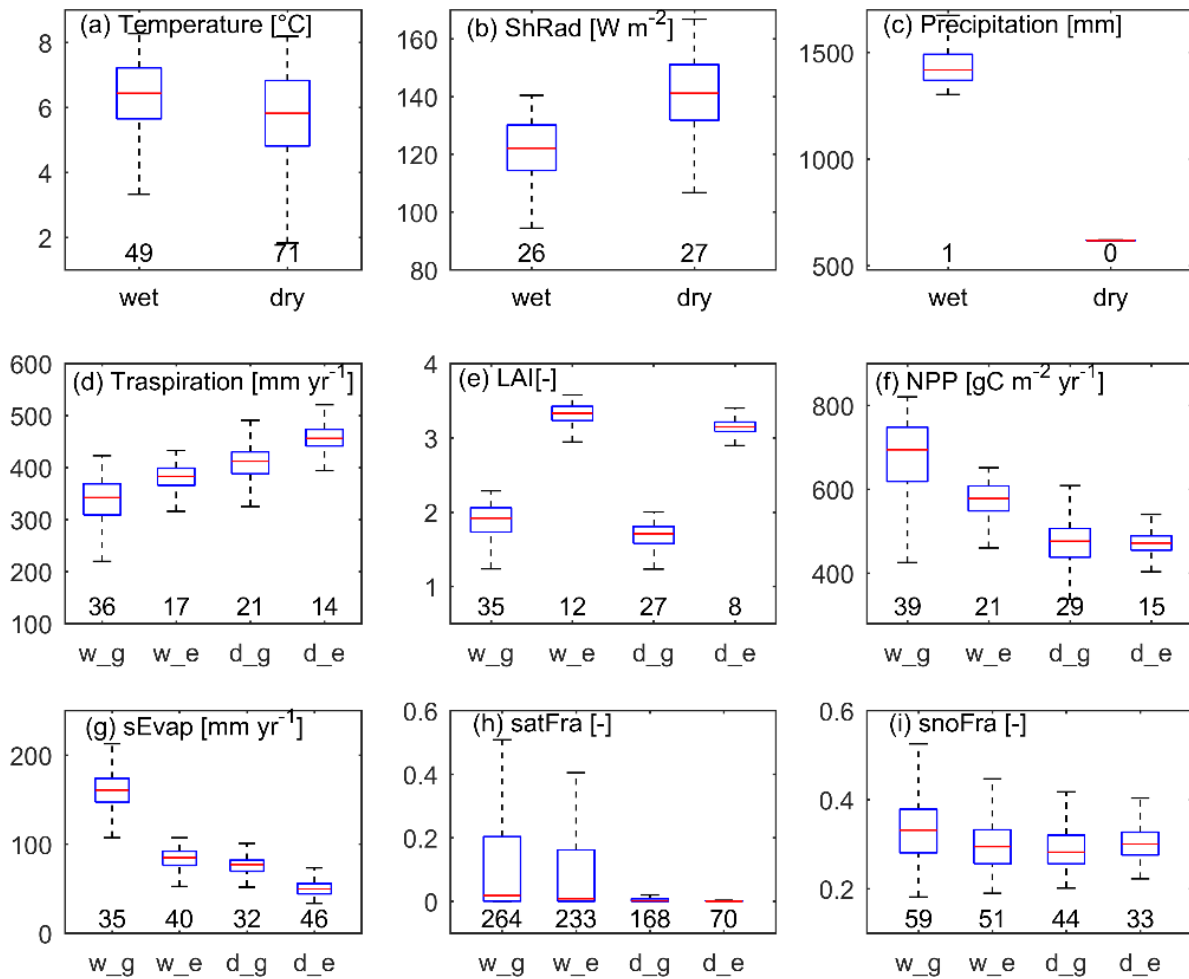


Figure 3.11 Range of spatial variability in the four experiments in the synthetic domain. Boxplots of (a) temperature, (b) shortwave radiation (ShRad), (c) precipitation, (d) transpiration, (e) leaf area index (LAI), (f) net primary production (NPP), (g) soil evaporation (sEvap), (h) fraction of time with soil saturation (satFra), and (i) fraction of time with snow cover (snoFra). For the meteorological forcing (a–c), we distinguish between the wet and dry experiments and for the ecohydrological variables we distinguish also between grassland and evergreen (using the symbols w_g, w_e, d_g, and d_e for wet grassland, wet evergreen forest, dry grassland, and dry evergreen forest, respectively). Each boxplot represents the 4-year average annual values for each simulated cell of the domain. The box length provides the interquartile range (I_{QR}), the bottom of the box the 25th percentile (first quartile, q_1), the top of the box the 75th percentile (third quartile, q_3), and the horizontal line within the box the median value. The lower whisker corresponds to $q_1 - 1.5I_{QR}$, or to the minimum estimate, and the upper whisker corresponds to $q_3 + 1.5I_{QR}$, or to the maximum estimate. The number on the x-axis is the range of variability (RV), as defined in Appendix A.4. Outliers outside the whiskers are not shown.

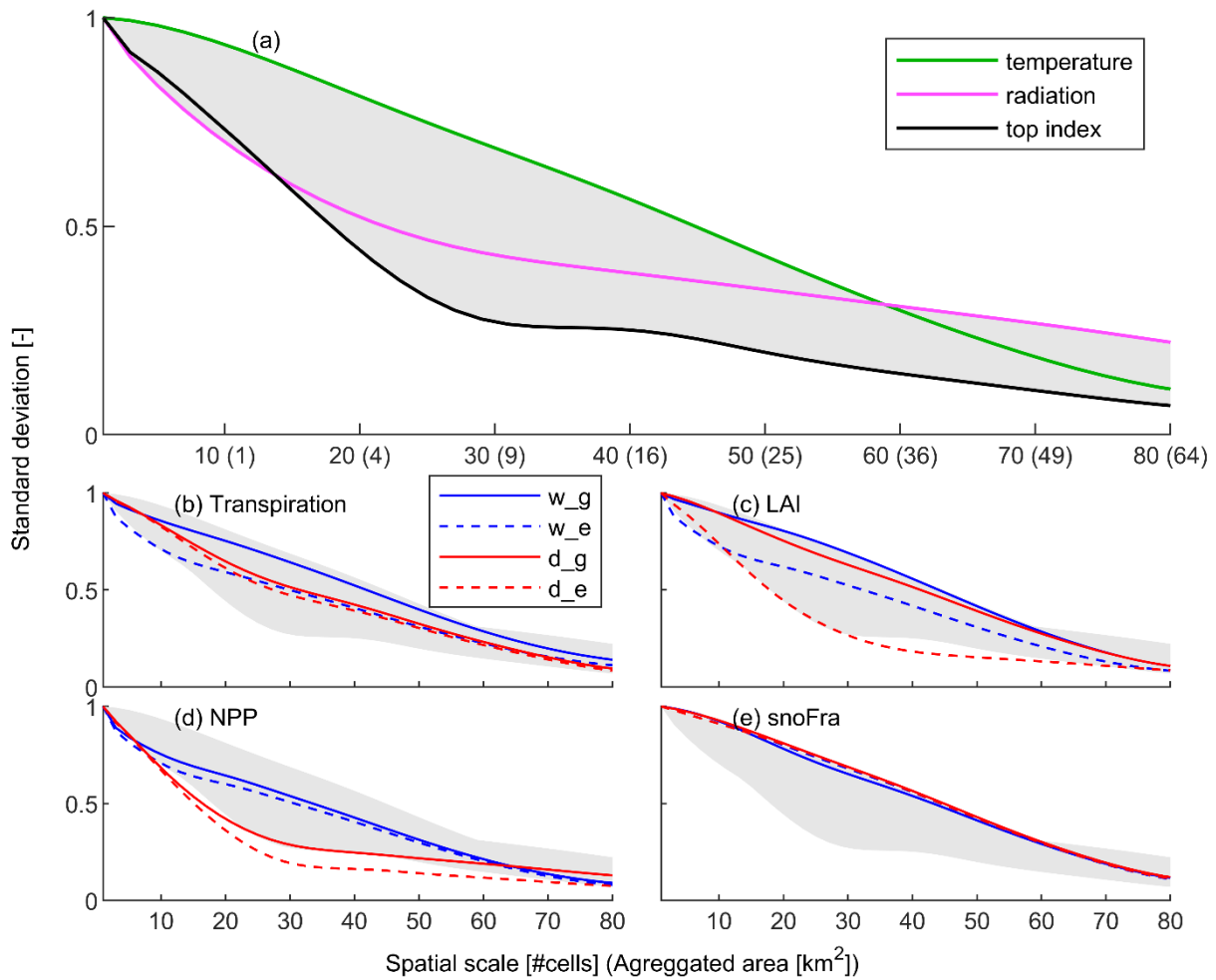


Figure 3.12 Meteorological, topographic, and ecosystem spatial variability in the four experiments on the synthetic domain. Normalized standard deviation as a function of spatial scale for (a) air temperature, shortwave radiation, and topographic index in green, magenta, and black, respectively; (b) transpiration; (c) leaf area index (LAI); (d) net primary production (NPP); and (e) fraction of time with snow cover (snoFra). In subplots (b–e), red lines represent the dry ecosystems and blue the wet ones; dashed lines are used for evergreen forest, and continuous lines are used for grassland (w_g, w_e, d_g, and d_e stand for wet grassland, wet evergreen forest, dry grassland, and dry evergreen forest, respectively). The three variables of subplot (a) create an envelope that contains most ecohydrological variables in all experiments (shaded). All variables are normalized so that the standard deviation equals one for the original resolution of the simulations (100-m grid). X-axis in subplot (a) also shows the area that is aggregated for each spatial scale (in km²).

3.4 DISCUSSION

3.4.1 Ecosystem sensitivities

The use of natural gradients is common when studying ecological responses to potential changes on climate (e.g., Dunne et al., 2004), but to our knowledge, no distributed ecohydrological modelling study has incorporated this approach to date. The advantage of this approach relies in using a single distributed simulation for each scenario where spatial gradients are exploited to infer ecohydrological sensitivities to a number of explanatory variables.

3.4.1.1 *Ecosystem sensitivity to air temperature*

We found that the vegetation is limited by low air temperature in large parts of both the Kleine Emme catchment (Figure 3.5a–d) and the synthetic domain (Figure 3.7a–d, B.14b–d, B.15a–d, and B.16a–d), as expected in an Alpine environment. Based on the model output, we are able to quantify these sensitivities, providing estimates of expected changes in NPP, ET, etc., for a unit change in air temperature. This temperature sensitivity is correlated with elevation; in higher (colder) parts, temperature is the strongest control of ecosystem response. In agreement with our results, a study on a coniferous forest in a slightly wetter environment compared with our dry evergreen forest also found that transpiration sensitivity to air temperature increases with elevation (Christensen, Tague, & Baron, 2008).

When moving to lower elevation, the sensitivity of several ecohydrological variables to temperature declines and can even reverse sign. Air temperature has a negative effect on NPP in the lower catchment parts in the two dry experiments (Figure 3.7c–d). This reveals a threshold below which the vegetation is water-limited and thus an increase in temperature enhances transpiration early in the growing season, and consequently reduces soil moisture and vegetation productivity at the annual scale. This threshold occurs at slightly higher elevation for the evergreen forest than for the grassland (around 1700 m a.s.l.), in agreement with a previous study (Rössler et al., 2012). The results of the dry grassland experiment confirm another modelling study in a dry Alpine hillslope (Della Chiesa et al., 2014); the presence of an elevation threshold reveals a shift from energy- to water-limited ecosystems in these inner-Alpine dry valleys. This threshold is a function of the amount and the elevational gradient of precipitation and of the fraction of precipitation falling as snowfall.

The wet evergreen forest stands out from the other ecosystems in terms of transpiration and ET sensitivity to temperature (Figures B.14a and B.16a). Transpiration sensitivity to air temperature does not change with elevation (unlike the other experiments) and the sensitivity of ET to temperature is negative at high elevations, mainly because of the contribution of sublimation. Indeed, snow sublimation ranges from close to zero at lower elevations up to roughly 200 mm yr⁻¹ in the top of the domain, in agreement with a previous study in the Alps (Strasser et al., 2008). Evaporation and sublimation from interception is higher in the evergreen forest due to the higher amount of snowfall interception and the larger exposure to wind (lower aerodynamic resistance). In this case, sublimation is negatively correlated with temperature and affects the sensitivity of the whole ET flux to temperature. These findings are also obtained for the evergreen forests in the Kleine Emme catchment, but the heterogeneous vegetation cover makes this pattern less evident (Figure 3.5a–b).

3.4.1.2 *Ecosystem sensitivity to shortwave radiation*

Transpiration and ET exhibit a positive sensitivity to radiation in most parts of the wet domains (Figure 3.5e–f, B.14e–f, and B.16e–f). The sensitivity of NPP and LAI to radiation depends on the slope orientation: south-facing slopes are radiation-saturated, whereas north-facing slopes are radiation-limited in Kleine Emme and the two wet experiments in the synthetic mountain (Figure 3.5g–h, Figure 3.7e–f, and B.15e–f).

In the dry climate, the negative effect of radiation is one order of magnitude larger than the positive effect in the wet climate in all ecohydrological variables. It is also stronger in south-facing slopes for all ecohydrological variables (Figure 3.7g–h, B.14g–h, B.15g–h, and B.16g–h), which shows that the south-facing slopes in the inner-Alpine valleys might be drought-prone. The negative effect of radiation is an indirect effect due to a temporary increase of transpiration and ET that leads to an emergence or a quicker onset of water stress and an overall reduction of NPP, LAI, transpiration, and ET at the annual scale.

3.4.1.3 Ecosystem sensitivity to water availability

The maps of topographic index sensitivity in Kleine Emme show that transpiration and ET are negatively correlated with topographic index (Figure 3.5i–j). The sensitivity of NPP and LAI to topographic index is mostly negative and only slightly positive along some ridges (Figure 3.5k–l), which may imply that an increase in soil moisture would be beneficial for vegetation in these steep hillslopes.

In the wet experiments, all ecosystem variables show a negative sensitivity to topographic index (Figure 3.7i–j, B.14i–j, B.15i–j, and B.16i–j), but, contrary to the Kleine Emme catchment, the sensitivity is uniform across elevations. The negative sensitivity is the result of temporary saturation and sporadic water logging in topographically convergent areas, which suppresses vegetation productivity.

In the dry scenarios, the sensitivity to topographic index is instead positive and relatively uniform throughout the domain (Figure 3.7k–l, B.14k–l, B.15k–l and B.16k–l). Topographic convergent areas, which are generally wetter (because they receive contributions of surface and subsurface water from upstream cells), are less water-limited. Studies of the spatiotemporal variability of transpiration and ET in a catchment covered by coniferous evergreen forest in the US (comparably dry to our dry scenarios) showed that the sensitivity to soil moisture depends on air temperature (or, equivalently, elevation) (Christensen et al., 2008; Lundquist & Loheide, 2011). However, we did not detect a significant interaction between the sensitivity of ET to topographic index and elevation in the dry experiments (Figure B.14i–l).

3.4.1.4 Which is the dominant driver of Alpine ecohydrological processes?

Air temperature emerges as the main control of NPP and LAI in most parts of the Kleine Emme catchment (Figure 3.6, and B.10). Temperature is also the dominant control of transpiration and ET at the highest elevation of the synthetic domain. The analysis in the synthetic domain verifies that in all cases (except for the wet evergreen forest transpiration and ET and the dry grassland ET) temperature is the dominant driver of ecohydrological processes, at least above 1800 m a.s.l. (Figure 3.8, B.17, B.18 and B.19); sensitivity patterns in wet ecosystems agree with the results from the Kleine Emme catchment. Many researchers have concluded that mountain ecosystems are particularly sensitive to temperature; from dry grasslands in the Tibetan Plateau (Saito, Kato, & Tang, 2009) to the treeline in the Patagonian mountains (Mayor et al., 2017) air temperature is a key ecosystem

driver. Thus, the dominant role of temperature does not come as a surprise, but its absolute quantification and relative comparison with the other variables is an innovative contribution of this modelling study.

In the dry scenarios, where the sensitivity to temperature changes from positive to negative when moving from higher to lower areas, we found an intermediate zone, in which topographic index is the dominant limiting factor, only because the other controls become much smaller. Note that in low-elevation areas, temperature exerts an important but indirect control because it reduces ET, transpiration, and vegetation productivity by enhancing water stress and altering the seasonal dynamics of these variables.

3.4.2 How important is catchment orientation?

The comparison between catchments with different orientation shows that the role of shortwave radiation is evident mostly in snow-related processes and runoff, whereas vegetation is less affected by aspect. Grasslands and forests show distinct patterns; In grasslands, snow stays up to roughly 10% longer in the north-facing compared with the south-facing catchments, but in the evergreen forests, this difference between snow duration in north- and south-facing catchments is only roughly 4% (Figure 3.9f). This implies that taller vegetation homogenizes the spatial variability of snow cover duration. Previous studies have found a similar homogenizing effect of tall vegetation on snow temporal distribution (e.g., Strasser, Warscher, & Liston, 2011) because tall canopies intercept snow, shade shortwave radiation and enhance longwave radiation in spring (Lundquist, Dickerson-Lange, Lutz, & Cristea, 2013).

A study in a relatively dry mountain in northern New Mexico, US, showed that the catchment orientation strongly controls vegetation productivity (Zapata-Rios et al., 2016) in an ecosystem that is severely energy-limited (thus, NPP is lower in the north-facing slopes). However, we found that dry evergreen NPP is uniform across catchments with different orientation for most experiments. Only NPP of the dry grassland peaks in the northeast-facing catchment, because water limitations are a dominant control and north-exposed catchments with lower radiation are less water-stressed (Figure 3.9d). The differences between the two studies might be due to the different elevational range and latitude; the case study of the aforementioned paper is higher and at lower latitude than our synthetic domain, and thus, differences in energy loads across catchments may be more pronounced.

We found that LAI in all cases is rather insensitive to the catchment orientation. Transpiration in the wet grassland peaks in the south-facing catchment, indicating an energy-limitation, but it is relatively insensitive in the other scenarios (Figure 3.9b). Overall, our findings show that the catchment-integrated effect of radiation on Alpine ecosystems is smaller than expectations based on the complex topography of these environments, because low air temperature is the most limiting “energy” control. However, these results are obtained with a relatively simplified experiment (e.g., uniform soil properties and vegetation) that may not capture all the complex signatures of aspects in the hillslopes (see 3.4.4.2).

3.4.3 Cross-scale spatial variability in Alpine ecohydrology

We examined how the spatial variability in major ecohydrological processes changes when aggregating the model results. Based on the simulations of a Swiss Alpine catchment and a synthetic mountainous domain (which mimics the complex topographic features that occur in steep Alpine valleys), we quantified the rapid loss of variability (20–40%) for many ecohydrological processes when averaging the results over a 20 times larger spatial resolution (2 km instead of 100 m, Figures 3.10 and 3.12). The integration in catchments of ~ 9 km² with different orientations in the synthetic domain, where differences are usually less than 10% for all simulated variables (Figure 3.9), supports the results obtained for the Kleine Emme catchment.

Interestingly, the decay in variability of ecosystem drivers (e.g., air temperature and topographic index) envelops the decay in variability of ecosystem responses (ecohydrological variables), thus highlighting that the ecosystems can buffer the topographic and meteorological variability not only in time (Pappas et al., 2017) but also in space (Figures 3.10 and 3.12). For the dry evergreen forest, LAI and NPP fall outside this envelope (Figure 3.12c–d), implying that probably the topographic index itself cannot fully explain the role of water availability. Using a coarser spatial resolution, beyond neglecting ecosystem spatial heterogeneity, can potentially also affect the overall mean in the domain and thus the large-scale fluxes (Pappas et al., 2015). The presented results reinforce several recent studies that have demonstrated the potential of high-resolution simulations in better capturing ecohydrological dynamics under current or future conditions (Etchanchu et al., 2017; Le & Kumar, 2017; Passalacqua et al., 2015), especially when identification of patterns is sought.

Another emerging aspect is the role of evergreen forests and dry climate in reducing the spatial heterogeneity in the ecohydrological response (Figure 3.11). When compared with grasslands, evergreen forests have deeper roots and larger LAI; thus, they tend to respond less than grasslands to local microclimatic conditions and elevation differences, which explains the reduced spatial variability in ecohydrological variables of the evergreen forests. A similar effect is generated by the dry climate in the synthetic mountain, which leads to more widespread water limitations, thus dampening spatial variability when compared with the wet scenario.

The spatial variability of each ecohydrological variable follows a different trajectory across aggregation scales. The proximity of the spatial variability of topographic or meteorological variables provides a qualitative link to the main driver of the ecohydrological dynamics. This is apparent in the snow-related variables (e.g., duration of snow cover), the variability of which follows air temperature in the Kleine Emme catchment (Figure 3.10) and in all the experiments on the synthetic domain (Figure 3.12e). Other variables are less easy to interpret, but in general, wet ecosystems and grasslands tend to be more temperature driven, whereas for dry ecosystems and for evergreen forests, soil moisture and radiation are also important. These findings confirm the results of the sensitivity analysis.

The analysis of spatial variability presented here, besides revealing the connections between the spatial scaling of ecohydrological and topographic/meteorological variables, represents a preliminary

step towards an improved understanding of the role of spatial scaling in ecohydrology. Previous modelling attempts explored the relations between hydrological processes and the spatial patterns of vegetation by using different aggregation methods, based on synthetic networks of flow paths (e.g., Thompson et al., 2011) or linking the hillslope scale to the catchment scale (e.g., Hwang, Band, & Hales, 2009). Results presented here, show that T&C could offer an opportunity to further explore these interactions.

3.4.4 Limits of interpretation

3.4.4.1 *Lateral water flows and soil moisture*

The T&C model simulates lateral surface and subsurface water flows, which are currently neglected in many land surface models. Recent studies showed that models incorporating these processes (e.g., Ivanov et al., 2008a) can simulate the heterogeneity of water and energy fluxes more realistically (Ji, Yuan, & Liang, 2017; Maxwell & Condon, 2016). This model advantage is reflected in the simulated patterns of soil effective saturation and subsequently on the spatial patterns of transpiration, LAI and NPP (Figures 3.2, 3.4, B.6, B.7 and B.8).

In both experiments on the wet climate, the soil in the valleys is saturated for almost the entire simulation period; this might be an artefact of the design of the synthetic domain, because each catchment is designed to maximize convergence and thus the collection the water. Another possible source of long-periods with saturation might be the assumption on which the model simulates the subsurface water flow. T&C uses the kinematic wave approximation (i.e. assumes that the hydraulic head parallels the surface topography), which is invalid in shallow terrains (Brutsaert, 2005; Chow, Maidment, & Mays, 1988; Vieira, 1983). For this reason, the model might overestimate the soil moisture in the near-stream areas. The use of uniform soil depth in both the synthetic domain and the Kleine Emme catchment might also bias the simulated soil moisture. Indeed, previous research showed that soil depth varies with elevation (e.g., Bertoldi, Rigon, & Over, 2006) and variations in soil depth can affect transpiration patterns (Tromp-van Meerveld & McDonnell, 2006) and thus soil moisture and discharge.

The calibration against discharge shows that T&C performs slightly poorer during periods of low flow (Figures B.3, B.4 and B.5), which may reflect effects of heterogeneity in the subsurface boundary conditions that the model either ignores or simulates in a simplistic way, such as variabilities in soil or root depth or the presence of groundwater. These can potentially contribute to streamflow and also to plant available water during periods of low soil moisture (Klos et al., 2018; Rodriguez-Iturbe, D'Odorico, Porporato, & Ridolfi, 1999). Especially, the assumption of a uniform soil depth and impermeable bedrock precludes the representation of deeper storage that could feed the stream during dry periods.

Another possible source of uncertainties is the use of the topographic index as a proxy for soil moisture effects on ecosystem functioning. This was a simplification imposed by the lack of a better independent proxy for soil moisture, and because the use of the simulated soil moisture would bias the robustness of the statistical analysis. Topographic index, being a steady-state metric, cannot

capture soil moisture temporal dynamics that are triggered by the timing of precipitation. Thus, the transitions between energy- and water-limited ecosystems shown in this study can only be regarded as a general overview of the main drivers of Alpine ecohydrology; the real patterns might be much more complex in space and variable in time.

Despite these possible sources of bias, our results for the Kleine Emme catchment (where grid cells close to the stream network, generally covered by grass, are saturated for about 80% of the time) are supported by a study in a pre-Alpine catchment (Hingerl et al., 2016). We note that (regardless of the validity of the simulated soil moisture) the grassland parameterization adopted for this environment might be unsuitable since near-stream and riparian areas are generally covered by vegetation adapted to wet environments (e.g., similar to wetlands). Therefore, the use of a single parameterization for grass probably leads to an overestimation of the ecosystem sensitivity to high soil moisture conditions in these areas.

3.4.4.2 Synthetic mountain set-up

Additional uncertainties arise from the simplicity of the synthetic domain. The choice of clay loam soil might lead to lower drainage capabilities and to overestimate soil moisture, since in most parts of the Alpine region soil texture is typically coarser (e.g., more sandy soils). We chose this solution to counterbalance the cumulative drainage imposed by the length of the continuous hillslopes, which is much longer in the synthetic domain than in reality. Additionally, beyond radiation, other ecosystem properties that we held constant in space in our analysis may co-vary with aspect. For example, soil texture and organic matter may differ between north- and south-facing slopes (e.g., Egli et al., 2009; Egli, Mirabella, Sartori, Zanelli, & Bischof, 2006), soil depth and vegetation characteristics may also covary with aspect (e.g., Hörsch, 2003) potentially producing indirect effects of aspect that cannot be accounted for in the presented analysis. For instance, a tree-ring study in the Italian Alps showed that the sensitivity of tree growth (which is related to variables we simulated, e.g., NPP) to air temperature changes with aspect (Leonelli et al., 2009). Indeed, a study in a Californian pine forest showed that tree sensitivity to temperature may even change sign from north- to south-facing slopes (Salzer, Larson, Bunn, & Hughes, 2014). However, we detected practically no interaction between ecosystem sensitivity to air temperature and aspect. This might be also due to the meteorological input we used for the model simulations, which was based on elevational lapse rates, thus, neglecting any effect of topographic features –other than elevation– on meteorological variables (e.g., T&C air temperature fields ignores the effect of aspect).

3.4.4.3 The use of the “space-for-time” approach

The innovative application of the “space-for-time” approach on model outputs offers an attractive alternative at the local scale to the traditional approach in which uncertainties from climate change projections and downscaling techniques would propagate and affect the model output (e.g., Rössler et al., 2012). However, the regressions between the ecohydrological responses and the three explanatory variables (i.e. air temperature, shortwave radiation and topographic index) cannot fully describe the spatial variability in the variables simulated by T&C. These regressions are slightly

poorer in Kleine Emme (insets in Figure 3.6, B.10, B.11, B.12 and B.13) than in the synthetic domain (insets in Figure 3.8, B.17, B.18, B.19 and B.20). We found that the three explanatory variables can describe the ecohydrological responses of grasslands better than those of evergreen forests in the synthetic domain (e.g., Figure 3.8c and d) but not in the Kleine Emme catchment (e.g., Figure 3.6a and c). Experiments in the synthetic domain show that ecosystems in dry climate are better approximated than ecosystems in wet climate (e.g., Figure 8a and 8c). Lower R^2 implies that the three explanatory variables do not explain completely the spatial variability in the dependent variable; indeed, evergreen forests are more difficult to describe with a simple regression than grasslands and, in wet conditions, the limitations by water ponding may also downgrade the explanatory power of the regressions. This is evident, for example, in the departure from the 1-1 line in the scatter inset of Figure 3.8c, B.17c and B.18c. The application of this approach for estimating climate change impacts on ecosystems also implies that the response of the ecosystems will follow the same principles that shaped its current spatial distribution, a hypothesis that might be invalid if the climate changes with unprecedented speed (e.g., Voepel et al., 2011). This hypothesis might also be inappropriate across large climatic and vegetation gradients where spatial sensitivities are typically larger than temporal ones (Faticchi & Ivanov, 2014; Hsu, Powell, & Adler, 2012; Huxman et al., 2004).

The space-for-time approach assumes that ecosystems will track changing climate in the same way that ecosystems currently vary with climatic variability in space (Dunne et al., 2004). However, many processes may confound the applicability of this approach (e.g. fine-scale environmental heterogeneity, Villalba, Veblen, & Ogden, 1994). Most importantly, the rapid pace of climate change may exceed the current climatic range pushing ecosystem to unexperienced limits (Davis, 1989; Diffenbaugh & Field, 2013).

3.4.4.4 Simulating vegetation fitness and mortality

The evergreen forest in the upper part of the dry synthetic domain (which is also slightly colder than the wet domain) showed declining activity throughout the five years of the simulation. This implies that the model would predict a climate-driven forest line roughly between 2100 and 2200 m a.s.l. in agreement with GIS estimates for Valais (Szerencsits, 2012). However, the evergreen forest in the wet climate did not show any decline with time even at the highest elevation (2500 m a.s.l.), although the forest line in the corresponding area (from which the meteorological data were used) lies even lower than in Valais (Szerencsits, 2012). This points to model limitations in capturing vegetation productivity decline near the tree line. More generally, the failure of the model to predict the tree line may also convey a poor representation of tree mortality and temperature limitations on tree growth (Leuzinger, Manusch, Bugmann, & Wolf, 2013). For example, while the model considers low-temperature stress in vegetation functioning, it ignores the effects of insects, which are an important disturbance for forests (Lindner et al., 2010; Rebetz & Dobbertin, 2004). It could also be a sign that reasons other than air temperature may also be important for the altitude of the forest line, such as changes in land use (Bolli, Rigling, & Bugmann, 2007), or windthrow (Elkin et al., 2013).

3.5 CONCLUSIONS

We used a spatially explicit mechanistic model to simulate with fine spatiotemporal resolution major ecohydrological processes in an Alpine catchment. The analysis of the spatial variability of several simulated ecohydrological variables shows that the vegetation in the wet Alpine areas is strongly temperature-limited, as previously found (Bolli et al., 2007), but the dry inner-Alpine catchments are water-limited, especially below 1700 m a.s.l. (Della Chiesa et al., 2014; Leitinger et al., 2015; Rebetz & Dobbertin, 2004; Rössler et al., 2012). Results on a synthetic domain show that the signal of radiation (associated with different aspects) on runoff is less than 10% for different climatic conditions and vegetation cover in the Alps. By examining how the variance of ecohydrological variables changes across spatial scales, we identified that spatial variability of ecosystem drivers envelopes that of ecosystem responses. Despite the simplifications, our analysis shows that in the absence of high-resolution measurements of ecohydrological variables, models offer a unique opportunity to explore the dependence of ecohydrological processes on spatial scales. The fact that different vegetation types exhibit different sensitivity patterns confirms that the ongoing changes in vegetation composition can affect the Alpine ecohydrology (Köplin et al., 2013; van den Bergh, Körner, & Hiltbrunner, 2017) in very complex ways. Mitigating the climate change effects in these ecosystems requires more large-scale high-resolution simulations at the Alpine scale, which can provide the framework to guide future monitoring campaigns and further improve our understanding of ecohydrological processes at mountain ecosystems.

Author contribution

S.F., T.M., C.P. and P.M. designed the study. T.M. performed the simulations and the analyses and plotted the figures. P.H. assisted with the code parallelization. T.M. wrote the manuscript with contributions from all authors.

Acknowledgements

T. M. and S. F. thank the support of the Stavros Niarchos Foundation and the ETH Zurich Foundation (Grant ETH-29 14-2). C. P. acknowledges the support of the Swiss National Science Foundation, the Stavros Niarchos Foundation, and the ETH Zurich Foundation (Grants P2EZP2_162293 and P300P2_174477).

More green and less blue water in the Alps during warmer summers

Abstract

Climate change can reduce surface-water supply by enhancing evapotranspiration in forested mountains, especially during heatwaves. We investigate this “drought paradox” for the European Alps combining a new database of 1212 stations and hyper-resolution ecohydrological simulations to quantify the blue (runoff) and green (evapotranspiration) water fluxes. Here, we found that during the historical 2003 heatwave, evapotranspiration was largely above average, despite the exceptionally low precipitation, amplifying the runoff deficit by 32% in the most runoff-productive areas (1300-3000 m a.s.l.). At the annual timescale, a 3°C temperature increase enhance annual evapotranspiration by up to 100 mm, which would reduce runoff similarly to a 3% precipitation decrease. This suggests that green water feedbacks, which are often poorly represented in large-scale assessments, pose an additional threat for water resources. We conclude that integrating hyper-resolution ecohydrological modelling into climate change impact assessments can support more realistic predictions of fresh water availability in mountain regions.

4.1 INTRODUCTION

Although relatively small in size, the European Alps (hereafter “Alps”) contribute a disproportionately large amount of water, especially during summer, to four major European rivers (Weingartner & Viviroli, 2007), in the basins of which reside more than 170 million people (European Environment Agency (EEA), 2009); hence the name “water towers of Europe” (Viviroli et al., 2007). However, droughts in central Europe are becoming more frequent (Briffa, van der Schrier, & Jones, 2009). The droughts of 2003, 2010, 2015 and 2018 have raised concerns about the vulnerability of the European water budget to climate change (European Environment Agency (EEA), 2009; Teuling, 2018) as these events have affected more than 17% of the European population (European Commission, 2007) with an annual economic impact exceeding USD 6.8 billion between 2001 and 2006. Temperature in the Alps is increasing at a fast pace (Brunetti et al., 2009), relative humidity is generally decreasing (Fatichi, Molnar, et al., 2015), evapotranspiration (ET) is increasing (Duethmann & Blöschl, 2018), while Alpine glaciers are shrinking and the distribution of snow is shifting to higher elevation (Beniston et al., 2018). Although there is consensus that climatic extremes will become more frequent (Samaniego et al., 2018), the complex topography, the interactions between water and vegetation, and the multiple processes shaping the water cycle in mountainous areas hinder the quantification of the different water budget components in traditional large-scale climate change assessment studies (Fan et al., 2019). For example, climatic change can shift the partitioning of water into blue (runoff) and green (ET) water fluxes (Falkenmark & Rockström, 2006; Orth & Destouni, 2018). Quantifying how these fluxes change seasonally and interannually is as much important as challenging.

Large uncertainties are associated with the vegetation response to water stress (Teuling, 2018). Studies in different parts of the Alps have found contrasting impacts of drought on vegetation (Jolly, Dobbertin, Zimmermann, & Reichstein, 2005), spanning from increased mortality in the dry inner-Alpine valleys (Timofeeva et al., 2017) to enhanced productivity in the wet pre-Alpine hills in the north (Seneviratne et al., 2012). These discrepancies emphasize that extrapolating results of specific case studies (e.g., Laghari, Vanham, & Rauch, 2012) to the entire Alpine domain or downscaling results of coarse resolution studies (e.g., Orth & Destouni, 2018) will lead to unreliable predictions (Mastrotheodoros et al., 2019). The largest component of land ET is plant transpiration (Good et al., 2015), which is poorly quantified due to the large variability in plant water use strategies and stomata sensitivity to water stress (Teuling et al., 2010). Land-surface models often represent the links between soil moisture and transpiration in a simplistic way (Seneviratne et al., 2006; Sheffield et al., 2012; Teuling, 2018). Most importantly, they do not resolve land-surface energy and water fluxes at sufficient resolutions to account for local topographic and microclimatic effects, and often ignore lateral flows of water in the subsurface (Bierkens et al., 2015; Fan et al., 2019; Rouholahnejad Freund & Kirchner, 2017; Wood et al., 2011).

Here, to overcome these limitations, we combined a new pan-Alpine database with hyper-resolution ecohydrological simulations to test the “drought paradox” hypothesis, i.e., that during droughts, ET may increase in a large fraction of the Alps at high elevations, thus amplifying the runoff deficits (Teuling et al., 2013). We used meteorological, discharge, and snow depth measurements at more

than 1200 stations across the entire Alpine domain together with distributed products of meteorological variables, soil texture, and land cover characteristics to drive the ecohydrological model Tethys-Chloris (T&C, Mastrotheodoros et al., 2018). The model resolves the water, carbon and energy budgets at the hourly time scale in a physically based and spatially explicit manner, accounting for lateral water transfer and topographic effects on radiation (see Appendices C.1-C.3). The model has been extensively validated in many ecosystems worldwide (Fatichi & Pappas, 2017; Fatichi, Rimkus, et al., 2015; Mastrotheodoros et al., 2019). To account for the high spatial heterogeneity of the region, we performed massively parallel simulations ($6.1 \cdot 10^5$ CPU hours) at an unprecedented high resolution (250 m grid) for the entire Alpine arch ($257,000 \text{ km}^2 - 4.12$ million pixels). The simulation period consisted of three years (2001-2003), including a very wet and a very dry year (2001 and 2003, respectively, Figures 4.1 and C.1, Tables C.1-C.5). We validated the model output against daily discharge and snow depth, with very satisfactory results, considering the lack of model calibration (Appendix C.5 and Figures C.2, C.3 and C.4). We partitioned the pan-Alpine water budget into blue and green water fluxes and quantified the sensitivity of each component to changes in precipitation and temperature.

4.2 DISSECTING THE WATER TOWER OF EUROPE

Simulation results indicate that latent heat, i.e. total ET expressed in units of equivalent energy, reaches its maximum values in wetter areas (e.g., in the north of Figure 4.1c, where annual precipitation exceeds 2000 mm), especially on south-facing slopes (Figure 4.1d) denoting that energy is the dominant driver of ET in this specific location. In drier regions, such as in the SE valley in Figure 4.1c (upper Rhone valley), latent heat is overall lower because precipitation ($\sim 500 \text{ mm yr}^{-1}$) becomes the critical constrain for annual ET. High-elevation areas are clearly distinguishable because rocks, snow and ice emit low latent heat (Figure 4.1, b and c).

Analysing the three-year average water fluxes across the entire elevation range, we found that ET peaks at 300 m a.s.l. and then steadily declines at higher elevations, despite the slightly increasing precipitation (Figure 4.2a). The elevational distribution of ET varies considerably between different catchments, due to vegetation heterogeneity and the interplay between water and energy limitations (Figure C.5, Della Chiesa et al., 2014). We used P-ET as a proxy for runoff at the annual time scale (Figure C.4, Goulden & Bales, 2014) since ice melt only marginally contributed to the water budget (less than 3%) at the annual scale, corresponding roughly to 4 km^3 , (Figure C.6). The runoff production, P-ET, peaks at 800 m a.s.l. (Figure 4.2a). More than 50% of this blue water originates from the areas between 1300 and 3000 m a.s.l., which correspond to only 35% of the total Alpine domain. This can be explained by the sharp decrease of ET with elevation due to temperature constraints (Figure 4.2a). The runoff production shows a great spatial variability as even neighbouring catchments, such as the upper Rhone and the Aare catchment in Switzerland, exhibit distinct P-ET patterns (Figure 4.2b).

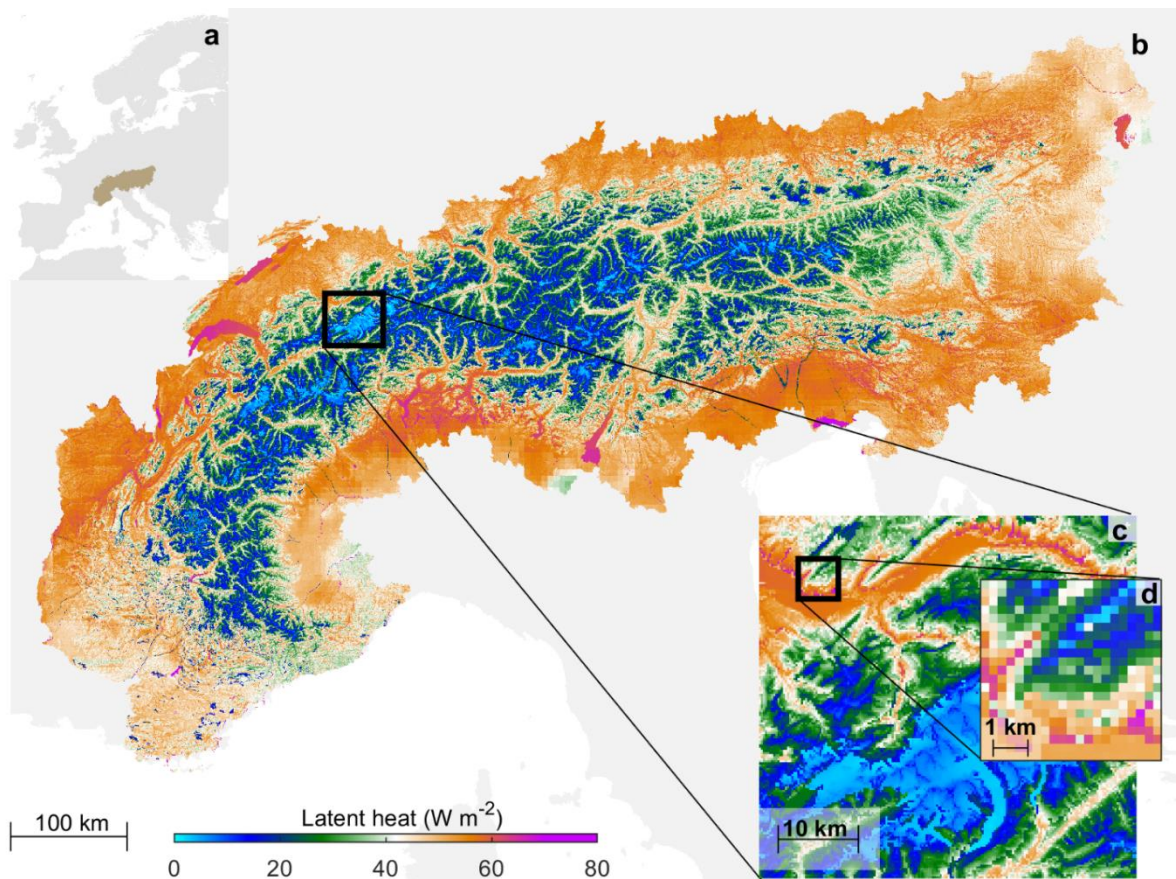


Figure 4.1 Simulation results reflect the high spatial heterogeneity in latent heat (evapotranspiration in energy units). (a) The spatial extent of the European Alps. (b) Three-year average latent heat flux (W m^{-2}) for the entire 257,000 km^2 domain simulated with Tethys-Chloris. (c) and (d) focus on the Bernese highlands, Switzerland, to reveal the small-scale spatial heterogeneity and the high-resolution simulation (250 m x 250 m pixels).

4.3 BLUE VS GREEN WATER DURING EXCEPTIONALLY DRY SUMMERS

The Alpine water budget also displays high elasticity in time (Figure 4.2c); P-ET in 2001 was 53% higher than in 2003 (Figure C.6a), which can be explained by both higher precipitation and lower ET. More specifically, the Alps received 250 mm more P in 2001 compared to 2003 while ET was 30 mm lower on average (Figure 4.2c).

Among the 381 monitored catchments, we selected 334 watersheds in which runoff and catchment-averaged P in 2003 were lower compared with each station's long-term average and the 2001-2003 mean. For these catchments, we compute how much ET contributed to amplifying the effect of precipitation deficit on runoff during the 2003 growing season (Figures 4.2b and C.9). We found that in 75% of the catchments, ET intensified the drought. The remaining 25% of the catchments - mostly located in the SW and NE of the pan-Alpine domain - experienced dry conditions with water-stressed vegetation and reduced ET. Considering the entire domain, ET increased during the drought in an area covering more than 144,000 km^2 (Figure C.10). Overall, the increase in green water amplified the precipitation-driven deficit by roughly 22% (Figures 4.2c and C.9). In the zone of 1300 to 3000 m a.s.l. elevation, enhanced ET created an additional water loss of more than 4 km^3 during the 2003

growing season compared with 2002, amplifying the precipitation impact on runoff by 32% (mean weighted by the area of each catchment).

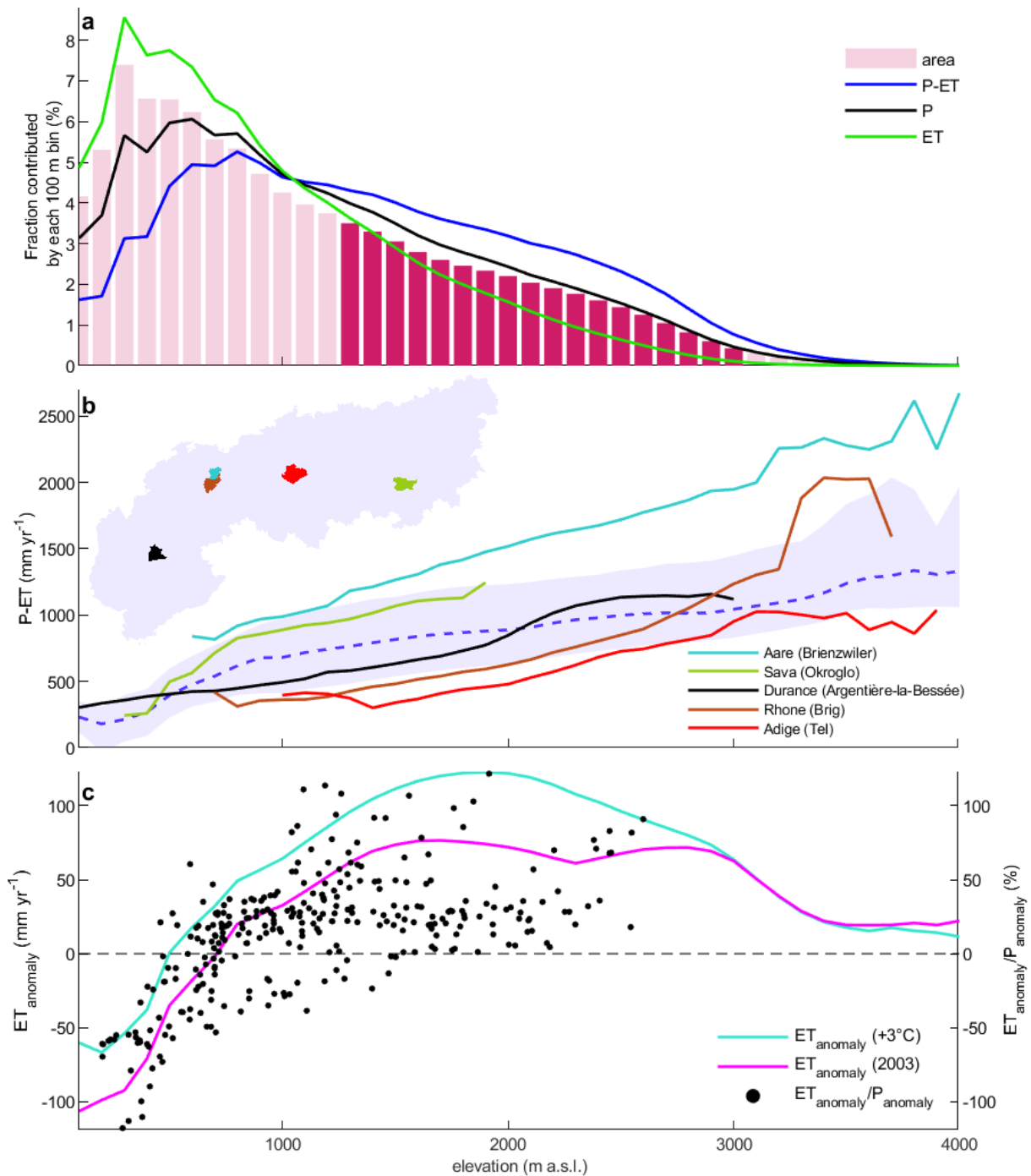


Figure 4.2 Relationship between elevation and blue and green water fluxes. (a) Percent contribution of each elevation class (grouped in 100 m elevational bins) to precipitation (P), evapotranspiration (ET) and P-ET, including the fractional area of each class (the fluxes are averaged over the entire simulation period, i.e. 2001-2003). The highlighted magenta bars show the most runoff-productive zone (1300-3000 m a.s.l.). (b) P-ET in mm yr^{-1} . The dashed line and the shaded area represent the median P-ET (averaged over the entire simulation period) over the entire domain and the interquartile range, respectively. Coloured lines show P-ET elevational distribution for selected catchments to illustrate the spatial variability. A locator map is included. (c) ET anomalies (solid lines-left y-axis) and ET contribution to the runoff deficits compared with the precipitation deficit during the 2003 growing season (scatter-right y-axis). The anomalies were computed based on the 2001-2003 mean and the fluxes were averaged in space based on the 100 m elevational bins. Each point of the scatter represents one of the 334 catchments (out of the 381 in total) for which both precipitation and runoff were lower in 2003 compared with the long-term average and the 2001-2003 mean, respectively.

To quantify the sensitivity of ET to warming and remove the effect of reduced precipitation, we performed a space-for-time substitution (see Appendix C.4). This procedure was necessary because the warm years in the Alps are well correlated with dry years (e.g., the 2003, Figure C.7). This analysis was based on regressions between ET components and temperature, accounting for regional variations and differences between land cover characteristics. We found that with a 3°C increase in air temperature, annual ET will increase on average by 6% (evaporation will increase by 9% and transpiration will increase by 5%) while P-ET will decrease by roughly 5% under the assumption of constant precipitation (Figure 4.2c). A similar effect on runoff is expected if annual precipitation is reduced by only 3%, which is likely to happen by the end of the century (Gobiet et al., 2014). The sensitivity of annual ET to temperature shifts from positive to negative below 700 m a.s.l., which implies that in a warmer climate ET will decrease at low elevations (Figures 4.2c and C.6).

During the growing season, precipitation is still the main source of blue water (81% on average), snowmelt comes second (16%), and ice melt accounts for the remaining 3% (Figure C.6b). Below 500 m a.s.l., the contribution of soil water storage dynamics is substantial (99 mm, compared with 464 mm ET, Figure C.6b). The simulated growing season ET for the $+3^{\circ}\text{C}$ scenario agrees well with ET simulated during 2003, when the growing season temperature anomaly was roughly $+3^{\circ}\text{C}$. This reinforces our confidence on the space-for-time approach employed here (Figure C.6b).

Blue and green water fluxes averaged over the entire domain show that ET sporadically exceeded precipitation during the growing season of 2001 and 2002. For 2003, however, ET was higher than precipitation (which was 32% lower than the long-term average) already before the beginning of the growing season (Figures C.8 and C.11). The earlier snowmelt, which peaked before the start of the growing season and plummeted afterwards, amplified this deficit. Early snowmelt is becoming more frequent with rising temperature (Beniston et al., 2018) and in 2003 it was only partly compensated by increased ice melt. The simulated ice melt during August 2003 was 38% of the total Alpine runoff, corresponding to about 2 km^3 of water.

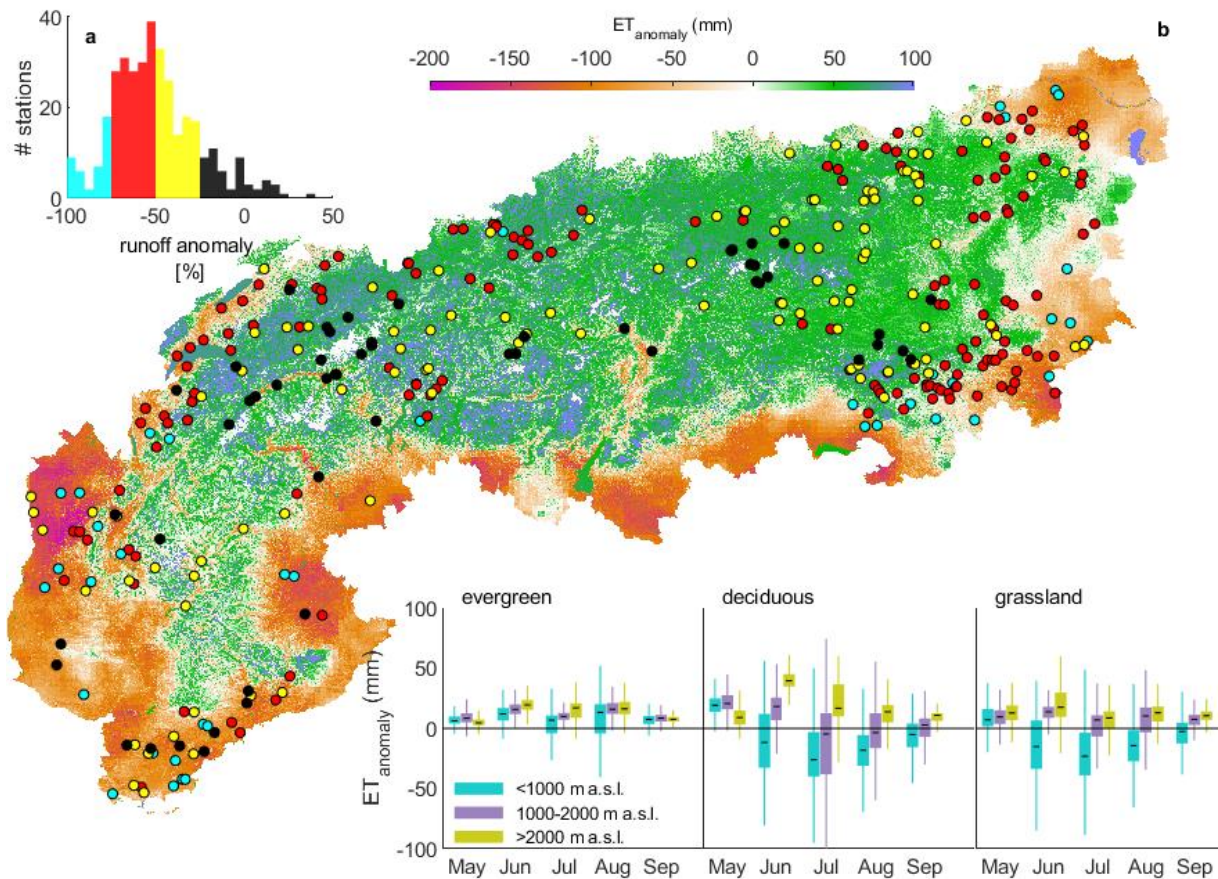


Figure 4.3 Analysis of anomalies in blue and green water fluxes during the 2003 drought. (a) Histogram of observed 2003 runoff anomalies in percentage for 381 locations (2003 compared with the long-term mean of each station), coloured according to the magnitude of the anomaly (>-75%: cyan, -50 to -75%: red, -25 to -50%: yellow and >-25%: black). (b) Spatial distribution of the simulated ET anomaly in mm during the 2003 growing season (May-September, here 2003 ET is compared with the 2001-2003 mean). The dots represent the locations of the 381 locations with hydrological measurements and are coloured as described in (a). The three insets in the lower right part show the boxplots of simulated ET anomaly for three different vegetation types (evergreen, deciduous, and grassland) in three elevational classes (<1000 m a.s.l., 1000-2000 m a.s.l. and >2000 m a.s.l.).

Considering all 381 catchments with runoff data, the observed runoff was on average 50% lower compared with the long-term mean between May and September 2003 (Figures 4.3 and C.8). Higher-than-average runoff occurred at a few locations, mostly in highly-glacierized catchments (Figure 4.3; Zappa & Kan, 2007). During this period, precipitation over the Alps was the lowest recorded between 1992-2008 and mean temperature was record-breaking high (Figure C.7). The detailed vegetation scheme in T&C allows an analysis of different vegetation responses to the 2003 drought (Figure 4.3). Most evergreen forests strongly benefited from the increased radiation and temperature, and did more so as the drought intensified during the summer months, mostly at high elevations, where ET increased. Grasslands and deciduous forests were water-stressed below 1000 m a.s.l., but benefited from the drought above 2000 m a.s.l., especially at the beginning of the growing season, when monthly ET increased by up to 100 mm (Figure 4.3). In most areas of the Northern Alps the simulated ET anomaly was positive throughout the summer, in agreement with local measurements (Leuzinger et al., 2005; Seneviratne et al., 2012). In all dry inner Alpine valleys (such as Valle d'Aosta and Val

d'Adige in Italy, Valais in Switzerland and the Mur valley in Austria), the increased water stress of 2003 reduced ET for all vegetation types (Dobbertin et al., 2005) but the area of these catchments is disproportionately smaller than the area with increased ET.

4.4 DISCUSSION

4.4.1 Limitations

Some limitations in this study should be noted. We used uniform soil depth throughout the entire domain in the absence of reliable datasets. Previous research, though, showed that soil depth varies with elevation in a catchment in the Italian Alps (Bertoldi, Rigon, & Over, 2006), while variations in soil depth can affect transpiration patterns (Tromp-van Meerveld & McDonnell, 2006) and thus soil moisture and discharge. Indeed, soil depth might be an important driver for key ecosystem properties, especially in mountain catchments (e.g., Woolhiser, Fedors, Smith, & Stothoff, 2006).

The use of a single vegetation parameterization for each plant functional type throughout the entire domain is another caveat. Intraspecific variations in vegetation traits can be considerable (Albert et al., 2011; Anderegg, 2015; Butler et al., 2017; J. Kattge et al., 2011; Siefert et al., 2015) and should be included in the representation of plant attributes in the vegetation component of the ecosystem models (Pappas et al., 2016), especially given the extent and the heterogeneities of the Alpine region.

Despite the very detailed approach for generating distributed meteorological input, some uncertainties are also unavoidably inserted by our poor knowledge of microclimatic conditions, as the monitoring networks are not dense enough in several parts of the Alps. The computational cost of the simulations also does not permit a longer analysis, which precludes a more robust estimation of the interannual variability in the water towers of Europe. Moreover, T&C represents groundwater processes in a simplified manner, and the analysis of the water budget assumed that the changes in soil water storage over three hydrological years are negligible. Although during each hydrological year the changes in soil water storage might act as a buffer for climatic variability (Brooks et al., 2015), in the course of three years, this should have minimal implications for the validity of our analysis.

Anthropogenic impact on the water cycle, such as flow regulation, was also ignored in this study, but the implications at the pan-Alpine scale should be minor, when compared to major local impact (de Jong, 2015). Although at the pan-Alpine scale the spatial resolution applied (250 m) can be regarded as hyper-resolution, several hydrological processes which depend on the fine-scale topographic variability might not be adequately captured (e.g., Son, Tague, & Hunsaker, 2016). Furthermore, the increase in fire occurrence in parts of the Alps (Dupire et al., 2017), also highlights that a more realistic representation of ecosystem dynamics should take large-scale disturbances into account (Hanan et al., 2018).

4.4.2 Conclusions

Our results indicate that at the annual timescale the “water towers of Europe” are largely vulnerable to precipitation decrease. Annual precipitation has shown no long-term trends so far (Casty, Wanner,

Luterbacher, Esper, & Böhm, 2005), but summer precipitation in central Europe has already decreased and could further do so in the future due to changes in atmospheric circulation patterns leading to more intense summer droughts (Pal, Giorgi, & Bi, 2004). Combined with the expected decrease in ice melt and earlier snowmelt (Beniston et al., 2018), our results demonstrate that blue water could be considerably reduced in the European Alps, but green water will continue to increase (Duethmann & Blöschl, 2018), leading to the oxymoron “lush vegetation-drier rivers”. The expected increase in water use efficiency with higher CO₂ concentration levels than present (Mastrotheodoros et al., 2017) may partially offset this ET feedback during warmer summers in the long-term but it will unlikely have a major role in the near future.

Understanding the partitioning of green and blue water fluxes and their spatial distribution from few square kilometers to the entire Alps is essential to manage the European water resources under current and future climatic conditions (European Environment Agency (EEA), 2009; Orth & Destouni, 2018). This partition has implications on ecosystem functioning, energy production, and water supply for agricultural and industrial uses. We showed that ecohydrological simulations driven by high-resolution hydrometeorological forcings improve the quantification and understanding of the water budget in mountainous areas and its vulnerability to climate, providing insights into processes that coarser-scale approaches fail to reproduce (e.g., Fan et al., 2019; Maxwell & Condon, 2016; Wood et al., 2011). The need for more realistic, high-resolution quantifications of water resources is urgent (Barnett et al., 2005); our study demonstrates that recent advances in ecohydrological modeling, combined with large scale datasets and new computational capabilities, offer the possibility to address this urgent need, thus helping towards defining strategies to counteract or adapt to climate change impacts in water resources.

Acknowledgements: T.M. wants to thank Daniela Anghileri for her support regarding the computational part of this study. Numerical simulations were performed on the ETH Euler cluster.

Funding: T.M. and S.F. thank the support of the Stavros Niarchos Foundation and the ETH Zurich Foundation (Grant ETH-29 14-2). C.P. acknowledges the support of the Swiss National Science Foundation (SNSF), the Stavros Niarchos Foundation and the ETH Zurich Foundation (Grants P2EZP2_162293 and P300P2_174477). GM was supported by the “The Branco Weiss Fellowship - Society in Science” administered by ETH Zurich.

Author contributions: S.F. and T.M. designed the study, J.P., R.R., B.S. and M.B. contributed with data, P.H. contributed to the code parallelization, T.M. performed the simulations and the analyses and made the figures, S.F., T.M. and C.P. synthesized the results, T.M. wrote the manuscript with contributions from all other authors.

Conclusions

5.1 MAJOR CONCLUSIONS

This work researched the ecohydrological sensitivity of the Alpine domain with physically-based modelling (ecohydrological model T&C) and dataset analysis. The main findings are centred on (a) the parameterization of hydrological models, (b) the topographic and climatic drivers of Alpine ecohydrology, and (c) the sensitivity of the pan-Alpine water budget to climate change.

5.1.1 Plasticity in plant traits

The larger-than-expected increase in water use efficiency (WUE) during the last decades observed in many forests in the Northern Hemisphere triggered a plethora of studies trying to explain the possible reasons for it (e.g., Cheng et al., 2017; Keenan et al., 2013; Knauer et al., 2017). As described in Chapter 2, at the stand scale plasticity in physiological parameters can explain the observed WUE increase. A 1% yr⁻¹ change in one or two vegetation parameters such as specific leaf area, or the coefficient of canopy nitrogen decay, may imply changes in the composition of the stand rather than changes in the traits of individual plants. There are demonstrations of such demographic changes in several ecosystems (e.g., Hardiman et al., 2013; Knapp et al., 2012; Urbanski et al., 2007).

A key parameter that can explain changes in WUE is the parameter that represents the sensitivity of stomatal conductance to assimilation rate and environmental drivers ([CO₂] and VPD) in the Leuning model of stomatal conductance (Leuning, 1995; Leuning et al., 1995). Although larger trends in this parameter might be unrealistic (Knauer et al., 2017), the results presented in Chapter 2 show that a 1% yr⁻¹ change in this parameter is plausible also at scales larger than the stand-scale because it only marginally affects evapotranspiration.

5.1.2 Drivers of Alpine ecohydrology

Simulations with high spatiotemporal resolution on synthetic and real topographies allowed the quantification of the relative importance of temperature, radiation, and water availability for ecohydrological processes, including runoff generation and plant-related variables, such as net primary production (Chapter 3). In agreement with previous studies, the ecohydrological model (T&C) detected large differences between the wet north pre-Alps and the dry inner-Alpine valleys (e.g., Bolli et al., 2007; Rössler et al., 2012). T&C also shows that different vegetation types exhibit different sensitivities to environmental factors; for example, dry grasslands are likely to experience higher water stress due to increased radiation, whereas dry evergreen forests are insensitive and wet

grasslands even benefit from increased radiation. This implies, for instance, that during heatwaves, we should expect very different vegetation responses across different Alpine areas.

These findings highlight the importance of performing high-resolution simulations. Detailed measurements in different sites across the Alps are invaluable for understanding how the steep climatic gradients affect vegetation functioning, but synthesizing the results of different case studies is not easy, due to the variability in the experimental designs and the specificity of each site. Moreover, the results presented in Chapter 3 display a very high spatial heterogeneity in ecohydrological fluxes, which implies that generalizing based on a given site is highly uncertain. These conclusions motivated the pan-Alpine assessment of the water and carbon balances presented in Chapter 4.

5.1.3 Pan-Alpine water budget

I performed ecohydrological simulations at unprecedented high resolution for the entire Alpine region (257,000 km² at 250 m grid, Chapter 4). The results of these simulations provide valuable insights into the so-called “water towers of Europe”. A key conclusion of my analyses is that although the annual runoff production in the Alps is largely precipitation-driven, increasing temperatures can increase ET and thus reduce runoff, especially during extreme heatwaves. This suggests that projections of runoff changes of large European rivers are uncertain mostly due to the uncertainty in future precipitation rather than because of the uncertainty in air temperature. T&C shows that the runoff reduction caused by a 3°C temperature increase is roughly equivalent to the runoff reduction caused by a 3% reduction in precipitation. This is particularly important, given that the uncertainties in the future annual precipitation in the Alps are large (different models estimate precipitation changes ranging between -1 to -11% for the next decades in the Alps, European Environment Agency (EEA), 2009).

The results of the pan-Alpine simulations concur with findings of previous studies regarding the drastic runoff reduction during summer in future (e.g., European Environment Agency (EEA), 2009). I found that during the 2003 drought, Alpine vegetation benefitted from the high temperatures and the increased radiation, across large parts of the Alps as shown by increased ET. This complements the results of previous studies (e.g., Seneviratne et al., 2012; Teuling et al., 2010, 2013), but provides a much more detailed picture of the heterogeneous responses of vegetation. On average, ET increased, amplifying the effects of precipitation deficit to runoff by up to 34% in the Alpine areas where most of the blue water (i.e. runoff) originates. However, T&C also identified hotspots where ET drastically decreased during the 2003 drought, due to water limitations. These include mountains near the French coast, large parts of the lower Rhone basin, the Austrian lowlands and notably many inner-Alpine valleys, such as Valais in Switzerland and Val d’Aosta in Italy.

This analysis shows that “lush vegetation and drier rivers” is a drought paradox to come soon true in the European Alps, as extreme events like the 2003 drought will become more frequent (Samaniego et al., 2018). This will be due to the enhanced ET resulting from the excess in temperature and radiation that are beneficial for plant activity in the most runoff productive areas.

5.2 OUTLOOKS

Research in this thesis was primarily based on ecohydrological modelling. Despite T&C is a state-of-the-art ecohydrological model, with very detailed process-descriptions, I identify four main areas where improvements are possible, new data are necessary and further research should be directed.

5.2.1 Adapting model parameterization

The results presented in Chapter 2 suggest that small trends in the order of 1% yr⁻¹ in key physiological parameters can affect how ecosystems respond to changing environmental conditions. However, we currently know little about how each physiological parameter responds to changing climatic factors. For some parameters there are even contrasting results between different studies (e.g., leaf-to-root ratio, H. H. Rogers et al., 1996). Ecosystem-scale trends are difficult to detect because many parameters are very heterogeneous not only between different species, but also between individual plants of the same species (which is currently poorly documented for most traits, Aubin et al., 2016) and even within the canopy (Albert et al., 2011; J. Kattge et al., 2011; Niinemets et al., 2015; Siefert et al., 2015). Most of the currently available measurements are usually available as snapshots on individual plants, thus conclusions about plasticity remain speculative. Clearly, we need new coordinated measurement campaigns to monitor both stand demography and multiple replicates of plant physiological measurements, especially in flux-tower sites, in order to identify which are the key processes behind the plant response to environmental changes (Dusenge, Duarte, & Way, 2019).

Modellers should further investigate the effects of vegetation plasticity in water, energy and carbon exchange across spatial scales (e.g., Knauer et al., 2017). Such modelling studies could further help monitoring campaigns by highlighting what are the key traits and how accurate the measurements should be, if we aim at studying trait plasticity. Vegetation modellers should in general revise the parametrization principles: many parameters that are currently held constant should become variable, accounting for changes in space and time. Increasing evidence indicates that this should be the way forward (Fyllas et al., 2014; Pappas et al., 2016; Pavlick et al., 2013; Sakschewski et al., 2015; Scheiter et al., 2013).

5.2.2 Ecohydrological models as tools for developing new theories

The study presented in Chapter 2 further shows that ecohydrological models can provide answers where simple theories fail to explain the observed response of vegetation to environmental changes. This implies that testing hypotheses through models can be a valuable tool for the development of new theories (Brewer et al., 2018). Indeed, despite the many recent advances in ecohydrology, there are still many open questions. For example, we are not able to fully capture several plant-related processes, such as carbon allocation (Hartmann & Trumbore, 2016), nutrient limitations to plant growth (Ågren, Wetterstedt, & Billberger, 2012), and the mesophyll conductance (A. Rogers et al., 2017). Models can play a key role in answering such open questions.

5.2.3 Towards hyper-resolution ecohydrology

The analyses presented in Chapters 3 and 4 show that ecohydrological simulations driven by high-resolution hydrometeorological forcing and solved at a high resolution grid improve the quantification and understanding of water resources vulnerability to climate and provide insights into processes that coarser-scale approaches fail to reproduce (e.g., Ko et al., 2018; Maxwell & Condon, 2016).

Studies of mountain hydrology have primarily focused on natural catchments (e.g., de Jong, 2015) and those studies that do include modified catchments usually simplify human intervention (e.g., Fatichi, Rimkus, et al., 2015), or totally ignore it. Given that mountain areas are under increased anthropogenic pressure, modelling human impacts on the water cycle is crucial (e.g., Jaramillo & Destouni, 2015). Hydropower, land use changes, irrigation and production of artificial snow affect the water budget and their effect downstream may be evident (de Jong, 2015). Thus, in the future, detailed hyper-resolution studies need to include anthropogenic influences in realistic ways to describe the actual hydrological budget.

For hydrology to take full advantage of the increasing availability in computational power, a close cooperation between hydrologists, mathematicians and computer scientists is needed; in other words, we need to develop a new interdisciplinary field to combine these disciplines. Based on my personal experience, I believe that enhancing the computational skills of students in hydrological sciences should be a priority, given the increasing reliance on computationally complex models.

5.2.4 Linking Earth system models to ecohydrology

Enhancing the computational efficiency of ecohydrological studies is a prerequisite for bridging the gap between detailed, mechanistic ecohydrological models and Earth system models. The latter aim at understanding and predicting global change, but they omit (or oversimplify) several key processes that occur at the hillslope scale (e.g., the lateral redistribution of subsurface water, Fan et al., 2019). They are thus often inaccurate (Rouholahnejad Freund & Kirchner, 2017).

On the other hand, high-resolution model simulations at regional or continental scales, that have profited from the increasing computational resources, have recently contributed to the scientific understanding of how hillslope-scale hydrologic processes can impact land-atmosphere exchanges and climate at larger spatial scales (e.g., Maxwell & Condon, 2016). The study presented in Chapter 4 demonstrates that the emergence of new distributed datasets combined with the rapidly increasing computational resources bring the scientific community closer to continental-scale simulations of hillslope processes. To better predict global change, we need to take advantage of the insights provided by such analyses, using them as a blueprint for identifying which are the key processes that Earth system models should account for (Fan et al., 2019). In this way, the scientific community will be able to make more realistic predictions of water resource availability in the near future.

A

Appendix A: Linking plant functional trait plasticity and the large increase in forest water use efficiency

A.1 WATER USE EFFICIENCY DEFINITION

The leaf-scale intrinsic water use efficiency (iWUE) is defined as (Beer et al., 2009):

$$\text{iWUE} = \frac{A_n}{1.6g_s} = \frac{A_n}{T} \text{VPD} \quad (\text{A.1})$$

where A_n [$\mu\text{mol CO}_2 \text{ s}^{-1} \text{ m}^{-2}$] is the net carbon assimilation rate, T [$\text{kg m}^{-2} \text{ s}^{-1}$] is the transpiration and VPD [Pa] is the vapor pressure deficit across the leaf interface. iWUE can be re-written explicating the stomatal conductance, g_s [$\mu\text{mol CO}_2 \text{ m}^{-2} \text{ leaf s}^{-1}$], as:

$$\text{iWUE} = \frac{g_s(C_a - C_i)}{1.6g_s \text{VPD } P_{atm}} \text{VPD} \quad (\text{A.2})$$

where C_a and C_i [Pa] are the CO_2 atmospheric concentration and leaf intercellular concentration respectively, P_{atm} is the atmospheric pressure [Pa]. It follows that iWUE scales proportionally to C_a if the ratio $C_i:C_a$ is constant:

$$\text{iWUE} = \frac{C_a}{1.6 P_{atm}} \left(1 - \frac{C_i}{C_a}\right) \propto C_a \quad (\text{A.3})$$

The ecosystem-scale intrinsic water use efficiency (IWUE) is defined as (Beer et al., 2009):

$$\text{IWUE} = \frac{\text{GPP}}{G_{s,\text{can}}} \quad (\text{A.4})$$

where GPP [$\text{mgC m}^{-2} \text{ s}^{-1}$] is the gross primary production and $G_{s,\text{can}}$ [$\mu\text{mol CO}_2 \text{ m}^{-2} \text{ s}^{-1}$] is the canopy conductance.

Here, we use eddy covariance measurements to approximate the ecosystem-scale intrinsic water use efficiency by the inherent water use efficiency (defined as $\text{IWUE} = \text{GEP}/\text{ET} \cdot \text{VPD}$). This approximation is based on the assumption of equal temperatures of leaves and atmosphere and negligible canopy-atmosphere decoupling (Beer et al., 2009). Thus, for decoupled canopies, the two definitions are not equivalent and the IWUE response to $[\text{CO}_2]$ is less than proportional to the $[\text{CO}_2]$ increase (De Kauwe et al., 2013).

A.2 FLUXNET DATA

In the Fluxnet2015 dataset, Net Ecosystem Exchange (NEE) and resulting products (Ecosystem Respiration (RECO) and GPP) are computed with two different methods (NEE_50 and NEE_REF, <http://fluxnet.fluxdata.org/data/fluxnet2015-dataset/fullset-data-product/>). For these products, we arbitrarily chose between the two versions since the differences are minimal. Regarding GPP, we preferred the product produced with the daytime partitioning method because it has no negative values. We used the Variable Ustar Threshold method that is available in the SUBSET. For the latent and heat fluxes, we used the products corrected by the energy balance closure correction factor (LE_CORR and H_CORR). In FI-Hyy, the GPP_DT_VUT_REF product was missing a whole year (2007), so we used the corresponding night time product (GPP_NT_VUT_REF). For data downloaded from <http://gaia.agraria.unitus.it/home>, we computed GPP as the average of the following: GPP_st_MDS, GPP_or_MDS, GPP_st_ANN and GPP_or_ANN. In case that one of those had gaps, it was not taken into account throughout the gap-period. For latent heat, we used LE_f.

A.3 THE T&C MODEL

Simulations were carried out using the mechanistic ecohydrological/biosphere model Tethys-Chloris (T&C), which is designed to simulate coupled dynamics of energy, water and vegetation at the land surface and at the hourly time-scale in different environments. All the principal components of the hydrological cycle, such as precipitation interception, transpiration, ground evaporation, infiltration, surface and subsurface water fluxes are accounted for. The model solves the ecohydrological dynamics over complex topography (e.g., a hillslope or a watershed), explicitly considering spatial variability of meteorological fields and the role of topography in controlling incoming radiation and transferring water laterally through the surface and subsurface. Heterogeneity in soil properties and vegetation can be accounted for. The basic computational elements are represented using cells of a regular grid. However, in this study, each location was assumed flat without lateral effects of mass and energy exchange and without an explicit areal dimension, essentially a one-dimensional representation.

Shortwave and longwave incoming radiation fluxes are explicitly transferred through vegetation. The energy, water and carbon exchanges between the surface (soil and vegetation) and the planetary boundary layer are computed with a resistance analogy scheme accounting for aerodynamic, under canopy and leaf boundary layer resistances, as well as for stomatal, soil-to-root and soil-to-air resistances (Sellers et al., 1997). The values of aerodynamic, and leaf boundary layer resistances defines the degree of coupling between the canopy and the atmosphere, with a much stronger coupling for taller forest with small leaves. The model can consider horizontal heterogeneity in vegetation since each element can account for multiple species or plant functional types. Rainfall interception follows an adaptation of the Rutter-model that accounts for throughfall, leaf and stem interception, and canopy dripping (Rutter et al., 1971, 1975). Vertical water content dynamics in the variably saturated soil profile are solved using the one-dimensional (1D) Richards equation. In case of snow occurrence, the energy balance of snowpack dynamics is computed. Snow can be intercepted by the vegetation or fall to the ground, where it can accumulate and melt. Runoff generation is made possible via saturation

excess and infiltration excess mechanisms. The soil heat flux is computed solving the heat diffusion equation. Water can pond at the surface modifying roughness, albedo and thermal properties and allowing direct evaporation from surface water.

Photosynthesis is simulated using the Farquhar biochemical model and subsequent modifications (Bonan et al., 2011; Farquhar et al., 1980). A "two big leaves" scheme, where sunlit and shaded leaves are treated separately is used to compute net assimilation and stomatal resistance. Stomatal resistance is computed with a revised version of the Leuning stomatal model (Leuning, 1990, 1995):

$$g_s = g_0 + a_1 \frac{A_n}{(C_i - \Gamma^*)} f(\text{VPD}) P_{atm} \quad (\text{A.5})$$

where a_1 [-] is an empirical parameter, g_s [$\mu\text{mol CO}_2 \text{ m}^{-2} \text{ s}^{-1}$] is the stomatal conductance to CO_2 , A_n [$\mu\text{mol CO}_2 \text{ s}^{-1} \text{ m}^{-2}$] is the net assimilation rate, C_i is the leaf interior partial CO_2 pressure, Γ^* [Pa] is the CO_2 compensation point, VPD [Pa] is the vapour pressure deficit, P_{atm} [Pa] is the atmospheric pressure and g_0 [$\mu\text{mol CO}_2 \text{ m}^{-2} \text{ s}^{-1}$] is the cuticular conductance when $A_n \leq 0$. $f(\text{VPD})$ is the function of sensitivity to vapor pressure deficit and is defined as:

$$f(\text{VPD}) = \frac{1}{1 + \text{VPD}/\text{VPD}_0} \quad (\text{A.6})$$

where VPD_0 [Pa] is the value of VPD at which $f(\text{VPD} = \text{VPD}_0) = 0.5$. The leaf interior partial CO_2 pressure (C_i) is also used in the equation:

$$A_n = \frac{C_a - C_i}{P_{atm}(1.64r_s + 1.37r_b + r_a)} \quad (\text{A.7})$$

where A_n [$\mu\text{mol CO}_2 \text{ s}^{-1} \text{ m}^{-2}$] is the net assimilation rate, C_a [Pa] is the atmospheric CO_2 concentration, P_{atm} [Pa] is the atmospheric pressure, and r_s , r_b and r_a [s m^{-1}] are the stomatal, leaf boundary layer and under canopy resistances, respectively.

Photosynthesis is upscaled from leaf to plant scale assuming an exponential profile of leaf nitrogen content per unit of area and therefore photosynthetic capacity (Bonan et al., 2011). Transpiration is automatically upscaled to the canopy level considering the sunlit and shaded fraction of LAI and different stomatal conductance for sunlit and shaded leaves. The wet fraction of the leaves (a prognostic variable in the model related to rainfall interception) does not transpire, while the dry fraction does. CO_2 assimilation is only inhibited by intercepted snow but not by intercepted water.

The scaling factor for the photosynthetic capacity of the sunlit ($F_{N,sun}$) and the shaded ($F_{N,shd}$) fractions of the leaf area index LAI are:

$$F_{N,sun} = \int_0^{LAI} e^{-K_{nit}x} e^{-K_{opt}x} dx = \frac{1 - e^{-(K_{nit}+K_{opt})LAI}}{K_{nit} + K_{opt}} \quad (\text{A.8})$$

$$\begin{aligned}
F_{N,shd} &= \int_0^{LAI} e^{-K_{nit}x} (1 - e^{-K_{opt}x}) dx & (A.9) \\
&= \frac{1 - e^{-K_{nit}LAI}}{K_{nit}} - \frac{1 - e^{-(K_{nit}+K_{opt})LAI}}{K_{nit} + K_{opt}}
\end{aligned}$$

where K_{nit} [-] is the nitrogen decay coefficient and K_{opt} [-] is a light extinction parameter computed in the radiation transfer module. The factors are used to obtain the estimate of photosynthetic quantities scaled from leaf to canopy. It follows that the maximum Rubisco capacity at 25°C, $V_{max,sun}$ [$\mu\text{mol CO}_2 \text{ m}^{-2} \text{ leaf s}^{-1}$] for unit of leaf area in the sunlit leaves (for the shaded respectively) is:

$$V_{max,sun} = V_{max}^T \frac{F_{N,sun}}{F_{sun} LAI} \quad (A.10)$$

where V_{max}^T [$\mu\text{mol CO}_2 \text{ m}^{-2} \text{ s}^{-1}$] is the maximum Rubisco capacity at 25°C at the top of the canopy, which is a model parameter, and F_{sun} is the fraction of sunlit canopy.

V_{max} is linked to the electron transport rate, J_{max} :

$$J_{max} = r_j V_{max} \quad (A.11)$$

where r_j is a model parameter ranging typically between 1.9 and 2.5.

Plant water stress in carbon uptake is introduced by multiplying A_n with a β correction factor, which has a sigmoidal shape that accounts for the root-zone integrated soil water potential and depends on two threshold parameters corresponding to the beginning of stomatal closure and to 50% stomatal closure (Brodribb & Holbrook, 2003).

The dynamics of seven carbon pools are explicitly simulated in the model and include green aboveground biomass (leaves), living sapwood, fine roots, carbohydrate reserve (non-structural carbohydrates), reproductive tissues (fruit and flowers), standing dead leaves and heartwood/dead-sapwood. The leaf area index (LAI, [-]) is derived from leaf carbon pool with the following structural equation:

$$LAI = C_{leaf} S_{LA} \quad (A.12)$$

where C_{leaf} [gC m^{-2}] is the green aboveground biomass and S_{LA} is the specific leaf area [$\text{m}^2 \text{ g}^{-1}\text{C}$].

The carbon assimilated through photosynthetic activity is used for maintenance and growth respiration otherwise is allocated to one of the first five pools. The different pools are undergoing tissue turnover in function of tissue longevity and environmental stresses, i.e., drought and low temperatures. Carbon allocation is a dynamic process that accounts for resource availability (light and water) and allometric constraints (Krunner et al., 2005), e.g., a minimum ratio of fine root to foliage carbon; and an upper limit for the storage of carbohydrate reserve. For instance, the allocation to C_{leaf} is constrained when

$$C_{leaf} > \text{LtR } C_{root} \quad (\text{A.13})$$

where LtR is the maximum leaf-to-root biomass ratio and C_{root} is the fine-root biomass.

Carbon allocated to reserves can be subsequently translocated to favour leaf expansion at the onset of the growing season or after severe disturbances. Phenology is simulated considering four states: dormant, maximum growth, normal growth, and senescence. Patterns of plant allocation are influenced by the phenological phase. Transition between phenological phases are prognostic in the model and controlled by soil temperature, soil moisture and photoperiod length. Nutrient dynamics and forest demography are neglected, which implies that vegetation is assumed to be in a mature phase and in equilibrium with its nutritional environment.

A.4 DATA-RELATED UNCERTAINTIES

Our aim was to detract as little as possible from the approach followed in Keenan et al. (2013), but data issues forced us to deviate. Due to data scarcity, we excluded one site (SE-Fla) and we prolonged time series length using the updated Fluxnet dataset; mean length is 13 years in our study and 10 years in Keenan et al. (2013). The time series analysed in our study were also taken in more recent years for several sites to avoid periods where large gaps in meteorological forcing would hinder the modelling analysis. These differences may partly explain the discrepancy between the two studies.

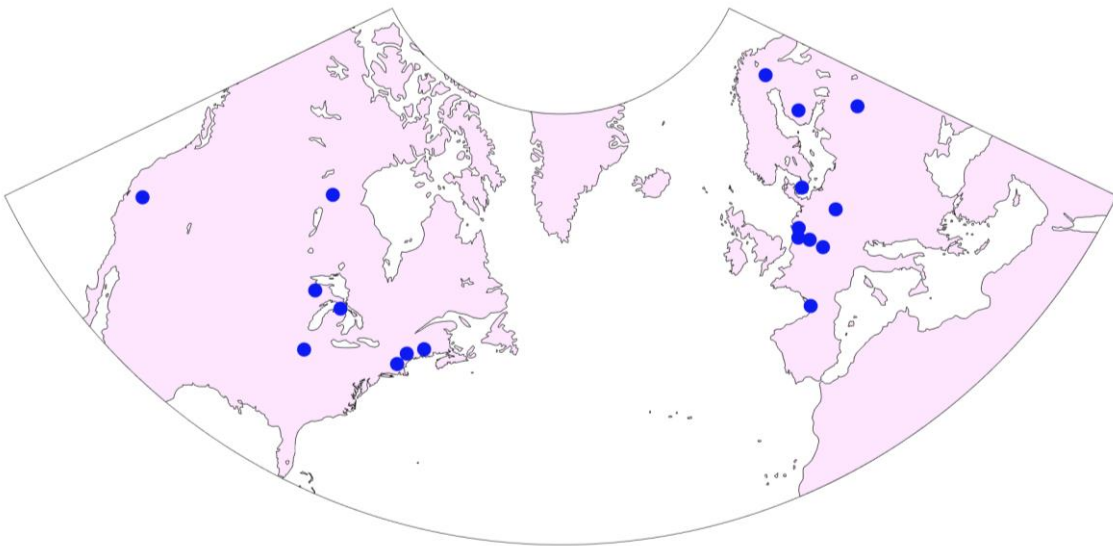


Figure A.1 Location of the 20 flux tower sites used in the study.

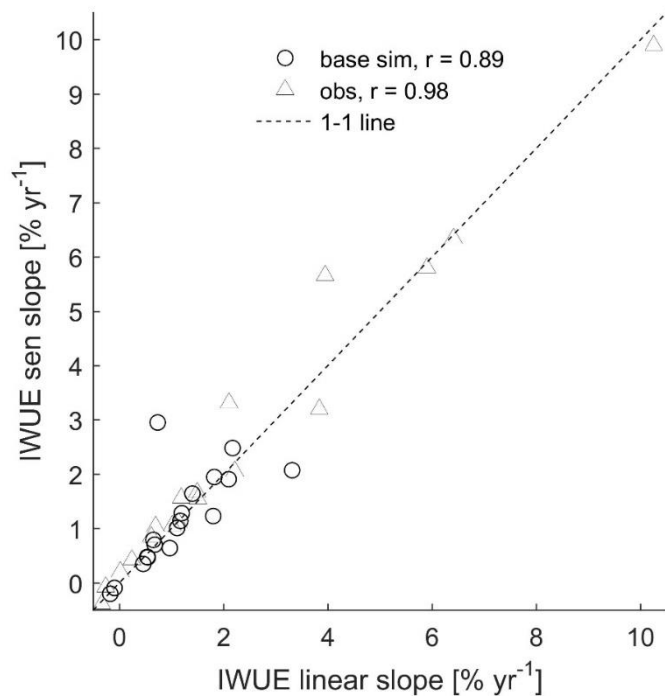


Figure A.2 Correlation and corresponding coefficients (r) between linear regression and Sen slope of the inherent water use efficiency (IWUE) computed in the 20 sites. We show the corresponding values obtained from both observations and Tethys-Chloris base simulations.

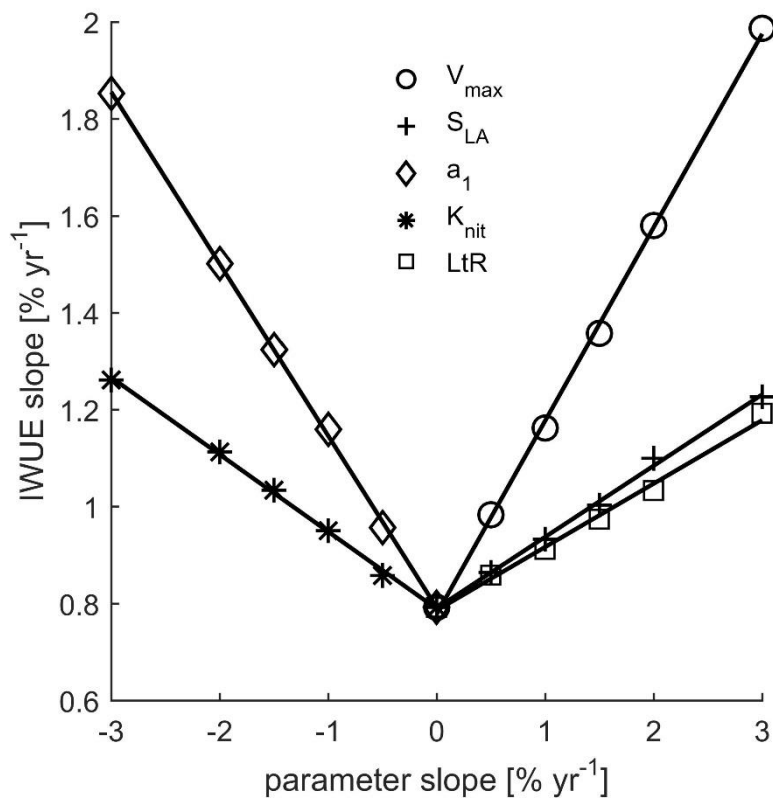


Figure A.3 Inherent water use efficiency (IWUE) response to perturbation of five parameters for the US-UMB site. Linear fit is also shown for each parameter.

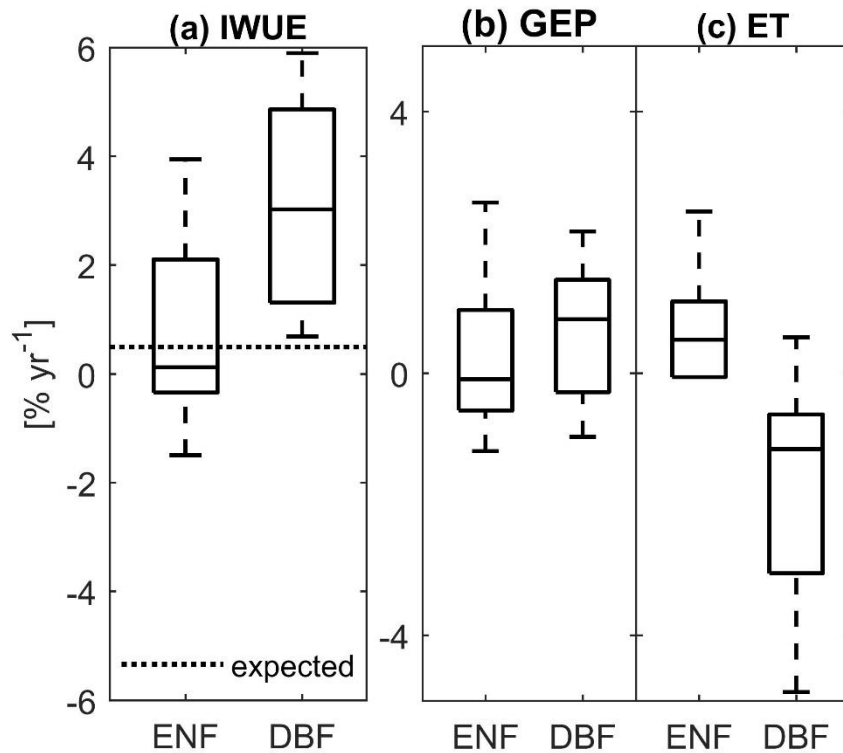


Figure A.4 Observed inherent water use efficiency (IWUE), gross ecosystem production (GEP) and evapotranspiration (ET) linear slopes in evergreen needleleaf forests (ENF) and deciduous broadleaf forests (DBF).

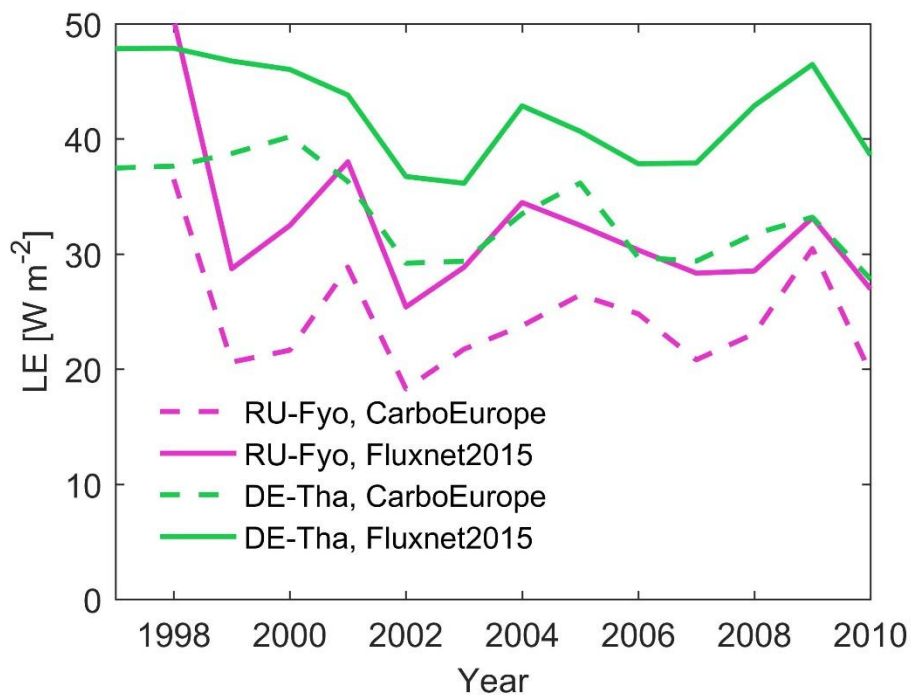


Figure A.5 Discrepancies between CarboEurope (dashed lines) and Fluxnet 2015 (continuous lines) in the reported observations of latent heat flux (LE), in RU-Fyo (magenta) and DE-Tha (green).

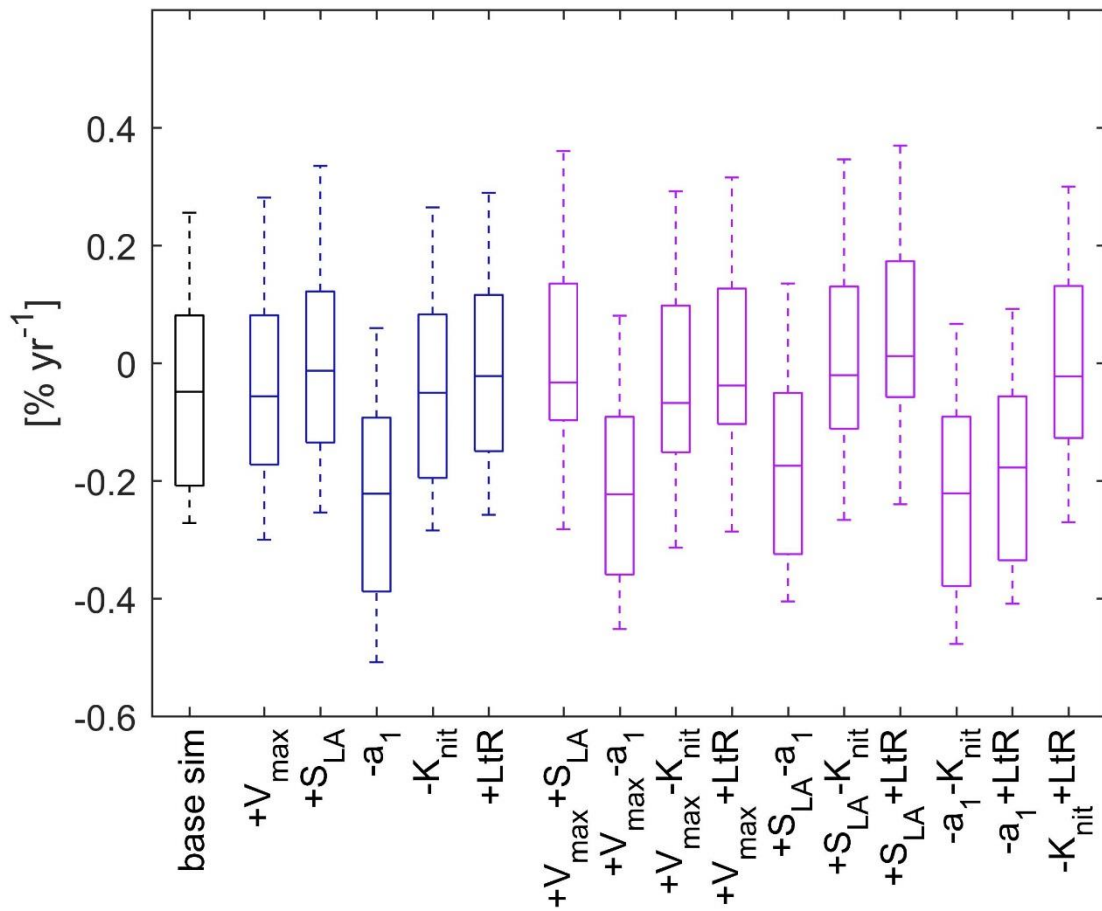


Figure A.6 Linear slopes in simulated C_i/C_a , where C_i is the intercellular CO_2 concentration estimated as the simple average of the annual C_i of sunlit and shaded leaves at the ecosystem scale and C_a is the annual atmospheric CO_2 concentration. Black represents the base simulations; blue the simulations for which only one parameter was perturbed, and magenta the simulations in which two parameters were perturbed.

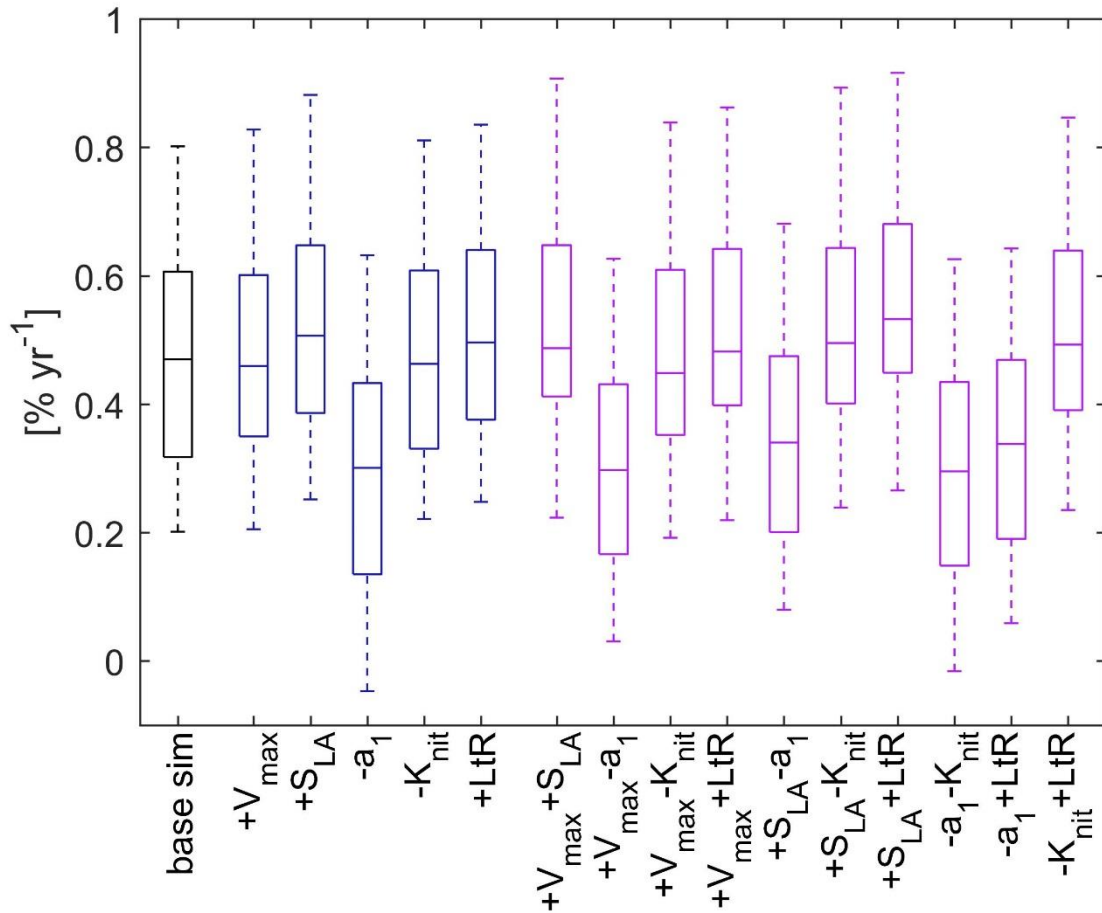


Figure A.7 Linear slopes in simulated C_i (intercellular CO_2 concentration estimated as the simple average of the annual intercellular CO_2 concentration of sunlit and shaded leaves at the ecosystem scale) for the 20 sites examined. Black represents the base simulations; blue the simulations for which only one parameter was perturbed, and magenta the simulations in which two parameters were perturbed.

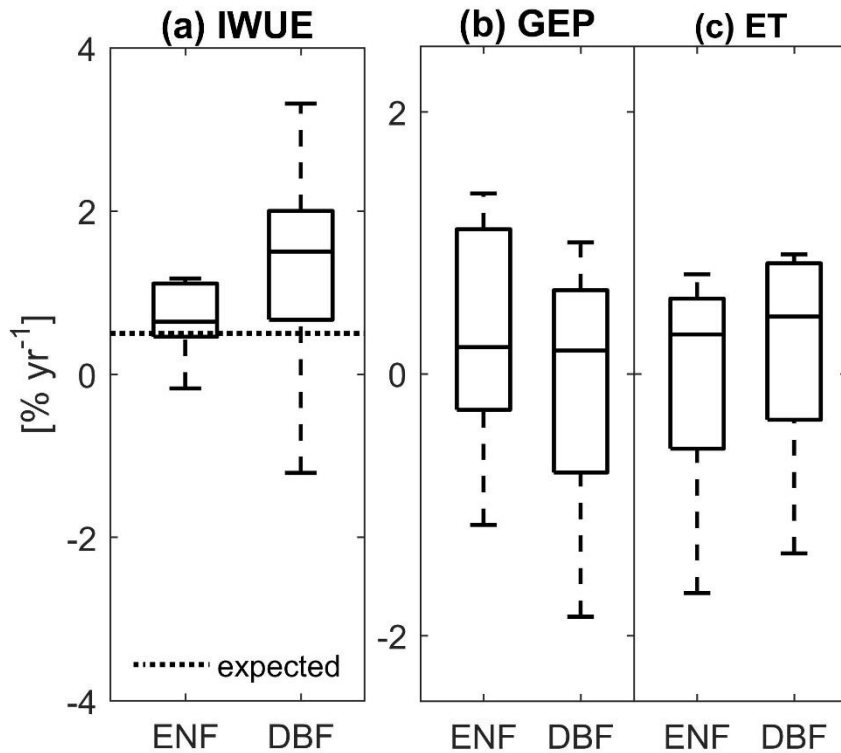


Figure A.8 Inherent water use efficiency (IWUE), gross ecosystem production (GEP) and evapotranspiration (ET) linear slopes in evergreen needleleaf forests (ENF) and deciduous broadleaf forests (DBF) for the base simulations.

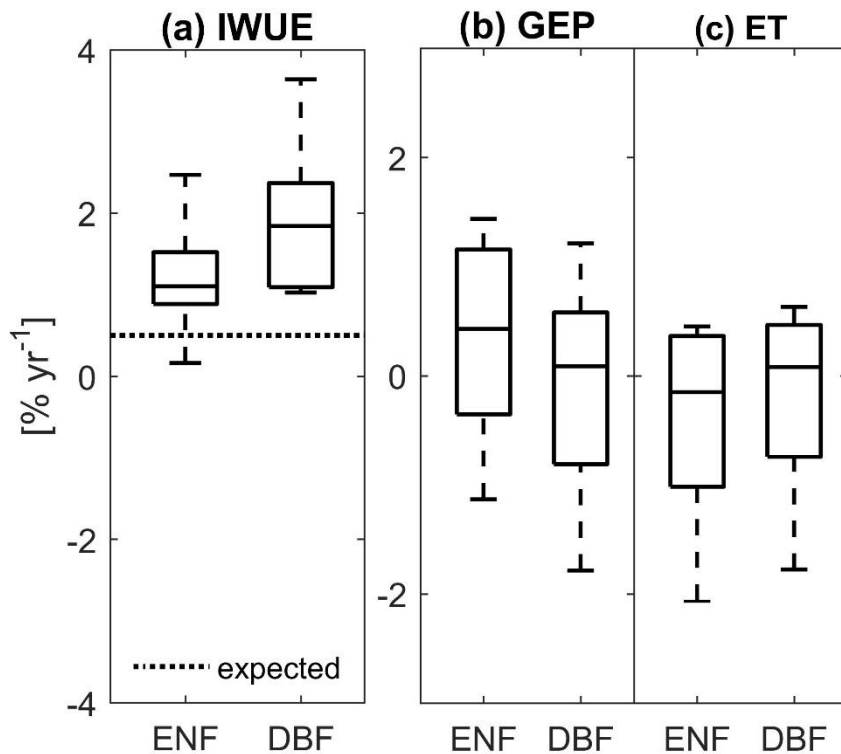


Figure A.9 Inherent water use efficiency (IWUE), gross ecosystem production (GEP) and evapotranspiration (ET) linear slopes in evergreen needleleaf forests (ENF) and deciduous broadleaf forests (DBF) for the numerical experiment in which we perturbed a_1 parameter (which connects stomatal aperture and net assimilation) by $-1\% \text{ yr}^{-1}$.

Table A.1 Summary of the 20 flux tower sites and of the periods used in the analysis. All sites represent temperate or boreal forest ecosystems. DBF = Deciduous broadleaf forest; ENF = Evergreen needleleaf forest; MF = Mixed Forest.

Site Code	Lat.	Lon.	Elevation [m. asl]	Years	Vegetation Type	Mean annual temperature [°C]	Years since the last disturbance	Annual precip. [mm]	Data source and download date	Reference
BE-Bra	51.31	4.52	16	2004-2014	MF	10.9	68	777	http://fluxnet.fluxdata.org/ , 22/7/2016	(Carrara et al., 2003)
BE-Vie	50.31	6.00	450	1996-2014	MF	8.3	61	952	http://fluxnet.fluxdata.org/ , 8/2/2016	(Aubinet et al., 2002)
CA-Man	55.88	-98.48	259	1994-2008	ENF	-1.3	~150	456	http://ameriflux.lbl.gov/	(Dunn et al., 2007)
DE-Tha	50.96	13.57	380	1996-2014	ENF	8.8	75	842	http://fluxnet.fluxdata.org/ , 8/2/2016	(Grünwald & Bernhofer, 2007)
DK-Sor	55.49	11.65	40	1996-2014	DBF	8.3	111	849	http://fluxnet.fluxdata.org/ , 22/7/2016	(Pilegaard et al., 2011)
FI-Hyy	61.85	24.30	181	1996-2014	ENF	4.4	34	604	http://fluxnet.fluxdata.org/ , 22/2/2016	(Suni et al., 2003)
FI-Sod	67.36	26.64	180	2000-2008	ENF	0.9	~100	545	http://gaia.agraria.unitus.it/home , 19/7/2015	(Thum et al., 2007)
FR-Hes	48.67	7.06	300	1997-2006	DBF	10.2	~30	937	http://gaia.agraria.unitus.it/home , 25/11/2015	(Granier et al., 2000)
FR-LBr	44.01	-0.77	61	2000-2008	ENF	13.3	30	828	http://gaia.agraria.unitus.it/home , 25/11/2015	(Berbigier et al., 2001)
NL-Loo	52.16	5.74	25	1997-2013	ENF	9.9	~100	842	http://fluxnet.fluxdata.org/ , 8/2/2016	(Dolman et al., 2002)
RU-Fyo	56.46	32.92	265	1998-2013	ENF	5.1	~200	582	http://fluxnet.fluxdata.org/ , 22/7/2016	http://fluxnet.fluxdata.org/
US-Bar	44.06	-71.28	272	2004-2010	DBF	7.5	73	1253	http://ameriflux.lbl.gov/ , 25/11/2015	(Jenkins et al., 2007)
US-Blo	38.90	-120.63	1315	1997-2007	ENF	11.1	6	1375	http://fluxnet.fluxdata.org/ , 8/2/2016	(Goldstein et al., 2000)
US-Ha1	42.54	-72.17	303	1992-2009	DBF	7.9	>50-100	1130	http://fluxnet.fluxdata.org/ , 8/2/2016	(Urbanski et al., 2007)
US-Ha2	42.54	-72.18	360	2005-2010	ENF	8.0	~100-230	1323	http://ameriflux.lbl.gov/ , 25/11/2015	(Hadley & Schedlbauer, 2002)
US-Ho1	45.20	-68.74	60	1996-2008	ENF	6.6	~90	846	http://ameriflux.lbl.gov/ , 8/9/2015	(Hollinger et al., 2004)
US-LPH	42.54	-72.19	360	2003-2010	DBF	7.8	46	1303	http://ameriflux.lbl.gov/ , 25/11/2015	(Davidson et al., 2006)
US-MMS	39.32	-86.41	275	1998-2014	DBF	12.4	~60-80	1097	http://fluxnet.fluxdata.org/ , 17/11/2015	(Schmid et al., 2000)
US-UMB	45.56	-84.71	234	1999-2014	DBF	7.2	76	890	http://ameriflux.lbl.gov/	(Curtis et al., 2005)
US-WCr	45.80	-90.08	520	1999-2006	DBF	5.6	~60-80	671	http://fluxnet.fluxdata.org/ , 8/2/2016	(Cook et al., 2004)

Table A.2 Linear slopes of inherent water use efficiency (IWUE), gross ecosystem production (GEP) and evapotranspiration (ET) for the 20 sites in [% yr⁻¹]; observed and base simulation slopes are shown as well as the slopes computed from simulations with de-trended temperature and relative humidity. We also show the output of the numerical experiments in which we perturbed the a_1 parameter (which connects stomatal aperture and net assimilation) by -1% yr⁻¹ ($[-a_1]$ simulations). For observations, the 5-95% uncertainty range is shown in parenthesis (the range is computed based on the normality assumption that residuals follow the Gaussian distribution).

Site Code	IWUE				GEP				ET			
	observations	Base sim	De- trended	$[-a_1]$ sim	observations	Base sim	De- trended	$[-a_1]$ sim	observations	Base sim	De- trended	$[-a_1]$ sim
BE-Bra	1.5 (-1.3, 4.3)	1.4	1.4	1.7	3.9 (1.1, 6.7)	0.1	0.4	0.0	2.5 (-0.1, 5.2)	-0.9	-0.6	-1.4
BE-Vie	1.0 (-0.9, 2.9)	-0.1	-0.2	0.2	1.1 (0.2, 1.9)	0.3	0.2	0.3	-0.8 (-1.9, 0.3)	-0.4	-0.5	-0.7
CA-Man	-0.3 (-2.2, 1.6)	1.0	0.4	1.4	-0.6 (-1.4, 0.3)	1.1	0.6	1.2	0.1 (-2.2, 2.3)	0.6	0.0	0.2
DE-Tha	0.6 (-0.8, 2.1)	1.1	0.7	1.5	0.6 (-0.5, 1.8)	0.3	0.5	0.5	0.9 (-0.9, 2.7)	0.6	0.5	0.4
DK-Sor	1.1 (-0.4, 2.7)	0.7	0.4	1.2	1.1 (0.6, 1.6)	0.8	1.2	1.2	0.6 (-0.7, 1.8)	0.8	0.8	0.6
FI-Hyy	0.2 (-1.0, 1.4)	0.5	0.4	1.0	1.0 (0.2, 1.7)	0.1	-0.1	0.0	1.1 (0.1, 2.1)	0.0	-0.2	-0.5
FI-Sod	3.9 (-5.5, 13.4)	0.7	0.4	1.2	-1.2 (-5.9, 3.6)	-1.2	-1.6	-1.1	-5.4 (-10.0, -0.8)	-3.4	-3.8	-3.8
FR-Hes	5.9 (-0.4, 12.2)	1.8	0.9	2.2	-3.2 (-8.3, 1.8)	-1.9	-1.5	-1.8	-4.9 (-11.1, 1.4)	0.5	0.2	0.2
FR-LBr	-1.1 (-8.0, 5.8)	-2.2	-1.3	-1.9	-0.5 (-6.8, 5.9)	0.9	1.1	0.9	0.1 (-7.2, 7.5)	2.9	3.3	2.6
NL-Loo	-0.3 (-2.3, 1.8)	0.5	0.4	0.9	0.1 (-0.9, 1.0)	-1.0	-0.9	-0.9	-0.1 (-1.0, 0.9)	-1.7	-1.7	-2.1
RU-Fyo	-1.5 (-5.4, 2.4)	-0.2	0.0	0.2	-0.3 (-1.8, 1.3)	1.3	1.2	1.3	1.0 (-0.9, 3.0)	0.8	0.8	0.4
US-Bar	3.8 (-2.9, 10.5)	-1.2	-0.7	-0.9	2.2 (-1.2, 5.5)	-0.6	-0.8	-0.7	-0.7 (-6.3, 4.9)	-1.4	-1.5	-1.8
US-Blo	6.4 (3.8, 9.1)	1.2	0.9	1.7	6.9 (2.7, 11.0)	0.1	0.4	0.4	1.9 (-0.1, 4.0)	0.5	0.5	0.3
US-Ha1	3.8 (2.2, 5.4)	1.2	0.2	1.5	1.2 (0.2, 2.3)	0.6	1.4	0.6	-1.2 (-2.2, -0.3)	0.8	-0.2	0.4
US-Ha2	2.1 (-6.5, 10.7)	2.1	2.2	2.5	2.6 (-5.5, 10.7)	-0.3	-0.3	-0.4	2.5 (-3.6, 8.6)	-0.6	-0.5	-1.0
US-Ho1	0.0 (-2.7, 2.7)	0.5	0.4	1.0	-1.1 (-2.3, 0.1)	1.4	1.4	1.4	-1.8 (-3.7, 0)	-0.2	-0.2	-0.5
US-LPH	10.3 (-0.7, 21.2)	3.3	1.4	3.6	0.6 (-2.5, 3.6)	0.2	-0.2	0.1	-7.3 (-17.5, 2.9)	0.9	-0.3	0.5
US-MMS	2.2 (0.3, 4.1)	1.8	1.3	2.1	-1.0 (-1.9, -0.1)	-0.9	-0.7	-0.9	-1.1 (-2.0, -0.2)	-0.6	-0.7	-0.9
US-UMB	1.5 (0.6, 2.4)	0.7	0.7	1.0	0.4 (-0.3, 1.1)	0.2	0.2	0.1	-0.6 (-1.7, 0.6)	-0.1	-0.1	-0.6
US-WCr	0.7 (-8.2, 9.6)	2.2	2.3	2.5	1.6 (-1.9, 5.2)	0.7	1.0	0.6	-1.2 (-6.1, 3.7)	0.3	0.6	-0.1

Table A.3 Correlation coefficients between modelled and observed latent heat (LE) and gross primary production (GPP) at the hourly and daily scale for the entire period modelled for each site (in parenthesis the coefficients for the filtered data, i.e. summer, non-rainy days and daytime only). The amount of data missing is also given (gaps in % of the total data). ‘-’ is used when no estimate of the gaps is available.

Site Code	Gaps in the hourly LE dataset [%]	LE Correlation Coefficient		Gaps in the hourly NEE dataset [%]	GPP Correlation Coefficient	
		Hourly	Daily		Hourly	Daily
BE-Bra	30.3	0.82 (0.61)	0.84	50.9	0.90 (0.31)	0.87
BE-Vie	73.3	0.88 (0.74)	0.87	75.3	0.92 (0.35)	0.89
CA-Man	34.4	0.80 (0.68)	0.80	60.2	0.88 (0.31)	0.92
DE-Tha	15.5	0.84 (0.66)	0.87	55.5	0.92 (0.48)	0.88
DK-Sor	42.7	0.83 (0.66)	0.86	40.5	0.94 (0.62)	0.95
FI-Hyy	50.9	0.83 (0.62)	0.88	59.5	0.89 (0.27)	0.92
FI-Sod	12.3	0.73 (0.41)	0.81	32.2	0.85 (0.31)	0.89
FR-Hes	8.4	0.81 (0.70)	0.81	40.2	0.90 (0.56)	0.92
FR-LBr	10.9	0.68 (0.54)	0.69	66.8	0.83 (0.32)	0.78
NL-Loo	34.9	0.82 (0.51)	0.79	62.2	0.93 (0.28)	0.89
RU-Fyo	25.2	0.84 (0.60)	0.85	61.2	0.90 (0.42)	0.89
US-Bar	-	0.84 (0.70)	0.87	-	0.92 (0.57)	0.95
US-Blo	37.4	0.83 (0.81)	0.66	76.8	0.83 (0.34)	0.69
US-Ha1	-	0.86 (0.74)	0.86	66.7	0.93 (0.59)	0.94
US-Ha2	-	0.89 (0.71)	0.60	-	0.89 (0.37)	0.91
US-Ho1	33.3	0.74 (0.69)	0.73	47.9	0.86 (0.26)	0.86
US-LPH	64.3	0.79 (0.59)	0.73	84.3	0.91 (0.59)	0.95
US-MMS	13.8	0.86 (0.76)	0.87	58.9	0.91 (0.53)	0.94
US-UMB	-	0.90 (0.77)	0.93	48.5	0.94 (0.58)	0.97
US-WCr	58.3	0.74 (0.64)	0.70	72.9	0.88 (0.36)	0.87

Table A.4 Annual trends in temperature and relative humidity.

Site Code	Temperature trend [$^{\circ}\text{C yr}^{-1}$]	Relative humidity trend [% yr^{-1}]
BE-Bra	-0.08	-0.21
BE-Vie	0.06	0.14
CA-Man	0.16	0.14
DE-Tha	0.08	-0.14
DK-Sor	0.06	-0.10
FI-Hyy	0.04	0.05
FI-Sod	0.07	0.02
FR-Hes	0.04	-0.63
FR-LBr	-0.14	0.20
NL-Loo	0.00	-0.06
RU-Fyo	0.02	0.23
US-Bar	0.07	0.54
US-Blo	0.05	-0.21
US-Ha1	0.11	-0.37
US-Ha2	0.01	0.09
US-Ho1	-0.04	-0.15
US-LPH	0.14	-0.85
US-MMS	-0.02	-0.39
US-UMB	-0.01	0.01
US-WCr	-0.09	-0.19

Table A.5 Parameters of the Tethys-Chloris (T&C) model included in the initial screening.

Symbol	Description	Units	Typical Range
a_l	Empirical parameter connecting stomatal aperture and net assimilation rate	[-]	3-11
K_{nit}	Canopy nitrogen decay coefficient	[-]	0.1-0.5
V_{max}	Maximum Rubisco capacity at 25 $^{\circ}\text{C}$ - leaf level	[$\mu\text{mol CO}_2/\text{m}^2 \text{s}$]	20-120
S_{LA}	Specific leaf area	[m^2/gC]	0.006-0.050
LtR	Maximum leaf-to-root biomass ratio	[-]	0.2-1.5
ZR95	Root depth (95 th percentile)	[mm]	200-1200
r	Maintenance respiration rate at 10 $^{\circ}\text{C}$	[$\text{gC gN}^{-1} \text{day}^{-1}$]	0.02-0.08
drn	Fine root turnover rate	[day^{-1}]	0.0001-0.0030
dsn	Living sapwood turnover rate	[day^{-1}]	0.0001-0.0030

Table A.6 Median linear slopes (in [% yr⁻¹]) of inherent water use efficiency (IWUE), gross ecosystem production (GEP) and evapotranspiration (ET) for observations and all T&C simulations and Euclidean distance between simulations and observations for all the experiments. Values for Sen slopes are given in parenthesis. Bold denotes the simulations in which the Euclidean distance is lower than that of the base simulations.

	IWUE	GEP	ET	Euclidean distance
observations	1.3 (1.3)	0.6 (0.6)	-0.3 (-0.3)	[-]
base simulations	0.9 (0.9)	0.2 (0.1)	0.2 (0.1)	0.8 (0.8)
base +V _{max}	1.3 (1.2)	1.1 (1.0)	0.7 (0.7)	1.1 (1.1)
base +S _{LA}	1.0 (0.9)	0.6 (0.6)	0.6 (0.5)	1.0 (0.9)
base -a₁	1.3 (1.4)	0.2 (0.1)	-0.3 (-0.4)	0.4 (0.6)
base -K_{nit}	1.0 (1.1)	0.6 (0.6)	0.5 (0.4)	0.8 (0.8)
base +LtR	1.0 (0.9)	0.6 (0.6)	0.6 (0.5)	1.0 (0.9)
base +V _{max} +S _{LA}	1.3 (1.2)	1.5 (1.5)	0.9 (0.9)	1.5 (1.5)
base +V _{max} -a ₁	1.7 (1.6)	1.0 (1.1)	0.4 (0.3)	0.9 (0.8)
base +V _{max} -K _{nit}	1.4 (1.4)	1.5 (1.5)	0.9 (0.9)	1.5 (1.4)
base +V _{max} +LtR	1.3 (1.2)	1.4 (1.5)	0.9(0.9)	1.4 (1.4)
base +S_{LA} -a₁	1.4 (1.3)	0.6 (0.6)	0.2 (0.1)	0.5 (0.4)
base +S _{LA} -K _{nit}	1.2 (1.0)	1.0 (1.0)	0.8 (0.7)	1.2 (1.1)
base +S _{LA} +LtR	1.0 (1.0)	1.0 (1.0)	0.8 (0.7)	1.2 (1.1)
base -a₁ -K_{nit}	1.5 (1.5)	0.6 (0.5)	-0.0 (-0.1)	0.3 (0.3)
base -a₁ +LtR	1.4 (1.3)	0.5 (0.6)	0.1 (0.0)	0.5 (0.4)
base -K _{nit} +LtR	1.1 (1.0)	0.9 (0.9)	0.8 (0.7)	1.1 (1.1)

Table A.7 Median linear slopes (in [% yr⁻¹]) of inherent water use efficiency (IWUE), gross ecosystem production (GEP) and evapotranspiration (ET) for observations and all T&C simulations and Euclidean distance between simulations and observations for all the experiments weighing by the length of time series. Values for Sen slopes are given in parentheses. Bold denotes the simulations in which the Euclidean distance is lower than that of the base simulations.

	IWUE	GEP	ET	Euclidean distance
observations	1.0 (1.1)	0.6 (0.6)	-0.1 (0.0)	[-]
base simulations	0.7 (0.8)	0.3 (0.2)	0.0 (0.1)	0.5 (0.5)
base +V _{max}	1.1 (1.2)	1.1 (1.0)	0.8 (0.8)	0.9 (0.9)
base +S _{LA}	0.8 (0.9)	0.6 (0.6)	0.7 (0.6)	0.7 (0.7)
base -a ₁	1.2 (1.4)	0.3 (0.1)	-0.5 (-0.5)	0.6 (0.7)
base -K_{nit}	0.8 (1.0)	0.6 (0.7)	0.4 (0.4)	0.5 (0.4)
base +LtR	0.8 (0.9)	0.6 (0.6)	0.6 (0.6)	0.8 (0.7)
base +V _{max} +S _{LA}	1.2 (1.2)	1.5 (1.5)	0.8 (0.9)	1.3 (1.4)
base +V _{max} -a ₁	1.5 (1.6)	1.1 (1.1)	0.4 (0.4)	0.8 (0.8)
base +V _{max} -K _{nit}	1.2 (1.2)	1.5 (1.4)	0.8 (1.0)	1.3 (1.3)
base +V _{max} +LtR	1.2 (1.1)	1.4 (1.4)	0.8 (0.9)	1.2 (1.3)
base +S_{LA}-a₁	1.2 (1.3)	0.6 (0.6)	0.1 (0.1)	0.3 (0.3)
base +S _{LA} -K _{nit}	1.0 (1.0)	1.0 (1.0)	0.7 (0.8)	0.9 (0.9)
base +S _{LA} +LtR	0.9 (1.0)	1.0 (1.0)	0.7 (0.9)	0.9 (1.0)
base -a₁-K_{nit}	1.2 (1.3)	0.7 (0.5)	-0.2 (-0.1)	0.2 (0.3)
base -a₁+LtR	1.2 (1.3)	0.6 (0.6)	0.1 (0.1)	0.2 (0.2)
base -K _{nit} +LtR	1.0 (1.0)	1.0 (0.9)	0.8 (0.8)	0.9 (0.9)

Appendix B: Ecohydrological dynamics in the Alps: Insights from a modelling analysis of the spatial variability

B.1 THE T&C MODEL

The T&C model uses the resistance analogy scheme to compute the energy, water, and carbon exchanges between the surface and the atmospheric surface layer (accounting for aerodynamic, undercanopy, and leaf boundary layer resistances, as well as for stomatal and soil resistances (Sellers et al., 1997). Each element includes up to two layers of vegetation, to simulate the coexistence of trees and grass. Horizontal composition of vegetation is also possible since each element can include multiple plant functional types (Fatichi, Ivanov, & Caporali, 2012; Fatichi & Leuzinger, 2013). Incoming shortwave and longwave radiation is explicitly transferred through the vegetation (Ivanov et al., 2008a).

Dynamics of water content in the soil profile are solved using the one-dimensional Richards equation for the vertical flow and the kinematic wave approximation for the lateral subsurface flow (quasi 3-D approach). Saturated and unsaturated parts of the soil column are explicitly identified. Surface overland and channel flow are also solved through the kinematic equation. The model simulates snowpack dynamics by solving the energy balance; snow either stays on the vegetation (snow interception) or falls to the ground, where it accumulates and successively it melts. In this study, snow redistribution was not simulated. Runoff is generated either by saturation excess or by infiltration excess mechanisms and depends on lateral moisture fluxes in the unsaturated and saturated zones and on the overland flow (Loague, Heppner, Ebel, & VanderKwaak, 2010).

Photosynthesis is simulated with a biochemical model (Collatz, Ball, Grivet, & Berry, 1991; Collatz, Ribas-Carbo, & Berry, 1992; Farquhar, von Caemmerer, & Berry, 1980) as it was modified by Bonan et al. (2011). Net assimilation and stomatal resistance are computed separately for sunlit and shaded leaves, following the two big-leaves approach (Dai, Dickinson, & Wang, 2004). Photosynthetic capacity decays exponentially through the canopy (Bonan et al., 2011; Ivanov et al., 2008). Stomatal resistance is parameterized as a function of assimilation rate and environmental conditions (Leuning, 1990, 1995; Tuzet, Perrier, & Leuning, 2003). The dynamics of five carbon pools are explicitly simulated in the model, i.e., green aboveground biomass, living sapwood (woody plants only), fine roots, carbohydrate reserve (non-structural carbohydrates), and standing dead biomass.

The carbon assimilated through photosynthesis is used for growth and reproduction and is lost in the process of maintenance and growth respiration and tissue turnover. Carbon allocation is a dynamic process that accounts for resource availability (light and water) and allometric constraints (Bonan,

Levis, & Sitch, 2003; Friedlingstein, Joel, Field, & Fung, 1999; Friend, Stevens, Knox, & Cannell, 1997; Kozlowski & Pallardy, 1997; Krinner et al., 2005). Carbon from reserves can be translocated to favour leaf expansion at the beginning of the growing season or after a severe disturbance (Chapin, Schulze, & Mooney, 1990; Fatichi et al., 2012; Gough, Flower, Vogel, & Curtis, 2010; Gough, Flower, Vogel, Dragoni, & Curtis, 2009). Organic matter turnover of the different carbon pools is a function of tissue longevity and environmental stresses, i.e., drought and low temperatures (Arora & Boer, 2005; Bonan et al., 2003; Fatichi et al., 2012; Ivanov et al., 2008; Sitch et al., 2003).

Four different phenological states control plant allocation (Arora & Boer, 2005): dormancy, maximum growth, normal growth, and senescence (Fatichi et al., 2012). Temperature, soil moisture and photoperiod define the beginning of the growing season. Nutrient dynamics and forest stand growth are neglected.

B.2 DETAILS ABOUT THE INDEPENDENT VARIABLES

To express soil moisture controls on ecosystems, we compared two topographic variables, the upstream area and the topographic wetness index (hereafter “topographic index”), defined as the logarithm of the ratio of the upstream area and the topographic slope. We computed both indices for each pixel of each domain based on the DEM. We considered the explanatory power of each variable when used as a third explanatory variable (Table B.2) when regressing several ecohydrological variables. We adopted the topographic index as the third variable, because it describes better the water fluxes in the more sensible dry case (in which we expected soil moisture to play a more important role) and it is superior to upstream area for all variables in the Kleine Emme catchment. This is not surprising, because the topographic index is by definition more appropriate to express soil moisture limitations (compared with the upstream area) as it accounts for the effect of slope. Since topographic index and air temperature are correlated in the synthetic domain (Table B.3), we applied residual regression. Following the methodology as previously described (Graham, 2003), topographic index was regressed against air temperature. Using the residuals of this regression, we substituted topographic index.

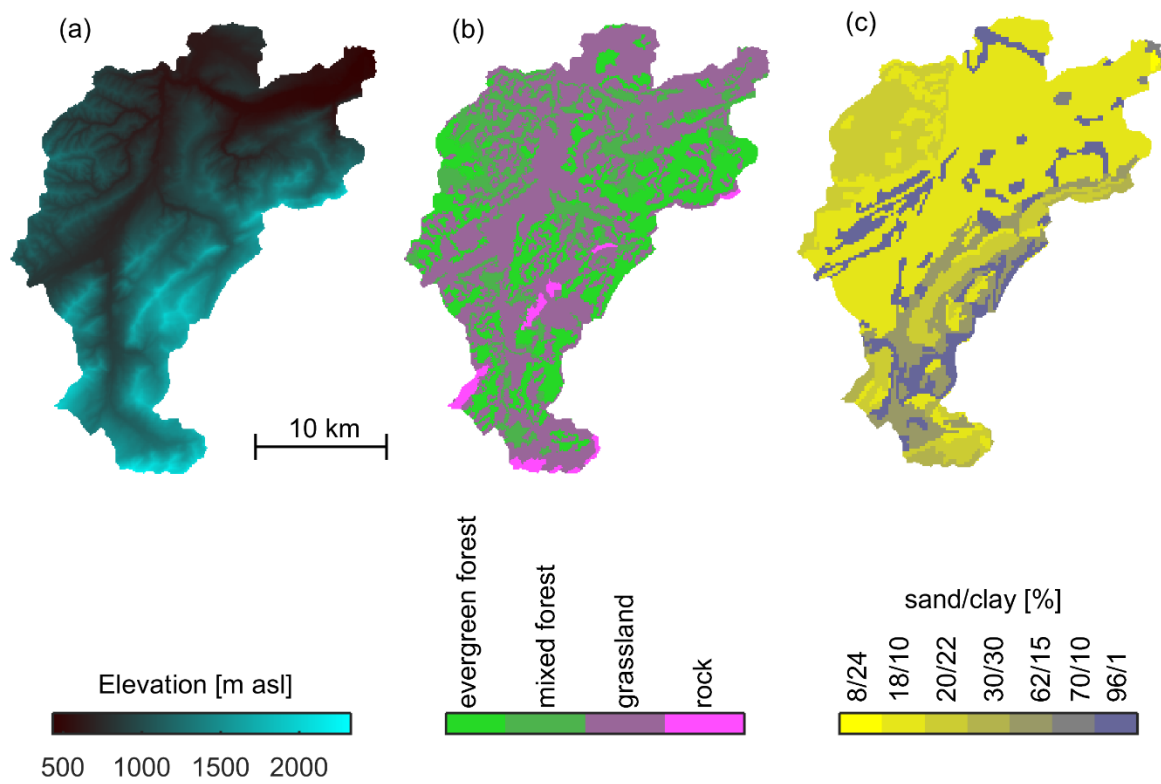


Figure B.1 The Kleine Emme catchment; elevation (a), land cover (b) and soil texture (c).

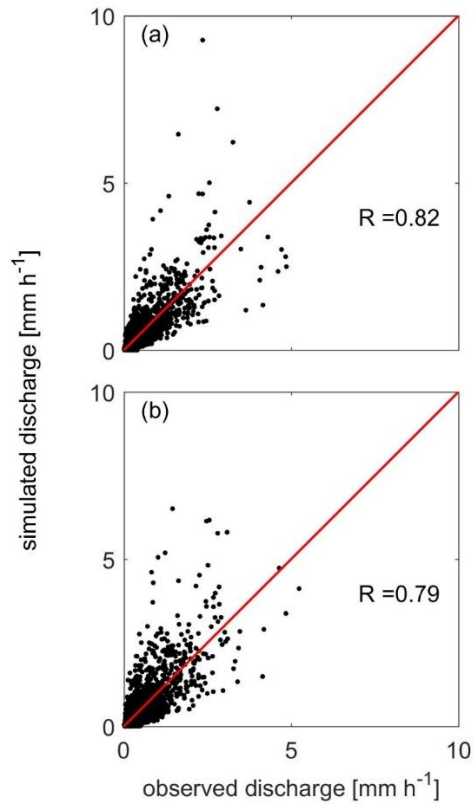


Figure B.2 Simulated and observed hourly discharge in Littau (a) and Werthenstein (b). For details about the two hydrological stations, refer to Table B.1.

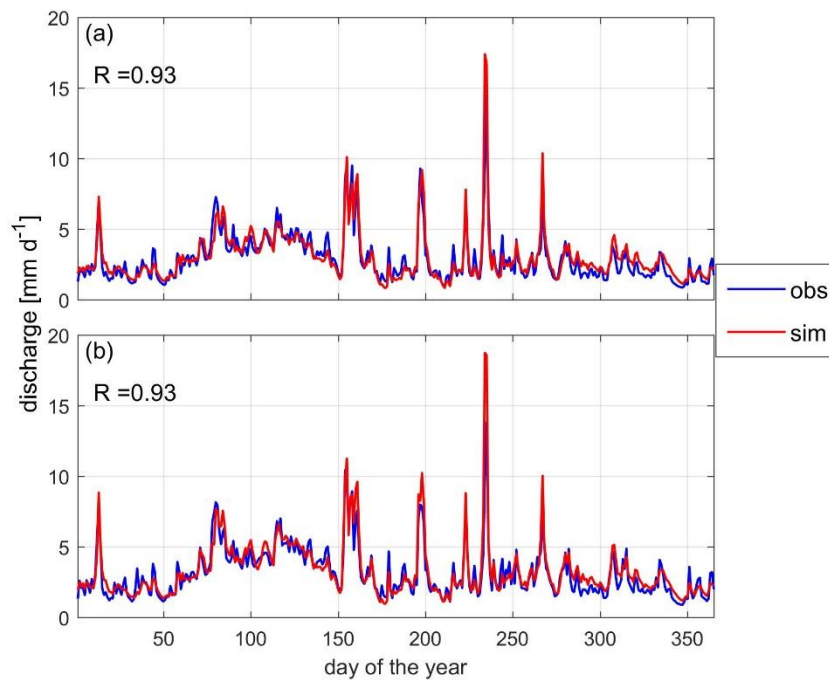


Figure B.3 Simulated and observed discharge seasonality for the simulated period (1/10/2000-30/9/2005) in Littau (a) and Werthenstein (b). For details about the two hydrological stations, refer to Table B.1.

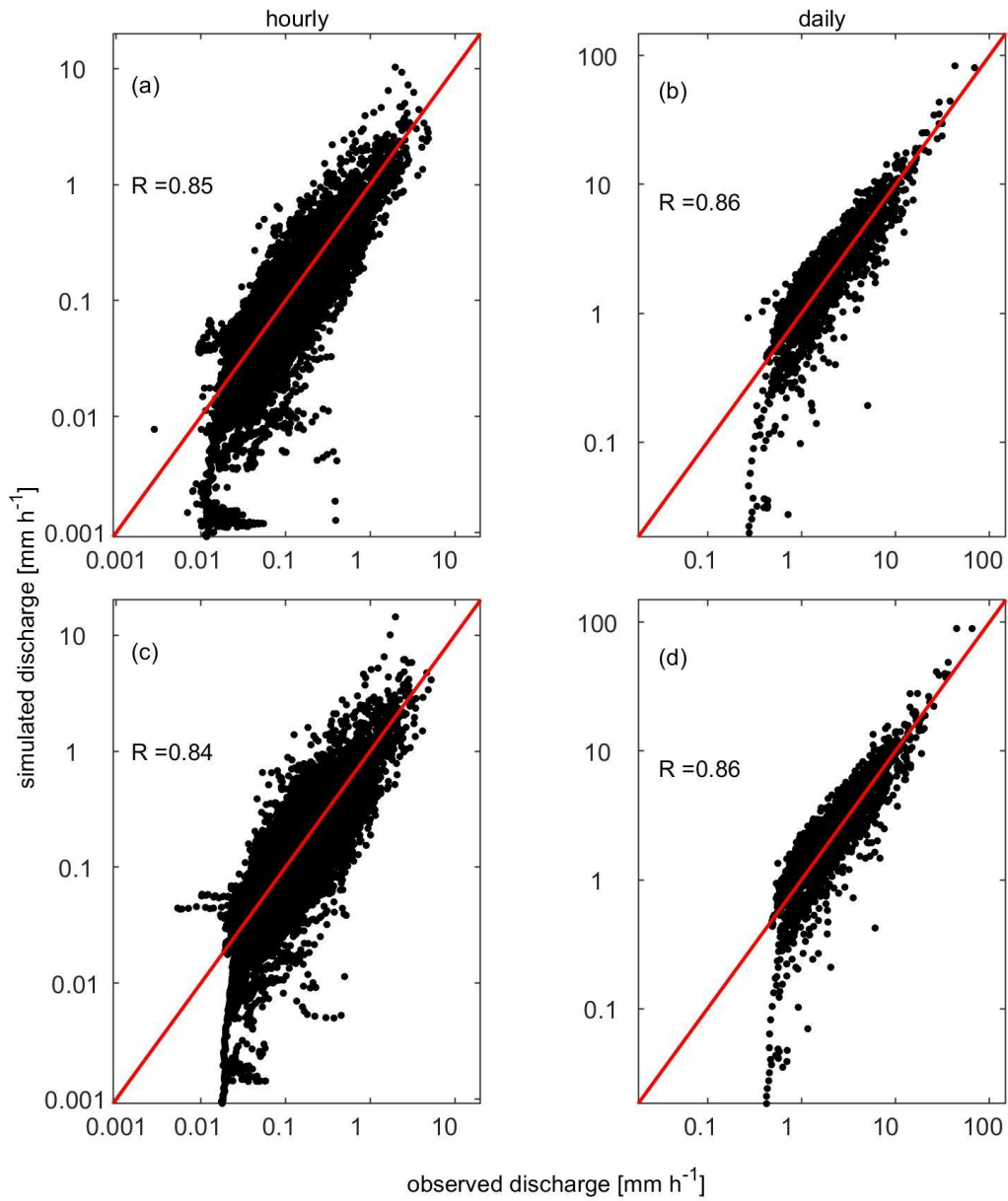


Figure B.4 Simulated and observed hourly (a and c) and daily (b and d) discharge in Littau (upper plots) and Werthenstein (lower plots) in logarithmic scale.

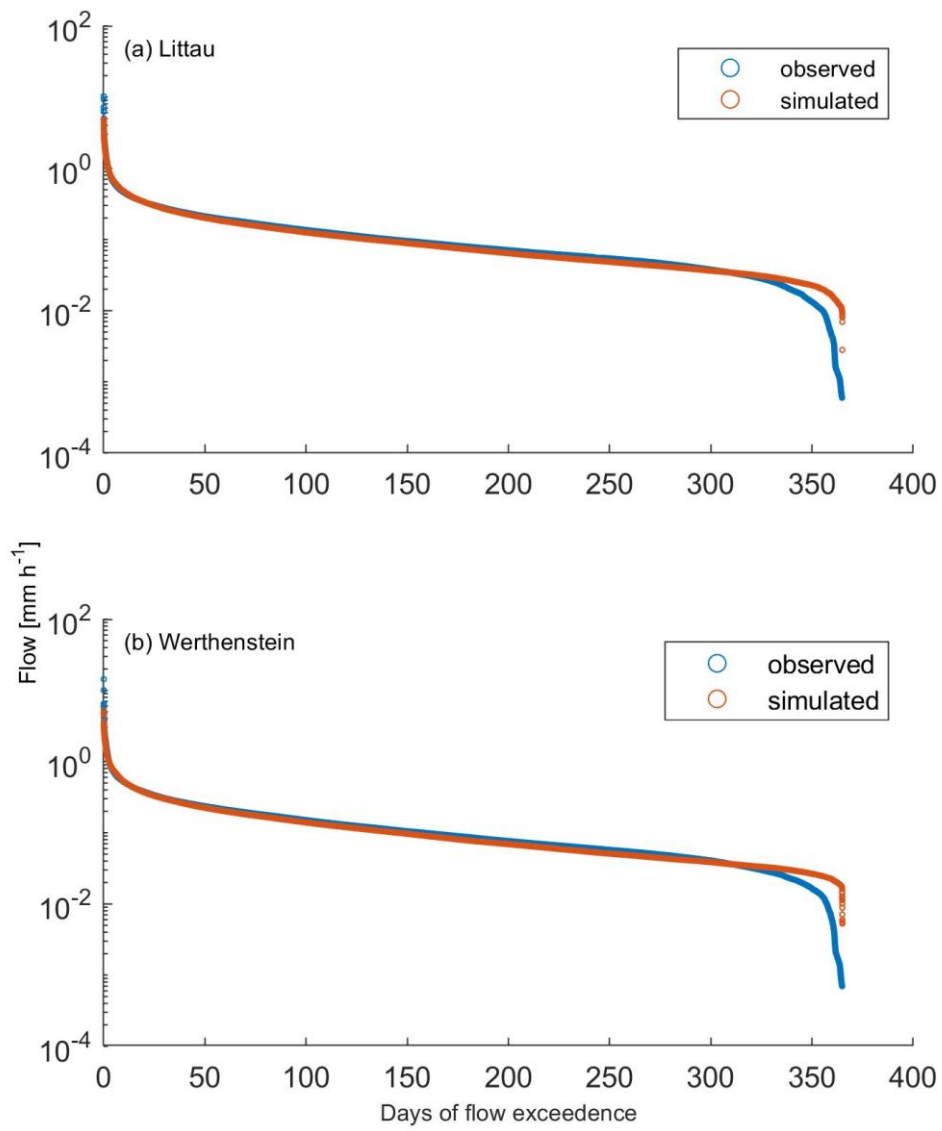


Figure B.5 Observed and simulated flow duration curves for Littau (a) and Werthenstein (b).

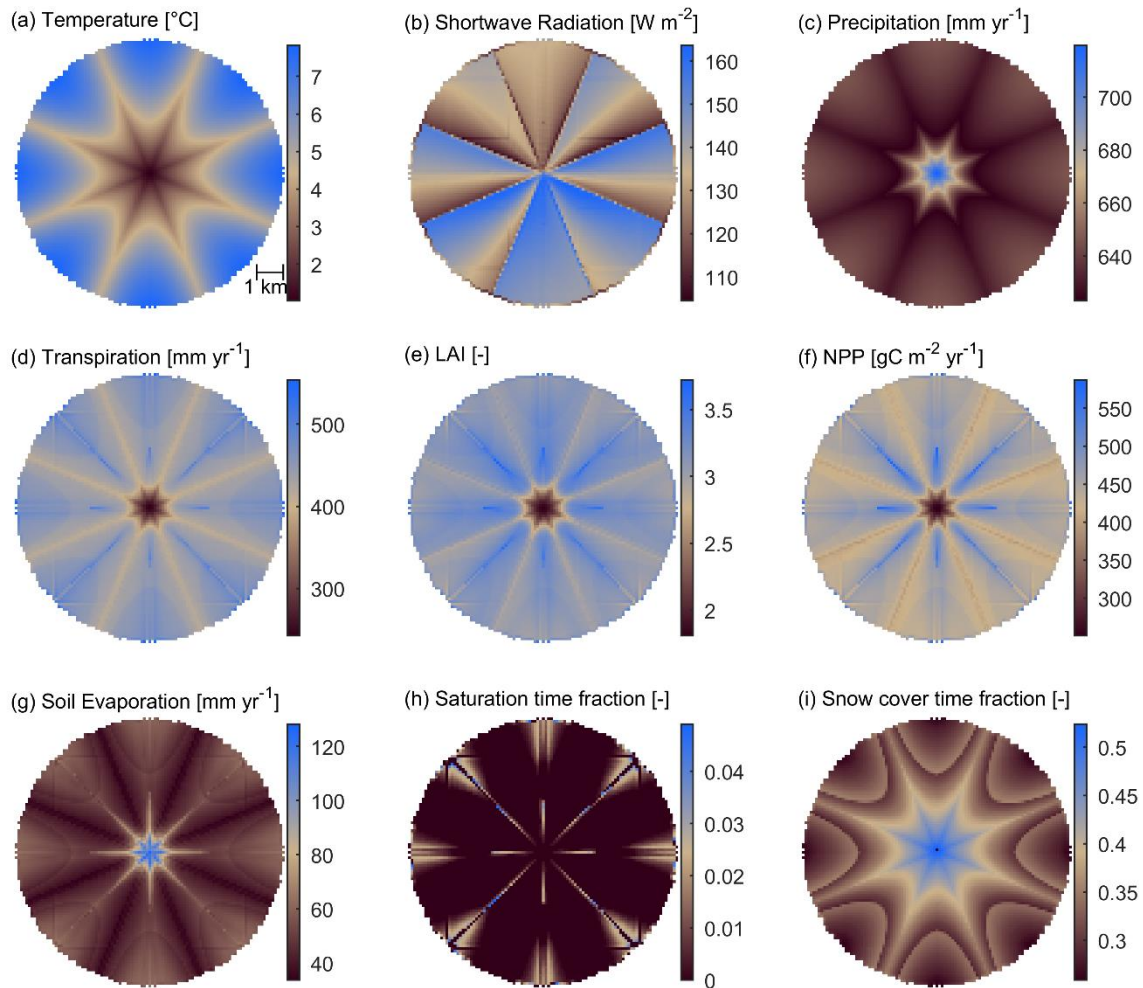


Figure B.6 Summary of the meteorological input and simulated ecohydrological variables for the dry evergreen forest experiment in the synthetic domain. The subplots show the four-year average of annual (a) temperature, (b) shortwave radiation, (c) precipitation, (d) transpiration, (e) leaf area index (LAI), (f) net primary production (NPP), (g) soil evaporation, (h) fraction of time with soil saturation, and (i) fraction of time with snow cover.

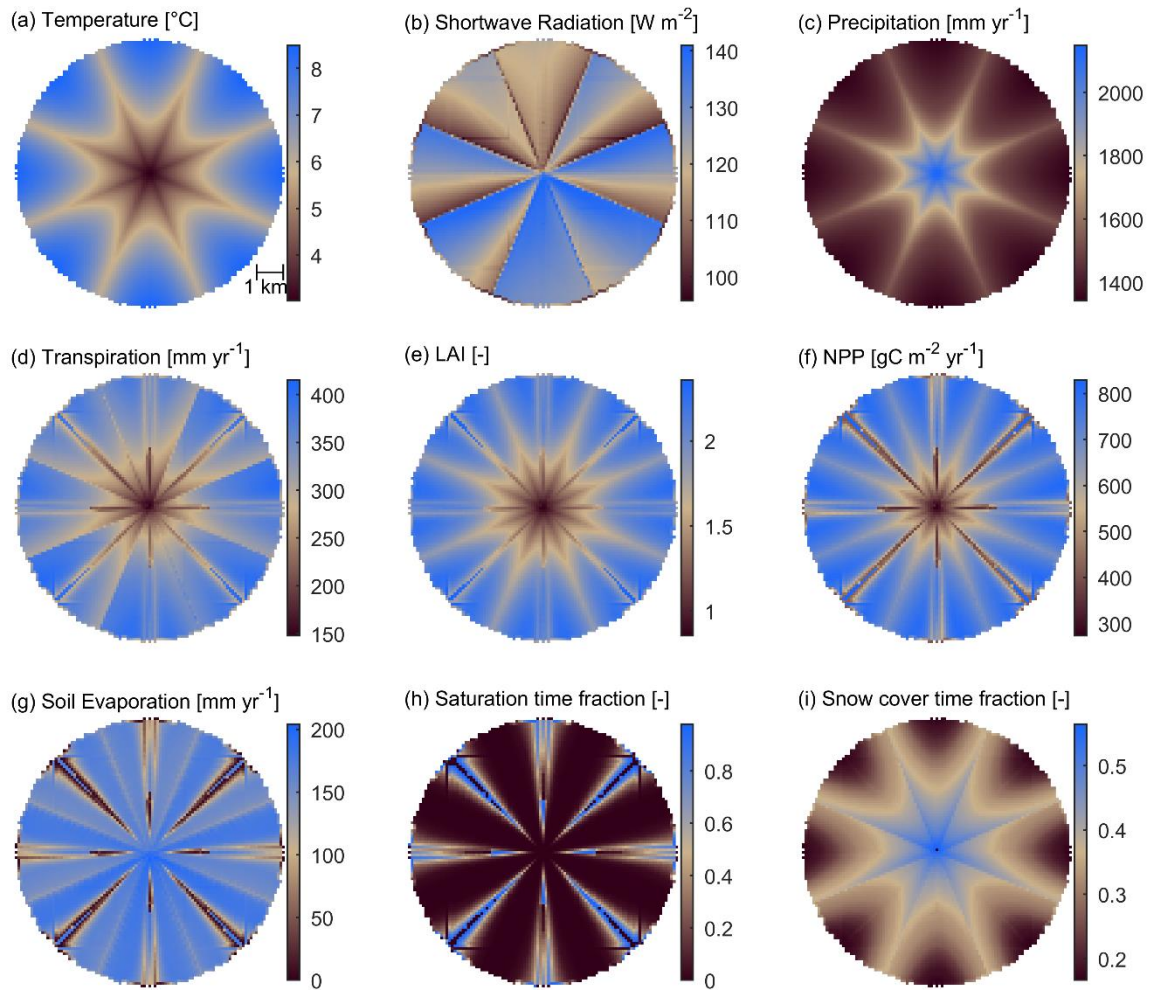


Figure B.7 Summary of the meteorological input and simulated ecohydrological variables for the wet grassland experiment in the synthetic domain. The subplots show the four-year average of annual (a) temperature, (b) shortwave radiation, (c) precipitation, (d) transpiration, (e) leaf area index (LAI), (f) net primary production (NPP), (g) soil evaporation, (h) fraction of time with soil saturation, and (i) fraction of time with snow cover.

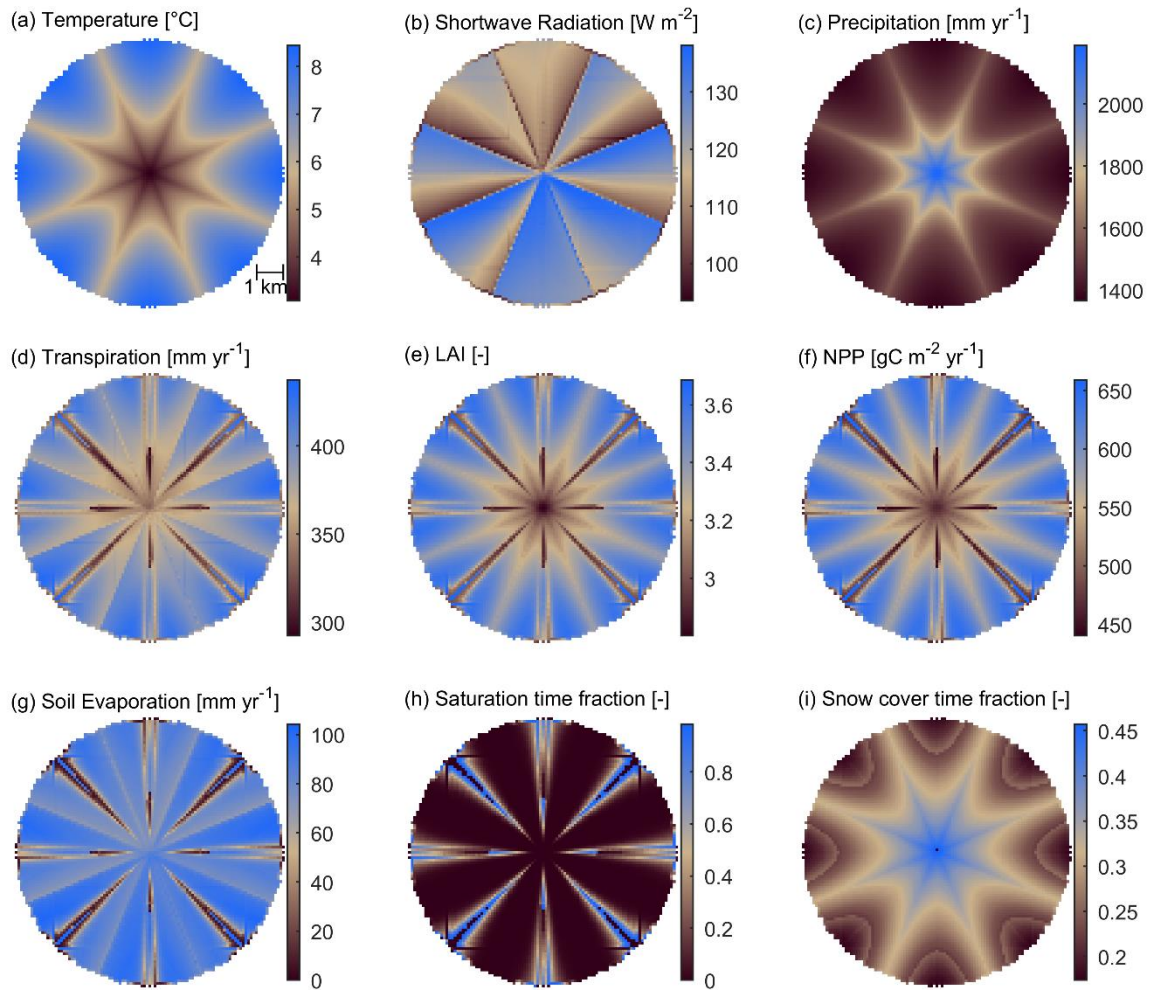


Figure B.8 Summary of the meteorological input and simulated ecohydrological variables for the wet evergreen forest experiment in the synthetic domain. The subplots show the four-year average of annual (a) temperature, (b) shortwave radiation, (c) precipitation, (d) transpiration, (e) leaf area index (LAI), (f) net primary production (NPP), (g) soil evaporation, (h) fraction of time with soil saturation, and (i) fraction of time with snow cover.

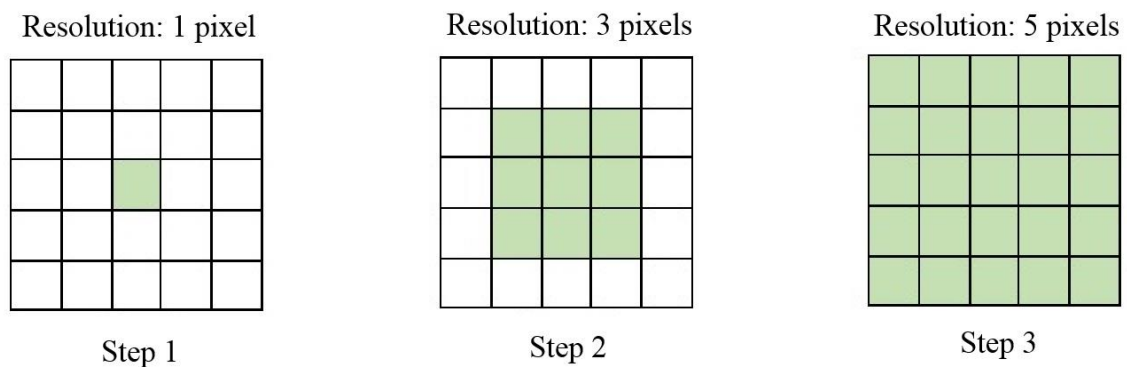


Figure B.9 Analysis of variance across spatial scales. The green colour shows the aggregation area, which is stepwise increased.

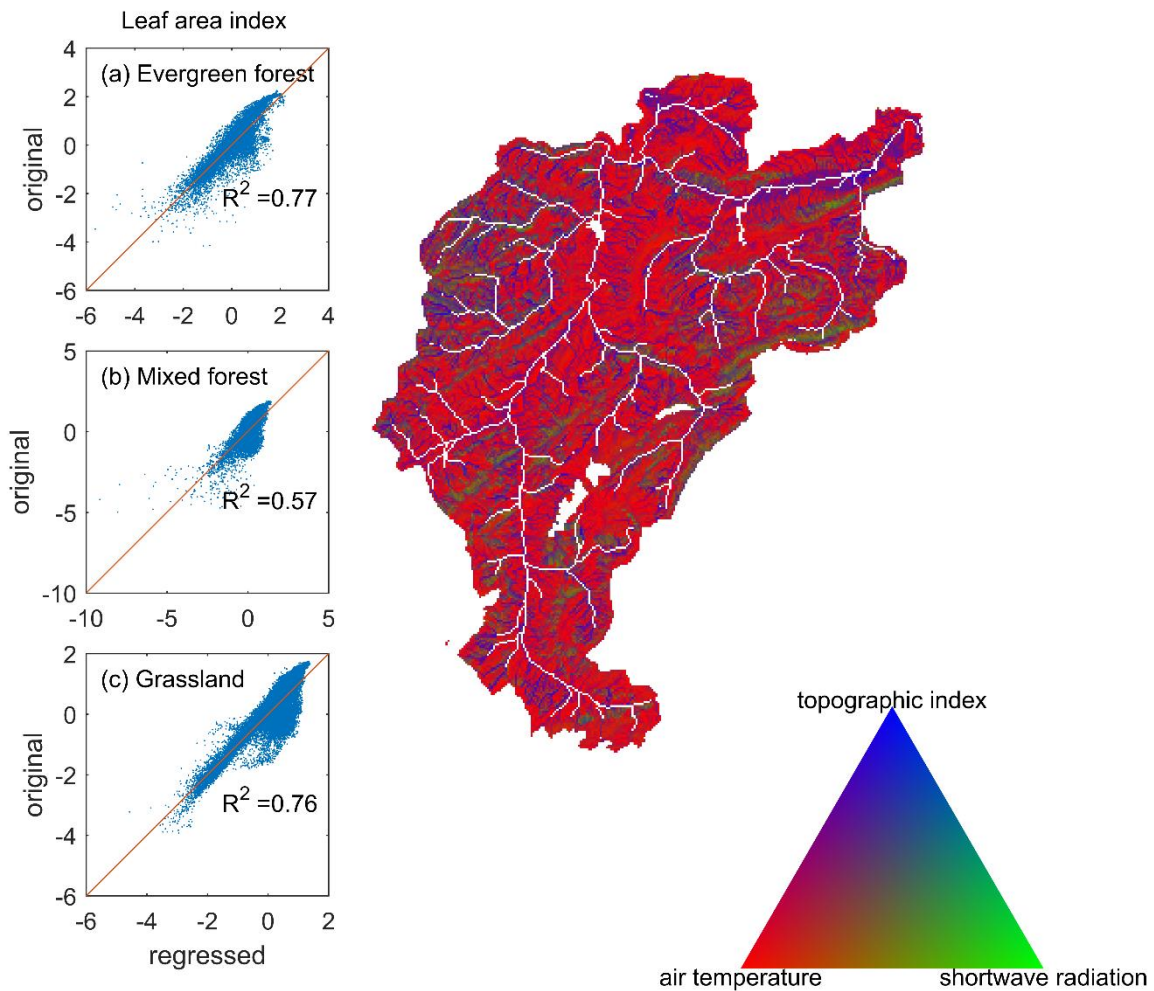


Figure B.10 Normalized sensitivity of leaf area index (LAI) to air temperature, shortwave radiation and topographic index in Kleine Emme. The red colour represents areas where temperature is the main control for LAI. Green represents the radiation-limited areas and blue is for areas where the topographic index is the dominant control. Inset scatter plots show the comparison between the original model output (“original”) and the values that are calculated with the regression formula that was used for the sensitivity analysis (“regressed”) for (a) evergreen forest, (b) mixed forest, and (c) grassland (the R^2 value of each regression is also shown). All variables are normalized.

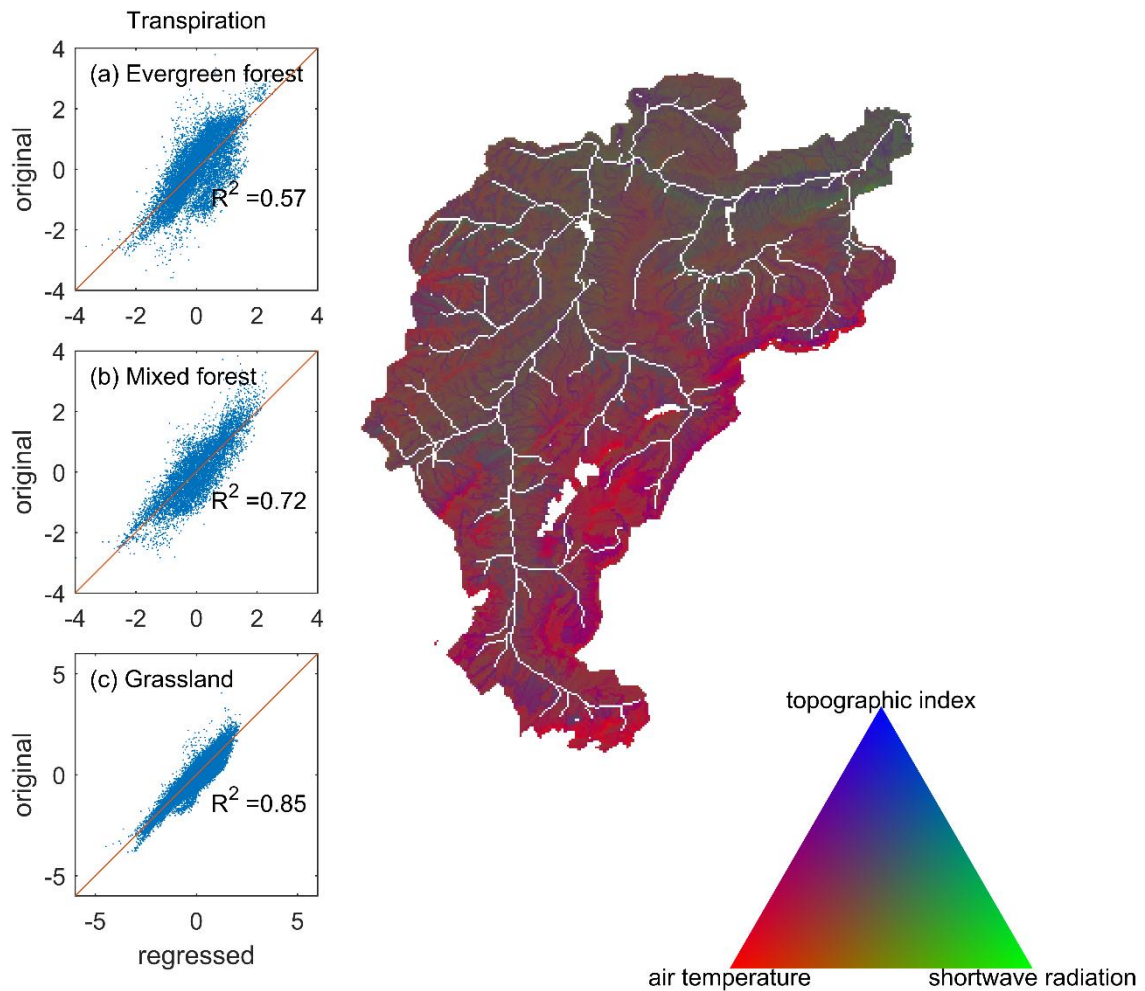


Figure B.11 Normalized sensitivity of transpiration (T) to air temperature, shortwave radiation and topographic index in Kleine Emme. The red colour represents areas where temperature is the main control for T. Green represents the radiation-limited areas and blue is for areas where the topographic index is the dominant control. Inset scatter plots show the comparison between the original model output (“original”) and the values that are calculated with the regression formula that was used for the sensitivity analysis (“regressed”) for (a) evergreen forest, (b) mixed forest, and (c) grassland (the R^2 value of each regression is also shown). All variables are normalized.

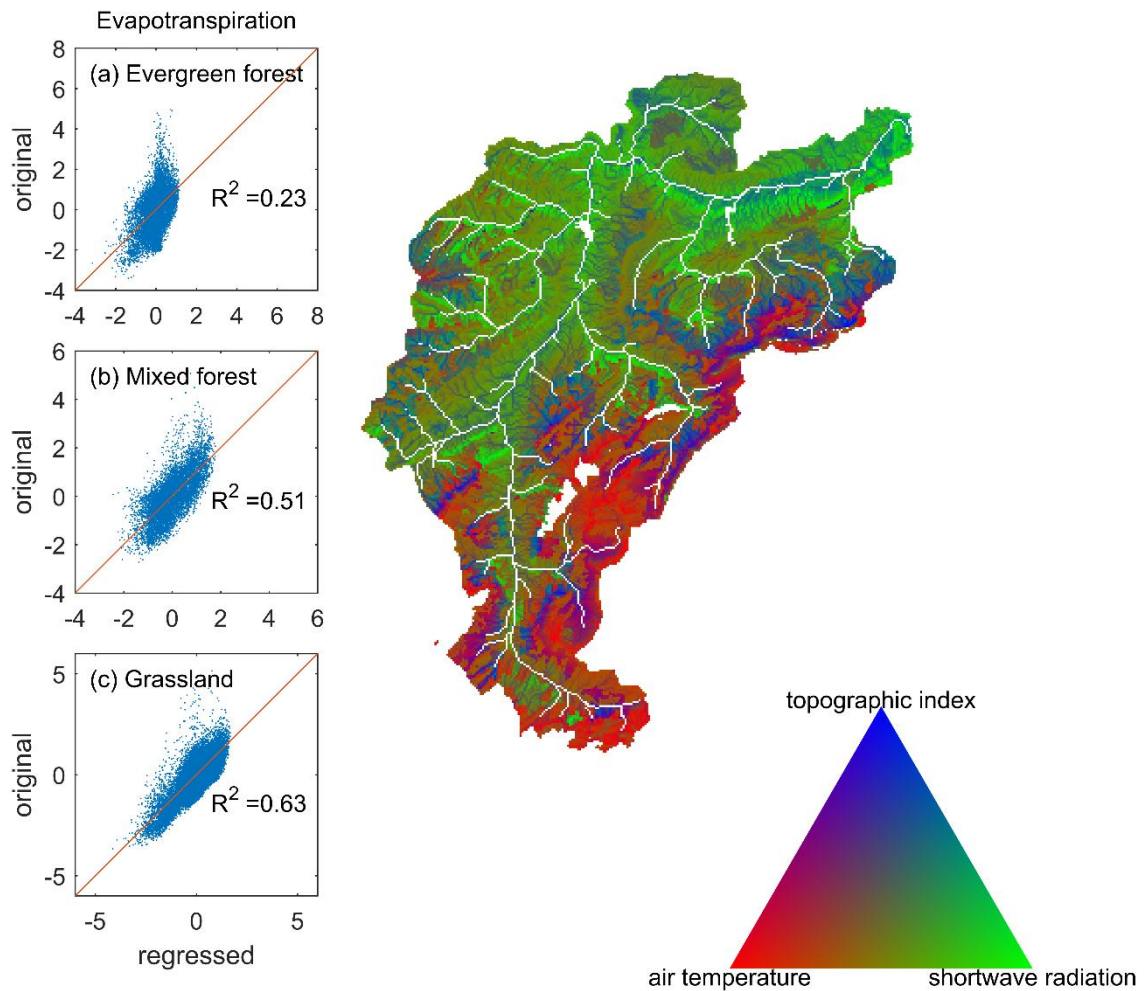


Figure B.12 Normalized sensitivity of evapotranspiration (ET) to air temperature, shortwave radiation and topographic index in Kleine Emme. The red colour represents areas where temperature is the main control for ET. Green represents the radiation-limited areas and blue is for areas where the topographic index is the dominant control. Inset scatter plots show the comparison between the original model output (“original”) and the values that are calculated with the regression formula that was used for the sensitivity analysis (“regressed”) for (a) evergreen forest, (b) mixed forest, and (c) grassland (the R^2 value of each regression is also shown). All variables are normalized.

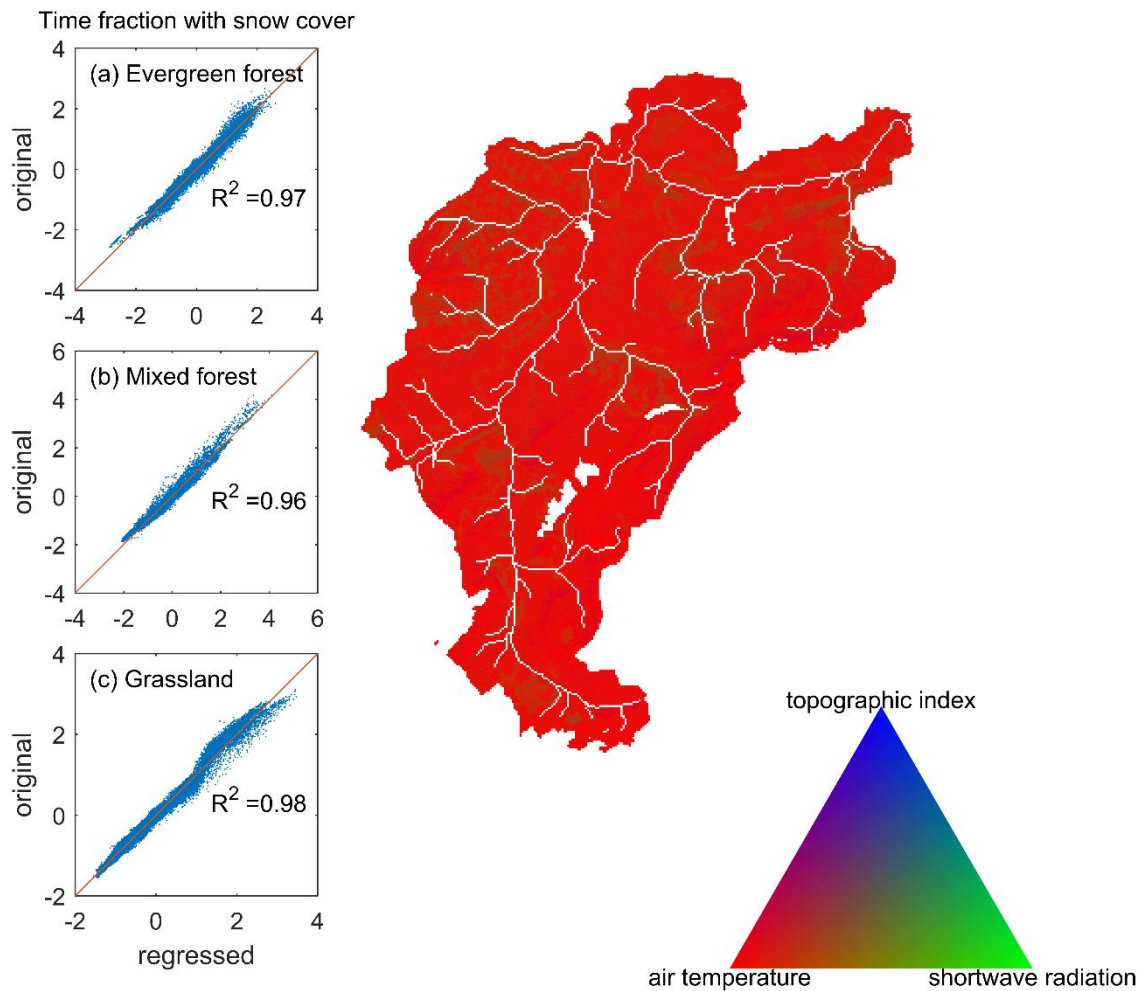


Figure B.13 Normalized sensitivity of the fraction of time with snow cover (snoFra) to air temperature, shortwave radiation and topographic index in Kleine Emme. The red colour represents areas where temperature is the main control for snoFra. Green represents the radiation-limited areas and blue is for areas where the topographic index is the dominant control. Inset scatter plots show the comparison between the original model output (“original”) and the values that are calculated with the regression formula that was used for the sensitivity analysis (“regressed”) for (a) evergreen forest, (b) mixed forest, and (c) grassland (the R^2 value of each regression is also shown). All variables are normalized.

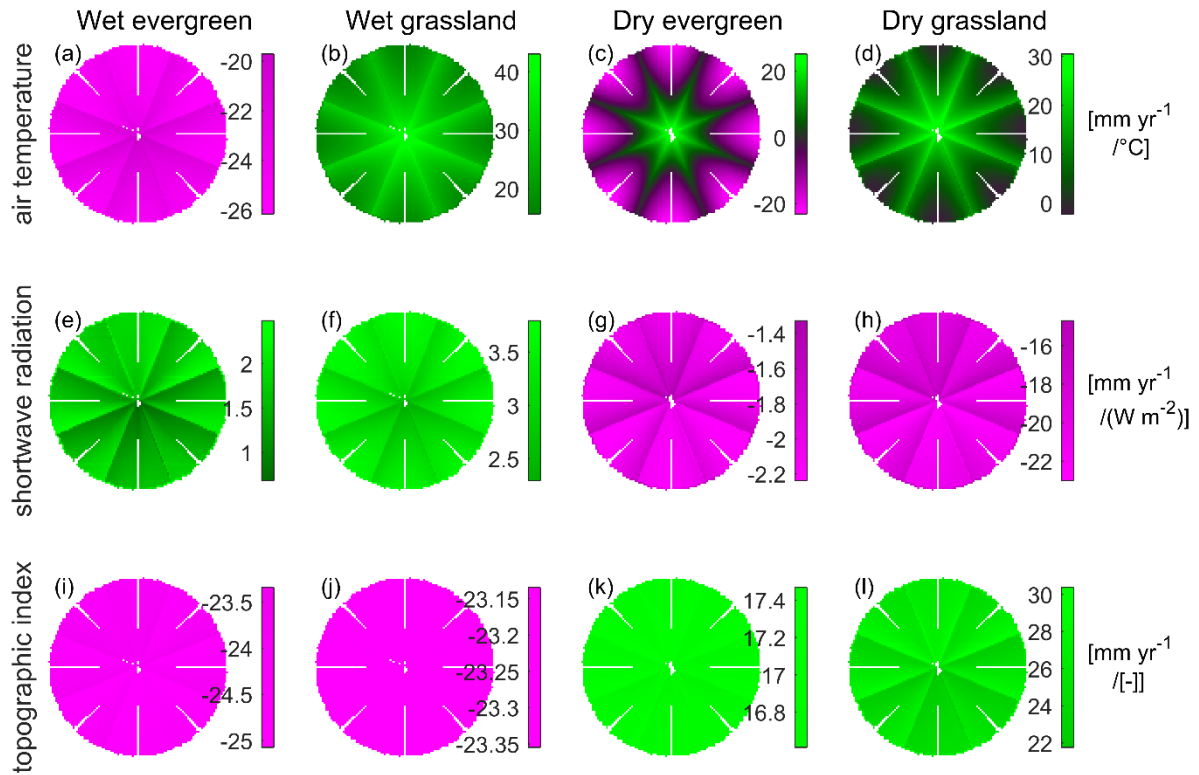


Figure B.14 Sensitivity of evapotranspiration (ET) to air temperature, shortwave radiation and topographic index in the four experiments on the synthetic domain. Green represents areas where an increase in the explanatory variable leads to an increase in ET and magenta is for areas where an increase in the explanatory variable leads to a decrease in ET. Areas shown in dark colour are those where ET is insensitive to respective explanatory variable.

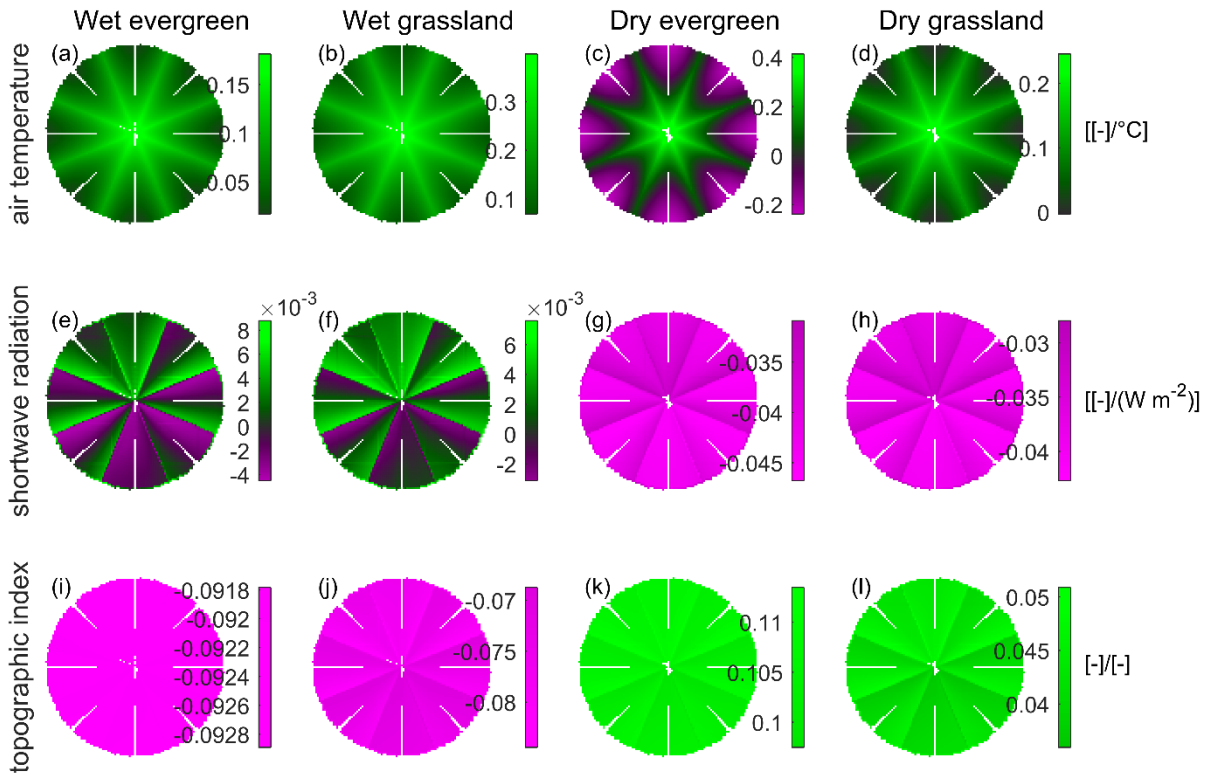


Figure B.15 Sensitivity of leaf area index (LAI) to air temperature, shortwave radiation and topographic index in the four experiments on the synthetic domain. Green represents areas where an increase in the explanatory variable leads to an increase in LAI and magenta is for areas where an increase in the explanatory variable leads to a decrease in LAI. Areas shown in dark colour are those where LAI is insensitive to respective explanatory variable.

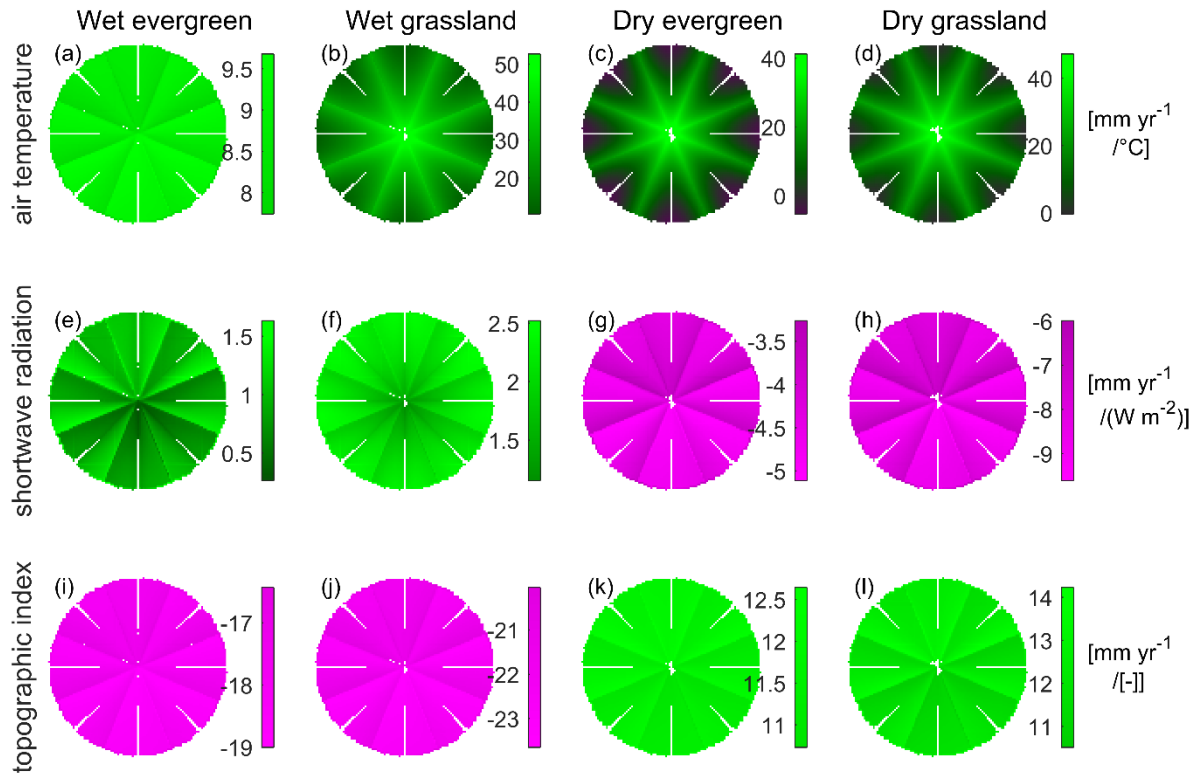


Figure B.16 Sensitivity of transpiration (T) to air temperature, shortwave radiation and topographic index in the four experiments on the synthetic domain. Green represents areas where an increase in the explanatory variable leads to an increase in T and magenta is for areas where an increase in the explanatory variable leads to a decrease in T . Areas shown in dark colour are those where T is insensitive to respective explanatory variable.

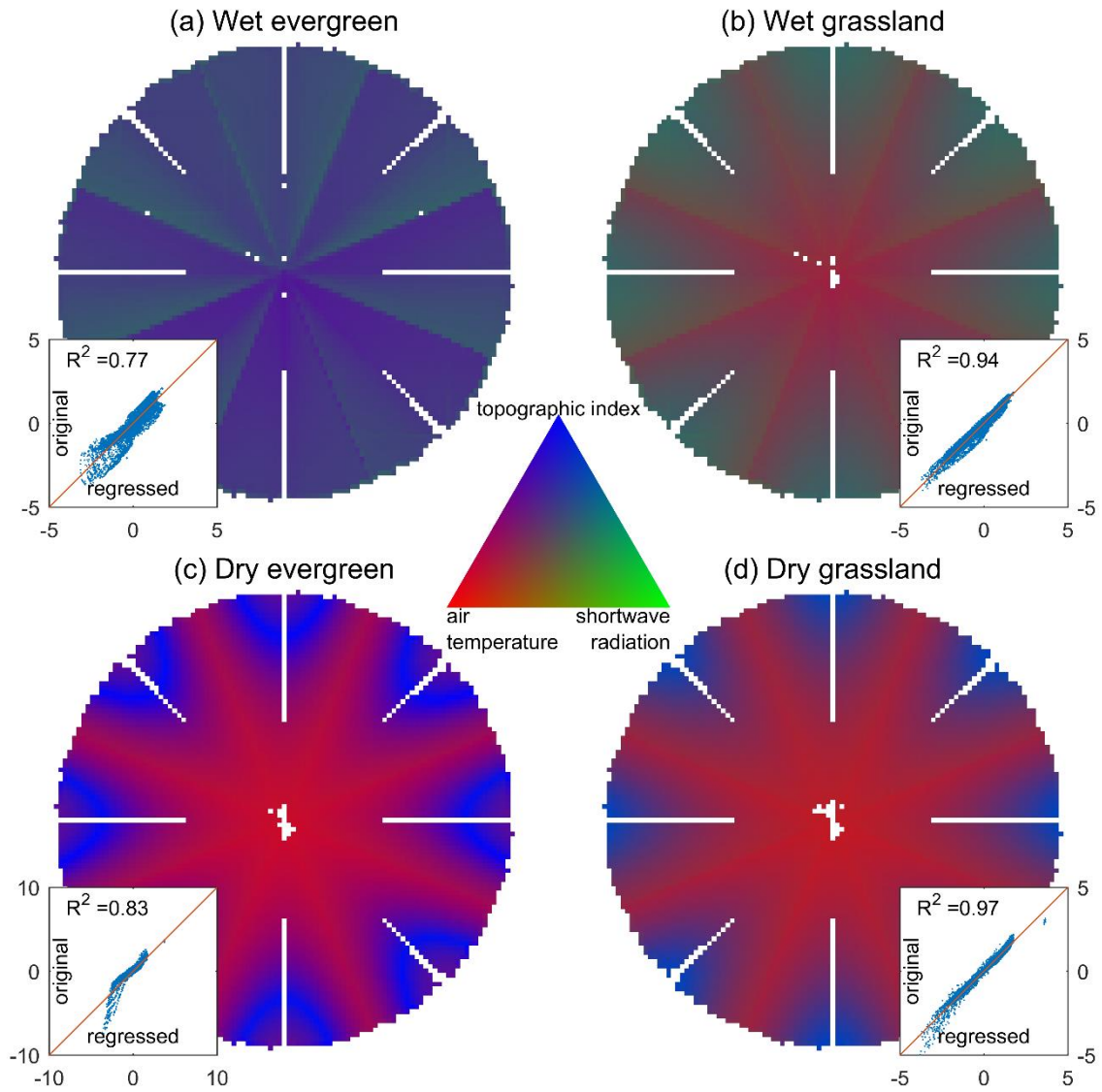


Figure B.17 Normalized transpiration (T) to air temperature, shortwave radiation and topographic index in the four experiments on the synthetic domain. The red colour represents areas where temperature is the main control for T. Green represents the radiation-limited areas and blue is for areas where the topographic index is the dominant control. Inset scatter plots show the comparison between the original model output (“original”) and the values that are calculated with the regression formula that was used for the sensitivity analysis (“regressed”, R^2 values are also shown). All variables are normalized.

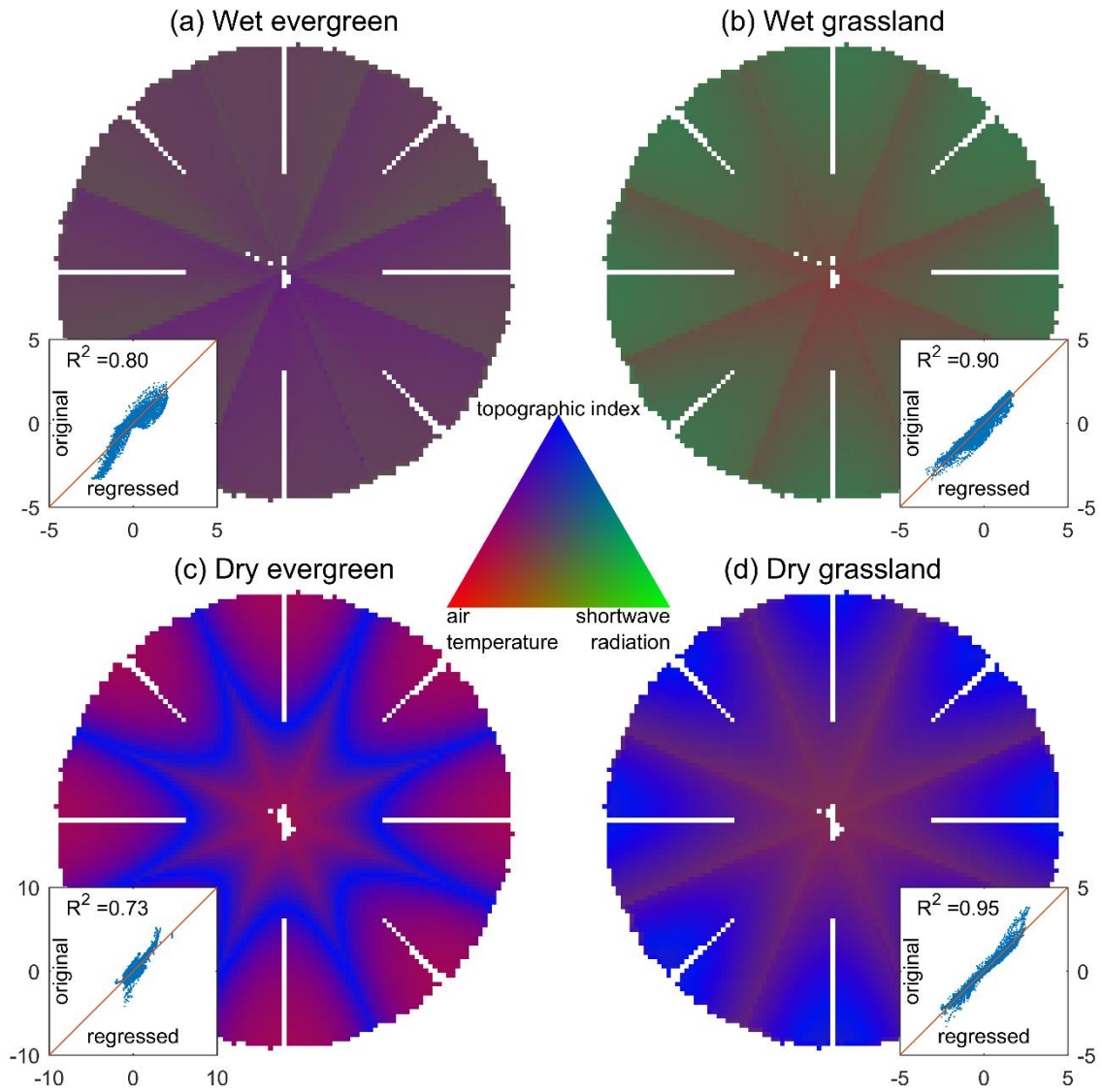


Figure B.18 Normalized sensitivity of evapotranspiration (ET) to air temperature, shortwave radiation and topographic index in the four experiments on the synthetic domain. The red colour represents areas where temperature is the main control for ET. Green represents the radiation-limited areas and blue is for areas where the topographic index is the dominant control. Inset scatter plots show the comparison between the original model output (“original”) and the values that are calculated with the regression formula that was used for the sensitivity analysis (“regressed”, R^2 values are also shown). All variables are normalized.

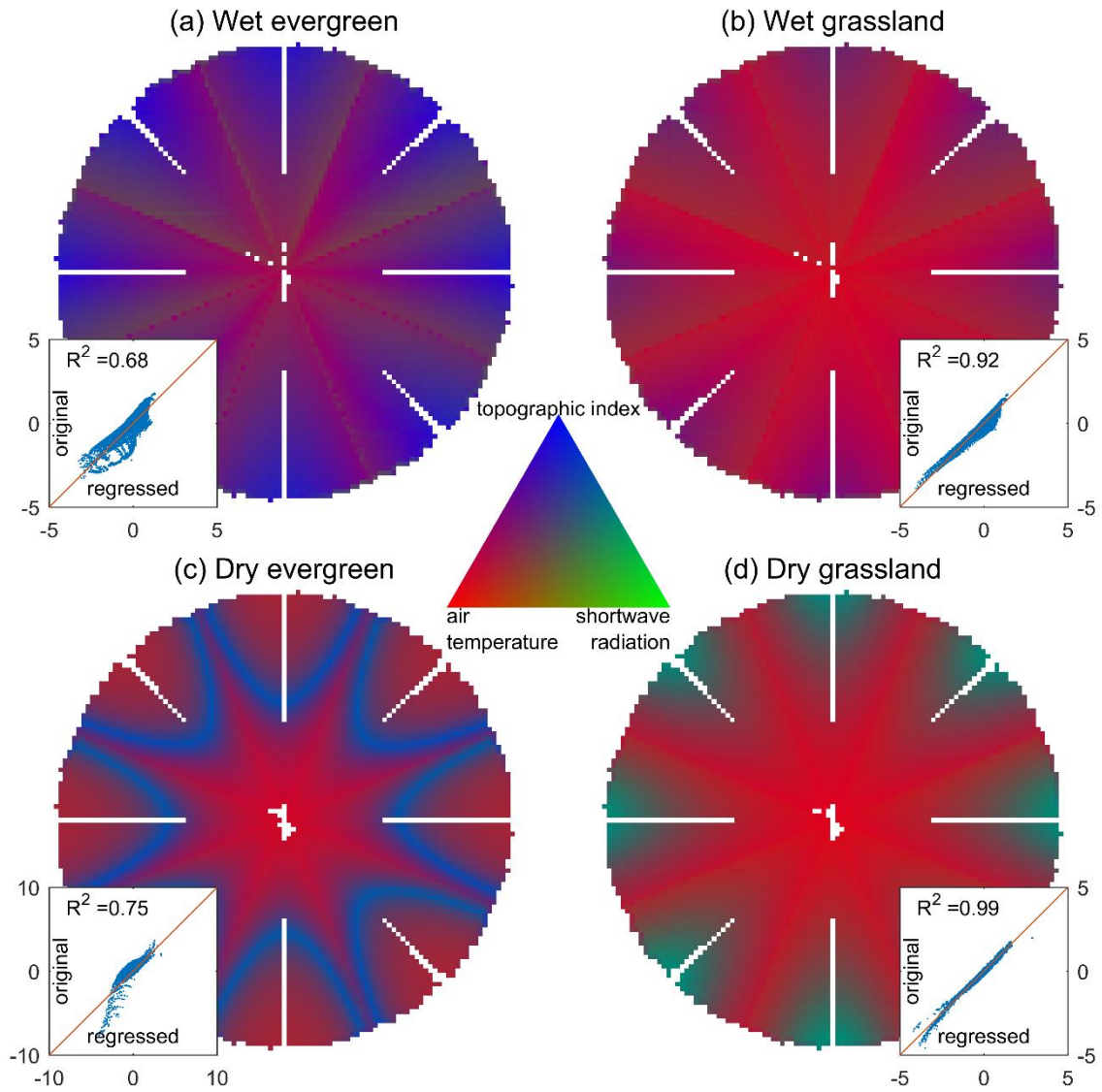


Figure B.19 Normalized sensitivity of leaf area index (LAI) to air temperature, shortwave radiation and topographic index in the four experiments on the synthetic domain. The red colour represents areas where temperature is the main control for LAI. Green represents the radiation-limited areas and blue is for areas where the topographic index is the dominant control. Inset scatter plots show the comparison between the original model output (“original”) and the values that are calculated with the regression formula that was used for the sensitivity analysis (“regressed”, R^2 values are also shown). All variables are normalized.

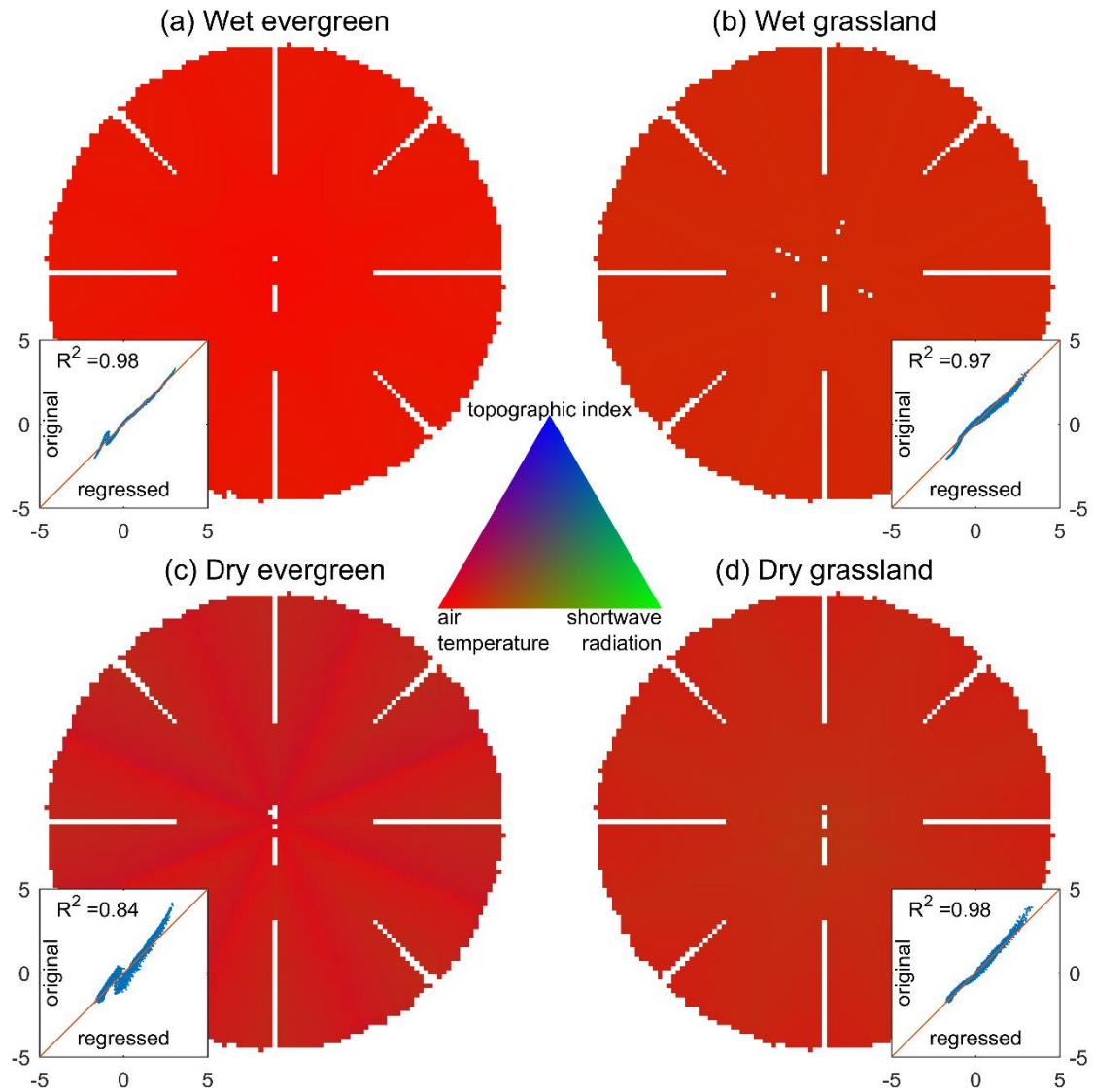


Figure B.20 Normalized sensitivity of the fraction of time with snow cover (snoFra) to air temperature, shortwave radiation and topographic index in the four experiments on the synthetic domain. The red colour represents areas where temperature is the main control for snoFra. Green represents the radiation-limited areas and blue is for areas where the topographic index is the dominant control. Inset scatter plots show the comparison between the original model output (“original”) and the values that are calculated with the regression formula that was used for the sensitivity analysis (“regressed”, R^2 values are also shown). All variables are normalized.

Table B.1. River discharge measurement stations in the Kleine Emme catchment.

Station name	Coordinates	Elevation [m]	Drainage area [km ²]
Emmen (Littau)	47°4' 0.1'' N, 8°17' 2.6'' E	430	478
Werthenstein	47°2' 5.6'' N, 8°4' 6.4'' E	540	311

Table B.2 Initial screening for the third explanatory variable to express water limitations. The table shows the explanatory power (R^2) of the regressions for transpiration (T), evapotranspiration (ET), net primary production (NPP), leaf area index (LAI), snow water equivalent (SWE) and the fraction of time with snow cover (snoFra) using air temperature, shortwave radiation and topographic index (upstream area).

	Wet	Wet	Dry	Dry	Kleine Emme		
	evergreen	grassland	evergreen	grassland	Evergreen	Mixed	Grassland
T	0.78 (0.86)	0.94 (0.94)	0.83 (0.77)	0.97 (0.92)	0.57 (0.52)	0.72 (0.61)	0.85 (0.78)
ET	0.80 (0.87)	0.90 (0.94)	0.73 (0.55)	0.95 (0.72)	0.23 (0.20)	0.51 (0.49)	0.63 (0.61)
NPP	0.65 (0.87)	0.74 (0.91)	0.80 (0.49)	0.95 (0.64)	0.72 (0.68)	0.42 (0.32)	0.42 (0.38)
LAI	0.68 (0.87)	0.92 (0.97)	0.75 (0.58)	0.99 (0.95)	0.77 (0.74)	0.57 (0.46)	0.76 (0.73)
SWE	0.98 (0.98)	0.98 (0.98)	0.38 (0.40)	0.89 (0.88)	0.75 (0.74)	0.67 (0.67)	0.90 (0.90)
snoFra	0.98 (0.98)	0.98 (0.98)	0.88 (0.89)	0.99 (0.99)	0.97 (0.97)	0.96 (0.96)	0.98 (0.98)

Table B.3 Correlation between the three explanatory variables in the wet and dry synthetic domains and in the Kleine Emme catchment.

	Air temperature			Shortwave radiation			Topographic index		
	wet	dry	Kl_Em	wet	dry	Kl_Em	wet	dry	Kl_Em
Air temperature	1	1	1	0	-0.02	0.24	0.67	0.67	0.33
Shortwave radiation	0	-0.02	0.24	1	1	1	0.10	0.08	0.24
Topographic index	0.67	0.67	0.33	0.10	0.08	0.24	1	1	1

Table B.4 Regression-derived relationships for transpiration (T), evapotranspiration (ET), net primary production (NPP) and leaf area index (LAI) in the Kleine Emme catchment (on normalized variables). y is the dependent variable and x_1 , x_2 and x_3 are the explanatory variables (air temperature, shortwave radiation and topographic index, respectively). The R^2 values are given in parenthesis after each equation.

	Evergreen forest	Mixed forest	Grassland
T	$y = 0.03 + 0.65x_1 + 0.24x_2 - 0.40x_3 + 0.14x_1x_2 - 0.02x_2x_3 - 0.001x_1^2 - 0.05x_3^2$ (0.57)	$y = -0.002 + 0.62x_1 + 0.40x_2 - 0.53x_3 + 0.09x_1x_2 - 0.05x_2x_3 + 0.005x_3^2$ (0.72)	$y = 0.06 + 0.77x_1 + 0.40x_2 - 0.45x_3 + 0.09x_1x_2 - 0.06x_2x_3 - 0.10x_1^2 + 0.05x_2^2 - 0.02x_3^2$ (0.85)
ET	$y = 0.21 + 0.07x_1 + 0.22x_2 - 0.33x_3 + 0.22x_1x_2 - 0.03x_2x_3 - 0.18x_1^2 - 0.06x_3^2$ (0.23)	$y = 0.06 + 0.30x_1 + 0.62x_2 - 0.11x_3 + 0.13x_1x_2 - 0.01x_2x_3 - 0.06x_3^2$ (0.51)	$y = 0.13 + 0.54x_1 + 0.48x_2 - 0.12x_3 + 0.12x_1x_2 - 0.03x_2x_3 - 0.17x_1^2 + 0.09x_2^2 - 0.08x_3^2$ (0.63)
NPP	$y = 0.40 + 0.67x_1 + 0.03x_2 + 0.04x_3 - 0.01x_1x_2 + 0.08x_2x_3 + 0.01x_1^2 - 0.14x_2^2 - 0.30x_3^2$ (0.72)	$y = 0.44 + 0.40x_1 - 0.08x_2 + 0.09x_3 + 0.03x_1x_2 + 0.08x_2x_3 - 0.14x_2^2 - 0.33x_3^2$ (0.42)	$y = 0.37 + 0.40x_1 + 0.003x_2 - 0.13x_3 + 0.004x_1x_2 + 0.07x_2x_3 - 0.09x_1^2 - 0.07x_2^2 - 0.22x_3^2$ (0.42)
LAI	$y = 0.39 + 0.70x_1 + 0.05x_2 - 0.05x_3 + 0.003x_1x_2 + 0.08x_2x_3 + 0.005x_1^2 - 0.14x_2^2 - 0.29x_3^2$ (0.77)	$y = 0.44 + 0.53x_1 - 0.06x_2 + 0.02x_3 + 0.03x_1x_2 + 0.06x_2x_3 - 0.13x_2^2 - 0.33x_3^2$ (0.57)	$y = 0.22 + 0.82x_1 + 0.01x_2 - 0.09x_3 + 0.01x_1x_2 + 0.04x_2x_3 - 0.05x_1^2 - 0.03x_2^2 - 0.14x_3^2$ (0.76)

Table B.5 Normalized sensitivity of T, ET, NPP and LAI to air temperature, shortwave radiation and topographic index for transpiration (T), net primary production (NPP) and leaf area index (LAI) along the altitudinal gradient in the Kleine Emme catchment. The values in the table represent the respective partial derivative (equation 3.2).

Altitude (m)	Transpiration			Evapotranspiration			NPP			LAI		
	Temp	Rad	topIn	Temp	Rad	topIn	Temp	Rad	topIn	Temp	Rad	topIn
<800	0.61	0.48	-0.49	0.20	0.65	-0.20	0.29	0	-0.27	0.69	0.01	-0.21
800-1200	0.70	0.39	-0.45	0.28	0.49	-0.16	0.47	-0.03	0.01	0.72	-0.01	-0.02
1200-1600	0.78	0.22	-0.42	0.56	0.21	-0.19	0.61	0.03	0.03	0.78	0.03	-0.01
1600-2000	1.00	0.15	-0.38	1.05	0.07	-0.06	0.74	0.01	0.18	0.93	-0.01	0.12
>2000	1.30	0.15	-0.37	1.49	0.02	0.07	0.97	0	0.29	1.11	-0.02	0.19

Table B.6 Normalized sensitivity of T, ET, NPP and LAI to air temperature, shortwave radiation and topographic index for transpiration (T), net primary production (NPP) and leaf area index (LAI) along the altitudinal gradient in the dry grassland numerical experiment. The values in the table represent the respective partial derivative (equation 3.2).

Altitude (m)	Transpiration			Evapotranspiration			NPP			LAI		
	Temp	Rad	topIn	Temp	Rad	topIn	Temp	Rad	topIn	Temp	Rad	topIn
<1700	0.22	0.16	0.40	0.09	-0.02	0.86	-0.57	-0.67	0.84	0.24	-0.30	0.29
1700-1900	0.62	0.19	0.19	0.34	0.08	0.86	1.07	-0.56	0.85	0.66	-0.24	0.29
1900-2100	1.01	0.22	0.22	0.59	0.18	0.86	1.71	-0.45	0.85	1.09	-0.18	0.30
2100-2300	1.44	0.25	0.25	0.86	0.28	0.85	1.41	-0.33	0.84	1.55	-0.12	0.29
>2300	1.83	0.27	0.27	1.10	0.37	0.85	2.04	-0.23	0.84	1.96	-0.06	0.29

Appendix C: More green and less blue water in the Alps during warmer summers

C.1 THE TETHYS-CHLORIS MODEL (T&C)

We performed simulations with the distributed ecohydrological model Tethys-Chloris (T&C). T&C simulates the coupled dynamics of energy, water, and vegetation and has been successfully applied to a very large spectrum of ecosystems and environmental conditions as summarized elsewhere (e.g., Fatichi et al., 2012a, 2012b; Fatichi & Leuzinger, 2013; Fatichi, Leuzinger, & Körner, 2014; Fatichi & Pappas, 2017; Fatichi, Zeeman, et al., 2014; Manoli et al., 2018; Mastrotheodoros et al., 2017, 2018; Wu et al., 2018).

The model simulates the energy, water, and carbon exchanges between the land surface and the atmospheric surface layer accounting for aerodynamic, undercanopy, and leaf boundary layer resistances, as well as for stomatal and soil resistances (Sellers et al., 1997). In each simulated grid cell, vegetation can occupy two vertical layers to mimic the coexistence of trees and bushes/grasses. Horizontal composition of vegetation is also possible since each element can account for multiple species or plant functional types (Fatichi et al., 2012a; Fatichi & Leuzinger, 2013). Dynamics of water content in the soil profile are solved using a quasi 3-D approach: the one-dimensional (1-D) Richards equation is used for the vertical flow and the kinematic wave equation is used for lateral subsurface flow. Saturated and unsaturated parts of the soil column are explicitly identified. Surface overland flow and channel flow are also solved by the kinematic equation. Snowpack dynamics are computed by the energy balance: snow can be intercepted by the vegetation or fall to the ground, where it accumulates and successively melts. Runoff generation occurs via saturation excess and infiltration excess mechanisms and depends on lateral moisture fluxes in the unsaturated and saturated zones as well as on overland flow (Loague et al., 2010). Soil water content, infiltration, and runoff production are estimated with an adaptive time step based on a maximum allowed water content difference (seconds to 5 min), and overland flow routing is computed with an adaptive time step that satisfies the Courant-Friedrichs-Lewy condition [seconds to 5 min, (Hunter, Horritt, Bates, Wilson, & Werner, 2005)]. The version of T&C used in this study does not include soil freezing and thawing processes and the water present in soil pores is always considered to be in a liquid state. The leakage from rocks is computed as the minimum between the intercepted water in rocks and the hydraulic conductivity of rocks (which is zero for compacted rocks and positive for fractured rocks). A free drainage condition can be also given: in that case, the intercepted water in rocks is completely infiltrated in the fractured rock and no water remains on the rock surface. The rock leakage supplies the fractured rock water storage. The soil biogeochemistry module is not activated, thus there is no evaporation from litter but only from soil.

Photosynthesis is simulated using the Farquhar biochemical model (Collatz et al., 1991, 1992; Farquhar et al., 1980) adapted with subsequent modifications and temperature dependence of biochemical parameters. The model follows the two big leaves scheme, where sunlit and shaded leaves are treated separately for estimating net assimilation and stomatal resistance (Dai et al., 2004; de Pury & Farquhar, 1997; Wang & Leuning, 1998). Leaf maintenance respiration is assumed equal to the leaf dark respiration and acclimation effects are not accounted for. For upscaling photosynthesis from leaf to plant scale, photosynthetic capacity is assumed to decay exponentially with canopy depth (Bonan et al., 2011; Ivanov et al., 2008a). The stomatal conductance parameterization accounts for net assimilation rate, leaf internal CO₂ concentration and vapour pressure deficit following the Leuning model (Leuning, 1990, 1995). The dynamics of seven carbon pools are explicitly simulated in the model and include leaves, living sapwood, fine roots, carbohydrate reserve (non-structural carbohydrates), reproductive tissues (fruit and flowers), standing dead leaves and heartwood/dead-sapwood. The carbon assimilated through photosynthetic activity is used for maintenance and growth respiration otherwise it is allocated to one of the first five pools. The different pools are undergoing tissue turnover in function of tissue longevity and environmental stresses, i.e., drought and low temperatures. Carbon allocation is a dynamic process that accounts for resource availability (light and water) and allometric constraints (Krinner et al., 2005), e.g., a minimum ratio of fine root to foliage carbon; and an upper limit for the storage of carbohydrate reserve (Friend et al., 1997; Kozłowski & Pallardy, 1997). Carbon allocated to reserves can be subsequently translocated to favour leaf expansion at the onset of the growing season or after severe disturbances (Fatichi et al., 2012a; Gough et al., 2009). Phenology for extratropical species is simulated considering four states (Arora & Boer, 2005): dormant, maximum growth, normal growth, and senescence. Patterns of plant allocation are influenced by the phenological phase (Farquhar et al., 1980). Transition between phenological phases are prognostic in the model and controlled by soil temperature, soil moisture and photoperiod length. The model assumes that vegetation is in a mature phase and in equilibrium with its nutritional environment. Further details of model computational set-up, structure, and description of process parameterizations are presented elsewhere (Fatichi et al., 2012a). Vegetation dynamics are solved at the daily time scale, energy fluxes at the hourly time scale.

C.2 DOMAIN SETUP

The land surface for the simulations was defined based on the 90 m resolution STRM digital elevation model (DEM) following the definition of the Alpine Region of the European Soil Data Center [ESDAC, project name: Eco-pedological Map for the Alpine Territory, https://esdac.jrc.ec.europa.eu/projects/Alpsis/Ecalp_data.html, (Panagos et al., 2012)]. This includes the entire alpine arch from the French coast in the southwest to the Austrian lowlands in the north east and from the Swiss plateau on the northwest to the Slovenian coast in the southeast. This DEM was resampled to the final resolution of our simulations (250 m) and the flow matrix used by T&C was calculated based on the D-infinity method (Tarboton, 1997). To compute the stream network, we set the threshold of upslope area above which a pixel is considered to belong to the channel network to 40 km². Therefore, small streams are not explicitly resolved.

For the subsurface computations, we also used a 250 m spatial resolution. Soil texture data were derived from the SoilGrids product at 250 m resolution (Hengl et al., 2014). We obtained sand, silt, clay, and organic content for seven different depths (at the ground surface and at 0.05, 0.10, 0.30, 1 and 2 m below the ground surface). Average soil properties were then computed considering the vertical discretization of the soil and assuming linearity. A uniform soil depth equal to 1 m was used for the entire area. This is clearly a simplification of the real system, since variability in soil depth can affect runoff generation mechanisms, but our choice is considered reasonable for large parts of the pan-Alpine domain, in the absence of consistent information about soil depth. We used land cover data from Corine (European Environment Agency, 2006), using seven different classes to summarize the information provided in the dataset. The classification we used is shown in Table C.1. Glaciers were initialized with 50 m depth. Lake depth was not explicitly simulated. In other words, we assured that there was always water available for evaporation for every lake-pixel (by automatically re-initializing a “dummy” lake depth), but the rivers flowing into the lakes did not interact with this “dummy” water.

For reasons of computational efficiency, the domain was divided into 8 subdomains, roughly equal in size, following the ridgelines; these subdomains were run independently of each other (no lateral exchange between the 8 domains, Fig C1). The total computational demand for the three-year simulation for each of these sub-regions is roughly 76,000 CPU hours. We initialized the model starting from a completely dry domain and we run the model twice with real meteorological forcing for the period September-October 2000. The final value of all state variables (e.g., soil moisture, surface temperature) was considered the initial condition for the numerical experiment presented in this study, which started on the 1st of November 2000.

C.3 METEOROLOGICAL INPUT

Obtaining hourly meteorological fields at the desired 250 m resolution for an area spanning 257,000 km² and seven countries (Austria, France, Germany, Italy, Lichtenstein, Slovenia and Switzerland) required the combination of distributed products and station data as described below.

Precipitation

We used the daily Alpine precipitation grid dataset (Isotta et al., 2014), which has a grid spacing of 5 km and daily time resolution. To obtain the required model input at hourly temporal resolution and 250 m spatial resolution we used ground measurements from 111 stations in Austria, France, Italy, Liechtenstein, and Switzerland (Table C.2). The computation of hourly precipitation was performed as the simulation was running, because of the impracticability of saving hourly precipitation fields for the entire period. Prior to the simulation, Thiessen polygons were defined based on the 111 stations, so that each pixel of the simulated domain was assigned to a single station. Each pixel was also assigned to the corresponding grid of the Alpine precipitation. Then, during the simulation, in hour 1:00 of each day, the daily sum of the distributed product was disaggregated to hourly precipitation proportionally to the hourly measurements of the corresponding station but preserving the amount of precipitation based on the gridded daily product. In case that the corresponding station recorded no precipitation in a day in which the gridded product did record some, the daily gridded sum was

assigned uniformly to the hours 18:00-22:00. These cases were however rare and mostly occurring at low rainfall intensities.

Air Temperature

For air temperature we used the ECMWF ERA INTERIM product (Dee et al., 2011) using time 00:00:00 and 12:00:00 and step 3/6/9/12. This corresponds to the forecasts that are issued twice a day for the next 12 hours with 3-hourly time step. Thus, we obtained 3-hourly data. We compared this to the product that includes analyses four times a day and only 3-hourly forecasts and the difference was minimal. We used the finest resolution available (0.125° , data downloaded from <https://apps.ecmwf.int/datasets/data/interim-full-daily/levtype=sfc/> on 23/2/2018). We first assigned the ERA INTERIM temperature to all the T&C cells within the corresponding ERA INTERIM grid and then we readjusted the temperature for each T&C grid cell for elevation to account for the elevation variability within each grid cell of the ERA INTERIM. For this readjustment, we used a single, temporally dynamic lapse rate over each subdomain. It was computed every three hours by using all the ERA INTERIM grid cells within the subdomain. The two hours between the three-hourly ERA INTERIM data were computed using linear interpolation.

Wind Speed

For wind speed, we used the corresponding variable of ERA INTERIM, as described for temperature above. A constant lapse rate was used for downscaling from ERA INTERIM to T&C grid cells throughout the entire simulation based on observations in Switzerland ($0.48 \text{ m s}^{-1} / 100 \text{ m}$). A lower limit to wind speed was also imposed to avoid numerical instabilities in the computation of turbulent fluxes at the surface (0.01 m s^{-1}).

Atmospheric Pressure

For surface pressure, we used the corresponding ERA INTERIM variable, as described for temperature and wind speed above. Between the three-hourly data, we performed linear regression and applied a specific exponential correction to account for the variations in elevation within each ERA INTERIM grid cell.

Relative Humidity

To compute the relative humidity, which is an additional necessary model input, we used dew temperature data from the ERA INTERIM product, and extrapolated it in space and time as described above for air temperature. Then, we combined hourly air temperature and dew point temperature to compute the hourly values of relative humidity for each cell in the T&C domain.

Solar Radiation

For computing distributed hourly radiation components for each pixel, we used measurements from 90 stations across the entire domain (stations with an asterisk * in Table C.1). We used the inverse distance weight to compute radiation in each T&C grid cell from the meteorological stations, which

means that more than one station is taken into account for each T&C grid cell. Radiation was corrected based on constant lapse rates that varied according to the radiation length (lapse rate $0.0015 \text{ W m}^{-2} \text{ m}^{-1}$ for shortwave radiation between 0.29 and $0.70 \mu\text{m}$, $0.0027 \text{ W m}^{-2} \text{ m}^{-1}$ for $0.70 - 4.0 \mu\text{m}$ and $0.0014 \text{ W m}^{-2} \text{ m}^{-1}$ for photosynthetically active radiation). T&C consequently adjusted radiation to account for local and remote topographic effects (sky view factor and terrain configuration factor scaling between 0 and 1).

Longwave Radiation

To compute the incoming longwave radiation we followed an empirical formula for the clear sky emissivity (Dilley & O'Brien, 1998), based on air temperature, vapour pressure (computed from relative humidity) and cloud cover. The latter was estimated for each of the stations with solar radiation measurements by comparing observed radiation and clear-sky radiation, simulated by a weather generator (Fatichi, Ivanov, & Caporali, 2011).

C.4 SPACE-FOR-TIME SUBSTITUTION

To compute the response of ET to changes in temperature, we applied a space-for-time substitution (e.g., Dunne et al., 2004). For each vegetation type (i.e. grassland, evergreen, deciduous and mixed forest) we fit a quadratic polynomial to describe evaporation (E) and transpiration (T) as a function of temperature. We also considered the sensitivity of water evaporation to temperature. We computed ET for the warmer climate by using the polynomial fitting function and the new temperature. Once the new reference values of ET were computed for each cell at the higher temperature, we also added the residuals of the regressions to preserve the spatial variability and the non-temperature-driven effects. At the annual scale, we performed separate regressions for each subdomain (Figure C.1), using linear fitting for E and quadratic fitting for T. For the growing season, the regressions were performed between ET and temperature at the pan-Alpine scale with quadratic fittings for forests and grasslands and linear fitting for lakes.

C.5 MODEL VALIDATION

We validated the model against satellite snow cover observations (<https://nsidc.org/data/mod10a2>). Using these distributed 8-daily dataset, we computed the time fraction with snow cover over the entire domain and compared it with the simulations (Figure C.2). The model tends to underestimate snow cover at lower elevations, and especially on the north facing slopes of the inner Alpine valleys. It also overestimates snow cover in the very wet pre Alpine mountains, which might be partly an artefact of the model spin-up (precipitation in October 2000 was very high). Overall, results are satisfying, considering that the model was run uncalibrated and MODIS may tend to overestimate snow cover at low elevations, because it assigns to all eight days the largest snow cover recorded in that period. In fact, comparison of simulated snow cover with station observations (Figure C.3f) suggests that bias in snow cover rarely exceeded 30 days (~ 0.082 in Figure C.2) and much larger errors could be a remote sensing artefact.

We validated the model against runoff measurements in 381 stations using daily time step (Table C.3) and against snow depth measurements in 720 stations in Switzerland, Austria, and Italy (Table C.4).

The results of the validation against station measurements are summarized in Figure C.3. Since T&C simulates only natural flows, (i.e. it does not account for human regulation, which is widespread in the Alps), we eliminated heavily regulated catchments. In order to do so, in the absence of a pan-Alpine database indicating which station is affected by regulation, dams, or water withdrawals, we visually inspected all the observed hydrographs to rank each station as regulated or natural. We found that the model shows a considerably higher performance when excluding the regulated catchments (Figure C.4). The correlation between simulated and observed runoff timeseries is higher for the natural catchments, compared with the regulated (R^2 equals 0.69 and 0.47, respectively). Mean bias is less than 0.01 mm hr^{-1} for both groups of catchments, but the sign is opposite: as expected, T&C tends to overestimate runoff in heavily regulated streamflows (due to water abstraction, which was not simulated). Since in our analysis we used P-ET as a proxy for runoff, the inset of Figure C.4 compares area-averaged P-ET with measured runoff and shows that our assumption is valid, especially for the natural and non-glacierised catchments. For glacierised catchments, indeed, icemelt should be added to P-ET.

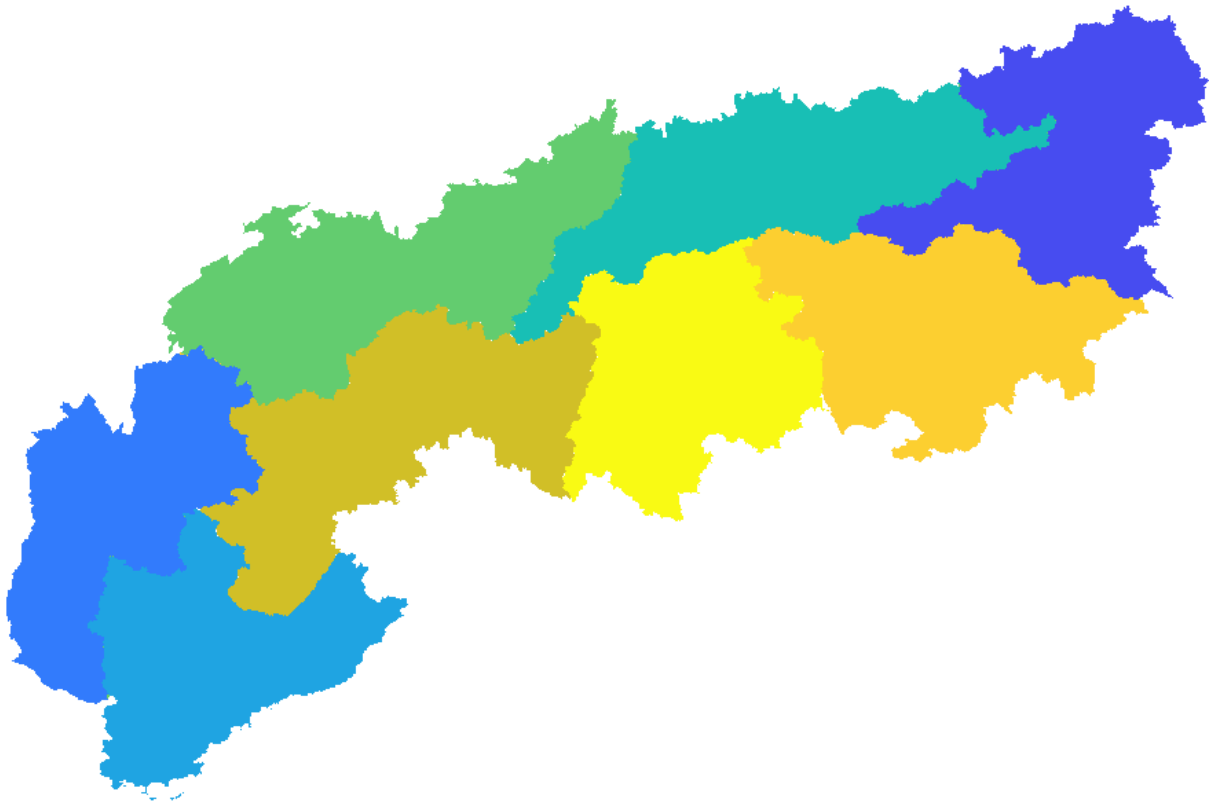


Figure C.1 Decomposition of the pan-Alpine domain into eight independent subdomains. The aim was to subdivide the computational load without affecting lateral connectivity and topographic influences, thus we followed the ridgelines and assumed no exchange between the different subdomains.

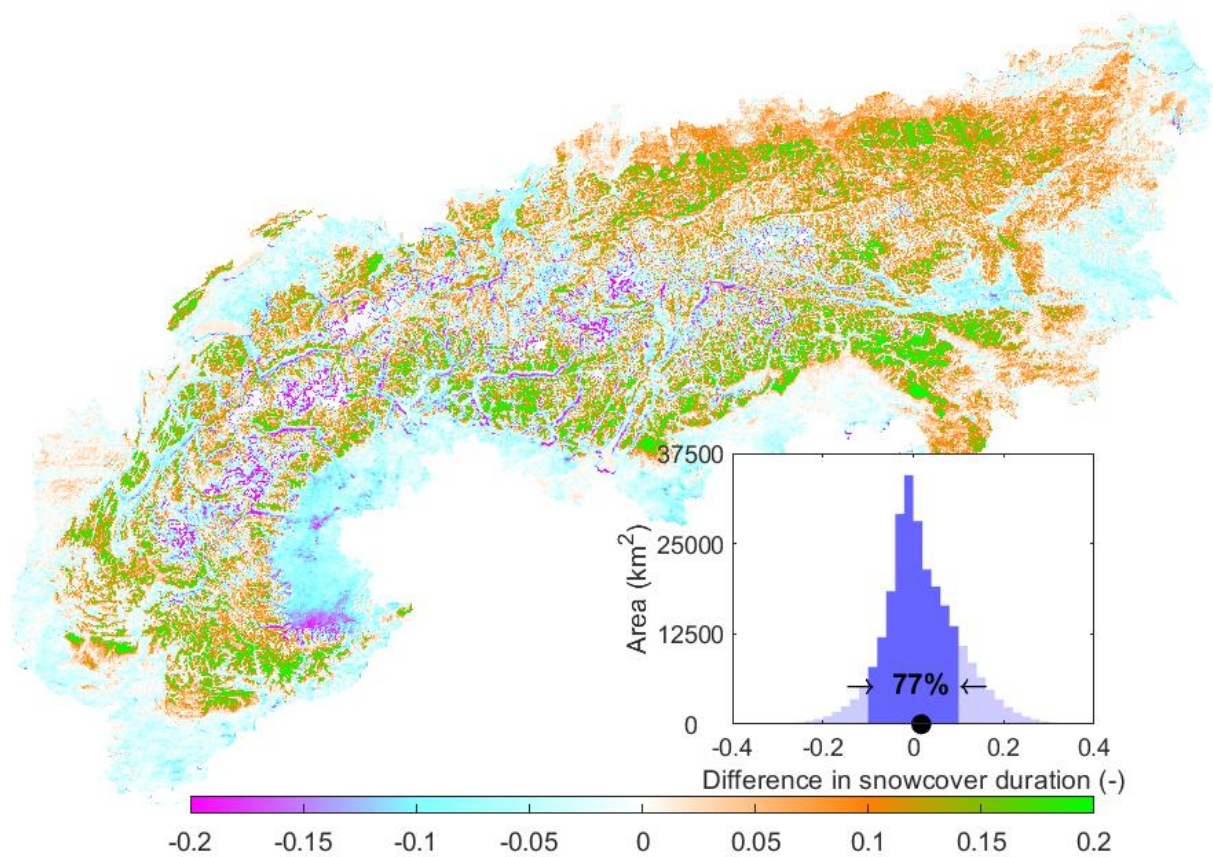


Figure C.2 Difference in fraction of time with snow cover [-] between MODIS observations for the period November 2000 to October 2003 and T&C simulations. The inset shows the respective histogram, including all the simulated pixels.

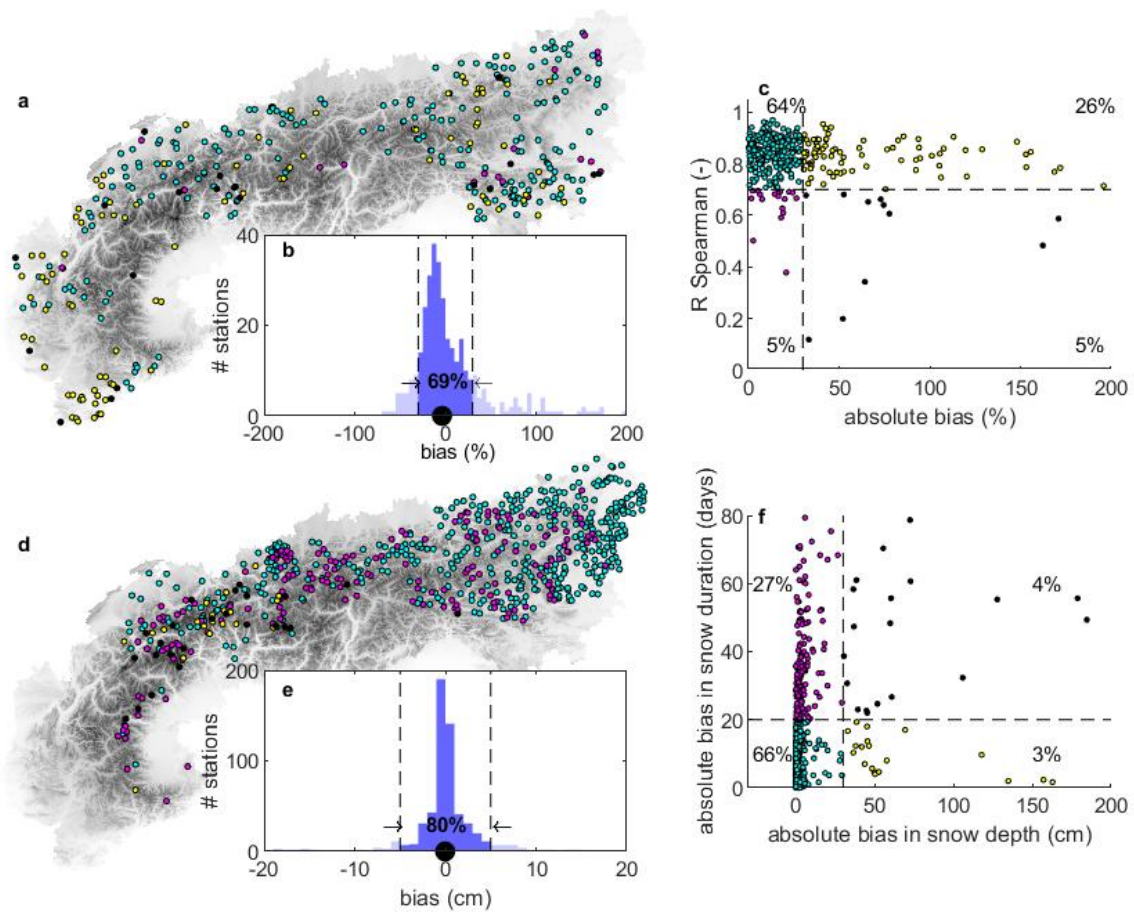


Figure C.3 Model validation against measured daily runoff (a-c) and snow depth (d-f). The latter was conducted accounting for the period with observed snow cover only. The maps (a, d) include the locations of each station, coloured according to model performance, as explained in subplots c and f for runoff and snow depth, respectively. Subplots B and E show the histogram of the percent bias and bias in cm, respectively for all the stations. For runoff, we used the Spearman R and the percent bias (c) and for snow we used the bias in snow duration and average snow depth (d). Both runoff (b) and snow depth (e) biases are close to zero for the majority of the stations.

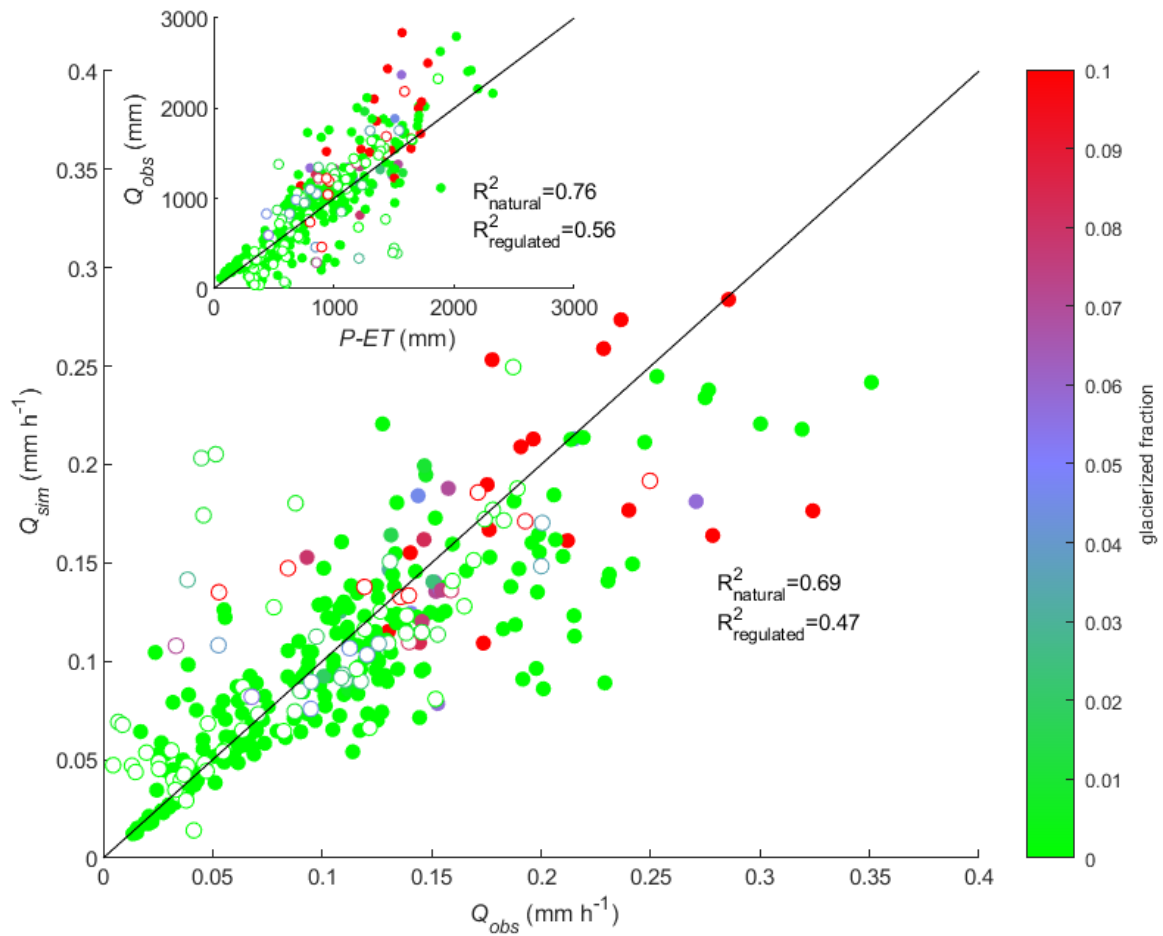


Figure C.4 Comparison between simulated (Q_{sim}) and observed (Q_{obs}) mean runoff for the entire simulation period in 381 locations (in mm hr^{-1}). The colour of the markers shows the degree of glaciation of each catchment. Closed circles are used for the natural catchments and open circles are used for the heavily regulated ones, the R^2 is reported separately for those two groups. The inset shows the comparison of catchment-averaged P-ET against measured runoff (Q_{obs}), using the same symbols. In both plots, the one-one line is also plotted.

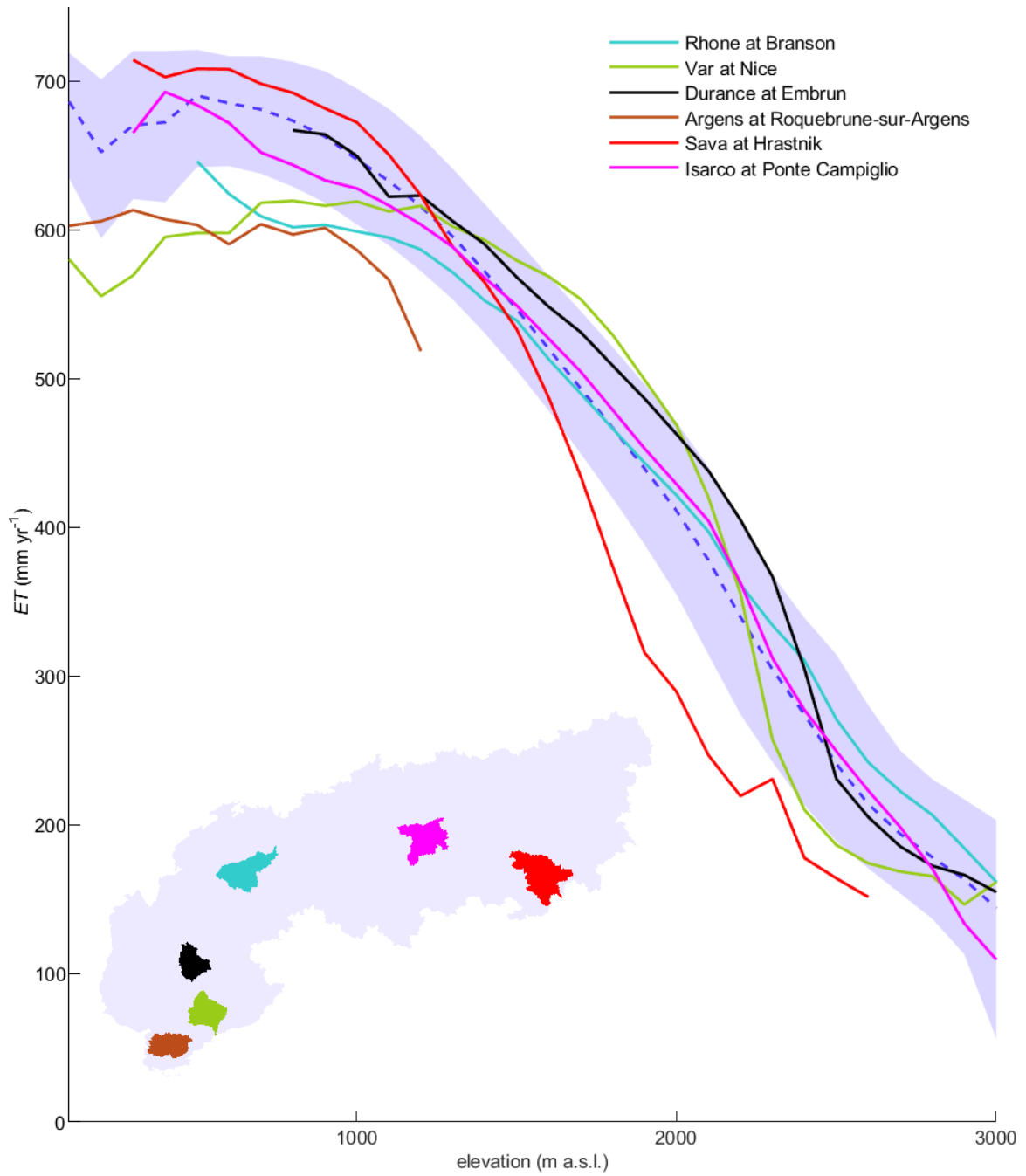


Figure C.5 ET elevational distribution. ET is averaged over 100 m elevation bins for the entire pan-Alpine domain (dashed line) and for selected catchments (solid lines, their locations are shown in the inset map). The shaded area represents the interquartile range of ET distribution across the entire pan-Alpine domain.

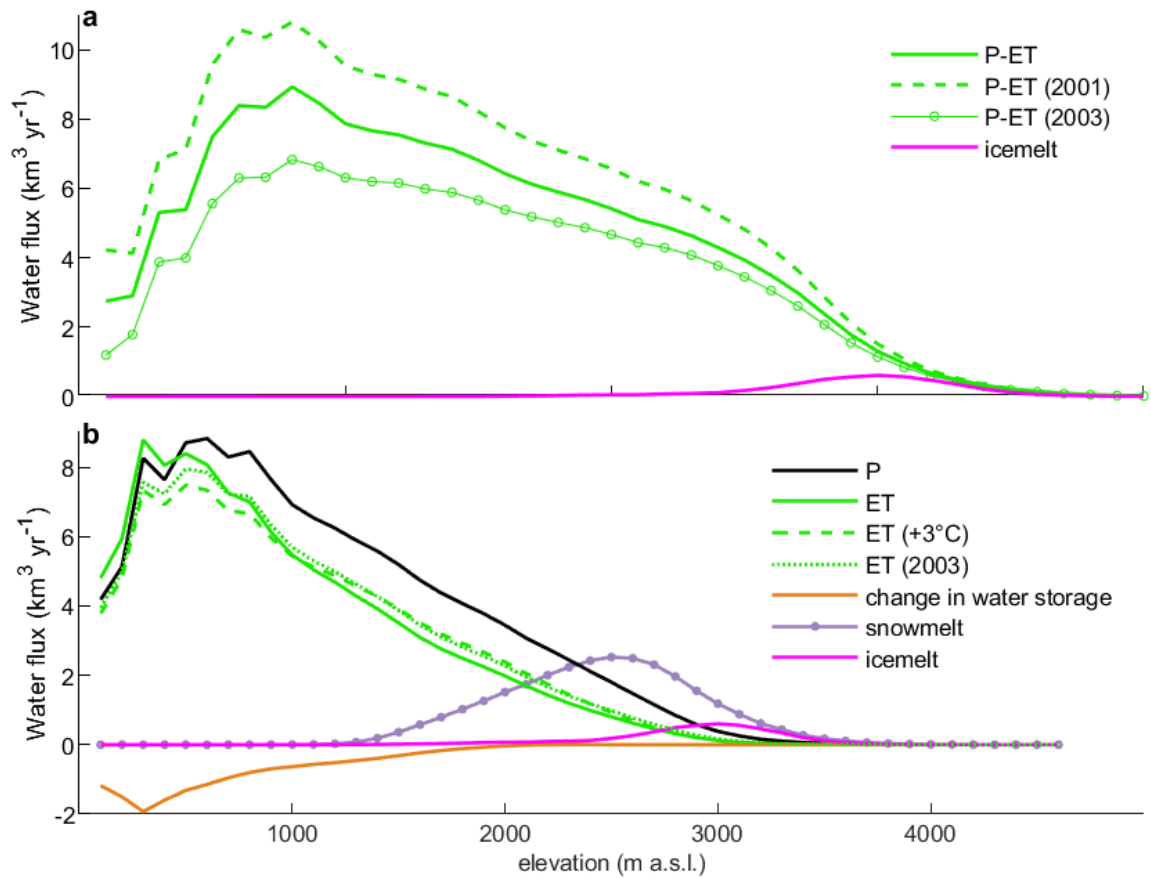


Figure C.6 Relationship between water fluxes (km^3) and elevation (a) annually and (b) for the growing season (May-September). Negative values on the y-axis denote supply of water from soil storage.

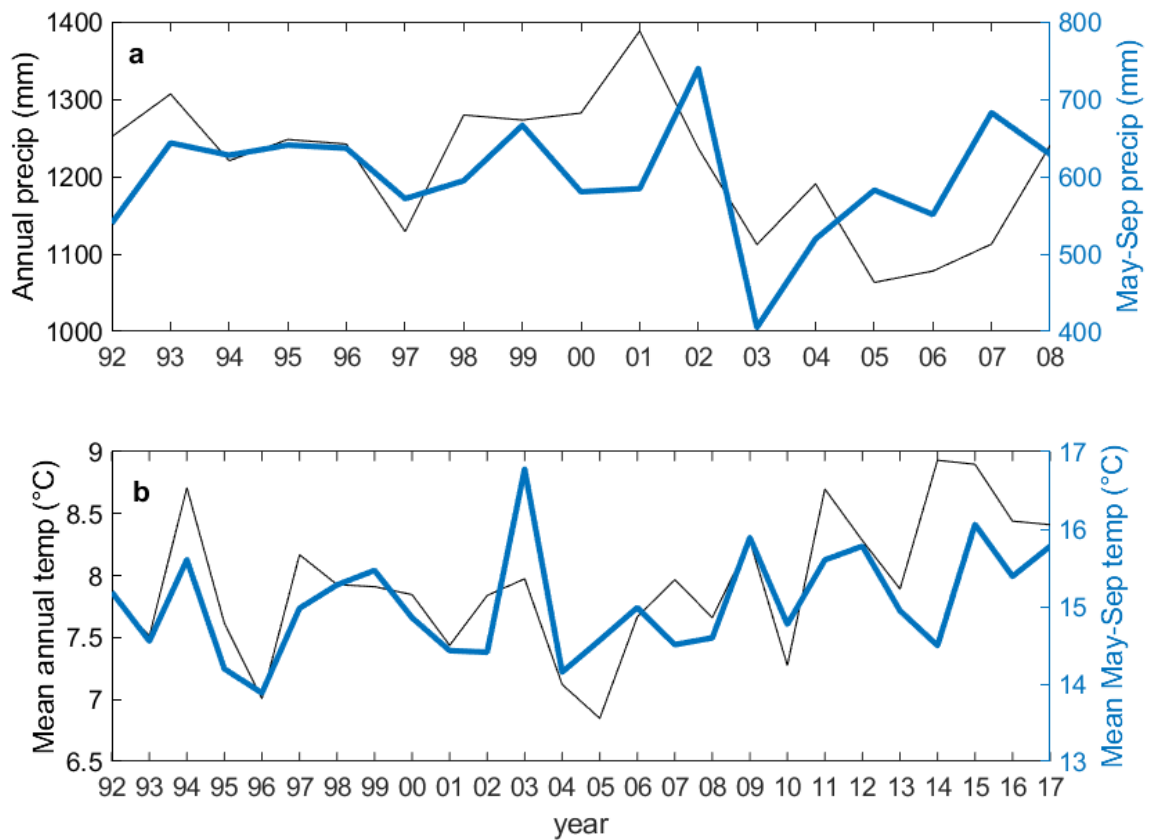


Figure C.7 Time series of mean annual (black) and growing season (blue bold) precipitation (a) and temperature (b) for the period 1992-2008 and 1992-2017, respectively. The growing season of 2002 and 2003, were the wettest and driest in the record, respectively; 2003 growing season was also the warmest. Hydrological years for computing the annual means, are defined as the period between November 1st of the previous year to October 31st, to be consistent with model simulations.

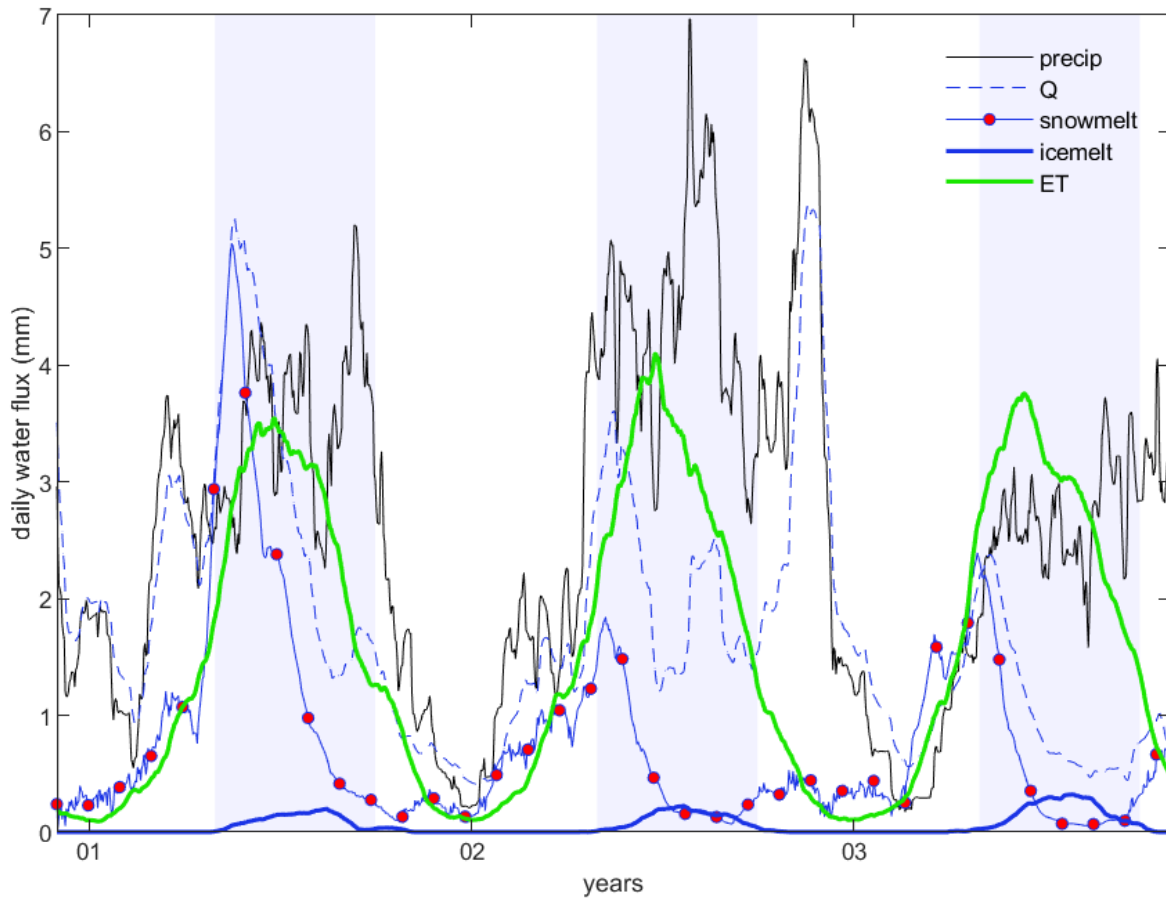


Figure C.8 Blue and green water daily fluxes averaged over the entire domain for the three simulated years (November 2000 excluded). Liquid precipitation (i.e. excluding snow), runoff (Q), snowmelt, icemelt and ET are shown in mm. All variables have been smoothed using a 30-days moving average. The three growing seasons (May-September) are highlighted (shaded areas).

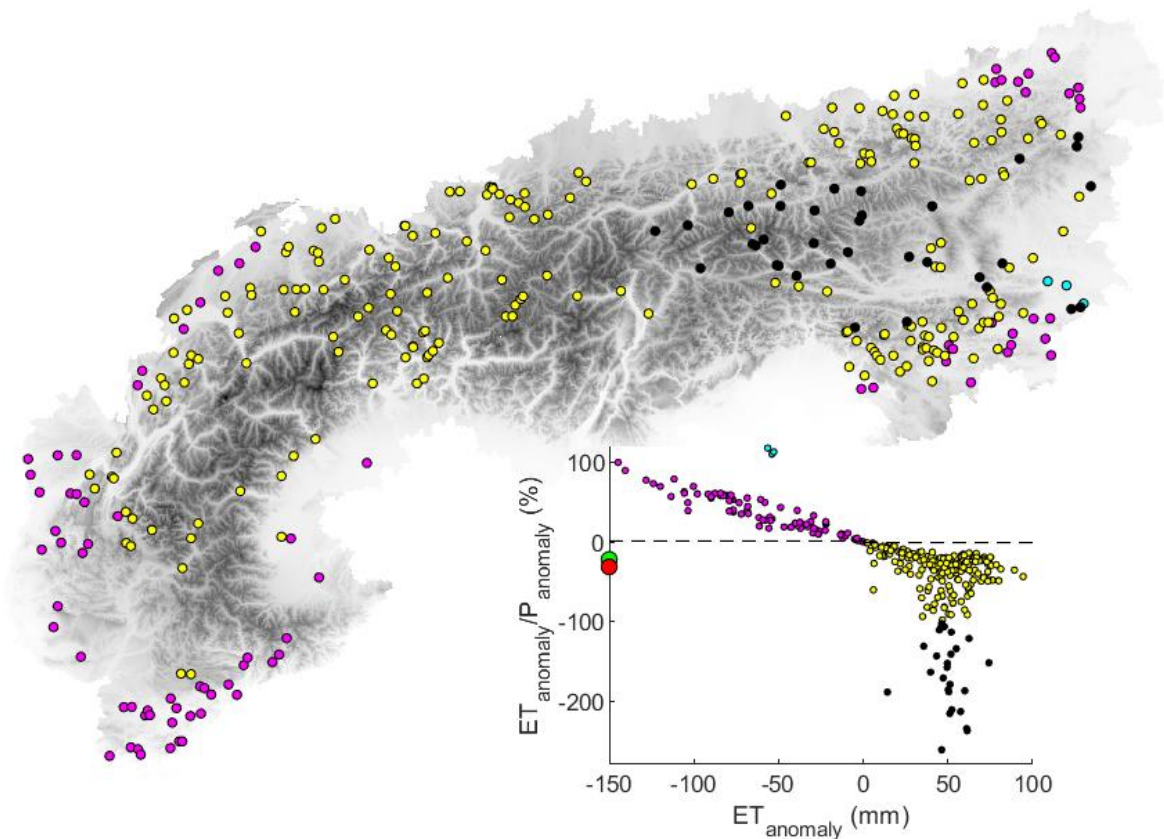


Figure C.9 Relative contribution of ET in comparison to P to the runoff deficit in 2003. Anomalies in ET and P are computed in comparison to the 2001-2003 mean in 334 catchments for which both precipitation and runoff were lower in 2003 compared with the 2001-2003 mean. The map shows the location of each runoff station coloured according to ET_{anomaly} and the ratio $ET_{\text{anomaly}}/P_{\text{anomaly}}$, as displayed in the inset. Yellow colour denotes the catchments for which ET increased in 2003, but the precipitation deficit was larger than the ET excess. Black colour shows the catchments in which ET excess in 2003 was larger than precipitation deficit. Magenta is used for the catchments where ET decreased in 2003 less than precipitation, and cyan for the catchments in which ET decreased more than precipitation. The green and the red dot on the y-axis show the median $ET_{\text{anomaly}}/P_{\text{anomaly}}$ across all catchments and in the catchments with mean elevation between 1300-3000 m a.s.l., respectively.

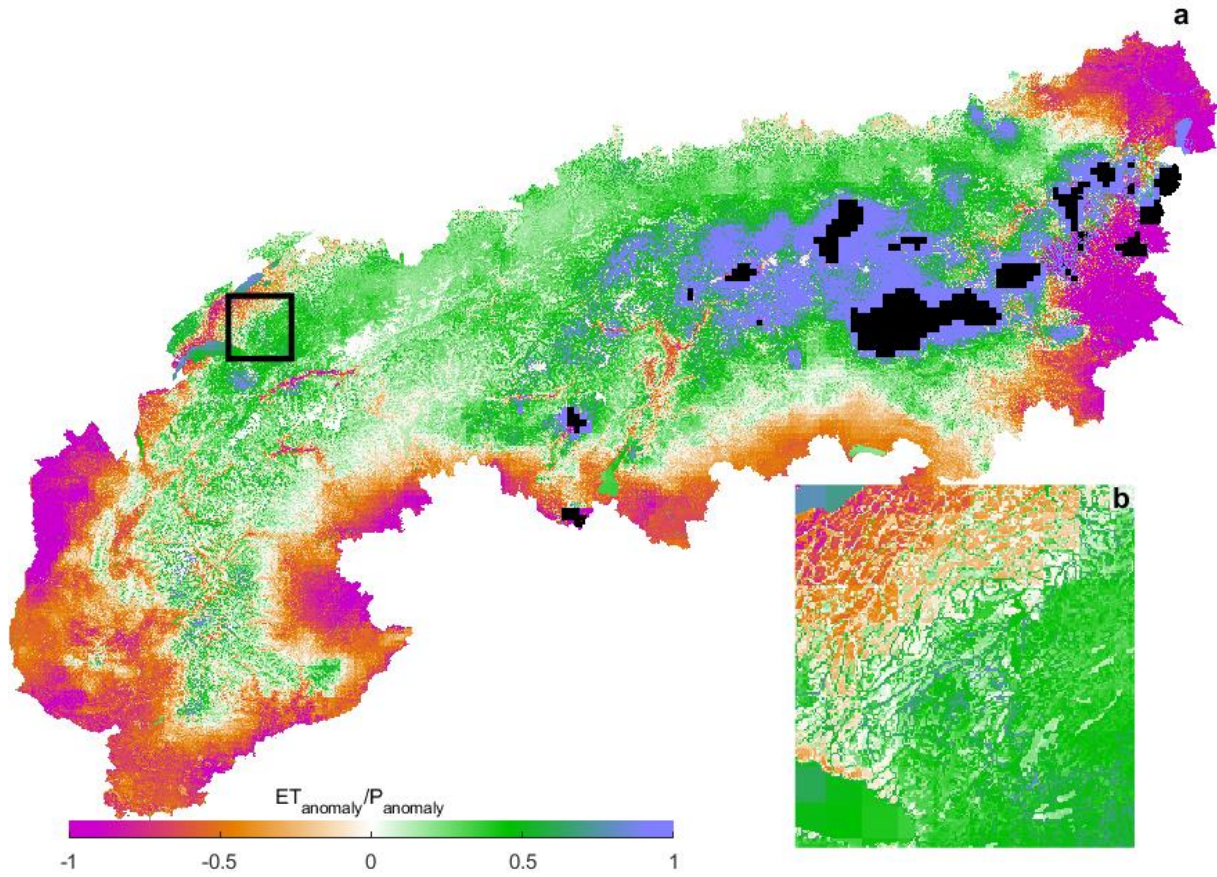


Figure C.10 Relative contribution of ET in comparison to precipitation to the runoff deficit in 2003. The maps show the ratio of the anomaly in ET over the anomaly in P (anomalies computed as the difference between 2003 and the mean over the entire simulation period, i.e. 2001-2003) over the entire Alps (a) and focusing in central Switzerland (b) to show the spatially complex patterns of changes in ET. Black represents the areas in which precipitation in 2003 was higher than the 2001-2003 mean.

Table C.1 Classification in the original Corine land cover product and correspondence with the classification used in this study. The contribution of each class to the total domain is shown. Original classes covering less than 0.005% of the pan-Alpine domain are omitted.

Original Corine classification	Classification for our study	% of total area
Continuous urban fabric	Grassland	0.09
Discontinuous urban fabric	Grassland	3.87
Industrial or commercial units	Grassland	0.51
Road and rail networks and associated land	Grassland	0.05
Port areas	Grassland	0.01
Airports	Grassland	0.06
Mineral extraction sites	Grassland	0.11
Construction sites	Grassland	0.01
Green urban areas	Grassland	0.03
Sport and leisure facilities	Grassland	0.14
Non-irrigated arable land	Grassland	10.17
Rice fields	Grassland	0.53
Vineyards	Grassland	1.14
Fruit trees and berry plantations	Grassland	0.41
Olive groves	Grassland	0.08
Pastures	Grassland	7.36
Annual crops associated with permanent crops	Grassland	0.01
Complex cultivation patterns	Grassland	5.34
Land principally occupied by agriculture with significant areas of natural vegetation	Grassland	3.52
Broad-leaved forest	Broad-leaved forest	10.63
Coniferous forest	Coniferous forest	18.20
Mixed forest	Mixed forest	11.33
Natural grasslands	Grassland	8.53
Moors and heathland	Grassland	2.36
Sclerophyllous vegetation	Grassland	0.59
Transitional woodland-shrub	Grassland	2.65
Beaches - dunes - sands	Rock	0.16
Bare rocks	Rock	5.32
Sparsely vegetated areas	Rock	4.14
Burnt areas	Rock	0.06
Glaciers and perpetual snow	Glaciers	0.93
Inland marshes	Water	0.14
Peat bogs	Water	0.06
Salt marshes	Water	0.01
Salines	Water	0.01
Water courses	Water	0.15
Water bodies	Water	1.23
Coastal lagoons	Water	0.05
Sea and ocean	Water	0.01

Table C.2 List of meteorological stations that were used for disaggregating daily precipitation provided by the Alpine precipitation to hourly values. The stations are presented in alphabetical order for each country, along with the ETRS coordinates and data sources. The asterisk denotes stations that were also used for the computation of radiation input.

##	Station name	ETRS-LAEA coordinates		Country/source/URL
		Longitude	Latitude	
1*	Acquarossa	4239236.79	2594736.78	Switzerland (Lichtenstein) MeteoSwiss
2*	Adelboden	4133612.54	2600862.77	
3*	Bern	4128032.22	2656447.66	
4*	Chur	4285276.35	2639889.52	
5*	Cimetta	4227725.34	2566145.74	
6*	Col du Grand St. Bernard	4101150.88	2532742.60	
7*	Davos	4309150.46	2633413.82	
8*	Evolene	4128277.23	2558807.82	
9*	Geneve	4022224.39	2578393.35	
10*	Grimsel	4193192.34	2608040.95	
11*	Interlaken	4157967.72	2620110.98	
12*	Locarno-Monti	4227361.81	2563045.14	
13*	Lugano	4240467.01	2544164.60	
14*	Luzern	4191856.30	2659702.62	
15*	Montana	4125250.65	2579641.80	
16*	Napf	4164308.52	2656871.60	
17*	Payerne	4087547.97	2638058.03	
18*	Pilatus	4188010.72	2653396.31	
19*	Piotta	4220311.64	2601179.57	
20*	Pully	4065121.05	2605749.65	
21*	Robiei	4206740.15	2593466.93	
22*	Säntis	4271380.78	2682105.75	
23*	Scuol	4342741.26	2631255.40	
24*	Sion	4114875.90	2571105.45	
25*	St. Gallen	4275695.30	2701628.80	
26*	Ulrichen	4191101.89	2600660.17	
27*	Visp	4284471.39	2668454.53	
28*	Wynau	4154734.79	2579172.26	
29*	Zermatt	4153497.84	2685007.91	
30*	Zürich Fluntern	4146924.71	2548994.75	

31*	Vaduz	4212710.01	2697210.44	
32	Embrun	4042709.91	2390356.77	France
33*	Lyon St. Exupery	3937648.03	2525313.45	Météo FR
34*	Montelimar	3902287.26	2400328.69	
35*	Nice	4095315.96	2286416.33	
36*	Avigliana	4115709.82	2446231.71	Italy
37*	Prerichard	4062177.37	2446244.48	ARPA Piemonte
38*	Borgone	4103911.33	2449155.52	
39*	Candia	4156083.68	2470188.58	
40*	Carmagnola	4138012.04	2422446.73	
41*	Cumiana	4114916.18	2431803.23	
42*	Bauducchi	4140003.45	2430581.58	
43*	Pino Torinese	4144729.95	2439454.54	
44*	Pietrastretta	4089060.95	2452555.73	
45*	Vercelli	4194632.89	2469605.81	
46*	Domodossola	4189671.43	2556140.65	
47*	Pallanza	4208375.36	2535883.35	
48*	Bra	4150511.34	2401534.43	
49*	Fossano	4144897.48	2383683.24	
50	Colle San Bernardo	4164665.58	2343106.46	
51	Bergalli	4175996.34	2368195.10	
52*	Alessandria Lobbi	4218612.31	2426137.88	
53*	Arquata Scrivia	4232198.87	2397678.36	
54*	Basaluzzo	4216464.98	2406750.60	
55*	Capanne di Cosola	4257543.95	2396578.65	
56*	Casale Monferrato	4203226.62	2448081.35	
57*	Isola S. Antonio	4230591.93	2435222.18	
58*	Novi Ligure	4222562.21	2409266.61	
59*	Ponzone Bric Berton	4204714.57	2379947.10	
60*	Sardigliano	4234356.36	2405809.02	
61*	Spineto Scrivia	4231482.24	2414249.62	
62	Paneveggio	4455748.42	2578956.86	Italy
63	Pieve Tesino (O.P. Enel)	4446458.90	2552172.80	University of Trento
64	Valda	4418893.74	2567063.47	
65	Segonzano (Scancio)	4418376.07	2565100.46	
66	Lisignago	4413182.67	2561436.00	
67	Vallarsa (Diga di Speccheri)	4409400.96	2517981.93	
68	Val di Genova (O.P. Enel)	4377228.39	2562113.03	
69	La Rocca (Centrale)	4375901.09	2545761.32	
70	Nembia (Centrale)	4393608.76	2555259.80	
71	Lago di Cavedine	4394780.80	2542849.75	
72	Vallarsa (Malga Boffetal)	4411648.59	2516037.67	
73*	Vivaro	4535391.36	2555494.68	Italy
74*	Trieste molo F.lli Bandiera	4613761.27	2511532.23	ARPA FVG-OSMER/GRN
75*	Tarvisio	4593763.86	2606242.15	
76*	Sgonico-Zgonik	4612497.73	2521250.77	
77*	Monte Lussari	4591495.76	2602987.24	
78	Gemona del Friuli	4561901.23	2577077.06	
79*	Enemonzo	4541272.72	2592818.70	
80	Cividale del Friuli	4585758.40	2558025.89	
81*	Cervignano del Friuli	4580440.45	2532115.85	
82*	Capriva del Friuli	4593514.28	2544788.43	
83*	Brugnera	4518647.02	2537282.14	
84*	Udine	4571010.96	2552339.67	
85*	Aigen Ennstal	4632627.12	2721954.32	Austria
86*	Alberschwende	4309576.64	2704888.35	Federal Ministry for sustainability and tourism
87*	Amstetten	4685673.40	2789263.12	
88*	Bad Mitterndorf	4617193.87	2723399.35	
89*	Braunau Ranshofen	4546043.38	2794685.76	
90	Eisenstadt-Nordost	4809872.94	2770557.94	
91*	Feldkirch	4291445.16	2684247.31	
92*	Graz-Universität	4734815.40	2677974.37	
93*	Jenbach	4453819.01	2698830.41	
94*	Kalwang	4680121.66	2712411.74	
95*	Katschberg	4595716.93	2667447.14	
96*	Kleinzicken	4800694.89	2697627.10	
97*	Koetschach-Mauthen	4550562.83	2622870.84	
98	Langenlebar	4774302.73	2819955.03	
99*	Lienz	4535275.40	2638730.19	
100*	Lofer Ort	4523960.13	2722494.05	
101	Lunz am See	4700104.49	2761980.67	
102*	Mariapfarr	4605111.01	2678110.83	
103	Neumarkt	4657139.97	2671832.37	
104*	Puchberg Schneeberg	4763315.29	2759530.07	
105*	Ramsau am Dachstein	4595268.02	2708028.53	
106*	Sillian	4506294.78	2628971.72	
107*	St. Michael B. Leoben	4699260.66	2704147.25	
108*	Weissensee-Gatschach	4572425.32	2628429.09	
109*	Wien-Hohe Warte	4792614.63	2813105.94	
110*	Wiener Neustadt Flugplatz	4787163.99	2766172.32	
111*	Zeltweg	4680687.29	2687764.16	

341	Lučnica	Lučc	57.39	57.26	SI	2594073.49	4686765.65	0
342	Višnjica	Trebnja Gorica	75.84	78	SI	2542487.45	4692584.21	0
343	Lavant	St.Gertraud	380.2	374.87	AT	2654644.72	4691971.27	1
344	Meža	Crna	95.17	91.63	SI	2607456.63	4693837.21	0
345	Sava	Litija I	4849.33	4702.66	SI	2561345.74	4694754.53	0
346	Dreta	Krase	100.82	102.85	SI	2587129.18	4699114.34	0
347	Lavant	Krottendorf	954.5	947.61	AT	2629413.56	4699633.91	1
348	Savinja	Nazarc	457.11	460.58	SI	2591454.47	4702879.93	0
349	Drava	HE Dravograd	12071.7	12061.74	SI	2621209.75	4706055.37	1
350	Meža	Otiški Vrh I	552.6	551.74	SI	2620264.82	4706675.44	0
351	Savinja	Letuš I	529.53	535.24	SI	2592272.20	4706839.43	0
352	Medinja	Zagorje I	96.97	101	SI	2569761.52	4707674.14	1
353	Mislinja	Otiški Vrh I	231.56	229.3	SI	2619188.26	4707616	0
354	Paka	Rečica	206.07	207.37	SI	2591879.61	4709484.99	0
355	Suhodolnica	Stari Trg I	59.45	59.82	SI	2612376.14	4710777.63	0
356	Sava	Hrastnik	5205.3	5067.43	SI	2570062.85	4714968.87	0
357	Paka	Velenje	63.36	63.38	SI	2596812.24	4715337.32	1
358	Mislinja	Dovže I	72.59	72.32	SI	2607284.12	4717170.58	0
359	Savinja	Veliko Sirje I	1847.14	1817.98	SI	2567308.85	4723034.93	0
360	Savinja	Laško I	1668.16	1678.2	SI	2574396.70	4725752.32	0
361	Savinja	Celje II - brv	1191.84	1169.67	SI	2582692.50	4726864.95	0
362	Sevnična	Orešje	39.78	40.37	SI	2561779.46	4731388.81	0
363	Dravinja	Zreče	42.75	42.67	SI	2600254.54	4735559.19	1
364	Gischloessbach	Innerschloess	39.30	40.46	AT	2670994.32	4507576.90	0
365	Oplotnica	Draža vas	85.81	83.66	SI	2594872.67	4744406.22	0
366	MestinjšCica	Sodna vas II	132.82	157.59	SI	2578560.76	4753950.39	0
367	Pesnica	Ranca	84.27	94.11	SI	2626291.33	4756654.49	0
368	Dravinja	Makole	303.21	302.61	SI	2595187.15	4758093.77	0
369	Bistrica	Zagaj I	94.01	91.6	SI	2564978.05	4758823.05	1
370	Tauernbach	Matreier Tauernhaus	59.90	62.9	AT	2670231.97	4510750.34	0
371	Pesnica	GoCova	281.77	296.46	SI	2622682.25	4771318.77	0
372	Rogatica	Podlechnik I	57.26	51.96	SI	2597894.88	4773967.85	0
373	Drava	Jez Markovci	13700.8	13938.63	SI	2604254.24	4777164.46	1
374	Isel	Waier	285.3	277.31	AT	2656823.63	4513281.27	0
375	Drava	Borl I	14642.08	14605.51	SI	2602885.30	4782678.09	1
376	Pesnica	Zamušani I	479.76	546.5	SI	2607899.02	4785205.66	0
377	Isel	Bruchl	518.4	480.84	AT	2654552.19	4515342.82	0
378	Adige	Spondigna	701.45	830.51	IT	2613869.80	4367254.10	1
379	Adige	Tel	1508.93	1664.52	IT	2618239.91	4403698.32	1
380	Isarço	Ponte Campiglio	3600.69	3766.03	IT	2598694.21	4426194.33	1
381	Aurino	S.Giorgio	614.56	608.32	IT	2635658.25	4468765.89	1

Table C.4 List of stations with daily snow depth measurements used for validation.

##	Station Name	Elevation (m. a.s.l.)	ETRS coordinates		Country
			Latitude	Longitude	
1	Illmitz (Biologische Station)	115	2762774.39	4826719.02	AT
2	Rust	118	2766377.36	4820654.09	AT
3	Andau	118	2765233.89	4847045.27	AT
4	Podersdorf am See	120	2772841.91	4831624.01	AT
5	Apetlon	120	2760293.20	4833778.76	AT
6	Frauenkirchen	122	2770234.69	4838916.83	AT
7	Winden am See	124	2783205.99	4824940.71	AT
8	Nickelsdorf	130	2783885.06	4848692.44	AT
9	Oggau	130	2769351.21	4819933.07	AT
10	Halbtorn	130	2775481.39	4842569.06	AT
11	Kleyhof	133	2778661.57	4848908.86	AT
12	Deutsch Jahrndorf	133	2791981.14	4850267.10	AT
13	Kittsee	135	2800723.89	4846952.64	AT
14	Donnerskirchen	136	2775570.53	4818405.82	AT
15	Pama	137	2795513.96	4845047.96	AT
16	Zurndorf	140	2788310.14	4843698.12	AT
17	Eckartsau	146	2804853.96	4826245.25	AT
18	Gattendorf	150	2791676.14	4841243.10	AT
19	Edmundshof	150	2779901.32	4843371.35	AT
20	St.Margarethen im Burgenland	151	2765350.74	4816148.90	AT
21	Franzensdorf	153	2808867.64	4814149.69	AT
22	Wien-Neueling	155	2812527.99	4806888.99	AT
23	Wien-Kagran	158	2813068.40	4798248.87	AT
24	Wien (Spargelfeld)	160	2812583.79	4801209.80	AT
25	Wulkaprodersdorf	170	2764602.70	4808798.88	AT
26	Matzen	171	2831760.57	4816553.68	AT
27	Mörbisch am See	175	276.47	4819751.50	AT
28	Eisenstadt	177	2769354.32	4808536.75	AT
29	Wien (Botanischer Garten)	180	2807283.51	4795197.51	AT
30	Pillichsdorf	180	2829251.21	4803476.50	AT
31	Parndorf	180	2788755.74	4831958.18	AT
32	Absdorf	182	2827718.49	4763170.50	AT
33	Ulrichskirchen	183	2830650.47	4801415.07	AT
34	Wien (Rathausplatz)	185	2808883.04	4793259.99	AT
35	Grafenwörth	189	2826696.04	4747242.19	AT
36	Vösendorf	190	2798725.49	4793035.44	AT
37	Deutschkreutz	195	2742976.64	4817678.33	AT
38	St.Margarethen-Berg	195	2765079.45	4818303.24	AT
39	Moosbrunn	198	2788587.19	4801599.74	AT
40	Lutzmannsburg	200	2728272.34	4821730.81	AT
41	Donnerskirchen (Waldgasse)	200	2777026.74	4816672.75	AT
42	Hagensdorf-Luising	200	2677033.67	4813361.85	AT
43	Zelting	200	2640098.52	4781356.57	AT
44	Magadino / Cadenazzo	203	2561488.69	4238638.15	CH
45	Magadino / Cadenazzo	203	2561488.69	4238638.15	CH
46	Frankenau	208	2726463.27	4818502.88	AT
47	Steinbrunn	210	2767135.56	4801275.27	AT
48	Pötsching	215	2763831.74	4798213.47	AT
49	Eberau	215	2687525.69	4811436.11	AT
50	Wien-Mauerbach	215	2808957.88	4782524.30	AT
51	Unterpurkla	220	2640947.05	4773063.37	AT
52	Heiligenkreuz	228	2672882.70	4796466.52	AT
53	Draburg	230	2758089.96	4807371.72	AT
54	Glasing	230	2680784.87	4801582.32	AT
55	Oberpullendorf	240	2730748.23	4810903.48	AT
56	Neumarkt an der Raab	240	2666355.07	4787318.69	AT
57	Eltendorf	240	2674770.55	4792029.78	AT
58	Nikitsch	245	2735290.14	4821160.02	AT
59	St.Leonhard am Forst	247	2794573.24	4713715.97	AT
60	Steinabrunn	247	2841521.11	4779367.38	AT
61	Nebersdorf	248	2733247.64	4815667.18	AT
62	Ennsbach	250	2794683.83	4697192.65	AT
63	Wien (Rosenhügel)	250	2802891.51	4788476.28	AT
64	Mannersdorf an der Rabnitz	250	2723025.58	4812615.15	AT
65	St.Michael im Burgenland	250	2688652.07	4796827.49	AT
66	Eisenberg an der Pinka	255	2695233.51	4807782.77	AT
67	Strass	256	2640977.91	4750818.92	AT
68	Schattendorf	260	2754617.55	4808777.36	AT
69	Kukmirn	260	2682509.20	4792694.56	AT
70	Fehring	260	2665245.44	4779085.68	AT
71	Wieselburg	263	2792604.47	4702492.70	AT
72	Kirchfidisch	265	2692611.44	4802548.40	AT
73	St.Peter am Ottersbach	270	2649002.01	4760569.62	AT

74	Lugano	273	2544164.60	4240467.01	CH
75	Lugano	273	2544164.60	4240467.01	CH
76	Growlfersdorf	275	2680820.56	4776760.74	AT
77	Tullnerbach	281	2804552.50	4776192.70	AT
78	Stephanshart	284	2794542	4679366.62	AT
79	Bad Waltersdorf	285	2691094.63	4776651.55	AT
80	Zehensdorf	288	2651377.11	4757265.29	AT
81	Dürnbach im Burgenland	291	2704125.62	4804185.76	AT
82	Kilb	295	2792221.41	4723979.23	AT
83	Pyhra	295	2799340.97	4744064.43	AT
84	Loretto	300	2775583.06	4808147.11	AT
85	Ollersbach	300	2806092.98	4753161.92	AT
86	Wetzelsdorf	303	2671136.38	4767618.87	AT
87	Ritzing	310	2743237.45	4809101.69	AT
88	Oberwart	315	2705155.40	4791569.91	AT
89	Hofstetten	318	2791136.54	4731483.85	AT
90	Laab im Walde	319	2801504.74	4780151.21	AT
91	Gross Sankt Florian	320	2649481.07	4726424.58	AT
92	Kobersdorf	320	2740625.88	4801565.77	AT
93	Grono	323	2571814.48	4256545.68	CH
94	Grono	323	2571814.48	4256545.68	CH
95	Pottenstein	327	2779944.02	4775812.29	AT
96	Scheibbs	330	2780349.08	4705649.10	AT
97	Sinabelkirchen	330	2683045.89	4763552.76	AT
98	Frauental	330	2648482.10	4721965.51	AT
99	Steyr	336	2780657.65	4650860.19	AT
100	Hochgleinz	340	2647118.36	4727991.69	AT
101	Sajach	340	2663506.39	4726534.34	AT
102	St.Nikolai im Sausal	340	2649423.18	4736696.89	AT
103	Stainz	340	2656725.81	4721719.34	AT
104	Stadt Haag	349	2787811.78	4661136.60	AT
105	Lavamünd	350	2626941.80	4699334.93	AT
106	Graz-Gries	350	2675362.61	4732969.29	AT
107	Forchtenstein	350	2753338.45	4796228.58	AT
108	Hartberg	350	2703812.30	4772677.43	AT
109	Riegersburg	350	2672511.63	4772430.81	AT
110	Seitenstetten	351	2779974.89	4667919.62	AT
111	Deutsch Kaltenbrunn	355	2683391.98	4785828.22	AT
112	Maria Laah	360	2787535.33	4645319	AT
113	Reichraming	360	2763360.99	4654887.47	AT
114	Oed	360	2789260.18	4674271.85	AT
115	Brand-Laaben	360	2794698.08	4757545.10	AT
116	Graz-Andritz	360	2680322.88	4731814.14	AT
117	Eibiswald	360	2634062.93	4723250.30	AT
118	Locarno / Monti	366	2563045.14	4227361.81	CH
119	Locarno / Monti	366	2563045.14	4227361.81	CH
120	Karl	370	2730992.47	4798762.88	AT
121	Pilgersdorf	370	2723780.85	4799595.16	AT
122	Ligist	370	2666678.84	4717200.84	AT
123	Leutschach	370	2630921.53	4739267.48	AT
124	Bonisdorf	370	2656401.01	4783415.37	AT
125	Oberdorf im Burgenland	374	2698787.86	4791012.19	AT
126	Aigle	381	2584299.56	4084026.76	CH
127	Alland-Groisbach	387	2788628.43	4772142.04	AT
128	Weissenbach bei Mödling	388	2795020.33	4783026.64	AT
129	Wies	390	2637498.52	4723270.80	AT
130	Gedersberg	390	2670123.66	4730734.55	AT
131	Gresten	398	2777033.46	4695732.05	AT
132	Gaissau	400	2706100.52	4290739.48	AT
133	Fussach	400	2707957.54	4295902.83	AT
134	St.Anton an der Jenitz	400	2774632.44	4709760.67	AT
135	Pinkafeld	400	2714214.23	4783187.92	AT
136	St.Ruprecht an der Raab	400	2686979.26	4750021.08	AT
137	Opponitz	402	2764929.84	4682248.96	AT
138	Montreux-Clarens	405	2597230.64	4082609.35	CH
139	Meiningen	410	2687808.23	4289234.90	AT
140	Lustenau	410	2702619.92	4295565.03	AT
141	Pottschach	411	2748725.23	4770703.45	AT
142	Altach	412	2694012.75	4294897.06	AT
143	Vorchdorf	415	2773989.70	4613329.41	AT
144	Markt Allhau	415	2704289.58	4783056.47	AT
145	Hinterlug	416	2769317.25	4676914.47	AT
146	Stadtschlaining	418	2710309.10	4794984.76	AT
147	Bromberg	419	2747292.37	4786724.24	AT
148	Mäder	420	2692793.60	4291803.86	AT
149	Hörbranz	420	2713831.09	4301181.38	AT

150	Vöcklabruck	420	2772464.70	4594473.21	AT
151	Hochstra	420	2722666.58	4803915.65	AT
152	Pöllau	420	2705569.05	4762107.53	AT
153	Frohnleiten	420	2698429.40	4723722.92	AT
154	Bämbach	420	2675399.58	4710937.45	AT
155	Glashütten bei Langeck	421	2716490.95	4802750.17	AT
156	Hohenlehen	424	2760782.36	4678429.48	AT
157	Ebensee (Wasserwerk)	425	2750655.66	4603987.08	AT
158	Kleinreifling	428	2755958.68	4668287.73	AT
159	Hainfeld	429	2785716.01	4752090.46	AT
160	Bregenz-Rieden	430	2708368.60	4301120.65	AT
161	Oberndorf	430	2765306.41	4541630.30	AT
162	Pechgraben	430	2765579.17	4659813.07	AT
163	Biel/Bienne	433	2671403.46	4112832.77	CH
164	Hohenems	433	2694836.30	4297063.49	AT
165	Dornbirn	435	2698521.78	4301674.20	AT
166	Molln	435	2761552.62	4639463.84	AT
167	Altdorf	438	2642608.52	4215971.11	CH
168	Babniak	440	2611838.35	4648804.72	AT
169	Wolfsberg	440	2646218.04	4690571.65	AT
170	Glanegg	440	2741844.58	4547464.31	AT
171	Laakirchen	440	2770686.54	4605752.68	AT
172	Laussa	440	2769932.97	4653585.93	AT
173	Waldneukirchen	440	2773601.54	4638704.49	AT
174	Unterhflein	441	2760841.74	4772628.51	AT
175	Klagenfurt	442	2621650.82	4651736.23	AT
176	Bregenz (Altreteweg)	443	2710492.85	4302656.62	AT
177	Hallein	443	2735335.62	4552942.78	AT
178	Pöggstall	445	2814121.97	4707352.66	AT
179	Stixenstein	448	2753443.33	4769286.06	AT
180	Sillehof	450	2627099.72	4660784.30	AT
181	Sieggraben	450	2747177.27	4799904.79	AT
182	St.Johann bei Herberstein	450	2695110.25	4761429.07	AT
183	Limberg	450	2639800.22	4719068.25	AT
184	Gmunden-Traundorf	451	2763635.56	4605712.05	AT
185	Luzern	454	2659703.51	4191859.33	CH
186	Klopein am Klopeiner See	455	2621309.60	4673811	AT
187	Kirchdorf an der Krems	456	2763899.78	4629054.92	AT
188	Vaduz	457	2668454.53	4284471.39	CH
189	Klaus an der Pyhrnbahn	458	2755181.59	4632403.29	AT
190	St. Margarethen ob Töllerberg	460	2628526.63	4671035.22	AT
191	Nudorf	460	2765153.09	4546247.28	AT
192	Pernegg	460	2709151.35	4723901.08	AT
193	Vigaun	460	2733983.14	4556047.15	AT
194	Frankenfels	468	2777550.67	4718540.85	AT
195	Weyregg	469	2761255.87	4587776.63	AT
196	Texing	469	2783273.60	4718470.76	AT
197	Bad Schönau	471	2728913.06	4790365.59	AT
198	Hörzendorf	475	2634223.18	4652137.16	AT
199	Weienbach am Attersee	475	2748686.97	4586074.25	AT
200	Attersee	475	2762084.23	4585076.06	AT
201	Gloggnitz	475	2746857.69	4765995.59	AT
202	Glanz	476	2630976.52	4742100.44	AT
203	Gutenstein	478	2769123.09	4761630.63	AT
204	Golling-Torren	480	2725614.33	4559047.64	AT
205	Scharfling	480	2748857.29	4575208.45	AT
206	Trassnitz	480	2772563.14	4729921.54	AT
207	Miesenbach	480	2765246.15	4768502.45	AT
208	Södingberg	480	2676799.95	4716364.37	AT
209	Sion	482	2571105.45	4114875.90	CH
210	Koppigen	485	2670314.65	4139242.37	CH
211	Scharnstein	485	2763136.27	4617945.99	AT
212	Kitzeck im Sausal	485	2646350.84	4737000.04	AT
213	Furth-Harras	488	2780761.18	4762264.98	AT
214	Payerne	490	2638058.03	4087547.97	CH
215	St.Georgen am Reith	494	2759627.59	4686316.87	AT
216	Behamberg	495	2779310.68	4656210.77	AT
217	Bad Ragaz	496	2656148.90	4283252.91	CH
218	Weiler	500	2688148.96	4294975.68	AT
219	St.Michael ob Bleiburg	505	2618870.83	4685142.11	AT
220	Bad Goisern	505	2733079.99	4592485.02	AT
221	Weienstein	510	2625965.95	4605931.25	AT
222	Bleistätter Moor	510	2628988.73	4630604.93	AT
223	St.Michael-Wolfsberg	510	2647390.53	4687204.34	AT
224	Lahn-Hallstatt	510	2722688.45	4595490.75	AT
225	Kirchenlandl	510	2738295.35	4676601.24	AT

226	Breitenau	510	2757940.65	4646998.34	AT
227	St.Pankraz	513	2748074.45	4636860.40	AT
228	Obertraun	515	2722575.20	4599433.15	AT
229	Frankenburg	515	2778846.49	4581372.23	AT
230	Ossiach	520	2627451.83	4626192.44	AT
231	Frastanz	520	2675364.50	4296982.87	AT
232	Kaiserbrunn	523	2752816.94	4755226.20	AT
233	Grünau-Almegg	525	2757028.81	4617640.82	AT
234	Altmünster	525	2758391.29	4602312.02	AT
235	Pöllau (Zentralstation)	525	2707562.16	4759890.74	AT
236	Keutschach	530	2617785.23	4640345.87	AT
237	Güttele	530	2697773.24	4304106.10	AT
238	Maria Lankowitz	530	2674549.69	4705789.49	AT
239	Velden-Weinzierl	535	2619780.65	4627762.75	AT
240	Eugendorf	540	2755416.56	4554353.60	AT
241	Strobl	540	2740431.19	4582743.03	AT
242	Unterlaussa	540	2744582.24	4662945.76	AT
243	Unken	540	2730371.91	4526522.59	AT
244	Ludesch	541	2674628.30	4304291.28	AT
245	Göstling an der Ybbs	544	2757406.80	4690150.08	AT
246	Schwaz	548	2693749.53	4450406.08	AT
247	Sachsenburg	550	2640989.42	4577025.72	AT
248	Thringen	550	2675896.09	4303431.23	AT
249	Strawalchen	550	2768345.83	4563954.79	AT
250	Friedberg-Ortgraben	550	2721236.72	4777052.04	AT
251	Bern / Zollikofen	552	2656447.66	4128032.22	CH
252	Chur	556	2639889.52	4285276.35	CH
253	Breitenau bei Mixnitz	560	2712590.68	4731588.96	AT
254	Grogmain	560	2739260.80	4540055.56	AT
255	Kirchberg am Wechsel	563	2740042.48	4771366.97	AT
256	Wernberg	565	2619948.28	4622231.83	AT
257	Ried im Zillertal	570	2689467.04	4462256.14	AT
258	Neustift an der Rosalia	570	2753086.50	4795099.01	AT
259	Boves	575	2361655.44	4126277.72	IT
260	Arnoldstein	576	2611500.69	4605157.90	AT
261	Faak am See	585	2613411.04	4621306.31	AT
262	Wolfsegg am Hausruck	585	2784523.22	4595133.04	AT
263	Meiringen	588	2626160.95	4181030.48	CH
264	Kössen	588	2731041.62	4501329.40	AT
265	Feistritz an der Gail	590	2613444.96	4597596.60	AT
266	Almsee-Fischerau	590	2747252.58	4617525.06	AT
267	Hinterstoder	590	2740653.69	4633052.02	AT
268	Zöbern	590	2730326.88	4782460.07	AT
269	Kreuzberg	590	2636863.78	4738440.19	AT
270	Millstatt	591	2638681.94	4593758.09	AT
271	Hopfgarten im Brixental	595	2706494.40	4483332.33	AT
272	Oberwang	595	2756648.94	4577295.38	AT
273	Brunnbach	595	2755013.36	4659026.36	AT
274	Hocheck	595	2776853.43	4571054.10	AT
275	Hall in Tirol	596	2686980.65	4434319.31	AT
276	Silbereg	598	2647802.95	4663707.94	AT
277	Andelsbuch	600	2698928.10	4311746.95	AT
278	St.Aegydt am Neuwalde	607	2764981	4737430.64	AT
279	Greifenburg	610	2631123.75	4564102.62	AT
280	Wildalpen	610	2739423.79	4695165.46	AT
281	Eichberg	610	2692753.46	4724413.79	AT
282	Priero	610	2365055.17	4170015.07	IT
283	Lunz am See	611	2762047.99	4700183.35	AT
284	Schwarzau im Gebirge	612	2759778.42	4747974.61	AT
285	Hochwolkersdorf	614	2747999.60	4792151.38	AT
286	Windischgarsten (Schule)	615	2743432.78	4646952.85	AT
287	Oberdrauburg	620	2630400.19	4548908.68	AT
288	Kleinvolderberg	620	2686439.13	4438011.07	AT
289	Eisenkappel	623	2606472.75	4673842.37	AT
290	Ebnat-Kappel	623	2684952.12	4253596.38	CH
291	Maria Neustift	625	2769113.30	4665424.89	AT
292	Wietersdorf	630	2648025.84	4666858.98	AT
293	Grubhof-St.Martin	630	2721915.58	4524189.83	AT
294	Spital am Pyhrn	630	2737903.49	4646537.02	AT
295	Telfs	633	2688587.42	4402434.73	AT
296	Waidegg	635	2619173.20	4568410.19	AT
297	Bodinggraben	640	2751691.71	4650109.43	AT
298	Nawald	648	2755174.49	4747714.66	AT
299	Stanz	648	2721538.17	4735360.66	AT
300	Fribourg / Posieux	650	2633074.28	4100455.96	CH
301	Grolobming	650	2685985.09	4685230	AT

302	Tröpolach	655	2616430.66	4572767.21	AT
303	Nikolsdorf	660	2634740.05	4543110.79	AT
304	Egg	660	2702380.57	4314583.36	AT
305	Walchsee	660	2728990.88	4495126.67	AT
306	Inzing	660	2685127.50	4410329.99	AT
307	Schwendt	660	2728648.06	4501801.81	AT
308	Trofaiach	660	2714479.52	4698771.90	AT
309	Veitsch	665	2733481.95	4734435.53	AT
310	Radweg-Gradisch	666	2627775.61	4637185.42	AT
311	Sankt Johann in Tirol-Almdorf	667	2714920.90	4505104.31	AT
312	Fuschl	670	2748253.81	4568712.47	AT
313	Semriach	670	2693694.67	4729285.11	AT
314	Stams	671	2685726.76	4396501.45	AT
315	Bizau	673	2695189.23	4315289.21	AT
316	Rohr im Gebirge	673	2770070.30	4749284.38	AT
317	Weichselboden	680	2742412.65	4709816.24	AT
318	Birkfeld (Schule)	680	2709677.61	4750865.73	AT
319	Tschagguns	681	2661554.85	4314601.36	AT
320	Thiersee-Landl	685	2721948.21	4474050.24	AT
321	Hollenthon	685	2739628.89	4791752.23	AT
322	Vorau	690	2716347.65	4765237.46	AT
323	Redlschlag	693	2722974.52	4795246.18	AT
324	Admont	700	2727231.89	4656381.01	AT
325	Hohenau an der Raab	702	2702991.15	4737814.31	AT
326	Mauthen-Würmlach	705	2621351.98	4551942.20	AT
327	Alberschwende	705	2704980.89	4309597.78	AT
328	Guttaring	710	2652999.73	4666289.29	AT
329	Doren	710	2708497.30	4310547.37	AT
330	Gössl	710	2733005.42	4613540.26	AT
331	Brunngraben	710	2748937.45	4717582.35	AT
332	Mautern	710	2710382.26	4685082.39	AT
333	Afritz	715	2631210.75	4611272.75	AT
334	Hirschenstein	719	2712746.18	4803885.36	AT
335	Breitenstein	722	2744313.95	4757778.90	AT
336	Grades-Klachel	725	2660682.86	4646810.10	AT
337	Bildstein	730	2706136.05	4304319.20	AT
338	Judenburg	730	2684368.04	4674459.67	AT
339	Thalgau	730	2755835.33	4561244.73	AT
340	Kleindorf	735	2651571.96	4558361.98	AT
341	Hochneukirchen	736	2724272.94	4789357.97	AT
342	Kleinlobming	740	2683009.64	4688457.99	AT
343	Langnau i.E.	743	2649941.97	4153930.36	CH
344	Unzmarkt	745	2685900.84	4657655.59	AT
345	Kernhof	751	2760907.64	4733912.16	AT
346	St.Johann im Walde	752	2646510.10	4521785.35	AT
347	Amerlügen	760	2677272.43	4291599.14	AT
348	Kelchsau	760	2698958.22	4482179.84	AT
349	Gosau	765	2725945.18	4587466.28	AT
350	Dürrnberg	770	2732932.44	4553102.97	AT
351	Trag	770	2726056.31	4703358.33	AT
352	Neuhof	770	2693457.20	4711201.69	AT
353	Feisoglio	770	2383745.70	4170779.86	IT
354	St. Gallen	775	2701628.80	4275695.30	CH
355	Oetz	775	2677085.28	4389241.56	AT
356	Schwarz-Radsberg	780	2616583.07	4657548.56	AT
357	Riefensberg	780	2710031.34	4318193.83	AT
358	Gasselsdorf	780	2687722.50	4671238.51	AT
359	Stuhlfelden	780	2689493.19	4512986.44	AT
360	St.Lorenzen	780	2631387.26	4716440.82	AT
361	Fieberbrunn	788	2711058.37	4513276.23	AT
362	Preblau	790	2657915.75	4686885.28	AT
363	Hittisau	790	2704815.56	4318379.93	AT
364	Grubegg	790	2722717.53	4616579.70	AT
365	Mitterbach	790	2758178.46	4716939.07	AT
366	Weissbriach	800	2623826.42	4571003.90	AT
367	Reichenfels	800	2666419.64	4682074.57	AT
368	Au	800	2689940.40	4319276.80	AT
369	Lackenhof	807	2764152.75	4706438.26	AT
370	Ellmau	810	2714142.96	4494321.32	AT
371	Mürzsteg	810	2744090.71	4731786.22	AT
372	Stall	820	2646475.93	4552398.41	AT
373	Birnberg	820	2706968.96	4602541.95	AT
374	Kirchberg in Tirol	823	2706778.11	4495801.62	AT
375	Imst-Oberstadt	826	2680247.69	4376573.12	AT
376	Malta	830	2655339.37	4588068.85	AT
377	Vils	835	2716321.22	4365766.75	AT

378	Wagrain	840	2696425.90	4570540.20	AT
379	Bramberg	844	2686027.87	4496767.57	AT
380	Sirnitz	850	2642938.08	4630826.30	AT
381	Meschach	850	2691410.33	4297175.35	AT
382	Nassereith	850	2689887.67	4383521.35	AT
383	Saalfelden	850	2707449.92	4536260.21	AT
384	Ingering II	850	2695479.31	4677026.57	AT
385	Neukirchen	857	2684768.46	4494995.37	AT
386	Rettenegg	860	2729442.65	4756145.99	AT
387	Höfen	870	2706846.09	4372902.26	AT
388	Sankt Ulrich-Pillersee	870	2714258.05	4516479.12	AT
389	St.Corona am Wechsel	870	2736981.75	4773348.20	AT
390	Sankt Martin am Grimming	875	2690483.68	4439526.89	AT
391	Obdach	875	2672998.98	4677584.54	AT
392	Ried im Oberinntal	880	2660601.12	4371079.21	AT
393	Breitenbach	880	2682673.44	4705146.10	AT
394	Axams	890	2680496.09	4417665.04	AT
395	Groarl	890	2685700.51	4563377.49	AT
396	Radstadt	890	2703167.69	4582179.76	AT
397	Wald am Schoberpass	890	2715782.06	4673801.54	AT
398	Preiner Gscheid	890	2744030.53	4748989.23	AT
399	Telfes im Stubai	895	2672836.38	4424286.11	AT
400	Silbertal	897	2664667.79	4319691.41	AT
401	Zell-Pfarre	900	2605367.22	4657610.05	AT
402	Blons	900	2679090.80	4308936.03	AT
403	Haidbach	900	2685445.46	4509268.16	AT
404	Hütten	900	2707475.43	4527113.22	AT
405	Flachau	900	2698506.19	4577597.57	AT
406	Forchach	905	2700513.54	4365050.79	AT
407	Einsiedeln	910	2669746.02	4226687.88	CH
408	Pleschkogel	910	2684671.19	4718279.34	AT
409	Magdalensberg	920	2633624.56	4659790.39	AT
410	Dalaas	920	2668277.84	4320472.67	AT
411	Festenburg-Hinterberg	920	2726071.94	4767153.24	AT
412	St.Jakob im Walde	922	2723160.67	4757000.90	AT
413	Annaberg	924	2765939.64	4722377.51	AT
414	Jauken	925	2622647.54	4553424.26	AT
415	Karbachalm (Talstation)	925	2701199.18	4555922.22	AT
416	Gaisberg	930	2661075.99	4657189.12	AT
417	Sibratsgfäll	930	2701235.69	4323726.56	AT
418	Hinterri	930	2706990.94	4431642.59	AT
419	Brandenberg	940	2710460.03	4464676.34	AT
420	Wildschnau-Mühlthal	940	2705876.28	4475695.13	AT
421	Kendlbruck	940	2669581.32	4615906.77	AT
422	Greith	945	2725509.45	4623659.61	AT
423	Obsteig	950	2687907.09	4390901.36	AT
424	Paal-Stadl	950	2670351.84	4623435.10	AT
425	Hochfilzen	952	2709382.97	4518364.16	AT
426	Elm	957	2646055.27	4258238.45	CH
427	Scharnitz	963	2697455.19	4416710.34	AT
428	Thringerberg	967	2678268.26	4304722.89	AT
429	Wastl am Wald	967	2770107.69	4716649.04	AT
430	Niederndorferberg	970	2733786.57	4489407.80	AT
431	Trahten	970	2648128.28	4712955.31	AT
432	Jochberg	980	2697764.93	4503636.91	AT
433	Seewiesen	980	2737241.61	4717223.25	AT
434	Donnersbachwald	985	2703951.96	4632468.70	AT
435	Piotta	990	2601179.57	4220311.64	CH
436	Am Nachtsöllberg	990	2704130.07	4489000.40	AT
437	Piotta	990	2601179.57	4220311.64	CH
438	Bodental	995	2605501.28	4646077.09	AT
439	Brental	1000	2604002.89	4640342.62	AT
440	Maitratten-Sonnleiten	1000	2638319.84	4621399	AT
441	Sulzberg	1000	2711824.78	4314217.05	AT
442	Schlitterberg	1000	2696947.30	4458923.34	AT
443	Steinberg am Rofan	1000	2713660.43	4455592.26	AT
444	St.Koloman	1000	2731634.58	4563938.24	AT
445	Pötschen	1000	2730271.97	4598829.39	AT
446	Osterwitz-Winkel	1000	2653944.58	4707576.16	AT
447	Matrei in Osttirol	1003	2659204.37	4513947.63	AT
448	Brand	1005	2665566.76	4301099.73	AT
449	Aschau	1005	2698859.80	4495369.86	AT
450	Mögggers	1010	2716467.56	4307047.59	AT
451	Schönberg im Stubaital	1010	2675421.27	4427190.49	AT
452	Hüttschlag	1010	2678931.27	4566128.08	AT
453	Kleinarl	1010	2690634.89	4572305.82	AT

454	Klein Pyhrgas	1010	2739602.94	4649135.99	AT
455	Salbertrand	1010	2445224.42	4076153.37	IT
456	Sll-Stockach	1020	2711044.63	4482659.25	AT
457	Alpl	1020	2725355.30	4747763.75	AT
458	Haringgraben	1020	2728347.39	4705616.24	AT
459	Klaushof	1022	2673512.13	4468444.18	AT
460	Château-d Oex	1028	2600634.92	4101235.77	CH
461	Hohegg	1030	2630988.79	4593732.67	AT
462	Bosruckhütte	1036	2734810.76	4649160.25	AT
463	Kreuzwirt	1038	2713382.47	4758290.21	AT
464	Seeburg	1040	2600516.39	4669979.70	AT
465	Innerlaterns	1040	2682630.16	4301326.43	AT
466	Schnenbach	1040	2695526.19	4323141.42	AT
467	Untertal-Tetter	1040	2700645.19	4601547.50	AT
468	Piedicavallo	1040	2510912.86	4161687.75	IT
469	Neuhaus am Zellerain	1048	2755023.56	4709562.08	AT
470	Knappenberg	1050	2656060	4668292.91	AT
471	St.Johann am Tauern	1050	2703845.72	4658841.61	AT
472	Pfänder	1056	2710579.87	4304436.77	AT
473	Noreia	1060	2666179.18	4665404.72	AT
474	Filzmoos	1060	2708798.90	4586919.58	AT
475	Oppenberg	1060	2717709.36	4642798.91	AT
476	Klösterle	1070	2668652.19	4327791.59	AT
477	See im Paznaun	1070	2663606.73	4356465.51	AT
478	Fladnitzberg	1070	2703560.21	4735476.89	AT
479	St.Lambrecht	1070	2670516.85	4647402.68	AT
480	Poschiavo / Robbia	1078	2581684.56	4325954.05	CH
481	Poschiavo / Robbia	1078	2581684.56	4325954.05	CH
482	Jerzens-Ritzenried	1080	2669165.09	4379210.30	AT
483	Inneralpbach	1080	2698172.18	4469392.48	AT
484	Hohenau am Wechsel	1080	2723492.31	4772039.56	AT
485	Ebnit	1085	2693090.67	4301572	AT
486	Thomatal	1090	2669812.44	4604777.17	AT
487	Sillian	1097	2629295	4505795.75	AT
488	Trattenbach (Schlaggraben)	1100	2739953.84	4762951.43	AT
489	Hopfgarten in Deferegg	1110	2648646.22	4513067.87	AT
490	Muhr	1110	2672267.85	4584759.87	AT
491	Pack	1115	2664498.78	4700372.03	AT
492	Jungholz	1120	2717792.77	4355716.45	AT
493	Böckstein	1120	2669024.34	4557673.98	AT
494	Sankt Nikolai im Sölktal	1120	2697991.81	4626983.02	AT
495	Gschmaidt	1128	2690163.15	4712331.27	AT
496	Leutasch-Kirchplatzl	1130	2695440.51	4406663.99	AT
497	Maria Luggau	1140	2624989.57	4531117.53	AT
498	Fontanella	1140	2681673.77	4314434.07	AT
499	Bucheiben	1140	2676346.43	4546448.74	AT
500	Soboth	1145	2633071.29	4710382.25	AT
501	Diex	1150	2636620.03	4673915.87	AT
502	Bödele	1150	2700852.50	4306548.23	AT
503	Flirsch	1150	2670647.73	4352205.57	AT
504	Hirscheegg	1158	2668374.08	4695418.80	AT
505	Gaberl	1160	2678921.28	4696790.73	AT
506	Klosterwinkel	1162	2658050.70	4709256.69	AT
507	Mönichkirchen	1179	2730064.70	4773244.27	AT
508	Dreifaltigkeit	1180	2642036.48	4648296.58	AT
509	Längenfeld	1180	2663051.17	4394685.24	AT
510	Bromberg	1180	2710640.81	4488852.46	AT
511	Lessach	1190	2682550.02	4609744.36	AT
512	Disentis	1197	2622262.22	4233338.97	CH
513	Pass Thurn	1200	2690329.59	4504776.46	AT
514	Postalm	1200	2732567.02	4579132.51	AT
515	Iselsberg-Penzelberg	1205	2641810.77	4539130.29	AT
516	Zederhaus	1205	2676978.70	4587690.47	AT
517	Trins	1210	2664400.25	4428658.76	AT
518	Seetal	1210	2679396.27	4620917.53	AT
519	Forno alpi graie	1215	2476282.07	4103319.36	IT
520	St.Peter im Katschtal	1220	2663840.49	4594617.87	AT
521	Osterwitz	1220	2652062.46	4708550.14	AT
522	Formazza bruggi	1226	2583085.23	4200013.43	IT
523	Tweng	1235	2681493.12	4594821.81	AT
524	Colleterto	1240	2484184.88	4137732.84	IT
525	Baad	1255	2688682.15	4330017.24	AT
526	Anras	1260	2632271.78	4516324.41	AT
527	Hohentauern	1265	2712515.67	4659530.57	AT
528	Paesana	1265	2398661.95	4103648.12	IT
529	St.Wolfgang	1275	2675866.47	4673032.90	AT

530	Gschnitz-Obertal	1280	2658111.40	4422370.62	AT
531	Kaunertal-Vergtschen	1285	2658044.54	4378053.60	AT
532	Jägerwirt	1300	2638593.35	4710165.54	AT
533	Scuol	1303	2631255.40	4342741.26	CH
534	Hebalpe	1310	2659051.15	4702614.16	AT
535	St.Oswald (Talstation)	1319	2644363.50	4608670.06	AT
536	Gramais	1320	2684069.17	4361557.93	AT
537	Adelboden	1322	2600862.77	4133612.54	CH
538	Prägraten	1340	2658954.04	4501732.71	AT
539	Berwang	1340	2699703.17	4377855.17	AT
540	Ulrichen	1345	2600666.92	4191109.12	CH
541	Schönbergalpe	1350	2720638.16	4600867.91	AT
542	Prerichard	1353	2446244.48	4062177.37	IT
543	Obernberg am Brenner	1360	2657423.54	4430161.73	AT
544	Macugnaga pecetto	1360	2542293.98	4162623.84	IT
545	Hutterer Böden	1370	2738439.29	4634907.45	AT
546	Sölden-Kaisers	1380	2650875.90	4398013.07	AT
547	Praly	1385	2426254.89	4088348.19	IT
548	Ladis-Neuegg	1390	2663526.52	4370399.61	AT
549	Valdieri	1390	2348021.66	4102308.76	IT
550	Navis	1400	2670211.21	4438359.86	AT
551	Kartitsch	1415	2626629.68	4512918.02	AT
552	Obertilliach	1430	2624580.64	4521515.52	AT
553	Flattnitz	1430	2655912.83	4628465.87	AT
554	Linzer Haus	1435	2735265.38	4643194.93	AT
555	Andermatt	1438	2614222.82	4212291.48	CH
556	Lech	1450	2677514.72	4331930.02	AT
557	Alpe cheggio	1460	2554499.99	4175181.66	IT
558	Bielmonte	1480	2507542.94	4170929.63	IT
559	Zug	1500	2676337.62	4329299.23	AT
560	Kappl-Oberbichl	1500	2661871.44	4349760.85	AT
561	Camparient	1515	2515386.99	4171833.18	IT
562	Pragelato - trampolino a valle	1525	2481150.82	4079609.80	IT
563	Barcenisio	1525	2458300.45	4083839.50	IT
564	Nafeld	1530	2610760.76	4572347.53	AT
565	Blatten, Lötschental	1538	2592264.83	4153579.13	CH
566	Piamprato	1555	2497103.27	4131346.15	IT
567	Davos/Stilli	1560	3251334.99	3735410.51	CH
568	Gries	1570	2662457.42	4398726.23	AT
569	Pontechianale	1575	2393805.90	4086734.22	IT
570	Ceresole villa	1581	2485157.14	4102596.07	IT
571	Davos	1594	2633413.82	4309150.46	CH
572	Grächen	1605	2567244.97	4153927.69	CH
573	Planneralm	1605	2708050.70	4638276.37	AT
574	Acceglio	1610	2379975.16	4080547.98	IT
575	Amden/Bärenfall	1610	3195426.32	3771436.67	CH
576	Plangero	1620	2652895.07	4386881.69	AT
577	Palanfre	1625	2346135.94	4119927.66	IT
578	Spiss	1630	2649676.69	4354116.71	AT
579	Innerschmirn-Obern	1630	2667591.82	4442907.89	AT
580	Glärnisch/Guppen	1630	3188298.77	3751717.17	CH
581	Alpe devero	1634	2579860.54	4186936.20	IT
582	S. Bernardino	1638	2594941.73	4258407.25	CH
583	Zermatt	1638	2549010.51	4146873.12	CH
584	S. Bernardino	1638	2594941.73	4258407.25	CH
585	Piaggia	1645	2332041.95	4138964.31	IT
586	Argentera	1680	2370159.47	4076819.28	IT
587	Samedan	1708	2601568.90	4311841.82	CH
588	Zürs	1720	2672920.12	4333456.18	AT
589	Castelmagno	1755	2369957.70	4095084.72	IT
590	Rifugio mondovi	1760	2345331.24	4139408.87	IT
591	Turracher Höhe	1767	2652778.40	4616651.49	AT
592	Elva	1770	2386389.17	4089378.96	IT
593	Lungern/Schönbüel	1770	3118360.81	3723948.25	CH
594	Gschwand	1775	2675244.08	4460094.70	AT
595	Ochsengarten-Obergut	1780	2680322.43	4393898.19	AT
596	Stockhorn/Vorderstocken	1780	3074151	3711270.03	CH
597	Malciaussia	1800	2459568.33	4096752.26	IT
598	Segl-Maria	1804	2591161.81	4302812.83	CH
599	Zettlersfeld	1820	2642970.60	4533911.44	AT
600	Evolène / Villa	1825	2558815.91	4128274.50	CH
601	Linthal/Ortstock Matt	1830	3182781.61	3742697.65	CH
602	Sauze cesana	1840	2425556.88	4077345	IT
603	Sieben Hengste	1850	3096262.91	3719566.37	CH
604	Larecchio	1860	2567222.74	4199901.81	IT
605	Brienzz/Rotschalp	1870	3110004.85	3723003.01	CH

606	Arosa	1878	2631194.25	4296572.14	CH
607	Vernago	1938	2625654.65	4383913.09	IT
608	Ladurns	1959	2647767.66	4425128.93	IT
609	Färnel/Färnelberg	1970	3073029.01	3693332.94	CH
610	Launen/Trütlisbergpass	1970	3064562.62	3682578.52	CH
611	Grimsel Hospiz	1980	2608040.95	4193192.34	CH
612	Le selle	1980	2443283.33	4077920.14	IT
613	Casa del Giovo	1986	2637530.82	4422296.16	IT
614	Piz la Ila (SOMMER)	2012	2607583.09	4467096.65	IT
615	Malga Merbe	2015	2660381.79	4482402.50	IT
616	Prati di Plan	2016	2631575.05	4405183.79	IT
617	Sestriere	2020	2431984.60	4074114.12	IT
618	Diga del chiotas	2020	2343006.26	4107425.79	IT
619	Frutigen/Otterer	2020	3078051.15	3695646.31	CH
620	Val d'Iliez/Les Collines	2020	3022895.93	3655189.76	CH
621	Schächental/Seewli	2030	3165030.41	3730116.61	CH
622	Krippenstein	2050	2719197.76	4599261.78	AT
623	Elm/Chüebodensee	2050	3196191.32	3745460.73	CH
624	Gadmen/Gschletteregg	2060	3141035.60	3721187.29	CH
625	Vals/Alp Calasa	2070	3203322.90	3716985.66	CH
626	Bedretto/Cassinello	2100	3152064.51	3693758.03	CH
627	Grindelwald/First	2110	3115975.67	3711572.14	CH
628	Gstaad/Ober Meiel	2110	3051764.95	3681627.25	CH
629	Guttannen/Homad	2110	3133146.57	3713553.20	CH
630	Pian delle baracche	2135	2386556.80	4092910.39	IT
631	Frutigen/Elsige	2140	3084222.48	3694790.39	CH
632	Klosters/Madrisa	2140	3252605.30	3746194.75	CH
633	Titlis	2140	3141658.73	3725802.86	CH
634	Clot della soma	2150	2435257.21	4079518.63	IT
635	Pian giasset	2150	2402160.97	4093093.84	IT
636	Hinterrhein/Alp Piänetsch	2150	3204123.09	3702626.11	CH
637	Kandersteg/Fisi	2160	3087050.02	3688517.75	CH
638	Männlichen	2165	3106935.49	3705644.72	CH
639	Taminatal/Schaftäli	2170	3221072.57	3742063.71	CH
640	Urseren/Giltnasen	2170	3150868.74	3704300.23	CH
641	Breil Tumpiv/Val Miez	2195	3188505.69	3727869.26	CH
642	Puzzetta, Medel/Il Plauns	2195	3177368.30	3710090.13	CH
643	Colle bercia	2200	2428943.47	4066735.37	IT
644	Hinterrhein/Unter Surettasee	2200	3215245.51	3702472.76	CH
645	Oberwald/Mällige	2200	3139088.24	3694918.57	CH
646	Meiental/Laucherer	2210	3152779.27	3721710.07	CH
647	Mund/Chiematte	2210	3107020.86	3674054.11	CH
648	Campolungo/Fontane	2220	3167253.71	3691722.86	CH
649	Chaussy/Pierres Fendues	2220	3048127.25	3676531.95	CH
650	Tujetsch/Nual	2220	3167857.27	3711855.40	CH
651	Conthey/Etang de Trente Pas	2230	3057076.18	3667127.96	CH
652	Finhaut/LEcreuleuse	2240	3033770.21	3645538.14	CH
653	Passo del Bernina	2260	2588560.89	4322604.27	CH
654	Tujetsch/Culmatsch	2270	3166352.05	3715896.16	CH
655	Lago pilone	2280	2437641.61	4074440.08	IT
656	Gütsch, Andermatt	2283	2616562.38	4214979.38	CH
657	Dresdner Hütte	2290	2654352.13	4407906.64	AT
658	Davos/Parsonn	2290	3247788.17	3739523.03	CH
659	Colle barant	2294	2411792.26	4088047.33	IT
660	Piz Lagrev/Materdell	2300	3242906.24	3691923.66	CH
661	Lago agnel	2304	2488442.61	4097088.30	IT
662	Colle lombarda	2305	2348729.49	4092682.49	IT
663	Bosco Gurin/Hendar Furggu	2310	3149069.32	3676214.67	CH
664	Klosters/Gatschiefer	2310	3257508.87	3739035.18	CH
665	Pian dei Cavalli	2314	2595668.44	4383313.26	IT
666	Crap Masegn	2330	3200407.63	3735855.14	CH
667	Schächental/Alpler Tor	2330	3169339.71	3738989.19	CH
668	Naluns/Schlivera	2350	3282431.92	3737994.05	CH
669	Schilthorn/Türliboden	2360	3098841.81	3700629.81	CH
670	Lago di valsoera	2365	2489629.39	4116993.56	IT
671	Distentis/Lumpegna	2388	3176650.47	3721720.22	CH
672	Arbaz, Val. Sionne/Donin du Jour	2390	3063995.35	3670907.19	CH
673	Flüela/Hospiz	2390	3259405.56	3729348.18	CH
674	Bocchetta delle pisse	2410	2531691.17	4157934.34	IT
675	Goms/Treichbode	2430	3129530.98	3692376.29	CH
676	Julier/Vairana	2430	3242093.46	3697815.70	CH
677	Oberwald/Jostsee	2430	3135938.64	3698921.96	CH
678	Piz Martegnas	2430	3229431.75	3708180.50	CH
679	Acquarossa/Piano del Simano	2450	3187482.14	3693120.61	CH
680	Bedretto/Cavanna	2450	3150953.64	3698436.95	CH
681	Davos/Hanengretji	2450	3245939.14	3732393.24	CH

682	Goms/Bodmerchumma	2450	3130232.38	3684896.55	CH
683	Bernina/Motta Bianca	2450	3268398.34	3693286.76	CH
684	Formazza	2453	2592721.75	4194781.78	IT
685	Taminatal/Wildsee	2460	3215424.65	3750333.27	CH
686	Leukerbad/Trubelboden	2480	3080720.76	3677121.16	CH
687	Saas/Seetal	2480	3104258.95	3656041.36	CH
688	Eggishorn	2495	3119390.34	3683875.02	CH
689	Säntis	2502	2682104.31	4271363.71	CH
690	Bever/Valetta	2510	3252685.48	3705312.70	CH
691	Simplon/Bortelsee	2520	3121454.80	3669937.63	CH
692	Samnaun/Ravaischer Salaas	2520	3287651.74	3754029.83	CH
693	Davos/Weissfluhjoch	2540	3248305.73	3737138.44	CH
694	Les Attelas	2545	3057485.84	3646855.90	CH
695	Lukmanier/Lai Verd	2550	3171411.84	3707295.32	CH
696	Davos/Bärentälli	2560	3250139.43	3722802.98	CH
697	Les Diablerets	2575	3054461.97	3669812.15	CH
698	Anniviers/Tracuit	2590	3087256.67	3649807.82	CH
699	Arolla/Bréona	2610	3080195.62	3645803.64	CH
700	Fully/Grand Cor	2610	3043170.21	3656245.34	CH
701	Bernina/Puoz Bass	2620	3259555.25	3694815.35	CH
702	Anniviers/Orzival	2630	3077596.31	3656836.63	CH
703	Rifugio gastaldi	2659	2469597.80	4096716.76	IT
704	Zernez/Pülschezza	2680	3265352.20	3723729.78	CH
705	Liddes/Pointe de Toules	2700	3055399.95	3633467.61	CH
706	Laucherenalp/Gandegg	2717	3093856.04	3684115.82	CH
707	Kesch/Porta dEs-cha	2725	3256740.37	3714662.94	CH
708	Piz Lagrev/Tscheppa	2730	3246296.95	3695124.67	CH
709	Vinadi/Alpetta	2730	3295762.25	3751939.62	CH
710	Rifugio vaccarone	2745	2454354	4078288.14	IT
711	Zermatt/Triftchumme	2750	3093166.35	3641293.39	CH
712	Saas/Schwarz mies	2810	3111878.13	3651173.05	CH
713	Madriccio	2818	2598036.40	4368229.13	IT
714	Passo del moro	2820	2545010.92	4164150.11	IT
715	Arolla/Les Fontanesses	2850	3071393.55	3638948.35	CH
716	St. Niklaus/Oberer Stelligletscher	2910	3094358.07	3655304.90	CH
717	La Fouly/Glacier de Saleina	2942	3040016.36	3631973.74	CH
718	Gornergrat	2950	3097767.04	3635413.01	CH
719	Giovo del Diavolo	3040	2630441.38	4379443.77	IT
720	Monviso	3325	2399039.93	4089801.52	IT

Table C.5 List of online data sources.

Product	Online source
Digital Elevation Model	https://esdac.jrc.ec.europa.eu/projects/Alpsis/Ecalp_data.html
Corine Land Cover	https://www.eea.europa.eu/data-and-maps/data/clc-2006-raster-4
MODIS snowcover	https://doi.org/10.5067/MODIS/MOD10A2.006
Discharge Data	AT https://ehyd.gv.at/
	CH https://www.hydrodaten.admin.ch/
	FR http://www.hydro.eaufrance.fr/
	I http://abouthydrology.blogspot.com/2016/09/the-adige-database-or-database-newage.html http://www.arpa.piemonte.it/
	SI http://www.arso.gov.si/vode/podatki/
Meteorological Data	AT https://ehyd.gv.at/
	CH https://gate.meteoswiss.ch/idaweb/more.do
	FR https://donneespubliques.meteofrance.fr/
	I http://www.meteo.fvg.it/archivio.php?ln=&p=dati http://www.arpa.piemonte.it/
Snow depth Data	AT https://ehyd.gv.at/
	CH https://gate.meteoswiss.ch/idaweb/more.do
	I http://abouthydrology.blogspot.com/2016/09/the-adige-database-or-database-newage.html http://www.arpa.piemonte.it/ http://www.meteo.fvg.it/archivio.php?ln=&p=dati

References

- Addor, N., Rohrer, M., Furrer, R., & Seibert, J. (2016). Propagation of biases in climate models from the synoptic to the regional scale: Implications for bias adjustment. *Journal of Geophysical Research: Atmospheres*, *121*(5), 2075–2089. <https://doi.org/10.1002/2015JD024040>
- Ågren, G. I., Wetterstedt, J. Å. M., & Billberger, M. F. K. (2012). Nutrient limitation on terrestrial plant growth - modeling the interaction between nitrogen and phosphorus. *New Phytologist*, *194*(4), 953–960. <https://doi.org/10.1111/j.1469-8137.2012.04116.x>
- Ainsworth, E. A., & Long, S. P. (2005). What have we learned from 15 years of free-air CO₂ enrichment (FACE)? A meta-analytic review of the responses of photosynthesis, canopy properties and plant production to rising CO₂. *New Phytologist*, *165*(2), 351–372. <https://doi.org/10.1111/j.1469-8137.2004.01224.x>
- Ainsworth, E. A., & Rogers, A. (2007). The response of photosynthesis and stomatal conductance to rising [CO₂]: Mechanisms and environmental interactions. *Plant, Cell and Environment*, *30*(3), 258–270. <https://doi.org/10.1111/j.1365-3040.2007.01641.x>
- Albert, C. H., Grassein, F., Schurr, F. M., Vieilledent, G., & Violle, C. (2011). When and how should intraspecific variability be considered in trait-based plant ecology? *Perspectives in Plant Ecology, Evolution and Systematics*, *13*(3), 217–225. <https://doi.org/10.1016/j.ppees.2011.04.003>
- Anderegg, W. R. L. (2015). Spatial and temporal variation in plant hydraulic traits and their relevance for climate change impacts on vegetation. *New Phytologist*, *205*(3), 1008–1014. <https://doi.org/10.1111/nph.12907>
- Arnth, A., Harrison, S. P., Zaehle, S., Tsigaridis, K., Menon, S., Bartlein, P. J., ... Vesala, T. (2010). Terrestrial biogeochemical feedbacks in the climate system. *Nature Geoscience*, *3*(8), 525–532. <https://doi.org/10.1038/ngeo905>
- Arora, V. K., & Boer, G. J. (2005). A parameterization of leaf phenology for the terrestrial ecosystem component of climate models. *Global Change Biology*, *11*(1), 39–59. <https://doi.org/10.1111/j.1365-2486.2004.00890.x>
- Aubin, I., Munson, A. D., Cardou, F., Burton, P. J., Isabel, N., Pedlar, J. H., ... McKenney, D. (2016). Traits to stay, traits to move: a review of functional traits to assess sensitivity and adaptive capacity of temperate and boreal trees to climate change. *Environmental Reviews*, *24*(2), 164–186. <https://doi.org/10.1139/er-2015-0072>
- Aubinet, M., Heinesch, B., & Longdoz, B. (2002). Estimation of the carbon sequestration by a heterogeneous forest: Night flux corrections, heterogeneity of the site and inter-annual variability. *Global Change Biology*, *8*(11), 1053–1071. <https://doi.org/10.1046/j.1365-2486.2002.00529.x>
- Ball, J. T., Wood, I. E., & Berry, J. A. (1987). A model predicting stomatal conductance and its

- contribution to the control of photosynthesis under different environmental conditions. *Progress in Photosynthesis Research*, *IV*(1), 221–224.
- Barnett, T. P., Adam, J. C., & Lettenmaier, D. P. (2005). Potential impacts of a warming climate on water availability in snow-dominated regions. *Nature*, *438*(7066), 303–309. <https://doi.org/10.1038/nature04141>
- Battipaglia, G., Saurer, M., Cherubini, P., Calfapietra, C., Mccarthy, H. R., Norby, R. J., & Francesca Cotrufo, M. (2013). Elevated CO₂ increases tree-level intrinsic water use efficiency: Insights from carbon and oxygen isotope analyses in tree rings across three forest FACE sites. *New Phytologist*, *197*(2), 544–554. <https://doi.org/10.1111/nph.12044>
- Beer, C., Ciais, P., Reichstein, M., Baldocchi, D., Law, B. E., Papale, D., ... Wohlfahrt, G. (2009). Temporal and among-site variability of inherent water use efficiency at the ecosystem level. *Global Biogeochemical Cycles*, *23*(2). <https://doi.org/10.1029/2008GB003233>
- Beniston, M. (2003). Climatic change in mountain regions: A review of possible impacts. *Climatic Change*, *59*(1–2), 5–31. <https://doi.org/10.1023/A:1024458411589>
- Beniston, M. (2006). Mountain weather and climate: A general overview and a focus on climatic change in the Alps. *Hydrobiologia*, *562*(1), 3–16. <https://doi.org/10.1007/s10750-005-1802-0>
- Beniston, M. (2012). Impacts of climatic change on water and associated economic activities in the Swiss Alps. *Journal of Hydrology*, *412–413*, 291–296. <https://doi.org/10.1016/j.jhydrol.2010.06.046>
- Beniston, M., Farinotti, D., Stoffel, M., Andreassen, L. M., Coppola, E., Eckert, N., ... Vincent, C. (2018). The European mountain cryosphere: a review of its current state, trends, and future challenges. *The Cryosphere*, *12*(2), 759–794. <https://doi.org/10.5194/tc-12-759-2018>
- Berbigier, P., Bonnefond, J. M., & Mellmann, P. (2001). CO₂ and water vapour fluxes for 2 years above Euroflux forest site. *Agricultural and Forest Meteorology*, *108*(3), 183–197. [https://doi.org/10.1016/S0168-1923\(01\)00240-4](https://doi.org/10.1016/S0168-1923(01)00240-4)
- Berry, J. A., Beerling, D. J., & Franks, P. J. (2010). Stomata: Key players in the earth system, past and present. *Current Opinion in Plant Biology*, *13*(3), 233–240. <https://doi.org/10.1016/j.pbi.2010.04.013>
- Bertoldi, G., Notarnicola, C., Leitinger, G., Endrizzi, S., Zebisch, M., Della Chiesa, S., & Tappeiner, U. (2010). Topographical and ecohydrological controls on land surface temperature in an alpine catchment. *Ecohydrology*, *3*, 189–204. <https://doi.org/10.1002/eco.129>
- Bertoldi, G., Rigon, R., & Over, T. M. (2006). Impact of Watershed Geomorphic Characteristics on the Energy and Water Budgets. *Journal of Hydrometeorology*, *7*(3), 389–403. <https://doi.org/10.1175/JHM500.1>
- Bierkens, M. F. P., Bell, V. A., Burek, P., Chaney, N., Condon, L. E., David, C. H., ... Wood, E. F. (2015). Hyper-resolution global hydrological modelling: what is next? *Hydrological Processes*,

- 29(2), 310–320. <https://doi.org/10.1002/hyp.10391>
- Boisvenue, C., & Running, S. W. (2006). Impacts of climate change on natural forest productivity - Evidence since the middle of the 20th century. *Global Change Biology*, *12*(5), 862–882. <https://doi.org/10.1111/j.1365-2486.2006.01134.x>
- Bolli, J. C., Rigling, A., & Bugmann, H. (2007). The influence of changes in climate and land-use on regeneration dynamics of Norway spruce at the treeline in the swiss alps. *Silva Fennica*, *41*(1), 55–70. <https://doi.org/10.14214/sf.307>
- Bonan, G. B. (2008). Forests and climate change: forcings, feedbacks, and the climate benefits of forests. *Science*, *320*(5882), 1444–1449. <https://doi.org/10.1126/science.1155121>
- Bonan, G. B., Lawrence, P. J., Oleson, K. W., Levis, S., Jung, M., Reichstein, M., ... Swenson, S. C. (2011). Improving canopy processes in the Community Land Model version 4 (CLM4) using global flux fields empirically inferred from FLUXNET data. *Journal of Geophysical Research: Biogeosciences*, *116*(G2), G02014. <https://doi.org/10.1029/2010JG001593>
- Bonan, G. B., Levis, S., & Sitch, S. (2003). A dynamic global vegetation model for use with climate models: concepts and description of simulated vegetation dynamics. *Global Change Biology*, *9*, 1543–1566. <https://doi.org/10.1046/j.1529-8817.2003.00681.x>
- Bonell, M. (2002). Ecohydrology—a completely new idea? *Hydrological Sciences Journal*, *47*(5), 809–810. <https://doi.org/10.1080/02626660209492984>
- Booth, R. K., Jackson, S. T., Sousa, V. A., Sullivan, M. E., Minckley, T. A., & Clifford, M. J. (2012). Multi-decadal drought and amplified moisture variability drove rapid forest community change in a humid region. *Ecology*, *93*(2), 219–226. <https://doi.org/10.1890/11-1068.1>
- Brewer, S. K., Worthington, T. A., Mollenhauer, R., Stewart, D. R., McManamay, R. A., Guertault, L., & Moore, D. (2018). Synthesizing models useful for ecohydrology and ecohydraulic approaches: An emphasis on integrating models to address complex research questions. *Ecohydrology*, *11*(7), 1–26. <https://doi.org/10.1002/eco.1966>
- Briffa, K. R., van der Schrier, G., & Jones, P. D. (2009). Wet and dry summers in Europe since 1750: evidence of increasing drought. *International Journal of Climatology*, *29*(13), 1894–1905. <https://doi.org/10.1002/joc.1836>
- Brodribb, T. J., & Holbrook, N. M. (2003). Stomatal closure during leaf dehydration, correlation with other leaf physiological traits. *Plant Physiology*, *132*(4), 2166–2173. <https://doi.org/10.1104/pp.103.023879>
- Brodribb, T. J., & McAdam, S. A. M. (2013). Unique responsiveness of angiosperm stomata to elevated CO₂ explained by calcium signalling. *PLoS ONE*, *8*(11), e82057. <https://doi.org/10.1371/journal.pone.0082057>
- Brooks, P. D., Chorover, J., Fan, Y., Godsey, S. E., Maxwell, R. M., McNamara, J. P., & Tague, C. (2015). Hydrological partitioning in the critical zone: Recent advances and opportunities for

- developing transferable understanding of water cycle dynamics. *Water Resources Research*, 51(9), 6973–6987. <https://doi.org/10.1002/2015WR017039>
- Brunetti, M., Lentini, G., Maugeri, M., Nanni, T., Auer, I., Böhm, R., & Schöner, W. (2009). Climate variability and change in the Greater Alpine Region over the last two centuries based on multi-variable analysis. *International Journal of Climatology*, 29, 2197–2225. <https://doi.org/10.1002/joc.1857>
- Brutsaert, W. (2005). *Hydrology: An Introduction*. Cambridge, UK: Cambridge University Press.
- Brzostek, E. R., Dragoni, D., Schmid, H. P., Rahman, A. F., Sims, D., Wayson, C. A., ... Phillips, R. P. (2014). Chronic water stress reduces tree growth and the carbon sink of deciduous hardwood forests. *Global Change Biology*, 20(8), 2531–2539. <https://doi.org/10.1111/gcb.12528>
- Buckley, T. N. (2008). The role of stomatal acclimation in modelling tree adaptation to high CO₂. *Journal of Experimental Botany*, 59(7), 1951–1961. <https://doi.org/10.1093/jxb/erm234>
- Buckley, T. N., Mott, K. A., & Farquhar, G. D. (2003). A hydromechanical and biochemical model of stomatal conductance. *Plant, Cell and Environment*, 26(10), 1767–1785. <https://doi.org/10.1046/j.1365-3040.2003.01094.x>
- Bunce, J. A. (2004). Carbon dioxide effects on stomatal responses to the environment and water use by crops under field conditions. *Oecologia*, 140(1), 1–10. <https://doi.org/10.1007/s00442-003-1401-6>
- Büntgen, U., Frank, D. C., Schmidhalter, M., Neuwirth, B., Seifert, M., & Esper, J. (2006). Growth/climate response shift in a long subalpine spruce chronology. *Trees - Structure and Function*, 20(1), 99–110. <https://doi.org/10.1007/s00468-005-0017-3>
- Butler, E. E., Datta, A., Flores-Moreno, H., Chen, M., Wythers, K. R., Fazayeli, F., ... Reich, P. B. (2017). Mapping local and global variability in plant trait distributions. *Proceedings of the National Academy of Sciences*, 114(51), E10937–E10946. <https://doi.org/10.1073/pnas.1708984114>
- Camarero, J. J., Gazol, A., Tardif, J. C., & Conciatori, F. (2015). Attributing forest responses to global-change drivers: Limited evidence of a CO₂-fertilization effect in Iberian pine growth. *Journal of Biogeography*, 42(11), 2220–2233. <https://doi.org/10.1111/jbi.12590>
- Cao, L., Bala, G., Caldeira, K., Nemani, R., & Ban-Weiss, G. (2010). Importance of carbon dioxide physiological forcing to future climate change. *Proceedings of the National Academy of Sciences*, 107(21), 9513–9518. <https://doi.org/10.1073/pnas.0913000107>
- Carlson, B. Z., Corona, M. C., Dentant, C., Bonet, R., Thuiller, W., & Choler, P. (2017). Observed long-term greening of alpine vegetation—a case study in the French Alps. *Environmental Research Letters*, 12(11), 114006. <https://doi.org/10.1088/1748-9326/aa84bd>
- Carrara, A., Kowalski, A. S., Neiryneck, J., Janssens, I. a., Yuste, J. C., & Ceulemans, R. (2003). Net ecosystem CO₂ exchange of mixed forest in Belgium over 5 years. *Agricultural and Forest*

- Meteorology*, 119(3–4), 209–227. [https://doi.org/10.1016/S0168-1923\(03\)00120-5](https://doi.org/10.1016/S0168-1923(03)00120-5)
- Casty, C., Wanner, H., Luterbacher, J., Esper, J., & Böhm, R. (2005). Temperature and precipitation variability in the European Alps since 1500. *International Journal of Climatology*, 25(14), 1855–1880. <https://doi.org/10.1002/joc.1216>
- Chapin, F. S., Schulze, E. D., & Mooney, H. (1990). The Ecology and Economics of Storage in Plants. *Annual Review of Ecology and Systematics*, 21(1), 423–447. <https://doi.org/10.1146/annurev.es.21.110190.002231>
- Cheng, L., Zhang, L., Wang, Y.-P., Canadell, J. G., Chiew, F. H. S., Beringer, J., ... Zhang, Y. (2017). Recent increases in terrestrial carbon uptake at little cost to the water cycle. *Nature Communications*, 8(1), 110. <https://doi.org/10.1038/s41467-017-00114-5>
- Chow, V. T., Maidment, D. R., & Mays, L. W. (1988). *Applied Hydrology*. New York, NY: McGraw-Hill.
- Christensen, L., Tague, C., & Baron, J. S. (2008). Spatial patterns of simulated transpiration response to climate variability in a snow dominated mountain ecosystem. *Hydrological Processes*, 22, 3576–3588. <https://doi.org/10.1002/hyp.6961>
- Churkina, G., & Running, S. W. (1998). Contrasting Climatic Controls on the Estimated Productivity of Global Terrestrial Biomes. *Ecosystems*, 1(2), 206–215. <https://doi.org/10.1007/s100219900016>
- Collatz, G. J., Ball, J. T., Grivet, C., & Berry, J. A. (1991). Physiological and environmental regulation of stomatal conductance, photosynthesis and transpiration: a model that includes a laminar boundary layer. *Agricultural and Forest Meteorology*, 54(2–4), 107–136. [https://doi.org/10.1016/0168-1923\(91\)90002-8](https://doi.org/10.1016/0168-1923(91)90002-8)
- Collatz, G. J., Ribas-carbo, M., & Berry, J. A. (1992). Coupled Photosynthesis-Stomatal Conductance Model for Leaves of C4 Plants. *Australian Journal of Plant Physiology*, 19(5), 519. <https://doi.org/10.1071/PP9920519>
- Cook, B. D., Davis, K. J., Wang, W., Desai, A. R., Berger, B. W., Teclaw, R. M., ... Heilman, W. (2004). Carbon exchange and venting anomalies in an upland deciduous forest in northern Wisconsin, USA. *Agricultural and Forest Meteorology*, 126(3–4), 271–295. <https://doi.org/10.1016/j.agrformet.2004.06.008>
- Curtis, P. S., Vogel, C. S., Gough, C. M., Schmid, H. P., Su, H. B., & Bovard, B. D. (2005). Respiratory carbon losses and the carbon-use efficiency of a northern hardwood forest, 1999–2003. *New Phytologist*, 167(2), 437–456. <https://doi.org/10.1111/j.1469-8137.2005.01438.x>
- Dai, Y., Dickinson, R. E., & Wang, Y. P. (2004). A two-big-leaf model for canopy temperature, photosynthesis, and stomatal conductance. *Journal of Climate*, 17(12), 2281–2299. [https://doi.org/10.1175/1520-0442\(2004\)017<2281:ATMFCT>2.0.CO;2](https://doi.org/10.1175/1520-0442(2004)017<2281:ATMFCT>2.0.CO;2)
- Damour, G., Simonneau, T., Cochard, H., & Urban, L. (2010). An overview of models of stomatal

- conductance at the leaf level. *Plant, Cell and Environment*, 33(9), 1419–1438. <https://doi.org/10.1111/j.1365-3040.2010.02181.x>
- Davidson, E. A., Savage, K. E., Trumbore, S., & Boroken, W. (2006). Vertical partitioning of CO₂ production within a temperate forest soil. *Global Change Biology*, 12(6), 944–956. <https://doi.org/10.1111/j.1365-2486.2006.01142.x>
- Davis, M. B. (1989). Lags in vegetation response to greenhouse warming. *Climatic Change*, 15(1–2), 75–82. <https://doi.org/10.1007/BF00138846>
- de Boer, H. J., Eppinga, M. B., Wassen, M. J., & Dekker, S. C. (2012). A critical transition in leaf evolution facilitated the Cretaceous angiosperm revolution. *Nature Communications*, 3(1), 1221. <https://doi.org/10.1038/ncomms2217>
- de Boer, H. J., Lammertsma, E. I., Wagner-Cremer, F., Dilcher, D. L., Wassen, M. J., & Dekker, S. C. (2011). Climate forcing due to optimization of maximal leaf conductance in subtropical vegetation under rising CO₂. *Proceedings of the National Academy of Sciences*, 108(10), 4041–4046. <https://doi.org/10.1073/pnas.1100555108>
- de Boer, H. J., Price, C. A., Wagner-Cremer, F., Dekker, S. C., Franks, P. J., & Veneklaas, E. J. (2016). Optimal allocation of leaf epidermal area for gas exchange. *New Phytologist*, 1219–1228. <https://doi.org/10.1111/nph.13929>
- de Jong, C. (2015). Challenges for mountain hydrology in the third millennium. *Frontiers in Environmental Science*, 3(May), 1–13. <https://doi.org/10.3389/fenvs.2015.00038>
- De Kauwe, M. G., Medlyn, B. E., Zaehle, S., Walker, A. P., Dietze, M. C., Hickler, T., ... Norby, R. J. (2013). Forest water use and water use efficiency at elevated CO₂: A model-data intercomparison at two contrasting temperate forest FACE sites. *Global Change Biology*, 19(6), 1759–1779. <https://doi.org/10.1111/gcb.12164>
- De Kauwe, M. G., Medlyn, B. E., Zaehle, S., Walker, A. P., Dietze, M. C., Wang, Y. P., ... Norby, R. J. (2014). Where does the carbon go? A model-data intercomparison of vegetation carbon allocation and turnover processes at two temperate forest free-air CO₂ enrichment sites. *New Phytologist*, 203(3), 883–899. <https://doi.org/10.1111/nph.12847>
- de Pury, D. G. G., & Farquhar, G. D. (1997). Simple scaling of photosynthesis from leaves to canopies without the errors of big-leaf models. *Plant, Cell and Environment*, 20(5), 537–557. <https://doi.org/10.1111/j.1365-3040.1997.00094.x>
- Dee, D. P., Uppala, S. M., Simmons, A. J., Berrisford, P., Poli, P., Kobayashi, S., ... Vitart, F. (2011). The ERA-Interim reanalysis: Configuration and performance of the data assimilation system. *Quarterly Journal of the Royal Meteorological Society*, 137(656), 553–597. <https://doi.org/10.1002/qj.828>
- Dekker, S. C., Groenendijk, M., Booth, B. B., Huntingford, C., & Cox, P. M. (2016). Spatial and temporal variations in plant water-use efficiency inferred from tree-ring, eddy covariance and atmospheric observations. *Earth System Dynamics*, 7, 525–533. <https://doi.org/doi:10.5194/esd->

- Della Chiesa, S., Bertoldi, G., Niedrist, G., Obojes, N., Endrizzi, S., Albertson, J. D., ... Tappeiner, U. (2014). Modelling changes in grassland hydrological cycling along an elevational gradient in the Alps. *Ecohydrology*, 7(6), 1453–1473. <https://doi.org/10.1002/eco.1471>
- Diffenbaugh, N. S., & Field, C. B. (2013). Changes in ecologically critical terrestrial climate conditions. *Science*, 341(6145), 486–492. <https://doi.org/10.1126/science.1237123>
- Dilley, A. C., & O'Brien, D. M. (1998). Estimating downward clear sky long-wave irradiance at the surface from screen temperature and precipitable water. *Quarterly Journal of the Royal Meteorological Society*, 124(549), 1391–1401. <https://doi.org/10.1256/smsqj.54902>
- Ding, R., Kang, S., Du, T., Hao, X., & Zhang, Y. (2014). Scaling Up Stomatal Conductance from Leaf to Canopy Using a Dual-Leaf Model for Estimating Crop Evapotranspiration. *PLoS ONE*, 9(4), e95584. <https://doi.org/10.1371/journal.pone.0095584>
- Dobbertin, M., Mayer, P., Wohlgemuth, T., Feldmeyer-Christe, E., Graf, U., Zimmermann, N. E., & Rigling, A. (2005). The decline of *Pinus sylvestris* L. forests in the Swiss Rhone valley - A result of drought stress? *Phyton - Annales Rei Botanicae*, 45(4), 153–156.
- Dolman, A. J., Moors, E. J., & Elbers, J. A. (2002). The carbon uptake of a mid latitude pine forest growing on sandy soil. *Agricultural and Forest Meteorology*, 111(3), 157–170. [https://doi.org/10.1016/S0168-1923\(02\)00024-2](https://doi.org/10.1016/S0168-1923(02)00024-2)
- Domec, J.-C., Palmroth, S., Ward, E. J., Maier, C. A., Thérézien, M., & Oren, R. (2009). Acclimation of leaf hydraulic conductance and stomatal conductance of *Pinus taeda* (loblolly pine) to long-term growth in elevated CO₂ (free-air CO₂ enrichment) and N-fertilization. *Plant, Cell and Environment*, 32(11), 1500–1512. <https://doi.org/10.1111/j.1365-3040.2009.02014.x>
- Drake, B. G., Gonzalez-Meler, M. a., & Long, S. P. (1997). MORE EFFICIENT PLANTS: A Consequence of Rising Atmospheric CO₂? *Annual Review of Plant Physiology and Plant Molecular Biology*, 48, 609–639. <https://doi.org/10.1146/annurev.arplant.48.1.609>
- Duethmann, D., & Blöschl, G. (2018). Why has catchment evaporation increased in the past 40 years? A data-based study in Austria. *Hydrology and Earth System Sciences*, 22(10), 5143–5158. <https://doi.org/10.5194/hess-22-5143-2018>
- Dunn, A. L., Barford, C. C., Wofsy, S. C., Goulden, M. L., & Daube, B. C. (2007). A long-term record of carbon exchange in a boreal black spruce forest: means, responses to interannual variability, and decadal trends. *Global Change Biology*, 13(3), 577–590. <https://doi.org/10.1111/j.1365-2486.2006.01221.x>
- Dunne, J. A., Saleska, S. R., Fischer, M. L., & Harte, J. (2004). INTEGRATING EXPERIMENTAL AND GRADIENT METHODS IN ECOLOGICAL CLIMATE CHANGE RESEARCH. *Ecology*, 85(4), 904–916. <https://doi.org/10.1890/03-8003>
- Dupire, S., Curt, T., & Bigot, S. (2017). Spatio-temporal trends in fire weather in the French Alps.

Science of the Total Environment, 595, 801–817.
<https://doi.org/10.1016/j.scitotenv.2017.04.027>

- Dusenge, M. E., Duarte, A. G., & Way, D. A. (2019). Plant carbon metabolism and climate change: elevated CO₂ and temperature impacts on photosynthesis, photorespiration and respiration. *New Phytologist*, 221(1), 32–49. <https://doi.org/10.1111/nph.15283>
- Eamus, D., & Jarvis, P. G. (1989). The Direct Effects of Increase in the Global Atmospheric CO₂ Concentration on Natural and Commercial Temperate Trees and Forests. *Advances in Ecological Research*, 19, 1–55. [https://doi.org/10.1016/S0065-2504\(03\)34001-2](https://doi.org/10.1016/S0065-2504(03)34001-2)
- Egli, M., Mirabella, A., Sartori, G., Zanelli, R., & Bischof, S. (2006). Effect of north and south exposure on weathering rates and clay mineral formation in Alpine soils. *Catena*, 67(3), 155–174. <https://doi.org/10.1016/j.catena.2006.02.010>
- Egli, M., Sartori, G., Mirabella, A., Favilli, F., Giaccari, D., & Delbos, E. (2009). Effect of north and south exposure on organic matter in high Alpine soils. *Geoderma*, 149(1–2), 124–136. <https://doi.org/10.1016/j.geoderma.2008.11.027>
- Ehlers, I., Augusti, A., Betson, T. R., Nilsson, M. B., Marshall, J. D., & Schleucher, J. (2015). Detecting long-term metabolic shifts using isotopomers: CO₂-driven suppression of photorespiration in C₃ plants over the 20th century. *Proceedings of the National Academy of Sciences*, 112(51), 201504493. <https://doi.org/10.1073/pnas.1504493112>
- Elkin, C., Gutiérrez, A. G., Leuzinger, S., Manusch, C., Temperli, C., Rasche, L., & Bugmann, H. (2013). A 2 °C warmer world is not safe for ecosystem services in the European Alps. *Global Change Biology*, 19(6), 1827–1840. <https://doi.org/10.1111/gcb.12156>
- Elsasser, H., & Bürki, R. (2002). Climate change as a threat to tourism in the Alps. *Climate Research*, 20(3), 253–257. <https://doi.org/10.3354/cr020253>
- Elsner, M. M., Gangopadhyay, S., Pruitt, T., Brekke, L. D., Mizukami, N., & Clark, M. P. (2014). How Does the Choice of Distributed Meteorological Data Affect Hydrologic Model Calibration and Streamflow Simulations? *Journal of Hydrometeorology*, 15(4), 1384–1403. <https://doi.org/10.1175/JHM-D-13-083.1>
- Etchanchu, J., Rivalland, V., Gascoin, S., Cros, J., Tallec, T., Brut, A., & Boulet, G. (2017). Effects of high spatial and temporal resolution Earth observations on simulated hydrometeorological variables in a cropland (southwestern France). *Hydrology and Earth System Sciences*, 21(11), 5693–5708. <https://doi.org/10.5194/hess-21-5693-2017>
- European Commission. (2007). *Water scarcity and droughts - In-depth assessment*. http://ec.europa.eu/environment/water/quantity/pdf/comm_droughts/2nd_int_report.pdf.
- European Environment Agency. (2006). *CORINE Land Cover 2006*. <https://www.eea.europa.eu/data-and-maps/data/clc-2006-raster-4>.
- European Environment Agency (EEA). (2009). *Regional climate change and adaptation. The Alps*

- facing the challenge of changing water resources*. <https://www.eea.europa.eu/publications/alps-climate-change-and-adaptation-2009>.
- Evans, N. P., Bauska, T. K., Gázquez-Sánchez, F., Brenner, M., Curtis, J. H., & Hodell, D. A. (2018). Quantification of drought during the collapse of the classic Maya civilization. *Science*, *361*(6401), 498–501. <https://doi.org/10.1126/science.aas9871>
- Falkenmark, M., & Rockström, J. (2006). The New Blue and Green Water Paradigm: Breaking New Ground for Water Resources Planning and Management. *Journal of Water Resources Planning and Management*, *132*(3), 129–132. [https://doi.org/10.1061/\(ASCE\)0733-9496\(2006\)132:3\(129\)](https://doi.org/10.1061/(ASCE)0733-9496(2006)132:3(129))
- Fan, Y., Clark, M., Lawrence, D. M., Swenson, S. C., Band, L. E., Brantley, S. L., ... Yamazaki, D. (2019). Hillslope Hydrology in Global Change Research and Earth System Modeling. *Water Resources Research*, 1–36. <https://doi.org/10.1029/2018WR023903>
- Farquhar, G. D., von Caemmerer, S., & Berry, J. A. (1980). A biochemical model of photosynthetic CO₂ assimilation in leaves of C₃ species. *Planta*, *149*(1), 78–90. <https://doi.org/10.1007/BF00386231>
- Fatichi, S., & Ivanov, V. Y. (2014). Interannual variability of evapotranspiration and vegetation productivity. *Water Resources Research*, *50*(4), 3275–3294. <https://doi.org/10.1002/2013WR015044>
- Fatichi, S., Ivanov, V. Y., & Caporali, E. (2011). Simulation of future climate scenarios with a weather generator. *Advances in Water Resources*, *34*(4), 448–467. <https://doi.org/10.1016/j.advwatres.2010.12.013>
- Fatichi, S., Ivanov, V. Y., & Caporali, E. (2012a). A mechanistic ecohydrological model to investigate complex interactions in cold and warm water-controlled environments: 1. Theoretical framework and plot-scale analysis. *Journal of Advances in Modeling Earth Systems*, *4*(2), M05002. <https://doi.org/10.1029/2011MS000086>
- Fatichi, S., Ivanov, V. Y., & Caporali, E. (2012b). A mechanistic ecohydrological model to investigate complex interactions in cold and warm water-controlled environments: 2. Spatiotemporal analyses. *Journal of Advances in Modeling Earth Systems*, *4*(5), M05003. <https://doi.org/10.1029/2011MS000087>
- Fatichi, S., Katul, G. G., Ivanov, V. Y., Pappas, C., Paschalis, A., Consolo, A., ... Burlando, P. (2015). Abiotic and biotic controls of soil moisture spatiotemporal variability and the occurrence of hysteresis. *Water Resources Research*, *51*(5), 3505–3524. [https://doi.org/10.1016/0022-1694\(68\)90080-2](https://doi.org/10.1016/0022-1694(68)90080-2)
- Fatichi, S., & Leuzinger, S. (2013). Reconciling observations with modeling: The fate of water and carbon allocation in a mature deciduous forest exposed to elevated CO₂. *Agricultural and Forest Meteorology*, *174–175*, 144–157. <https://doi.org/10.1016/j.agrformet.2013.02.005>
- Fatichi, S., Leuzinger, S., & Körner, C. (2014). Moving beyond photosynthesis: From carbon source

- to sink-driven vegetation modeling. *New Phytologist*, 201(4), 1086–1095. <https://doi.org/10.1111/nph.12614>
- Fatichi, S., Leuzinger, S., Paschalis, A., Langley, J. A., Donnellan Barraclough, A., & Hovenden, M. J. (2016). Partitioning direct and indirect effects reveals the response of water-limited ecosystems to elevated CO₂. *Proceedings of the National Academy of Sciences*, 113(45), 12757–12762. <https://doi.org/10.1073/pnas.1605036113>
- Fatichi, S., Molnar, P., Mastrotheodoros, T., & Burlando, P. (2015). Diurnal and seasonal changes in near-surface humidity in a complex orography. *Journal of Geophysical Research: Atmospheres*, 120(6), 2358–2374. <https://doi.org/10.1002/2014JD022537>
- Fatichi, S., & Pappas, C. (2017). Constrained variability of modeled T:ET ratio across biomes. *Geophysical Research Letters*, 44(13), 6795–6803. <https://doi.org/10.1002/2017GL074041>
- Fatichi, S., Pappas, C., & Ivanov, V. Y. (2016). Modeling plant-water interactions: an ecohydrological overview from the cell to the global scale. *Wiley Interdisciplinary Reviews: Water*, 3(3), 327–368. <https://doi.org/10.1002/wat2.1125>
- Fatichi, S., Rimkus, S., Burlando, P., Bordoy, R., & Molnar, P. (2015). High-resolution distributed analysis of climate and anthropogenic changes on the hydrology of an Alpine catchment. *Journal of Hydrology*, 525, 362–382. <https://doi.org/10.1016/j.jhydrol.2015.03.036>
- Fatichi, S., Zeeman, M. J., Fuhrer, J., & Burlando, P. (2014). Ecohydrological effects of management on subalpine grasslands: From local to catchment scale. *Water Resources Research*, 50(1), 148–164. <https://doi.org/10.1002/2013WR014535>
- Field, C. B., Jackson, R. B., & Mooney, H. (1995). Stomatal responses to increased CO₂: Implications from the plant to the global scale. *Plant, Cell and Environment*, 18(10), 1214–1225. <https://doi.org/10.1111/j.1365-3040.1995.tb00630.x>
- Flexas, J., Díaz-Espejo, A., Conesa, M. À., Coopman, R. E., Douthe, C., Gago, J., ... Niinemets, Ü. (2016). Mesophyll conductance to CO₂ and Rubisco as targets for improving intrinsic water use efficiency in C₃ plants. *Plant, Cell and Environment*, 39(5), 965–982. <https://doi.org/10.1111/pce.12622>
- Foken, T. (2008). The Energy Balance Closure Problem: an Overview. *Ecological Applications*, 18(6), 1351–1367. <https://doi.org/doi:10.1890/06-0922.1>
- Forkel, M., Carvalhais, N., Rodenbeck, C., Keeling, R., Heimann, M., Thonicke, K., ... Reichstein, M. (2016). Enhanced seasonal CO₂ exchange caused by amplified plant productivity in northern ecosystems. *Science*, 351(6274), 696–699. <https://doi.org/10.1126/science.aac4971>
- Francey, R. J., Trudinger, C. M., van der Schoot, M., Law, R. M., Krummel, P. B., Langenfelds, R. L., ... Rodenbeck, C. (2013). Atmospheric verification of anthropogenic CO₂ emission trends. *Nature Climate Change*, 3(5), 520–524. <https://doi.org/10.1038/nclimate1817>
- Frank, D. C., Poulter, B., Saurer, M., Esper, J., Huntingford, C., Helle, G., ... Weigl, M. (2015).

- Water-use efficiency and transpiration across European forests during the Anthropocene. *Nature Climate Change*, 5(6), 579–583. <https://doi.org/10.1038/nclimate2614>
- Franks, P. J., Adams, M. A., Amthor, J. S., Barbour, M. M., Berry, J. A., Ellsworth, D. S., ... von Caemmerer, S. (2013). Sensitivity of plants to changing atmospheric CO₂ concentration: From the geological past to the next century. *New Phytologist*, 197(4), 1077–1094. <https://doi.org/10.1111/nph.12104>
- Franks, P. J., W. Doheny-Adams, T., Britton-Harper, Z. J., & Gray, J. E. (2015). Increasing water-use efficiency directly through genetic manipulation of stomatal density. *New Phytologist*, 207(1), 188–195. <https://doi.org/10.1111/nph.13347>
- Franks, S. J., Sim, S., & Weis, A. E. (2007). Rapid evolution of flowering time by an annual plant in response to a climate fluctuation. *Proceedings of the National Academy of Sciences*, 104(4), 1278–1282. <https://doi.org/10.1073/pnas.0608379104>
- Frei, C. (2014). Interpolation of temperature in a mountainous region using nonlinear profiles and non-Euclidean distances. *International Journal of Climatology*, 34(5), 1585–1605. <https://doi.org/10.1002/joc.3786>
- Friedlingstein, P., Joel, G., Field, C. B., & Fung, I. Y. (1999). Toward an allocation scheme for global terrestrial carbon models. *Global Change Biology*, 5, 755–770. <https://doi.org/10.1046/j.1365-2486.1999.00269.x>
- Friend, A. D., Stevens, A. K., Knox, R. G., & Cannell, M. G. R. (1997). A process-based, terrestrial biosphere model of ecosystem dynamics (Hybrid v3.0). *Ecological Modelling*, 95(2–3), 249–287. [https://doi.org/10.1016/S0304-3800\(96\)00034-8](https://doi.org/10.1016/S0304-3800(96)00034-8)
- Fyllas, N. M., Gloor, E., Mercado, L. M., Sitch, S., Quesada, C. A., Domingues, T. F., ... Lloyd, J. (2014). Analysing Amazonian forest productivity using a new individual and trait-based model (TFS v.1). *Geoscientific Model Development*, 7(4), 1251–1269. <https://doi.org/10.5194/gmd-7-1251-2014>
- Fyllas, N. M., Patiño, S., Baker, T. R., Nardoto, G. B., Martinelli, L. A., Quesada, C. A., ... Lloyd, J. (2009). Basin-wide variations in foliar properties of Amazonian forest: phylogeny, soils and climate. *Biogeosciences*, 6, 2677–2708. <https://doi.org/10.5194/bgd-6-3707-2009>
- Galmés, J., Andralojc, P. J., Kapralov, M. V., Flexas, J., Keys, A. J., Molins, A., ... Conesa, M. À. (2014). Environmentally driven evolution of Rubisco and improved photosynthesis and growth within the C₃ genus *Limonium* (Plumbaginaceae). *New Phytologist*, 203(3), 989–999. <https://doi.org/10.1111/nph.12858>
- Gedney, N., Cox, P. M., Betts, R. A., Boucher, O., Huntingford, C., & Stott, P. A. (2006). Detection of a direct carbon dioxide effect in continental river runoff records. *Nature*, 439(7078), 835–838. <https://doi.org/10.1038/nature04504>
- GEOSTAT. (2000). *Digitale Bodeneignungskarte der Schweiz*. Swiss Federal Statistical Office.

- Gobiet, A., Kotlarski, S., Beniston, M., Heinrich, G., Rajczak, J., & Stoffel, M. (2014). 21st century climate change in the European Alps-A review. *Science of the Total Environment*, *493*, 1138–1151. <https://doi.org/10.1016/j.scitotenv.2013.07.050>
- Goldstein, A., Hultman, N. E., Fracheboud, J. M., Bauer, M. R., Panek, J. A., Xu, M., ... Baugh, W. (2000). Effects of climate variability on the carbon dioxide, water, and sensible heat fluxes above a ponderosa pine plantation in the Sierra Nevada (CA). *Agricultural and Forest Meteorology*, *101*(2–3), 113–129. [https://doi.org/10.1016/S0168-1923\(99\)00168-9](https://doi.org/10.1016/S0168-1923(99)00168-9)
- Good, S. P., Noone, D., & Bowen, G. (2015). Hydrologic connectivity constrains partitioning of global terrestrial water fluxes. *Science*, *349*(6244), 175–177. <https://doi.org/10.1126/science.aaa5931>
- Gottfried, M., Pauli, H., Futschik, A., Akhalkatsi, M., Barančok, P., Benito Alonso, J. L., ... Grabherr, G. (2012). Continent-wide response of mountain vegetation to climate change. *Nature Climate Change*, *2*(2), 111–115. <https://doi.org/10.1038/nclimate1329>
- Gough, C. M., Flower, C. E., Vogel, C. S., & Curtis, P. S. (2010). Phenological and temperature controls on the temporal non-structural carbohydrate dynamics of *Populus grandidentata* and *Quercus rubra*. *Forests*, *1*(1), 65–81. <https://doi.org/10.3390/f1010065>
- Gough, C. M., Flower, C. E., Vogel, C. S., Dragoni, D., & Curtis, P. S. (2009). Whole-ecosystem labile carbon production in a north temperate deciduous forest. *Agricultural and Forest Meteorology*, *149*(9), 1531–1540. <https://doi.org/10.1016/j.agrformet.2009.04.006>
- Gough, C. M., Hardiman, B. S., Nave, L. E., Bohrer, G., Maurer, K. D., Vogel, C. S., ... Curtis, P. S. (2013). Sustained carbon uptake and storage following moderate disturbance in a Great Lakes forest. *Ecological Applications*, *23*(5), 1202–1215. <https://doi.org/10.1890/12-1554.1>
- Goulden, M. L., & Bales, R. C. (2014). Mountain runoff vulnerability to increased evapotranspiration with vegetation expansion. *Proceedings of the National Academy of Sciences*, *111*(39), 14071–14075. <https://doi.org/10.1073/pnas.1319316111>
- Goward, S. N., & Prince, S. D. (1995). Transient effects of climate on vegetation dynamics : satellite observations. *Journal of Biogeography*, *22*(2), 549–564.
- Graham, M. H. (2003). Confronting multicollinearity in ecological multiple regression. *Ecology*, *84*(11), 2809–2815. <https://doi.org/10.1890/02-3114>
- Granier, A., Bréda, N., Longdoz, B., Gross, P., & Ngao, J. (2008). Ten years of fluxes and stand growth in a young beech forest at Hesse, North-eastern France. *Annals of Forest Science*, *65*(7), 704–716. <https://doi.org/10.1051/forest:2008052>
- Granier, A., Ceschia, E., Damesin, C., Dufrêne, E., Epron, D., Gross, P., ... Saugier, B. (2000). The carbon balance of a young beech forest. *Functional Ecology*, *14*(3), 312–325. <https://doi.org/10.1046/j.1365-2435.2000.00434.x>
- Grünwald, T., & Bernhofer, C. (2007). A decade of carbon, water and energy flux measurements of

- an old spruce forest at the Anchor Station Tharandt. *Tellus B*, 59(3), 387–396. <https://doi.org/10.1111/j.1600-0889.2007.00259.x>
- Guerrieri, R., Mencuccini, M., Sheppard, L. J., Saurer, M., Perks, M. P., Levy, P., ... Grace, J. (2011). The legacy of enhanced N and S deposition as revealed by the combined analysis of $\delta^{13}\text{C}$, $\delta^{18}\text{O}$ and $\delta^{15}\text{N}$ in tree rings. *Global Change Biology*, 17(5), 1946–1962. <https://doi.org/10.1111/j.1365-2486.2010.02362.x>
- Gutiérrez-Jurado, H. A., & Vivoni, E. R. (2013). Ecogeomorphic expressions of an aspect-controlled semiarid basin: II. Topographic and vegetation controls on solar irradiance. *Ecohydrology*, 6(1), 24–37. <https://doi.org/10.1002/eco.1263>
- Hadley, J. L., & Schedlbauer, J. L. (2002). Carbon exchange of an old-growth eastern hemlock (*Tsuga canadensis*) forest in central New England. *Tree Physiology*, 22, 1079–1092.
- Hall, D. K., & Riggs, G. A. (2016). *MODIS/Terra Snow Cover 8-Day L3 Global 500m Grid, Version 6.MOD10A2*. Colorado USA. NASA National Snow and Ice Data Center Distributed Active Archive Center. <https://doi.org/https://doi.org/10.5067/MODIS/MOD10A2.006>
- Hanan, E. J., Tague, C., Choate, J., Liu, M., Kolden, C., & Adam, J. (2018). Accounting for disturbance history in models: using remote sensing to constrain carbon and nitrogen pool spin-up. *Ecological Applications*, 28(5), 1197–1214. <https://doi.org/10.1002/eap.1718>
- Hardiman, B. S., Gough, C. M., Halperin, A., Hofmeister, K. L., Nave, L. E., Bohrer, G., & Curtis, P. S. (2013). Maintaining high rates of carbon storage in old forests: A mechanism linking canopy structure to forest function. *Forest Ecology and Management*, 298, 111–119. <https://doi.org/10.1016/j.foreco.2013.02.031>
- Hartmann, H., & Trumbore, S. (2016). Understanding the roles of nonstructural carbohydrates in forest trees - from what we can measure to what we want to know. *New Phytologist*, 211(2), 386–403. <https://doi.org/10.1111/nph.13955>
- Hengl, T., de Jesus, J. M., MacMillan, R. a., Batjes, N. H., Heuvelink, G. B. M., Ribeiro, E., ... Gonzalez, M. R. (2014). SoilGrids1km — Global Soil Information Based on Automated Mapping. *PLoS ONE*, 9(8), e105992. <https://doi.org/10.1371/journal.pone.0105992>
- Hereş, A.-M., Voltas, J., López, B. C., & Martínez-Vilalta, J. (2014). Drought-induced mortality selectively affects Scots pine trees that show limited intrinsic water-use efficiency responsiveness to raising atmospheric CO₂. *Functional Plant Biology*, 41(3), 244. <https://doi.org/10.1071/FP13067>
- Hetherington, A. M., & Woodward, F. I. (2003). The role of stomata in sensing and driving environmental change. *Nature*, 424(6951), 901–908. <https://doi.org/10.1038/nature01843>
- Hinckley, E.-L. S., Ebel, B. A., Barnes, R. T., Anderson, R. S., Williams, M. W., & Anderson, S. P. (2014). Aspect control of water movement on hillslopes near the rain-snow transition of the Colorado Front Range. *Hydrological Processes*, 28(1), 74–85. <https://doi.org/10.1002/hyp.9549>

- Hingerl, L., Kunstmann, H., Wagner, S., Mauder, M., Bliefernicht, J., & Rigon, R. (2016). Spatio-temporal variability of water and energy fluxes – a case study for a mesoscale catchment in pre-alpine environment. *Hydrological Processes*, 30(21), 3804–3823. <https://doi.org/10.1002/hyp.10893>
- Hollinger, D. Y., Aber, J., Dail, B., Davidson, E. A., Goltz, S. M., Hughes, H., ... Walsh, J. (2004). Spatial and temporal variability in forest-atmosphere CO₂ exchange. *Global Change Biology*, 10(10), 1689–1706. <https://doi.org/10.1111/j.1365-2486.2004.00847.x>
- Hörsch, B. (2003). Modelling the spatial distribution of montane and subalpine forests in the central Alps using digital elevation models. *Ecological Modelling*, 168(3), 267–282. [https://doi.org/10.1016/S0304-3800\(03\)00141-8](https://doi.org/10.1016/S0304-3800(03)00141-8)
- Hsu, J. S., Powell, J., & Adler, P. B. (2012). Sensitivity of mean annual primary production to precipitation. *Global Change Biology*, 18(7), 2246–2255. <https://doi.org/10.1111/j.1365-2486.2012.02687.x>
- Huang, J.-G., Bergeron, Y., Denneler, B., Berninger, F., & Tardif, J. C. (2007). Response of Forest Trees to Increased Atmospheric CO₂. *Critical Reviews in Plant Sciences*, 26(5–6), 265–283. <https://doi.org/10.1080/07352680701626978>
- Huang, M., Piao, S. L., Sun, Y., Ciais, P., Cheng, L., Mao, J., ... Wang, Y. (2015). Change in terrestrial ecosystem water-use efficiency over the last three decades. *Global Change Biology*, 21(6), 2366–2378. <https://doi.org/10.1111/gcb.12873>
- Huang, M., Piao, S., Zeng, Z., Peng, S., Ciais, P., Cheng, L., ... Wang, Y. (2016). Seasonal responses of terrestrial ecosystem water-use efficiency to climate change. *Global Change Biology*, 22(6), 2165–2177. <https://doi.org/10.1111/gcb.13180>
- Hunter, N. M., Horritt, M. S., Bates, P. D., Wilson, M. D., & Werner, M. G. F. (2005). An adaptive time step solution for raster-based storage cell modelling of floodplain inundation. *Advances in Water Resources*, 28(9), 975–991. <https://doi.org/10.1016/j.advwatres.2005.03.007>
- Huxman, T. E., Smith, M. D., Fay, P. A., Knapp, A. K., Shaw, M. R., Loik, M. E., ... Williams, D. G. (2004). Convergence across biomes to a common rain-use efficiency. *Nature*, 429(6992), 651–654. <https://doi.org/10.1038/nature02561>
- Hwang, T., Band, L. E., & Hales, T. C. (2009). Ecosystem processes at the watershed scale: Extending optimality theory from plot to catchment. *Water Resources Research*, 45(11), 1–20. <https://doi.org/10.1029/2009WR007775>
- Immerzeel, W. W., van Beek, L. P. H., & Bierkens, M. F. P. (2010). Climate Change Will Affect the Asian Water Towers. *Science*, 328(5984), 1382–1385. <https://doi.org/10.1126/science.1183188>
- Ishizaki, S., Hikosaka, K., & Hirose, T. (2003). Increase in leaf mass per area benefits plant growth at elevated CO₂ concentration. *Annals of Botany*, 91(7), 905–914. <https://doi.org/10.1093/aob/mcg097>

- Isotta, F. A., Frei, C., Weigluni, V., Perčec Tadić, M., Lassègues, P., Rudolf, B., ... Vertačnik, G. (2014). The climate of daily precipitation in the Alps: Development and analysis of a high-resolution grid dataset from pan-Alpine rain-gauge data. *International Journal of Climatology*, 34(5), 1657–1675. <https://doi.org/10.1002/joc.3794>
- Ito, A., & Inatomi, M. (2012). Water-use efficiency of the terrestrial biosphere: a model analysis focusing on interactions between the global carbon and water cycles. *Journal of Hydrometeorology*, 13(2), 681–694. <https://doi.org/10.1175/JHM-D-10-05034.1>
- Ivanov, V. Y., Bras, R. L., & Vivoni, E. R. (2008a). Vegetation-hydrology dynamics in complex terrain of semiarid areas: 1. A mechanistic approach to modeling dynamic feedbacks. *Water Resources Research*, 44(3), W03429. <https://doi.org/10.1029/2006WR005588>
- Ivanov, V. Y., Bras, R. L., & Vivoni, E. R. (2008b). Vegetation-hydrology dynamics in complex terrain of semiarid areas: 2. Energy-water controls of vegetation spatiotemporal dynamics and topographic niches of favorability. *Water Resources Research*, 44(3), 1–20. <https://doi.org/10.1029/2006WR005595>
- Jaramillo, F., & Destouni, G. (2015). Local flow regulation and irrigation raise global human water consumption and footprint. *Science*, 350(6265), 1248–1251. <https://doi.org/10.1126/science.aad1010>
- Jarvis, P. G., & McNaughton, K. G. (1986). Stomatal Control of Transpiration: Scaling Up from Leaf to Region. *Advances in Ecological Research*, 15(C), 1–49. [https://doi.org/10.1016/S0065-2504\(08\)60119-1](https://doi.org/10.1016/S0065-2504(08)60119-1)
- Jenkins, J. P., Richardson, A. D., Braswell, B. H., Ollinger, S. V., Hollinger, D. Y., & Smith, M. L. (2007). Refining light-use efficiency calculations for a deciduous forest canopy using simultaneous tower-based carbon flux and radiometric measurements. *Agricultural and Forest Meteorology*, 143(1–2), 64–79. <https://doi.org/10.1016/j.agrformet.2006.11.008>
- Jennings, K. A., Guerrieri, R., Vadeboncoeur, M. A., & Asbjornsen, H. (2016). Response of *Quercus velutina* growth and water use efficiency to climate variability and nitrogen fertilization in a temperate deciduous forest in the northeastern USA. *Tree Physiology*, 36(4), 428–443. <https://doi.org/10.1093/treephys/tpw003>
- Ji, P., Yuan, X., & Liang, X.-Z. (2017). Do Lateral Flows Matter for the Hyperresolution Land Surface Modeling? *Journal of Geophysical Research: Atmospheres*, 122(22), 12,077–12,092. <https://doi.org/10.1002/2017JD027366>
- Jolly, W. M., Dobbertin, M., Zimmermann, N. E., & Reichstein, M. (2005). Divergent vegetation growth responses to the 2003 heat wave in the Swiss Alps. *Geophysical Research Letters*, 32(18), 1–4. <https://doi.org/10.1029/2005GL023252>
- Jung, M., Reichstein, M., Margolis, H. A., Cescatti, A., Richardson, A. D., Arain, M. A., ... Williams, C. A. (2011). Global patterns of land-atmosphere fluxes of carbon dioxide, latent heat, and sensible heat derived from eddy covariance, satellite, and meteorological observations. *Journal*

- of Geophysical Research: Biogeosciences*, 116(3), 1–16. <https://doi.org/10.1029/2010JG001566>
- Kattge, J., Diaz, S., Lavorel, S., Prentice, I. C., Leadley, P., Bönsch, G., ... Wirth, C. (2011). TRY - a global database of plant traits. *Global Change Biology*, 17(9), 2905–2935. <https://doi.org/10.1111/j.1365-2486.2011.02451.x>
- Kattge, Jens, & Knorr, W. (2007). Temperature acclimation in a biochemical model of photosynthesis: A reanalysis of data from 36 species. *Plant, Cell and Environment*, 30(9), 1176–1190. <https://doi.org/10.1111/j.1365-3040.2007.01690.x>
- Katul, G. G., Manzoni, S., Palmroth, S., & Oren, R. (2010). A stomatal optimization theory to describe the effects of atmospheric CO₂ on leaf photosynthesis and transpiration. *Annals of Botany*, 105(3), 431–442. <https://doi.org/10.1093/aob/mcp292>
- Keenan, T. F., Davidson, E. A., Moffat, A. M., Munger, J. W., & Richardson, A. D. (2012). Using model-data fusion to interpret past trends, and quantify uncertainties in future projections, of terrestrial ecosystem carbon cycling. *Global Change Biology*, 18(8), 2555–2569. <https://doi.org/10.1111/j.1365-2486.2012.02684.x>
- Keenan, T. F., Hollinger, D. Y., Bohrer, G., Dragoni, D., Munger, J. W., Schmid, H. P., & Richardson, A. D. (2013). Increase in forest water-use efficiency as atmospheric carbon dioxide concentrations rise. *Nature*, 499(7458), 324–327. <https://doi.org/10.1038/nature12291>
- Kenney, J. F., & Keeping, E. S. (1962). *Mathematics of Statistics. 3rd Ed. Princeton, NJ: Van Nostrand, Part I*. Retrieved from <http://books.google.fr/books?id=UdILAAAAMAAJ>
- Klemeš, V. (1987). The modelling of mountain hydrology: the ultimate challenge. *Hydrology of Mountainous Areas*, (190), 29–44. [https://doi.org/10.1641/0006-3568\(2001\)051\[0227:HIOEPA\]2.0.CO;2](https://doi.org/10.1641/0006-3568(2001)051[0227:HIOEPA]2.0.CO;2)
- Klos, P. Z., Goulden, M. L., Riebe, C. S., Tague, C., O'Geen, A. T., Flinchum, B. A., ... Bales, R. C. (2018). Subsurface plant-accessible water in mountain ecosystems with a Mediterranean climate. *Wiley Interdisciplinary Reviews: Water*, 5(3), e1277. <https://doi.org/10.1002/wat2.1277>
- Knapp, A. K., Briggs, J. M., & Smith, M. D. (2012). Community stability does not preclude ecosystem sensitivity to chronic resource alteration. *Functional Ecology*, 26(6), 1231–1233. <https://doi.org/10.1111/j.1365-2435.2012.02053.x>
- Knauer, J., Zaehle, S., Reichstein, M., Medlyn, B. E., Forkel, M., Hagemann, S., & Werner, C. (2017). The response of ecosystem water-use efficiency to rising atmospheric CO₂ concentrations: sensitivity and large-scale biogeochemical implications. *New Phytologist*, 213(4), 1654–1666. <https://doi.org/10.1111/nph.14288>
- Ko, A., Mascaro, G., & Vivoni, E. R. (2018). Strategies to Improve Physics-Based Hyperresolution Hydrologic Simulations at Regional Basin Scales. *Water Resources Research*, (88 m), 1–24. <https://doi.org/10.1029/2018WR023521>
- Köplin, N., Schädler, B., Viviroli, D., & Weingartner, R. (2013). The importance of glacier and forest

- change in hydrological climate-impact studies. *Hydrology and Earth System Sciences*, 17(2), 619–635. <https://doi.org/10.5194/hess-17-619-2013>
- Koutavas, A. (2013). CO₂ fertilization and enhanced drought resistance in Greek firs from Cephalonia Island, Greece. *Global Change Biology*, 19(2), 529–539. <https://doi.org/10.1111/gcb.12053>
- Kozłowski, T. T., & Pallardy, S. G. (1997). *Physiology of wood plants*. San Diego, California: Academic Press.
- Krinner, G., Viovy, N., de Noblet-Ducoudré, N., Ogée, J., Polcher, J., Friedlingstein, P., ... Prentice, I. C. (2005). A dynamic global vegetation model for studies of the coupled atmosphere-biosphere system. *Global Biogeochemical Cycles*, 19(1), GB1015. <https://doi.org/10.1029/2003GB002199>
- Laghari, A. N., Vanham, D., & Rauch, W. (2012). To what extent does climate change result in a shift in Alpine hydrology? A case study in the Austrian Alps. *Hydrological Sciences Journal*, 57(1), 103–117. <https://doi.org/10.1080/02626667.2011.637040>
- Lammertsma, E. I., Boer, H. J. d., Dekker, S. C., Dilcher, D. L., Lotter, A. F., & Wagner-Cremer, F. (2011). Global CO₂ rise leads to reduced maximum stomatal conductance in Florida vegetation. *Proceedings of the National Academy of Sciences*, 108(10), 4035–4040. <https://doi.org/10.1073/pnas.1100371108>
- Lawson, T., & McElwain, J. C. (2016). Evolutionary trade-offs in stomatal spacing. *New Phytologist*, 210(4), 1149–1151. <https://doi.org/10.1111/nph.13972>
- Le, P. V. V., & Kumar, P. (2017). Interaction Between Ecohydrologic Dynamics and Microtopographic Variability Under Climate Change. *Water Resources Research*, 53(10), 8383–8403. <https://doi.org/10.1002/2017WR020377>
- Leakey, A. D. B., Ainsworth, E. A., Bernacchi, C. J., Rogers, A., Long, S. P., & Ort, D. R. (2009). Elevated CO₂ effects on plant carbon, nitrogen, and water relations: Six important lessons from FACE. *Journal of Experimental Botany*, 60(10), 2859–2876. <https://doi.org/10.1093/jxb/erp096>
- Leitinger, G., Ruggenthaler, R., Hammerle, A., Lavorel, S., Schirpke, U., Clement, J. C., ... Tappeiner, U. (2015). Impact of droughts on water provision in managed alpine grasslands in two climatically different regions of the Alps. *Ecohydrology*, 8(8), 1600–1613. <https://doi.org/10.1002/eco.1607>
- Lemordant, L., Gentine, P., Stéfanon, M., Drobinski, P., & Fatichi, S. (2016). Modification of land-atmosphere interactions by CO₂ effects: Implications for summer dryness and heat wave amplitude. *Geophysical Research Letters*, 43(19), 10,240–10,248. <https://doi.org/10.1002/2016GL069896>
- Lemordant, L., Gentine, P., Swann, A. S., Cook, B. I., & Scheff, J. (2018). Critical impact of vegetation physiology on the continental hydrologic cycle in response to increasing CO₂. *Proceedings of the National Academy of Sciences*, 115(16), 4093–4098. <https://doi.org/10.1073/pnas.1720712115>

- Leonardi, S., Gentilesca, T., Guerrieri, R., Ripullone, F., Magnani, F., Mencuccini, M., ... Borghetti, M. (2012). Assessing the effects of nitrogen deposition and climate on carbon isotope discrimination and intrinsic water-use efficiency of angiosperm and conifer trees under rising CO₂ conditions. *Global Change Biology*, *18*(9), 2925–2944. <https://doi.org/10.1111/j.1365-2486.2012.02757.x>
- Leonelli, G., Pelfini, M., Battipaglia, G., & Cherubini, P. (2009). Site-aspect influence on climate sensitivity over time of a high-altitude *Pinus cembra* tree-ring network. *Climatic Change*, *96*(1), 185–201. <https://doi.org/10.1007/s10584-009-9574-6>
- Leuning, R. (1990). Modelling Stomatal Behaviour and Photosynthesis of *Eucalyptus grandis*. *Australian Journal of Plant Physiology*, *17*(2), 159–175. <https://doi.org/10.1071/PP9900159>
- Leuning, R. (1995). A critical appraisal of a combined stomatal-photosynthesis model for C₃ plants. *Plant, Cell & Environment*, *18*(4), 339–355. <https://doi.org/10.1111/j.1365-3040.1995.tb00370.x>
- Leuning, R., Kelliher, F. M., de Pury, D. G. G., & Schulze, E. D. (1995). Leaf nitrogen, photosynthesis, conductance and transpiration: Scaling from leaves to canopies. *Plant, Cell and Environment*, *18*(10), 1183–1200. <https://doi.org/10.1111/j.1365-3040.1995.tb00628.x>
- Leuning, R., van Gorsel, E., Massman, W. J., & Isaac, P. R. (2012). Reflections on the surface energy imbalance problem. *Agricultural and Forest Meteorology*, *156*, 65–74. <https://doi.org/10.1016/j.agrformet.2011.12.002>
- Leuzinger, S., Luo, Y., Beier, C., Dieleman, W., Vicca, S., & Körner, C. (2011). Do global change experiments overestimate impacts on terrestrial ecosystems? *Trends in Ecology and Evolution*, *26*(5), 236–241. <https://doi.org/10.1016/j.tree.2011.02.011>
- Leuzinger, S., Manusch, C., Bugmann, H., & Wolf, A. (2013). A sink-limited growth model improves biomass estimation along boreal and alpine tree lines. *Global Ecology and Biogeography*, *22*(8), 924–932. <https://doi.org/10.1111/geb.12047>
- Leuzinger, S., Zotz, G., Asshoff, R., & Korner, C. (2005). Responses of deciduous forest trees to severe drought in Central Europe. *Tree Physiology*, *25*(6), 641–650. <https://doi.org/10.1093/treephys/25.6.641>
- Lexer, M. J., Hönninger, K., Scheifinger, H., Matulla, C., Groll, N., Kromp-Kolb, H., ... Englisch, M. (2001). The sensitivity of the austrian forests to scenarios of climatic change. A large-scale risk assessment. *Monographien (Umweltbundesamt)*, *132*. <https://doi.org/10.1016/j.jcep.2010.06.003>
- Lin, Y.-S., Medlyn, B. E., Duursma, R. A., Prentice, I. C., Wang, H., Baig, S., ... Wingate, L. (2015). Optimal stomatal behaviour around the world. *Nature Climate Change*, *5*(5), 459–464. <https://doi.org/10.1038/nclimate2550>
- Lindner, M., Maroschek, M., Netherer, S., Kremer, A., Barbati, A., Garcia-Gonzalo, J., ... Marchetti, M. (2010). Climate change impacts, adaptive capacity, and vulnerability of European forest

- ecosystems. *Forest Ecology and Management*, 259(4), 698–709. <https://doi.org/10.1016/j.foreco.2009.09.023>
- Liu, X., Wang, W., Xu, G., Zeng, X., Wu, G., Zhang, X., & Qin, D. (2014). Tree growth and intrinsic water-use efficiency of inland riparian forests in northwestern China: Evaluation via $\delta^{13}\text{C}$ and $\delta^{18}\text{O}$ analysis of tree rings. *Tree Physiology*, 34(9), 966–980. <https://doi.org/10.1093/treephys/tpu067>
- Liu, Y., Xiao, J., Ju, W., Zhou, Y., Wang, S., & Wu, X. (2015). Water use efficiency of China's terrestrial ecosystems and responses to drought. *Scientific Reports*, 5(1), 13799. <https://doi.org/10.1038/srep13799>
- Loague, K., Heppner, C. S., Ebel, B. A., & VanderKwaak, J. E. (2010). The quixotic search for a comprehensive understanding of hydrologic response at the surface: Horton, Dunne, Dunton, and the role of concept-development simulation. *Hydrological Processes*, 24(17), 2499–2505. <https://doi.org/10.1002/hyp.7834>
- Lombardozzi, D. L., Bonan, G. B., Smith, N. G., Dukes, J. S., & Fisher, R. A. (2015). Temperature acclimation of photosynthesis and respiration: A key uncertainty in the carbon cycle-climate feedback. *Geophysical Research Letters*, 42(20), 8624–8631. <https://doi.org/10.1002/2015GL065934>
- Long, S. P., Ainsworth, E. A., Rogers, A., & Ort, D. R. (2004). Rising atmospheric carbon dioxide: plants FACE the future. *Annual Review of Plant Biology*, 55, 591–628. <https://doi.org/10.1146/annurev.arplant.55.031903.141610>
- Lundquist, J. D., Dickerson-Lange, S. E., Lutz, J. A., & Cristea, N. C. (2013). Lower forest density enhances snow retention in regions with warmer winters: A global framework developed from plot-scale observations and modeling. *Water Resources Research*, 49(10), 6356–6370. <https://doi.org/10.1002/wrcr.20504>
- Lundquist, J. D., & Loheide, S. P. (2011). How evaporative water losses vary between wet and dry water years as a function of elevation in the Sierra Nevada, California, and critical factors for modeling. *Water Resources Research*, 47(5), 1–13. <https://doi.org/10.1029/2010WR010050>
- Ma, S., Baldocchi, D. D., Mambelli, S., & Dawson, T. E. (2011). Are temporal variations of leaf traits responsible for seasonal and inter-annual variability in ecosystem CO_2 exchange? *Functional Ecology*, 25(1), 258–270. <https://doi.org/10.1111/j.1365-2435.2010.01779.x>
- Maillard, P., Guehl, J.-M., Muller, J. F., & Gross, P. (2001). Interactive effects of elevated CO_2 concentration and nitrogen supply on partitioning of newly fixed ^{13}C and ^{15}N between shoot and roots of pedunculate oak seedlings (*Quercus robur*). *Tree Physiology*, 21(2–3), 163–172. Retrieved from isi:000166829300012
- Manoli, G., Ivanov, V. Y., & Fatichi, S. (2018). Dry-Season Greening and Water Stress in Amazonia: The Role of Modeling Leaf Phenology. *Journal of Geophysical Research: Biogeosciences*, 123(6), 1909–1926. <https://doi.org/10.1029/2017JG004282>

- Manzoni, S., Vico, G., Katul, G. G., Fay, P. A., Polley, W., Palmroth, S., & Porporato, A. (2011). Optimizing stomatal conductance for maximum carbon gain under water stress: A meta-analysis across plant functional types and climates. *Functional Ecology*, *25*(3), 456–467. <https://doi.org/10.1111/j.1365-2435.2010.01822.x>
- Manzoni, S., Vico, G., Palmroth, S., Porporato, A., & Katul, G. G. (2013). Optimization of stomatal conductance for maximum carbon gain under dynamic soil moisture. *Advances in Water Resources*, *62*(PA), 90–105. <https://doi.org/10.1016/j.advwatres.2013.09.020>
- Maseyk, K., Hemming, D. L., Angert, A., Leavitt, S. W., & Yakir, D. (2011). Increase in water-use efficiency and underlying processes in pine forests across a precipitation gradient in the dry Mediterranean region over the past 30 years. *Oecologia*, *167*(2), 573–585. <https://doi.org/10.1007/s00442-011-2010-4>
- Mastrotheodoros, T., Pappas, C., Molnar, P., Burlando, P., Hadjidoukas, P., & Fatichi, S. (2019). Ecohydrological dynamics in the Alps: Insights from a modelling analysis of the spatial variability. *Ecohydrology*, *12*(1), e2054. <https://doi.org/10.1002/eco.2054>
- Mastrotheodoros, T., Pappas, C., Molnar, P., Burlando, P., Keenan, T. F., Gentine, P., ... Fatichi, S. (2017). Linking plant functional trait plasticity and the large increase in forest water use efficiency. *Journal of Geophysical Research: Biogeosciences*, *122*(9), 2393–2408. <https://doi.org/10.1002/2017JG003890>
- Matamala, R., & Schlesinger, W. H. (2000). Effects of elevated atmospheric CO₂ on fine root production and activity in an intact temperate forest ecosystem. *Global Change Biology*, *6*(8), 967–979. <https://doi.org/10.1046/j.1365-2486.2000.00374.x>
- Maxwell, R. M., & Condon, L. E. (2016). Connections between groundwater flow and transpiration partitioning. *Science*, *353*(6297), 377–380. <https://doi.org/10.1126/science.aaf7891>
- Mayor, J. R., Sanders, N. J., Classen, A. T., Bardgett, R. D., Clément, J. C., Fajardo, A., ... Wardle, D. A. (2017). Elevation alters ecosystem properties across temperate treelines globally. *Nature*, *542*(7639), 91–95. <https://doi.org/10.1038/nature21027>
- McAusland, L., Vialet-Chabrand, S., Davey, P., Baker, N. R., Brendel, O., & Lawson, T. (2016). Effects of kinetics of light-induced stomatal responses on photosynthesis and water-use efficiency. *New Phytologist*, *211*(4), 1209–1220. <https://doi.org/10.1111/nph.14000>
- Medlyn, B. E., Barton, C. V. M., Broadmeadow, M. S. J., Ceulemans, R., De Angelis, P., Forstreuter, M., ... Jarvis, P. G. (2001). Stomatal conductance of forest species after long-term exposure to elevated CO₂ concentration: A synthesis. *New Phytologist*, *149*(2), 247–264. <https://doi.org/10.1046/j.1469-8137.2001.00028.x>
- Medlyn, B. E., & De Kauwe, M. G. (2013). Biogeochemistry: Carbon dioxide and water use in forests. *Nature*, *499*(7458), 287–289. <https://doi.org/10.1038/nature12411>
- Medlyn, B. E., De Kauwe, M. G., Lin, Y.-S., Knauer, J., Duursma, R. A., Williams, C. A., ... Wingate, L. (2017). How do leaf and ecosystem measures of water-use efficiency compare? *New*

Phytologist, 216(3), 758–770. <https://doi.org/10.1111/nph.14626>

- Medlyn, B. E., Duursma, R. a., Eamus, D., Ellsworth, D. S., Prentice, I. C., Barton, C. V. M., ... Wingate, L. (2011). Reconciling the optimal and empirical approaches to modelling stomatal conductance. *Global Change Biology*, 17(6), 2134–2144. <https://doi.org/10.1111/j.1365-2486.2010.02375.x>
- Medlyn, B. E., Zaehle, S., De Kauwe, M. G., Walker, A. P., Dietze, M. C., Hanson, P. J., ... Norby, R. J. (2015). Using ecosystem experiments to improve vegetation models. *Nature Climate Change*, 5(6), 528–534. <https://doi.org/10.1038/nclimate2621>
- Middelkoop, H., Daamen, K., Gellens, D., Grabs, W., Kwadijk, J. C. J., Lang, H., ... Wilke, K. (2001). Impact of climate change on hydrological regimes and water resources management in the Rhine basin. *Climatic Change*, 49(1–2), 105–128. <https://doi.org/10.1023/A:1010784727448>
- Miglietta, F., Peressotti, A., Viola, R., Korner, C., & Amthor, J. S. (2011). Stomatal numbers, leaf and canopy conductance, and the control of transpiration. *Proceedings of the National Academy of Sciences*, 108(28), E275–E275. <https://doi.org/10.1073/pnas.1105831108>
- Miralles, D. G., Jiménez, C., Jung, M., Michel, D., Ershadi, A., McCabe, M. F., ... Fernández-Prieto, D. (2015). The WACMOS-ET project – Part 2: Evaluation of global terrestrial evaporation data sets. *Hydrology and Earth System Sciences*, 20, 823–842. <https://doi.org/doi:10.5194/hess-20-823-2016>.
- Montanari, A., Young, G., Savenije, H., Hughes, D., Wagener, T., Ren, L. L., ... Belyaev, V. (2013). “Panta Rhei-Everything Flows”: Change in hydrology and society-The IAHS Scientific Decade 2013-2022. *Hydrological Sciences Journal*, 58(6), 1256–1275. <https://doi.org/10.1080/02626667.2013.809088>
- Moore, B. D., Cheng, S. H., Sims, D., & Seemann, J. R. (1999). The biochemical and molecular basis for photosynthetic acclimation to elevated atmospheric CO₂. *Plant Cell and Environment*, 22(6), 567–582. <https://doi.org/10.1046/j.1365-3040.1999.00432.x>
- Morison, J. I. L. (1985). Sensitivity of stomata and water use efficiency to high CO₂. *Plant, Cell and Environment*, 8(6), 497–474. <https://doi.org/10.1111/j.1365-3040.1985.tb01682.x>
- Morison, J. I. L., & Gifford, R. M. (1984). Plant Growth and Water Use with Limited Water Supply in High CO₂ Concentrations. II*. Plant Dry Weight, Partitioning and Water Use Efficiency. *Australian Journal of Plant Physiology*, 11, 375–384. <https://doi.org/10.1071/PP9840375>
- Nelson, J. A., Morgan, J. A., LeCain, D. R., Mosier, A. R., Milchunas, D. G., & Parton, B. A. (2004). Elevated CO₂ increases soil moisture and enhances plant water relations in a long-term field study in semi-arid shortgrass steppe of Colorado. *Plant and Soil*, 259(1–2), 169–179. <https://doi.org/10.1023/B:PLSO.0000020957.83641.62>
- Nemani, R., Keeling, C. D., Hashimoto, H., Jolly, W. M., Piper, S. C., Tucker, C. J., ... Running, S. W. (2003). Climate-Driven Increases in Global Terrestrial Net Primary Production from 1982 to 1999. *Science*, 300(5625), 1560–1563. <https://doi.org/10.1126/science.1082750>

- Nicotra, A. B., Atkin, O. K., Bonser, S. P., Davidson, A. M., Finnegan, E. J., Mathesius, U., ... van Kleunen, M. (2010). Plant phenotypic plasticity in a changing climate. *Trends in Plant Science*, *15*(12), 684–692. <https://doi.org/10.1016/j.tplants.2010.09.008>
- Niinemets, Ü. (2007). Photosynthesis and resource distribution through plant canopies. *Plant, Cell and Environment*, *30*(9), 1052–1071. <https://doi.org/10.1111/j.1365-3040.2007.01683.x>
- Niinemets, Ü., Keenan, T. F., & Hallik, L. (2015). A worldwide analysis of within-canopy variations in leaf structural, chemical and physiological traits across plant functional types. *New Phytologist*, *205*(3), 973–993. <https://doi.org/10.1111/nph.13096>
- Novick, K. A., Ficklin, D. L., Stoy, P. C., Williams, C. A., Bohrer, G., Oishi, A. C., ... Phillips, R. P. (2016). The increasing importance of atmospheric demand for ecosystem water and carbon fluxes. *Nature Climate Change*, *6*(11), 1023–1027. <https://doi.org/10.1038/nclimate3114>
- Novick, K. A., Oishi, A. C., Ward, E. J., Siqueira, M. B. S., Juang, J. Y., & Stoy, P. C. (2015). On the difference in the net ecosystem exchange of CO₂ between deciduous and evergreen forests in the southeastern United States. *Global Change Biology*, *21*(2), 827–842. <https://doi.org/10.1111/gcb.12723>
- Orth, R., & Destouni, G. (2018). Drought reduces blue-water fluxes more strongly than green-water fluxes in Europe. *Nature Communications*, *9*(1), 3602. <https://doi.org/10.1038/s41467-018-06013-7>
- Pal, J. S., Giorgi, F., & Bi, X. (2004). Consistency of recent European summer precipitation trends and extremes with future regional climate projections. *Geophysical Research Letters*, *31*(13), 20–23. <https://doi.org/10.1029/2004GL019836>
- Palmroth, S., Oren, R., McCarthy, H. R., Johnsen, K. H., Finzi, A. C., Butnor, J. R., ... Schlesinger, W. H. (2006). Aboveground sink strength in forests controls the allocation of carbon below ground and its [CO₂]-induced enhancement. *Proceedings of the National Academy of Sciences*, *103*(51), 19362–19367. <https://doi.org/10.1073/pnas.0609492103>
- Panagos, P., Van Liedekerke, M., Jones, A., & Montanarella, L. (2012). European Soil Data Centre: Response to European policy support and public data requirements. *Land Use Policy*, *29*(2), 329–338. <https://doi.org/10.1016/j.landusepol.2011.07.003>
- Pappas, C., Fatichi, S., & Burlando, P. (2016). Modeling terrestrial carbon and water dynamics across climatic gradients: Does plant trait diversity matter? *New Phytologist*, *209*(1), 137–151. <https://doi.org/10.1111/nph.13590>
- Pappas, C., Fatichi, S., Leuzinger, S., Wolf, A., & Burlando, P. (2013). Sensitivity analysis of a process-based ecosystem model: Pinpointing parameterization and structural issues. *Journal of Geophysical Research: Biogeosciences*, *118*(2), 505–528. <https://doi.org/10.1002/jgrg.20035>
- Pappas, C., Fatichi, S., Rimkus, S., Burlando, P., & Huber, M. O. (2015). The role of local-scale heterogeneities in terrestrial ecosystem modeling. *Journal of Geophysical Research: Biogeosciences*, *120*(2), 341–360. <https://doi.org/10.1002/2014JG002735>

- Pappas, C., Mahecha, M. D., Frank, D. C., Babst, F., & Koutsoyiannis, D. (2017). Ecosystem functioning is enveloped by hydrometeorological variability. *Nature Ecology & Evolution*, *1*(9), 1263–1270. <https://doi.org/10.1038/s41559-017-0277-5>
- Paschalis, A., Fatichi, S., Katul, G. G., & Ivanov, V. Y. (2015). Cross-scale impact of climate temporal variability on ecosystem water and carbon fluxes. *Journal of Geophysical Research: Biogeosciences*, *120*(9), 1716–1740. <https://doi.org/10.1002/2015JG003002>
- Paschalis, A., Katul, G. G., Fatichi, S., Palmroth, S., & Way, D. A. (2016). On the variability of the ecosystem response to elevated atmospheric CO₂ across spatial and temporal scales at the Duke Forest FACE experiment Agricultural and Forest Meteorology. *Agricultural and Forest Meteorology*, *232*, 367–383. <https://doi.org/10.1016/j.agrformet.2016.09.003>
- Passalacqua, P., Belmont, P., Staley, D. M., Simley, J. D., Arrowsmith, J. R., Bode, C. A., ... Wheaton, J. M. (2015). Analyzing high resolution topography for advancing the understanding of mass and energy transfer through landscapes: A review. *Earth-Science Reviews*, *148*, 174–193. <https://doi.org/10.1016/j.earscirev.2015.05.012>
- Pauli, H., Gottfried, M., Reiter, K., Klettner, C., & Grabherr, G. (2007). Signals of range expansions and contractions of vascular plants in the high Alps: Observations (1994–2004) at the GLORIA *master site Schrankogel, Tyrol, Austria. *Global Change Biology*, *13*(1), 147–156. <https://doi.org/10.1111/j.1365-2486.2006.01282.x>
- Pavlick, R., Drewry, D. T., Bohn, K., Reu, B., & Kleidon, A. (2013). The Jena Diversity-Dynamic Global Vegetation Model (JeDi-DGVM): a diverse approach to representing terrestrial biogeography and biogeochemistry based on plant functional trade-offs. *Biogeosciences*, *10*(6), 4137–4177. <https://doi.org/10.5194/bgd-9-4627-2012>
- Penman, H. L. (1948). Natural evaporation from open water, bare soil and grass. *Proceedings of the Royal Society of London. Series A, Mathematical and Physical Sciences*, *193*(1032), 120–145. <https://doi.org/10.1098/rspa.1948.0037>
- Peñuelas, J., Canadell, J. G., & Ogaya, R. (2011). Increased water-use efficiency during the 20th century did not translate into enhanced tree growth. *Global Ecology and Biogeography*, *20*(4), 597–608. <https://doi.org/10.1111/j.1466-8238.2010.00608.x>
- Peñuelas, J., & Matamala, R. (1990). Changes in N and S leaf content, stomatal density and specific leaf-area of 14 plant-species during the last 3 centuries of CO₂ increase. *Journal of Experimental Botany*, *41*(9), 1119–1124. <https://doi.org/10.1093/jxb/41.9.1119>
- Perroud, M., & Bader, S. (2013). Klimaänderung in der Schweiz. *Bundesamt Für Umwelt (BAFU)*, 86. <https://doi.org/Umwelt-Zustand Nr. 1308>
- Pilegaard, K., Ibrom, A., Courtney, M. S., Hummelshøj, P., & Jensen, N. O. (2011). Increasing net CO₂ uptake by a Danish beech forest during the period from 1996 to 2009. *Agricultural and Forest Meteorology*, *151*(7), 934–946. <https://doi.org/10.1016/j.agrformet.2011.02.013>
- Poorter, H., & Nagel, O. (2000). The role of biomass allocation in the growth response of plants to

- different levels of light, CO₂, nutrients and water: a quantitative review. *Australian Journal of Plant Physiology*, 27(12), 595–607. <https://doi.org/10.1071/PP99173>
- Potter, K. a., Arthur Woods, H., & Pincebourde, S. (2013). Microclimatic challenges in global change biology. *Global Change Biology*, 19(10), 2932–2939. <https://doi.org/10.1111/gcb.12257>
- Prentice, I. C., Liang, X.-Z., Medlyn, B. E., & Wang, Y.-P. (2015). Reliable, robust and realistic: The three R's of next-generation land-surface modelling. *Atmospheric Chemistry and Physics*, 15(10), 5987–6005. <https://doi.org/10.5194/acp-15-5987-2015>
- Priestley, C. H. B., & Taylor, R. J. (1972). On the Assessment of Surface Heat Flux and Evaporation Using Large-Scale Parameters. *Monthly Weather Review*, 100(2), 81–92. [https://doi.org/10.1175/1520-0493\(1972\)100<0081:OTAOSH>2.3.CO;2](https://doi.org/10.1175/1520-0493(1972)100<0081:OTAOSH>2.3.CO;2)
- Radoglou, K. M., Aphalo, P., & Jarvis, P. G. (1992). Response of Photosynthesis, Stomatal Conductance and Water-Use Efficiency to Elevated CO₂ and Nutrient Supply in Acclimated Seedlings of Phaseolus-Vulgaris L. *Annals of Botany*, 70(3), 257–264. <https://doi.org/10.1093/oxfordjournals.aob.a088467>
- Rebetez, M., & Dobbertin, M. (2004). Climate change may already threaten Scots pine stands in the Swiss Alps. *Theoretical and Applied Climatology*, 79(1–2), 1–9. <https://doi.org/10.1007/s00704-004-0058-3>
- Reich, P. B., Sendall, K. M., Stefanski, A., Wei, X., Rich, R. L., & Montgomery, R. A. (2016). Boreal and temperate trees show strong acclimation of respiration to warming. *Nature*, 531(7596), 633–636. <https://doi.org/10.1038/nature17142>
- Reichstein, M., Falge, E., Baldocchi, D. D., Papale, D., Aubinet, M., Berbigier, P., ... Valentini, R. (2005). On the separation of net ecosystem exchange into assimilation and ecosystem respiration: Review and improved algorithm. *Global Change Biology*, 11(9), 1424–1439. <https://doi.org/10.1111/j.1365-2486.2005.001002.x>
- Reichstein, M., Papale, D., Valentini, R., Aubinet, M., Bernhofer, C., Knohl, A., ... Seufert, G. (2007). Determinants of terrestrial ecosystem carbon balance inferred from European eddy covariance flux sites. *Geophysical Research Letters*, 34(1), L01402. <https://doi.org/10.1029/2006GL027880>
- Reid, C. D., Maherali, H., Johnson, H. B., Smith, S. D., Wullschleger, S. D., & Jackson, R. B. (2003). On the relationship between stomatal characters and atmospheric CO₂. *Geophysical Research Letters*, 30(19), 1983. <https://doi.org/10.1029/2003GL017775>
- Rigden, A. J., & Salvucci, G. D. (2017). Stomatal response to humidity and CO₂ implicated in recent decline in US evaporation. *Global Change Biology*, 23(3), 1140–1151. <https://doi.org/10.1111/gcb.13439>
- Rigling, A., Bigler, C., Eilmann, B., Feldmeyer-Christe, E., Gimmi, U., Ginzler, C., ... Dobbertin, M. (2013). Driving factors of a vegetation shift from Scots pine to pubescent oak in dry Alpine forests. *Global Change Biology*, 19(1), 229–240. <https://doi.org/10.1111/gcb.12038>

- Rixen, C., Teich, M., Lardelli, C., Gallati, D., Pohl, M., Pütz, M., & Bebi, P. (2011). Winter Tourism and Climate Change in the Alps: An Assessment of Resource Consumption, Snow Reliability, and Future Snowmaking Potential. *Mountain Research and Development*, 31(3), 229–236. <https://doi.org/10.1659/MRD-JOURNAL-D-10-00112.1>
- Rodriguez-Iturbe, I., D’Odorico, P., Porporato, A., & Ridolfi, L. (1999). On the spatial and temporal links between vegetation, climate, and soil moisture. *Water Resources Research*, 35(12), 3709–3722. <https://doi.org/10.1029/1999WR900255>
- Rogers, A., Medlyn, B. E., Dukes, J. S., Bonan, G. B., von Caemmerer, S., Dietze, M. C., ... Zaehle, S. (2017). A roadmap for improving the representation of photosynthesis in Earth system models. *New Phytologist*, 213(1), 22–42. <https://doi.org/10.1111/nph.14283>
- Rogers, H. H., Stephen, A. P., Runion, G. B., & Mitchell, R. J. (1996). Root to shoot ratio of crops as influenced by CO₂. *Plant and Soil*, 187(2), 229–248. <https://doi.org/10.1007/BF00017090>
- Rössler, O., Diekkrüger, B., & Löffler, J. (2012). Potential drought stress in a Swiss mountain catchment-Ensemble forecasting of high mountain soil moisture reveals a drastic decrease, despite major uncertainties. *Water Resources Research*, 48(4), 1–19. <https://doi.org/10.1029/2011WR011188>
- Rouholahnejad Freund, E., & Kirchner, J. W. (2017). A Budyko framework for estimating how spatial heterogeneity and lateral moisture redistribution affect average evapotranspiration rates as seen from the atmosphere. *Hydrology and Earth System Sciences*, 21(1), 217–233. <https://doi.org/10.5194/hess-21-217-2017>
- Rutter, A. J., Kershaw, K. A., Robins, P. C., & Morton, A. J. (1971). A predictive model of rainfall interception in forests. 1. Derivation of the model from observation in a plantation of Corsican pine. *Agricultural Meteorology*, 9, 367–384. [https://doi.org/10.1016/0002-1571\(71\)90034-3](https://doi.org/10.1016/0002-1571(71)90034-3)
- Rutter, A. J., Morton, A. J., & Robins, P. C. (1975). A Predictive Model of Rainfall Interception in Forests 2. Generalization of the Model and Comparison With Observations in Some Coniferous and Hardwood Stands. *The Journal of Applied Ecology*, 12(1), 367–380.
- Ryan, M. G. (1991). Effects of Climate Change on Plant Respiration. *Ecological Applications*, 1(2), 157–167. <https://doi.org/10.2307/1941808>
- Sage, R. F. (1994). Acclimation of photosynthesis to increasing atmospheric CO₂: The gas exchange perspective. *Photosynthesis Research*, 39(3), 351–368. <https://doi.org/10.1007/BF00014591>
- Saito, M., Kato, T., & Tang, Y. (2009). Temperature controls ecosystem CO₂ exchange of an alpine meadow on the northeastern Tibetan Plateau. *Global Change Biology*, 15(1), 221–228. <https://doi.org/10.1111/j.1365-2486.2008.01713.x>
- Sakschewski, B., von Bloh, W., Boit, A., Rammig, A., Kattge, J., Poorter, L., ... Thonicke, K. (2015). Leaf and stem economics spectra drive diversity of functional plant traits in a dynamic global vegetation model. *Global Change Biology*, 21(7), 2711–2725. <https://doi.org/10.1111/gcb.12870>

- Saltelli, A., & Annoni, P. (2010). How to avoid a perfunctory sensitivity analysis. *Environmental Modelling and Software*, 25(12), 1508–1517. <https://doi.org/10.1016/j.envsoft.2010.04.012>
- Saltelli, A., Ratto, M., Andres, T., Campolongo, F., Cariboni, J., Gatelli, D., ... Stefano, T. (2008). Global Sensitivity Analysis. The Primer. *John Wiley & Sons, Ltd.* <https://doi.org/10.1002/9780470725184>
- Salzer, M. W., Larson, E. R., Bunn, A. G., & Hughes, M. K. (2014). Changing climate response in near-treeline bristlecone pine with elevation and aspect. *Environmental Research Letters*, 9(11), 114007. <https://doi.org/10.1088/1748-9326/9/11/114007>
- Samaniego, L., Thober, S., Kumar, R., Wanders, N., Rakovec, O., Pan, M., ... Marx, A. (2018). Anthropogenic warming exacerbates European soil moisture droughts. *Nature Climate Change*, 8(5), 421–426. <https://doi.org/10.1038/s41558-018-0138-5>
- Saurer, M., Siegwolf, R. T. W., & Schweingruber, F. H. (2004). Carbon isotope discrimination indicates improving water-use efficiency of trees in northern Eurasia over the last 100 years. *Global Change Biology*, 10(12), 2109–2120. <https://doi.org/10.1111/j.1365-2486.2004.00869.x>
- Saurer, M., Spahni, R., Frank, D. C., Joos, F., Leuenberger, M., Loader, N. J., ... Young, G. H. F. (2014). Spatial variability and temporal trends in water-use efficiency of European forests. *Global Change Biology*, 20(12), 3700–3712. <https://doi.org/10.1111/gcb.12717>
- Scheiter, S., Langan, L., & Higgins, S. I. (2013). Next-generation dynamic global vegetation models: learning from community ecology. *The New Phytologist*, 198(3), 957–969. <https://doi.org/10.1111/nph.12210>
- Schmid, H. P., Grimmond, C. S. B., Cropley, F., Offerle, B., & Su, H. B. (2000). Measurements of CO₂ and energy fluxes over a mixed hardwood forest in the mid-western United States. *Agricultural and Forest Meteorology*, 103(4), 357–374. [https://doi.org/10.1016/S0168-1923\(00\)00140-4](https://doi.org/10.1016/S0168-1923(00)00140-4)
- Schumacher, S., & Bugmann, H. (2006). The relative importance of climatic effects, wildfires and management for future forest landscape dynamics in the Swiss Alps. *Global Change Biology*, 12(8), 1435–1450. <https://doi.org/10.1111/j.1365-2486.2006.01188.x>
- Schymanski, S. J., & Or, D. (2015). Wind increases leaf water use efficiency. *Plant, Cell & Environment*, 39(7), 1448–1459. <https://doi.org/10.1111/pce.12700>
- Seddon, A. W. R., Macias-Fauria, M., Long, P. R., Benz, D., & Willis, K. J. (2016). Sensitivity of global terrestrial ecosystems to climate variability. *Nature*, 531(7593), 229–232. <https://doi.org/10.1038/nature16986>
- Sellers, P. J., Dickinson, R. E., Randall, D. A., Betts, A. K., Hall, F. G., Berry, J. A., ... Henderson-Sellers, A. (1997). Modeling the exchanges of energy, water, and carbon between continents and the atmosphere. *Science*, 275(5299), 502–509. <https://doi.org/10.1126/science.275.5299.502>
- Sen, P. K. (1968). Estimates of the regression coefficient based on Kendall's tau. *Journal of American*

- Statistical Association*, 63(324), 1379–1389. <https://doi.org/10.1017/CBO9781107415324.004>
- Seneviratne, S. I., Lehner, I., Gurtz, J., Teuling, A. J., Lang, H., Moser, U., ... Zappa, M. (2012). Swiss prealpine Rietholzbach research catchment and lysimeter: 32 year time series and 2003 drought event. *Water Resources Research*, 48(6), 1–20. <https://doi.org/10.1016/j.ajhg.2014.01.010>
- Seneviratne, S. I., Lüthi, D., Litschi, M., & Schär, C. (2006). Land-atmosphere coupling and climate change in Europe. *Nature*, 443(7108), 205–209. <https://doi.org/10.1038/nature05095>
- Sheffield, J., Wood, E. F., & Roderick, M. L. (2012). Little change in global drought over the past 60 years. *Nature*, 491(7424), 435–438. <https://doi.org/10.1038/nature11575>
- Siefert, A., Violle, C., Chalmandrier, L., Albert, C. H., Taudiere, A., Fajardo, A., ... Wardle, D. A. (2015). A global meta-analysis of the relative extent of intraspecific trait variation in plant communities. *Ecology Letters*, 18(12), 1406–1419. <https://doi.org/10.1111/ele.12508>
- Silva, L. C. R., & Anand, M. (2013). Probing for the influence of atmospheric CO₂ and climate change on forest ecosystems across biomes. *Global Ecology and Biogeography*, 22(1), 83–92. <https://doi.org/10.1111/j.1466-8238.2012.00783.x>
- Sitch, S., Smith, B., Prentice, I. C., Arneth, A., Bondeau, A., Cramer, W., ... Venevsky, S. (2003). Evaluation of ecosystem dynamics, plant geography and terrestrial carbon cycling in the LPJ dynamic global vegetation model. *Global Change Biology*, 9(2), 161–185. <https://doi.org/10.1046/j.1365-2486.2003.00569.x>
- Smith, N. G., & Dukes, J. S. (2013). Plant respiration and photosynthesis in global-scale models: Incorporating acclimation to temperature and CO₂. *Global Change Biology*, 19(1), 45–63. <https://doi.org/10.1111/j.1365-2486.2012.02797.x>
- Smith, N. G., Malyshev, S. L., Shevliakova, E., Kattge, J., & Dukes, J. S. (2016). Foliar temperature acclimation reduces simulated carbon sensitivity to climate. *Nature Climate Change*, 6(4), 407–411. <https://doi.org/10.1038/nclimate2878>
- Son, K., Tague, C., & Hunsaker, C. (2016). Effects of Model Spatial Resolution on Ecohydrologic Predictions and Their Sensitivity to Inter-Annual Climate Variability. *Water*, 8(8), 321. <https://doi.org/10.3390/w8080321>
- Stager, J. C., Ryves, D. B., Chase, B. M., & Pausata, F. S. R. (2011). Catastrophic Drought in the Afro-Asian Monsoon Region During Heinrich Event 1. *Science*, 331(6022), 1299–1302. <https://doi.org/10.1126/science.1198322>
- Strasser, U., Bernhardt, M., Weber, M., Liston, G. E., & Mauser, W. (2008). Is snow sublimation important in the alpine water balance? *The Cryosphere*, 2(1), 53–66. <https://doi.org/10.5194/tc-2-53-2008>
- Strasser, U., Warscher, M., & Liston, G. E. (2011). Modeling Snow–Canopy Processes on an Idealized Mountain. *Journal of Hydrometeorology*, 12(4), 663–677.

<https://doi.org/10.1175/2011JHM1344.1>

- Stuart-Haëntjens, E. J., Curtis, P. S., Fahey, R. T., Vogel, C. S., & Gough, C. M. (2015). Net primary production of a temperate deciduous forest exhibits a threshold response to increasing disturbance severity. *Ecology*, *96*(9), 2478–2487. <https://doi.org/10.1890/14-1810.1>
- Su, H., Schmid, H. P., Grimmond, C. S. B., Vogel, C. S., & Oliphant, A. J. (2004). Spectral Characteristics and Correction of Long-Term Eddy-Covariance Measurements Over Two Mixed Hardwood Forests in Non-Flat Terrain. *Boundary-Layer Meteorology*, *110*(2), 213–253. <https://doi.org/10.1023/A:1026099523505>
- Sun, Y., Gu, L., Dickinson, R. E., Norby, R. J., Pallardy, S. G., & Hoffman, F. M. (2014). Impact of mesophyll diffusion on estimated global land CO₂ fertilization. *Proceedings of the National Academy of Sciences*, *111*(44), 15774–15779. <https://doi.org/10.1073/pnas.1418075111>
- Sundqvist, M. K., Sanders, N. J., & Wardle, D. A. (2013). Community and Ecosystem Responses to Elevational Gradients: Processes, Mechanisms, and Insights for Global Change. *Annual Review of Ecology, Evolution, and Systematics*, *44*(1), 261–280. <https://doi.org/10.1146/annurev-ecolsys-110512-135750>
- Suni, T., Rinne, J., Reissell, A., Altimir, N., Keronen, P., Rannik, Ü., ... Vesala, T. (2003). Long-term measurements of surface fluxes above a Scots pine forest in Hyytiälä, southern Finland, 1996–2001. *Boreal Environment Research*, *8*(4), 287–301.
- Szerencsits, E. (2012). Swiss tree lines - a GIS-based Approximation. *Landscape Online*, *28*(1), 1–18. <https://doi.org/10.3097/LO.201228>
- Tague, C., Heyn, K., & Christensen, L. (2009). Topographic controls on spatial patterns of conifer transpiration and net primary productivity under climate warming in mountain ecosystems. *Ecohydrology*, *2*(4), 541–554. <https://doi.org/10.1002/eco.88>
- Tague, C., McDowell, N. G., & Allen, C. D. (2013). An Integrated Model of Environmental Effects on Growth, Carbohydrate Balance, and Mortality of *Pinus ponderosa* Forests in the Southern Rocky Mountains. *PLoS ONE*, *8*(11), e80286. <https://doi.org/10.1371/journal.pone.0080286>
- Tague, C., & Peng, H. (2013). The sensitivity of forest water use to the timing of precipitation and snowmelt recharge in the California Sierra: Implications for a warming climate. *Journal of Geophysical Research: Biogeosciences*, *118*(2), 875–887. <https://doi.org/10.1002/jgrg.20073>
- Tague, C., Seaby, L., & Hope, A. (2009). Modeling the eco-hydrologic response of a Mediterranean type ecosystem to the combined impacts of projected climate change and altered fire frequencies. *Climatic Change*, *93*(1–2), 137–155. <https://doi.org/10.1007/s10584-008-9497-7>
- Tang, X., Li, H., Desai, A. R., Nagy, Z., Luo, J., Kolb, T. E., ... Ammann, C. (2014). How is water-use efficiency of terrestrial ecosystems distributed and changing on Earth? *Scientific Reports*, *4*, 7483. <https://doi.org/10.1038/srep07483>
- Tarboton, D. G. (1997). A new method for the determination of flow directions and upslope areas in

- grid digital elevation models. *Water Resources Research*, 33(2), 309–319. <https://doi.org/10.1029/96WR03137>
- Teuling, A. J. (2018). A hot future for European droughts. *Nature Climate Change*, 8(5), 364–365. <https://doi.org/10.1038/s41558-018-0154-5>
- Teuling, A. J., Seneviratne, S. I., Stöckli, R., Reichstein, M., Moors, E. J., Ciais, P., ... Wohlfahrt, G. (2010). Contrasting response of European forest and grassland energy exchange to heatwaves. *Nature Geoscience*, 3(10), 722–727. <https://doi.org/10.1038/ngeo950>
- Teuling, A. J., Van Loon, A. F., Seneviratne, S. I., Lehner, I., Aubinet, M., Heinesch, B., ... Spank, U. (2013). Evapotranspiration amplifies European summer drought. *Geophysical Research Letters*, 40(10), 2071–2075. <https://doi.org/10.1002/grl.50495>
- Thompson, S. E., Harman, C. J., Troch, P. A., Brooks, P. D., & Sivapalan, M. (2011). Spatial scale dependence of ecohydrologically mediated water balance partitioning: A synthesis framework for catchment ecohydrology. *Water Resources Research*, 47(5), 1–20. <https://doi.org/10.1029/2010WR009998>
- Thum, T., Aalto, T., Laurila, T., Aurela, M., Kolari, P., & Hari, P. (2007). Parametrization of two photosynthesis models at the canopy scale in a northern boreal Scots pine forest. *Tellus B*, 59(5), 874–890. <https://doi.org/10.1111/j.1600-0889.2007.00305.x>
- Timofeeva, G., Treydte, K., Bugmann, H., Rigling, A., Schaub, M., Siegwolf, R. T. W., & Saurer, M. (2017). Long-term effects of drought on tree-ring growth and carbon isotope variability in Scots pine in a dry environment. *Tree Physiology*, 37(8), 1028–1041. <https://doi.org/10.1093/treephys/tpx041>
- Tor-ngern, P., Oren, R., Ward, E. J., Palmroth, S., Mccarthy, H. R., & Domec, J.-C. (2015). Increases in atmospheric CO₂ have little influence on transpiration of a temperate forest canopy. *New Phytologist*, 205(2), 518–525. <https://doi.org/10.1111/nph.13148>
- Tromp-van Meerveld, H. J., & McDonnell, J. J. (2006). On the interrelations between topography, soil depth, soil moisture, transpiration rates and species distribution at the hillslope scale. *Advances in Water Resources*, 29(2), 293–310. <https://doi.org/10.1016/j.advwatres.2005.02.016>
- Tuzet, A., Perrier, A., & Leuning, R. (2003). A coupled model of stomatal conductance, photosynthesis and transpiration. *Plant, Cell and Environment*, 26(7), 1097–1116. <https://doi.org/10.1046/j.1365-3040.2003.01035.x>
- Urbanski, S., Barford, C., Wofsy, S. C., Kucharik, C., Pyle, E., Budney, J., ... Munger, J. W. (2007). Factors controlling CO₂ exchange on timescales from hourly to decadal at Harvard Forest. *Journal of Geophysical Research: Biogeosciences*, 112(2), 1–25. <https://doi.org/10.1029/2006JG000293>
- Valentini, R., Gamon, J. A., & Field, C. B. (1995). Ecosystem Gas Exchange in a California Grassland : Seasonal Patterns and Implications for Scaling. *Ecology*, 76(6), 1940–1952.

- Valladares, F., Gianoli, E., & Gómez, J. M. (2007). Ecological limits to plant phenotypic plasticity. *New Phytologist*, *176*(4), 749–763. <https://doi.org/10.1111/j.1469-8137.2007.02275.x>
- van den Bergh, T., Körner, C., & Hiltbrunner, E. (2017). *Alnus* shrub expansion increases evapotranspiration in the Swiss Alps. *Regional Environmental Change*, 1–11. <https://doi.org/10.1007/s10113-017-1246-x>
- van der Sleen, P., Groenendijk, P., Vlam, M., Anten, N. P. R., Boom, A., Bongers, F., ... Zuidema, P. A. (2015). No growth stimulation of tropical trees by 150 years of CO₂ fertilization but water-use efficiency increased. *Nature Geoscience*, *8*(1), 24–28. <https://doi.org/10.1038/ngeo2313>
- Van Dijk, A. I. J. M., Gash, J. H., Van Gorsel, E., Blanken, P. D., Cescatti, A., Emmel, C., ... Wohlfahrt, G. (2015). Rainfall interception and the coupled surface water and energy balance. *Agricultural and Forest Meteorology*, *214–215*, 402–415. <https://doi.org/10.1016/j.agrformet.2015.09.006>
- Venturas, M. D., Sperry, J. S., & Hacke, U. G. (2017). Plant xylem hydraulics: What we understand, current research, and future challenges. *Journal of Integrative Plant Biology*, *59*(6), 356–389. <https://doi.org/10.1111/jipb.12534>
- Vicente-Serrano, S. M., Camarero, J. J., Zabalza, J., Sangüesa-Barreda, G., López-Moreno, J.-I., & Tague, C. (2015). Evapotranspiration deficit controls net primary production and growth of silver fir: Implications for Circum-Mediterranean forests under forecasted warmer and drier conditions. *Agricultural and Forest Meteorology*, *206*, 45–54. <https://doi.org/10.1016/j.agrformet.2015.02.017>
- Vickers, D., Thomas, C. K., Pettijohn, C., Martin, J. G., & Law, B. E. (2012). Five years of carbon fluxes and inherent water-use efficiency at two semi-arid pine forests with different disturbance histories. *Tellus, Series B: Chemical and Physical Meteorology*, *64*(1), 1–14. <https://doi.org/10.3402/tellusb.v64i0.17159>
- Vieira, J. H. D. (1983). Conditions governing the use of approximations for the Saint-Venant equations for shallow surface water flow. *Journal of Hydrology*, *60*(1–4), 43–58. [https://doi.org/10.1016/0022-1694\(83\)90013-6](https://doi.org/10.1016/0022-1694(83)90013-6)
- Villalba, R., Veblen, T. T., & Ogden, J. (1994). Climatic Influences on the Growth of Subalpine Trees in the Colorado Front Range. *Ecology*, *75*(5), 1450–1462. <https://doi.org/10.2307/1937468>
- Viviroli, D., Archer, D. R., Buytaert, W., Fowler, H. J., Greenwood, G. B., Hamlet, A. F., ... Woods, R. (2011). Climate change and mountain water resources: overview and recommendations for research, management and policy. *Hydrology and Earth System Sciences*, *15*(2), 471–504. <https://doi.org/10.5194/hess-15-471-2011>
- Viviroli, D., Messerli, B., Meybeck, M., & Weingartner, R. (2007). Mountains of the world, water towers for humanity: Typology, mapping, and global significance. *Water Resources Research*, *43*(7), 1–13. <https://doi.org/10.1029/2006WR005653>
- Viviroli, D., & Weingartner, R. (2004). The hydrological significance of mountains: from regional to

- global scale. *Hydrology and Earth System Sciences*, 8(6), 1017–1030. <https://doi.org/10.5194/hess-8-1017-2004>
- Vivoni, E. R., Rodríguez, J. C., & Watts, C. J. (2010). On the spatiotemporal variability of soil moisture and evapotranspiration in a mountainous basin within the North American monsoon region. *Water Resources Research*, 46(2), 1–18. <https://doi.org/10.1029/2009WR008240>
- Voepel, H., Ruddell, B., Schumer, R., Troch, P. A., Brooks, P. D., Neal, A., ... Sivapalan, M. (2011). Quantifying the role of climate and landscape characteristics on hydrologic partitioning and vegetation response. *Water Resources Research*, 47(8), 1–13. <https://doi.org/10.1029/2010WR009944>
- Vörösmarty, C. J., Lévêque, C., & Revenga, C. (2005). Fresh Water. In *Millennium Ecosystems Assessment, vol. 1 Ecosystems and Human Well-Being: Current State and Trends* (eds Hassan, pp. 165–207). <https://doi.org/10.1007/BF03007034>
- Wang, Y. P., & Leuning, R. (1998). A two-leaf model for canopy conductance, photosynthesis and partitioning of available energy I: Model description and comparison with a multi-layered model. *Agricultural and Forest Meteorology*, 91(1–2), 89–111. [https://doi.org/10.1016/S0168-1923\(98\)00061-6](https://doi.org/10.1016/S0168-1923(98)00061-6)
- Wang, Y. P., Lu, X. J., Wright, I. J., Dai, Y., Rayner, P. J., & Reich, P. B. (2012). Correlations among leaf traits provide a significant constraint on the estimate of global gross primary production. *Geophysical Research Letters*, 39(19), L19405. <https://doi.org/10.1029/2012GL053461>
- Ward, E. J., Oren, R., Bell, D. M., Clark, J. S., McCarthy, H. R., Kim, H. S., & Domec, J.-C. (2013). The effects of elevated CO₂ and nitrogen fertilization on stomatal conductance estimated from 11 years of scaled sap flux measurements at Duke FACE. *Tree Physiology*, 33(2), 135–151. <https://doi.org/10.1093/treephys/tps118>
- Warren, J. M., Jensen, A. M., Medlyn, B. E., Norby, R. J., & Tissue, D. T. (2015). Carbon dioxide stimulation of photosynthesis in *Liquidambar styraciflua* is not sustained during a 12-year field experiment. *AoB PLANTS*, 7(1), plu074. <https://doi.org/10.1093/aobpla/plu074>
- Wassen, M. J., & Grootjans, A. P. (1996). Ecohydrology: An Interdisciplinary Approach for Wetland Management and Restoration. *Source: Vegetatio*, 126(1), 1–4.
- Way, D. A., Oren, R., & Kroner, Y. (2015). The space-time continuum: the effects of elevated CO₂ and temperature on trees and the importance of scaling. *Plant, Cell & Environment*, 38(6), 991–1007. <https://doi.org/10.1111/pce.12527>
- Wehr, R., Munger, J. W., McManus, J. B., Nelson, D. D., Zahniser, M. S., Davidson, E. A., ... Saleska, S. R. (2016). Seasonality of temperate forest photosynthesis and daytime respiration. *Nature*, 534(7609), 680–683. <https://doi.org/10.1038/nature17966>
- Weingartner, R., & Viviroli, D. (2007). Water resources in mountain regions: a methodological approach to assess the water balance in a highland-lowland-system. *Hydrological Processes*, 21(5), 578–585. <https://doi.org/10.1002/hyp.6268>

- Williams, C. J., McNamara, J. P., & Chandler, D. G. (2009). Controls on the temporal and spatial variability of soil moisture in a mountainous landscape: the signature of snow and complex terrain. *Hydrology and Earth System Sciences*, *13*(7), 1325–1336. <https://doi.org/10.5194/hess-13-1325-2009>
- Wohlfahrt, G., & Gu, L. (2015). The many meanings of gross photosynthesis and their implication for photosynthesis research from leaf to globe. *Plant, Cell and Environment*, *38*(12), 2500–2507. <https://doi.org/10.1111/pce.12569>
- Wolf, A., Anderegg, W. R. L., & Pacala, S. W. (2016). Optimal stomatal behavior with competition for water and risk of hydraulic impairment. *Proceedings of the National Academy of Sciences*, *113*(46), E7222–E7230. <https://doi.org/10.1073/pnas.1615144113>
- Wolf, S., Eugster, W., Ammann, C., Häni, M., Zielis, S., Hiller, R., ... Buchmann, N. (2013). Contrasting response of grassland versus forest carbon and water fluxes to spring drought in Switzerland. *Environmental Research Letters*, *8*(3). <https://doi.org/10.1088/1748-9326/8/3/035007>
- Wood, E. F., Roundy, J. K., Troy, T. J., van Beek, L. P. H., Bierkens, M. F. P., Blyth, E., ... Whitehead, P. (2011). Hyperresolution global land surface modeling: Meeting a grand challenge for monitoring Earth's terrestrial water. *Water Resources Research*, *47*(5), 1–10. <https://doi.org/10.1029/2010WR010090>
- Woolhiser, D. A., Fedors, R. W., Smith, R. E., & Stothoff, S. A. (2006). Estimating Infiltration in the Upper Split Wash Watershed, Yucca Mountain, Nevada. *Journal of Hydrologic Engineering*, *11*(2), 123–133. [https://doi.org/10.1061/\(asce\)1084-0699\(2006\)11:2\(123\)](https://doi.org/10.1061/(asce)1084-0699(2006)11:2(123))
- Wu, D., Ciais, P., Viovy, N., Knapp, A. K., Wilcox, K., Bahn, M., ... Piao, S. L. (2018). Asymmetric responses of primary productivity to altered precipitation simulated by ecosystem models across three long-term grassland sites. *Biogeosciences*, *15*(11), 3421–3437. <https://doi.org/10.5194/bg-15-3421-2018>
- Wüest, M., Frei, C., Altenhoff, A., Hagen, M., Litschi, M., & Schär, C. (2010). A gridded hourly precipitation dataset for Switzerland using rain-gauge analysis and radar-based disaggregation. *International Journal of Climatology*, *30*(12), 1764–1775. <https://doi.org/10.1002/joc.2025>
- Wullschleger, S. D., Gunderson, C. A., Hanson, P. J., Wilson, K. B., & Norby, R. J. (2002). Sensitivity of stomatal and canopy conductance to elevated CO₂ concentration - interacting variable and perspectives of scale. *New Phytologist*, *153*(3), 485–496. <https://doi.org/10.1046/j.0028-646X.2001.00333.x>
- Wullschleger, S. D., Tschaplinski, T. J., & Norby, R. J. (2002). Plant water relations at elevated CO₂ - Implications for water-limited environments. *Plant, Cell and Environment*, *25*(2), 319–331. <https://doi.org/10.1046/j.1365-3040.2002.00796.x>
- Xue, B.-L., Guo, Q., Otto, A., Xiao, J., Tao, S., & Li, L. (2015). Global patterns, trends, and drivers of water use efficiency from 2000 to 2013. *Ecosphere*, *6*(10), 174. <https://doi.org/10.1890/ES14->

- Yin, X. (2002). Responses of leaf nitrogen concentration and specific leaf area to atmospheric CO₂ enrichment: A retrospective synthesis across 62 species. *Global Change Biology*, 8(7), 631–642. <https://doi.org/10.1046/j.1365-2486.2002.00497.x>
- Zapata-Rios, X., Brooks, P. D., Troch, P. A., McIntosh, J., & Guo, Q. (2016). Influence of terrain aspect on water partitioning, vegetation structure and vegetation greening in high-elevation catchments in northern New Mexico. *Ecohydrology*, 9(5), 782–795. <https://doi.org/10.1002/eco.1674>
- Zappa, M., & Kan, C. (2007). Extreme heat and runoff extremes in the Swiss Alps. *Natural Hazards and Earth System Sciences*, 7(3), 375–389. <https://doi.org/10.5194/nhess-7-375-2007>
- Zhou, S. X., Medlyn, B. E., & Prentice, I. C. (2016). Long-term water stress leads to acclimation of drought sensitivity of photosynthetic capacity in xeric but not riparian Eucalyptus species. *Annals of Botany*, 117(1), 133–144. <https://doi.org/10.1093/aob/mcv161>
- Zhou, S., Yu, B., Huang, Y., & Wang, G. (2015). Daily underlying water use efficiency for AmeriFlux sites. *Journal of Geophysical Research Biogeosciences*, 120(5), 887–902. <https://doi.org/10.1002/2015JG002947>
- Zierl, B., Bugmann, H., & Tague, C. (2007). Water and carbon fluxes of European ecosystems: an evaluation of the ecohydrological model RHESSys. *Hydrological Processes*, 21(24), 3328–3339. <https://doi.org/10.1002/hyp.6540>
- Zscheischler, J., Fatichi, S., Wolf, S., Blanken, P. D., Bohrer, G., Clark, K., ... Seneviratne, S. I. (2016). Short-term favorable weather conditions are an important control of interannual variability in carbon and water fluxes. *Journal of Geophysical Research: Biogeosciences*, 121(8), 2186–2198. <https://doi.org/10.1002/2016JG003503>

Curriculum Vitae

Personal information

Name	Theodoros Mastrotheodoros
Father's Name	Panagiotis Mastrotheodoros
Address	Holderbachweg 14, 8046, Zürich
Phone	+41786773426
E-mail	mastrotheodoros@ifu.baug.ethz.ch
Nationality	Greek
Date of Birth	14 June 1990

Education

<i>5/2019-present</i>	Post-doctoral fellow Institute of Environmental Engineering, ETH Zürich, Switzerland Group of Hydrology and Water Resources Management PhD student (ALPHSENS project funded by ETH Grants and Stavros Niarchos Foundation: A pan-Alpine high-resolution carbon and water budget and its sensitivity to climate changes)
<i>3/2015-4/2019</i>	PhD in Environmental Engineering Institute of Environmental Engineering, ETH Zürich, Switzerland Group of Hydrology and Water Resources Management Supervisor: Prof. Dr. Peter Molnar Dissertation title: <i>Ecohydrological sensitivity to climatic variables: dissecting the water tower of Europe</i>
<i>9/2008-12/2013</i>	Diploma degree in Civil Engineering Specialization in Hydraulics, Hydrology and Water Resources Management, Department of Water Resources and Environmental Engineering, Faculty of Civil Engineering, National Technical University of Athens, Athens, Greece 5-year studies equivalent to Master, 300 ECTS, GPA 9.55/10 (graduated 3 rd) Diploma Thesis: <i>A Monte Carlo simulation approach for generating flood hydrographs in Mediterranean basins</i> Supervisor: Prof. Dr. Demetris Koutsoyiannis

Professional Experience

<i>3/2019-7/2019</i>	<i>Institute of Environmental Engineering, ETH Zürich, Switzerland</i> Scientific assistant
<i>5/2014-11/2014</i>	<i>Hellenic Army, Corps of Engineers</i> Redaction of Hellenic Military Academy's Curriculum Guide
<i>2/2014-4/2014</i>	<i>Institute of Environmental Engineering, ETH Zürich, Switzerland</i>

Work as a research assistant on a trend analysis project for a variety of meteorological variables in Switzerland with emphasis on the seasonality of trends in near surface humidity (Fatichi, S., Molnar, P., Mastrotheodoros, T., & Burlando, P. (2015). Diurnal and seasonal changes in near-surface humidity in a complex orography. *Journal of Geophysical Research: Atmospheres*, 120(6), 2358–2374. <https://doi.org/10.1002/2014JD022537>)

9/2013-10/2013

National Technical University of Athens and Raycap

Extension of the research program 62/2740, “Evaluation of the proposition to install fuse gates on the spillways of five dams that are managed by the Greek public power corporation”. Investigation of the possibility to install fuse gates on 18 dams in Thessaly, central Greece. Work included localization of dams, photography of each dam, spillways and surroundings, report with detailed technical data regarding each dam, questionnaire about reservoir operation, water uses and water availability in the area of each dam

7/2012-8/2012

Mashhoor Engineering Consultancy, Muscat, Oman

PO Box 374, PC 100, <http://mashhoor.org/>

Autocad design and on-site work in Yiti village, Oman

Publications in peer-reviewed journals

Fatichi, S., P. Molnar, **T. Mastrotheodoros**, and P. Burlando (2015), Diurnal and seasonal changes in near surface humidity in a complex orography, *Journal of Geophysical Research: Atmospheres*, 119, <https://doi.org/10.1002/2014JD022537>

Mastrotheodoros, T., Pappas, C., Molnar, P., Burlando, P., Keenan, T. F., Gentine, P., Gough C. M., Fatichi, S. (2017). Linking plant functional trait plasticity and the large increase in forest water use efficiency. *Journal of Geophysical Research: Biogeosciences*, 122(9), 2393–2408. <https://doi.org/10.1002/2017JG003890>

Mastrotheodoros, T., Pappas, C., Molnar, P., Burlando, P., Hadjidoukas, P., & Fatichi, S. (2019). Ecohydrological dynamics in the Alps: insights from a modelling analysis of the spatial variability. *Ecohydrology*, 12(1), e2054. <https://doi.org/10.1002/eco.2054>

Mastrotheodoros T., Pappas C., Molnar P., Burlando P., Manoli G., Parajka J., Rigon R., Bottazzi M., Szeles B., Hadjidoukas P., and Fatichi S., (under review), More green and less blue water in the Alps during warmer summers, *Nature Climate Change*

Conferences

T. Mastrotheodoros, C. Pappas, P. Molnar, P. Burlando, J. Parajka, R. Rigon, B. Szeles, M. Bottazzi, P. Hadjidoukas and S. Fatichi, A high-resolution ecohydrological analysis of the European Alps, EGU General Assembly 2019, Vienna (oral)

T. Mastrotheodoros, C. Pappas, P. Molnar, P. Burlando, P. Hadjidoukas, and S. Fatichi, Alpine ecohydrology: exploring the interactions between topographic, climatic and vegetation gradients, CMWR XXII, Saint-Malo, France, 2018 (oral)

T. Mastrotheodoros, C. Pappas, P. Molnar, P. Burlando, P. Hadjidoukas, and S. Fatichi, Alpine Ecohydrology Across Scales: Propagating Fine-scale Heterogeneity to the Catchment and Beyond, AGU, Fall Meeting 2017, New Orleans (oral)

T. Mastrotheodoros, C. Pappas, P. Molnar, P. Burlando, P. Hadjidoukas, and S. Fatichi, Alpine ecohydrology across scales: propagating fine-scale heterogeneity to the catchment and beyond, 15th Swiss Geoscience Meeting, Davos 2017 (oral)

T. Mastrotheodoros, C. Pappas, P. Molnar, P. Burlando, T. F. Keenan, P. Gentine, and S. Fatichi, Trends in ecosystem water use efficiency are potentially amplified by plasticity in plant functional traits, EGU General Assembly 2017, Vienna (poster)

T. Mastrotheodoros, S. Fatichi, C. Pappas, P. Molnar, and P. Burlando, Does plasticity in plant physiological traits explain the rapid increase in water use efficiency? An ecohydrological modeling approach, EGU General Assembly 2016, Vienna (poster)

E.-M. Michaelidi, **T. Mastrotheodoros**, A. Efstratiadis, A. Koukouvinos and D. Koutsoyiannis, Flood modelling in river basins with highly variable runoff, 5th EGU Leonardo Conference - Hydrofractals 2013 - STAHY '13, Kos Island, Greece (available online <http://itia.ntua.gr/en/docinfo/1385/>, poster)

E. Anagnostopoulou, A. Galani, P. Dimas, A. Karanasios, **T. Mastrotheodoros**, E.-M. Michaelidi, D. Nikolopoulos, S. Pontikos, F. Sourla, A. Chazapi, S. M. Papalexiou and D. Koutsoyiannis, Record breaking events for typical autocorrelation structures, EGU General Assembly 2013, Vienna (available online <http://itia.ntua.gr/en/docinfo/1331/>, poster)

Personal Skills

Languages

Greek	Mother tongue
English	Excellent Knowledge (Certificate of Proficiency in English of Cambridge and Michigan University, C2)
German	Excellent Knowledge (Goethe Institut Certificate for Language Proficiency, C1)
French	Basic knowledge

Computer Skills

Excellent command of Microsoft Office tools and Matlab, Very good C++ knowledge

Hobbies

2013	Degree in violin with Grade A
2010-2013	Experience in several youth orchestras playing in first or second violins, and as a first viola player (Greek Youth Orchestra, Athenian Symphonic Youth Orchestra, Camerata Junior)
2010	Certificate in Counterpoint with Grade A
2009	Primary Certificate of Mountaineering, Hellenic Federation of Mountaineering and Climbing
2008, 2010, 2012, 2014	Participation in the Athens Classic Marathon Race

2007	Certificate in Harmony of Music with Grade A
2004	Certificate in Theory of Music with Grade A
2003-Today	Participation in mountain running races in Greece and Switzerland

Manuscript Reviewer

Hydrological Processes
Geophysical Research Letters
Hydrology and Earth System Sciences
Agricultural and Forest Meteorology
Atmosphere